Scaling-up of the Electrochemical Leaf System



Beichen Cheng

Trinity Term 2022

A Thesis Submitted for the Degree of
Doctor of Philosophy, University of Oxford

© Beichen Cheng 2022

ABSTRACT

This thesis presents an exploration of the Electrochemical Leaf (e-Leaf) with a novel application-oriented direction. The e-Leaf, a recent breakthrough made in the Armstrong group in the area of bio-electrochemical catalysis, is inspired by the natural leaf: enzyme cascade is immobilised in the nanopores of the electrode, allowing multi-step biotransformations to be energised, controlled, and monitored in real time. Ferredoxin $NADP^+$ reductase (FNR) is the key enzyme in the e-Leaf, catalysing the interconversion of $NADP^+$/NADP(H). Other co-entrapped NADP(H)-dependent enzyme(s) catalyse reactions coupled to this regeneration, achieving a fast conversion due to the very high effective concentration of enzymes and short distances for cofactor and reactants to diffuse between the enzymes in the nanopores. The e-Leaf is a powerful tool for the investigation of biocatalytic processes and potentially for the production of valuable chemicals.

In this work, the e-Leaf has been exploited for its versatility in application. First, the e-Leaf has been scaled up from a 4 mL lab-scale cell to a 500 mL pilot level reactor with new reactor designs, optimisations of the electrode construction and optimisation of reaction conditions. The productivity scales up linearly with the size of the reactor, showing the feasibility and potential of scaling up an electrochemical system.

The e-Leaf has also been explored to function as a biphasic reactor. The introduction of an organic layer containing substrate and(or) solvent has provided the electrochemical system with a sustainable substrate supply with simultaneous relief of product-inhibition. The final step in engineering the e-Leaf has been its transformation from an original batch design into a flow reactor in which the electrochemical reactions have been performed under flow as a proof of concept. The e-Leaf therefore has the potential to

work in series continuously with high space-time-yield to accommodate complex requirements for industry-level syntheses.

In a separate branch of work, the e-Leaf has been exploited to achieve the deracemisation and stereoinversion of a secondary alcohol in a dually-controlled method, with the ability to switch the direction of the redox reaction and to change the enantioselectivity of the electrode. The reaction process is monitored in real-time to complete a one-pot, one-step deracemisation (or stereoinversion).

ACKNOWLEDGEMENTS

First of all, I would like to thank Fraser for giving me the opportunity to be a DPhil student, studying and doing research in the group. His encouragement has always been valuable to me since I was not confident when I first stepped on this journey. I remembered the first week in the lab Fraser said to me 'You should always try the difficult way. Don't simply pick an easy one.' I have learned perseverance as well as knowledges.

I would like to thank my parents and my wife, for providing the endless support and love. I feel strong and determined with you standing by my side. I have been enjoying every day in my life and I am willing to build a bright future with you.

Thanks to all the Armstrong group's brothers and sisters. It was a great journey with all of you on the way: Bhavin, Clare, Non, Liyun, Kourosh, Leonie, Kavita, Sarah, Adam, Ros, Tom, Cam, Sacha, and Alice, as well as the visiting students Matteo and Oliver. Thanks to my buddies Giorgio, Lei and Ryan, who provided great professional suggestions for research and also fantastic casual chatting topics. I remember those hilarious moments when the group was having game night and the pool for the world cup, and birthdays when I could get cakes. Special thanks to Bhavin and Clare, who have been offering generous help from day one of my DPhil, and I cannot finish this thesis without their help. I received valuable research suggestions and creative ideas from those brilliant minds, and the mentality reinforcement from their warm-hearted encouragement. This thesis was proofread by Bhavin and Clare and great improvement has been made. Thanks for the valuable time and patience you have provided.

Thanks to the staff working in the ICL to keep the lab working safely. Special thanks to Terri who made me cells of different designs which are vital for my project. Thanks to Nenad and Alex for fixing our electrical devices. I would also want to thank St Hugh's college for providing the cheap and delicious food to keep me healthy.

PUBLICATIONS

- **Cheng, B.**; Heath, R. S.; Turner, N. J.; Armstrong, F. A.; Megarity, C. F. Deracemisation and Stereoinversion by a Nanoconfined Bidirectional Enzyme Cascade: Dual Control by Electrochemistry and Selective Metal Ion Activation. *Chem. Commun*. 2022.

- **Cheng, B.**; Wan, L.; Armstrong, F. A. Progress in Scaling up and Streamlining a Nanoconfined, Enzyme-Catalyzed Electrochemical Nicotinamide Recycling System for Biocatalytic Synthesis. *ChemElectroChem* 2020, 7 (22), 4672–4678.

- Megarity, C. F.; Siritanaratkul, B.; **Cheng, B.**; Morello, G.; Wan, L.; Sills, A. J.; Heath, R. S.; Turner, N. J.; Armstrong, F. A. Electrified Nanoconfined Biocatalysis with Rapid Cofactor Recycling. *ChemCatChem* 2019, 11 (23), 5662–5670.

- Armstrong, F. A.; Siritanaratkul, B.; Megarity, C. F.; Herold, R. A.; **Cheng, B**. From Protein Film Electrochemistry to Nanoconfined Enzyme Cascades and the Electrochemical Leaf. *Chem. Rev.* 2022.

ABBREVIATIONS

A	Ampere
ADH	Alcohol dehydrogenase
Ar	Argon
ATP	Adenosine triphosphate
BSA	Bovine serum albumin
C	Coulomb
CE	Counter electrode
CV	Cyclic voltammetry
Da	Dalton
DTT	Dithiothreitol
δ	Chemical shift
E	Potential
E. coli.	Escherichia coli
E1	Enzyme 1
E2	Enzyme 2
EDTA	Ethylenediaminetetraacetic acid
ee	Enantiomeric excess
EPD	Electrophoretic deposition
F	Faraday constant
FAD	Flavin adenine dinucleotide
Fd	Ferredoxin
FDH	Formate dehydrogenase
FNR	Ferredoxin NADP+ reductase
FTO	Fluorine-doped tin oxide
GC-FID	Gas chromatography - flame ionization detector
GDH	Glucose dehydrogenase
GLDH	Glutamate dehydrogenase
HEPES	4-(2-hydroxyethyl)-1-piperazineethanesulfonic acid

i	Current density
I	Current
ID	Inner diameter
IPTG	Isopropyl β-d-1-thiogalactopyranoside
ITO	Indium tin oxide
k_{cat}	turnover number
K_i	Inhibition constant
K_m	Michaelis constant
LK	Lactobacillus kefir
MTBE	Methyl tert-butyl ether
MV	Methyl viologen
NADP	Nicotinamide adenine dinucleotide phosphate
NMR	Nuclear magnetic resonance
OD	Optical density
OD	Outer diameter
PBER	Packed-bed electrochemical reactor
PCR	Polymerase chain reaction
PDB	Protein data bank
PGE	Pyrolytic graphite edge
pI	Isoelectric point
Pt	Platinum
Q	Quantity of charges
RE	Reference electrode
rpm	Rotation per minute
RT	Room temperature
SA	Surface area
SCE	Standard calomel electrode
SDS	Sodium dodecyl sulphate
SEM	Scanning electron microscopy
SHE	Standard hydrogen electrode
T	Temperature

TAPS	[tris(hydroxymethyl)methylamino] propanesulfonic acid
Ti	Titanium
TMSP	Trimethylsilylpropanoic acid
TOF	Turnover frequency
TTN	Total turnover number
UV-Vis	Ultraviolet - visible
V	Volt
v	Reaction rate
v_{max}	Maximum reaction rate
WE	Working electrode
Zn	Zinc

CONTENTS

Abstract I

Acknowledgements III

Publications IV

Abbreviations V

Contents VIII

Chapter I Introduction of the Electrochemical Leaf 1

1.1. Introduction 2

1.2. Biocatalysis: Enzyme Catalysed Reactions 3

1.3. Nicotinamide Cofactor 4

1.4. Ferredoxin-NADP+ Reductase (FNR) 10

1.5. The Electrochemical Leaf 13

1.5.1. E-Leaf basics: from the Nature Leaf to the E-Leaf 13

1.5.2. Features of the E-Leaf 16

1.6. Downstream Enzyme (E2) Reactions 18

1.6.1. Glutamate Dehydrogenase (GLDH) 18

1.6.2. Alcohol Dehydrogenase (ADH) 18

1.7. Construction of the E-Leaf 19

1.7.1. Electrode Manufacturing: ITO Coating 19

1.7.2. Enzyme Loading 20

1.7.3. Electrochemical Cell 21

1.8. Electrochemistry Analysis Methods 23

1.8.1. Cyclic Voltammetry 23

1.8.2. Chronoamperometry 26

Chapter II Optimisation of the Initial E-Leaf System 29

2.1. Introduction 30

2.2. Electrode Support Material 31

2.2.1. Titanium Tube 31

2.2.2. Titanium Foam 33

2.2.3. Titanium Mesh 34

2.2.4. Titanium Wire and Titanium Foil (twisted) 35

2.3. Indium Tin Oxide (ITO) Coating 37

2.3.1. Alternative ITO coating - Doctor's Blade Pasting method 38

2.3.2. Deposition Time and ITO Amount in EPD 40

2.4. Enzyme Loading Optimisation with FNR Preloaded 43

2.4.1. FNR Loading Method: Stir-loading and Drop-casting 43

2.4.2. Live Injection Amount of E2 44

2.4.3. Membrane for Enzyme Confining with E2 Live Injection 45

2.5. Enzyme Loading Optimisation: Stepwise Loading 48

2.6. Enzyme Co-loading by Drop-casting 49

2.6.1. Enzyme Loading Ratio (FNR to GLDH) 49

2.6.2. Enzyme Usage in Loading 50

2.6.3. Drop-casting Volume (Drop Concentration) 52

2.6.4. Incubation Time 54

2.7. Reaction Optimisation 55

2.7.1. Reactor 55

2.7.2. Cofactor NADP(H) Concentration in Bulk Solution 55

2.8. Summary 59

Chapter III Scaling-up of the Electrochemical Leaf for Biocatalytic Synthesis 61

3.1. Abstract 62

3.2. GLDH-catalysed Reaction 63

3.2.1. GLDH: The Model Reaction 63

3.2.2. Kinetics by Solution Assay 63

3.3. Optimisation Before Scaling-up 65

3.3.1. Electrode Design and Scale with Enzyme Loading methods – Ti foil 65

3.3.2. Enzyme Ratios (FNR to GLDH), $NADP^+$ and pH 67

3.4. Cell Design and Reactions in Scaling-up 69

3.4.1. 4 mL Prototype Cell Design and Reaction 69

3.4.2. Intermediate 40 mL Cell Design and Reaction 72

3.4.3. Large-scale Modular Cell Configuration (80 mL) 78

3.4.4. Large-scale Bulk Synthesis in a 0.5 Litre Reaction 80

3.4.5. Product Separation of L-glutamic Acid 88

3.5. Conclusion and Possibilities of the E-Leaf 92

Chapter IV Dual Control of a Bidirectional Nanoconfined Enzyme Cascade: A Novel Approach for Deracemisation and Inversion 95

4.1. Introduction 96

4.2. Characteristics of Three Alcohol Dehydrogenases 99

4.2.1. Enantioselectivity 100

4.2.1.1. Cyclic Voltammetry of W110A and LK 100

4.2.1.2. Chronoamperometry of the Enantiomer-specific Conversion Catalysed by W110A, LK and W110V 101

4.2.2. Product-inhibition in ADH-Catalysed Oxidation 106

4.3. LK and W110A Nanoconfined Together in a Single Electrode: Real-time Investigative Experiments 107
4.3.1. The Effect of Changing Enantiomers and the Addition of EDTA in Real-time, on each Enzyme Separately 107
4.3.2. Investigating the Effect of Changing the Alcohol and the Addition of EDTA in Real-time on LK and W110A Co-entrapped in One Electrode 110
4.4. The Magnesium Effect 113
4.4.1. W110A: A Mg^{2+} Titration 114
4.4.2. Further Investigations of the Mg^{2+} effect by EDTA Titration on LK and W110A 115
4.4.2.1. Small Scale EDTA Titration with Rotating Disk Electrode 115
4.4.2.2. EDTA Titration with Ti Foil Electrode 117
4.5. The Electrochemical Leaf: Optimisation for Inversion and Deracemisation 127
4.5.1. A Two-electrode Deracemisation System 128
4.5.2. Inversion (*R* to *S*): (LK + W110A) Co-entrapped in a Single Electrode 131
4.5.2.1. Initial Design for Inversion 131
4.5.2.2. Inverter Improved by pH Adjustment 133
4.5.3. Deracemisation (Racemic to S): LK + W110A Co-entrapped in a Single Electrode 136
4.5.3.1. Initial design for deracemisation 136
4.5.3.2. Deracemiser Improved by pH Adjustment 138
4.6. A New ADH Variant: W110V 140
4.7. The Optimised Inverter and Deracemiser: with W110V Substituting W110A 141
4.8. Inverter and Deracemiser: with More Substrate 144
4.9. The Electrochemical Leaf: Bulk Deracemisation 147
4.10. Conclusion and Potential Improvement 150

Chapter V Biphasic Electrochemical Leaf for Sustainable Substrate Supply and Product-Inhibition Relief 152

5.1. Introduction 153

5.2. Enzyme and Reaction Involved 156

5.3. Condition Optimisation 158

5.3.1. Enzyme Loading 158

5.3.2. Scaling-up Feasibility 159

5.4. Organic Solvent 161

5.4.1. Organic Solvent Partition Numbers Tested by NMR 162

5.4.2. Effect of Additional Solvent Layer on Enzyme Stability 165

5.5. Initial Experiments with Real-time Addition of ADH 169

5.5.1. The Electrochemical Leaf Setup as a Biphasic Reactor 170

5.5.2. Benchmarks and First Trials 170

5.5.3. Biphasic Reactions with Hexane and Pure Substrates 173

5.5.4. Supplementary Test for Initial Experiments 179

5.6. Later-stage Experiments in a Glovebox with Enzyme Pre-loaded 182

5.6.1. Reduction with Pure Substrate: Substrate Replenishing and Deactivation 183

5.6.2. Organic Phase in Oxidation for Product Inhibition relief 186

5.7. Conclusion and Potential Improvement 193

Chapter VI The Electrochemical Leaf Under Flow 195

6.1. Introduction 196

6.2. Flow Cell I 200

6.2.1. Cell Design 200

6.2.2. Experiment Results and Discussion - Flow Cell I 201

6.3. Flow Cell II 206
6.3.1. Cell design 206
6.3.2. Flow cell II Test with Ferro-ferricyanide Oxidation 207
6.3.2.1. Cell Construction and Feasibility Test 207
6.3.2.2. Improved Flow Cell II with Tube Electrodes 212
6.3.3. Flow cell II: GLDH-catalysed Reduction with Ti Tube Electrodes 216
6.3.3.1. Cell Setup 216
6.3.3.2. GLDH-catalysed reduction in flow cell II 217
6.4. Flow cell III 220
6.4.1. Cell Design 220
6.4.2. Batch Mode Test with Ti mesh 222
6.4.3. First Trial in Flow Cell III Under Flow 224
6.4.4. Flow cell III in the Glovebox 226
6.5. Conclusion and Potential Improvement 232
Chapter VII Experimental Methods and Materials 234
7.1. Introduction 235
7.2. Enzyme Production 235
7.2.1. Enzyme Preparation and Purification 235
7.2.2. Visualisation of Enzyme Purity by gel Electrophoresis and Determination of Enzyme Concentration 240
7.3. Electrode Construction 241
7.3.1. Electrode Materials 241
7.3.2. Enzyme Loading 243
7.4. Electrochemistry 244
7.4.1. Three-electrode System 244

7.4.2. Cell Operation in measurement 245
7.5. Detection of Product and Monitoring Enzyme Activity 246
7.5.1. Ultraviolet–visible (UV-VIS) Spectroscopy 246
7.5.2. Proton Nuclear Magnetic Resonance (^{1}H NMR) 247
7.5.3. Gas Chromatography - Flame Ionization Detection (GC-FID) 248
7.6. Equipment and Chemicals 249
7.6.1. Glovebox 249
7.6.2. Potentiostat 249
7.6.3. Peristaltic Pump 249
7.6.4. Key Chemicals 249
Appendix 251
Reference 308

CHAPTER I

1. Introduction of the Electrochemical Leaf

1.1. Introduction

This chapter presents an introduction of the 'Electrochemical Leaf' (e-Leaf), the nanoconfined bio-electrochemical system that catalyses cofactor NADP(H) regeneration and enzymatic reactions in an innovative and efficient way. The e-Leaf is inspired by the biological leaf. It was developed in the Armstrong group in 2017 as a nicotinamide cofactor recycling system.[1] It has been developed into an efficient and scalable platform to drive and monitor biocatalytic process. The e-Leaf is a technology combining biocatalysts, nanoconfinement and electrochemical method, that energizes, controls and monitors the biocatalytic process at the 'touch of a button'.

The e-Leaf (figure 1.1 showing the conceptual sketch) is the nanoporous electrode with at least two enzymes entrapped operating in a cascade, one of these is ferredoxin-$NADP^+$ reductase (FNR). Enzyme cascade including FNR and downstream enzymes (denoted in the thesis as E2, E3 …) is packed easily on a material, abbreviated as (FNR + E2 + …) on ITO/Ti, where indium tin oxide (ITO) is the nanoporous coating material and titanium (Ti) is the support material. The system is powered by electricity through a potentiostat driving the cofactor regeneration. At least one of the downstream enzyme(s) is an NADP(H)-dependent enzyme.

This chapter includes the introduction of biocatalyst, nicotinamide cofactors, ferredoxin $NADP^+$ reductase (FNR), electrochemistry and the principle of the e-Leaf. Projects and topics in this thesis are application oriented. Subsequent chapters in this thesis present several different application-oriented explorations of the e-Leaf. The e-Leaf has been scaled up to half-litre size. The feature of bidirectionality and real-time control of the e-Leaf has led to a new process of chiral deracemisation and inversion. The system has also been tested with bi-phasic reaction conditions and been made into a flow reactor.

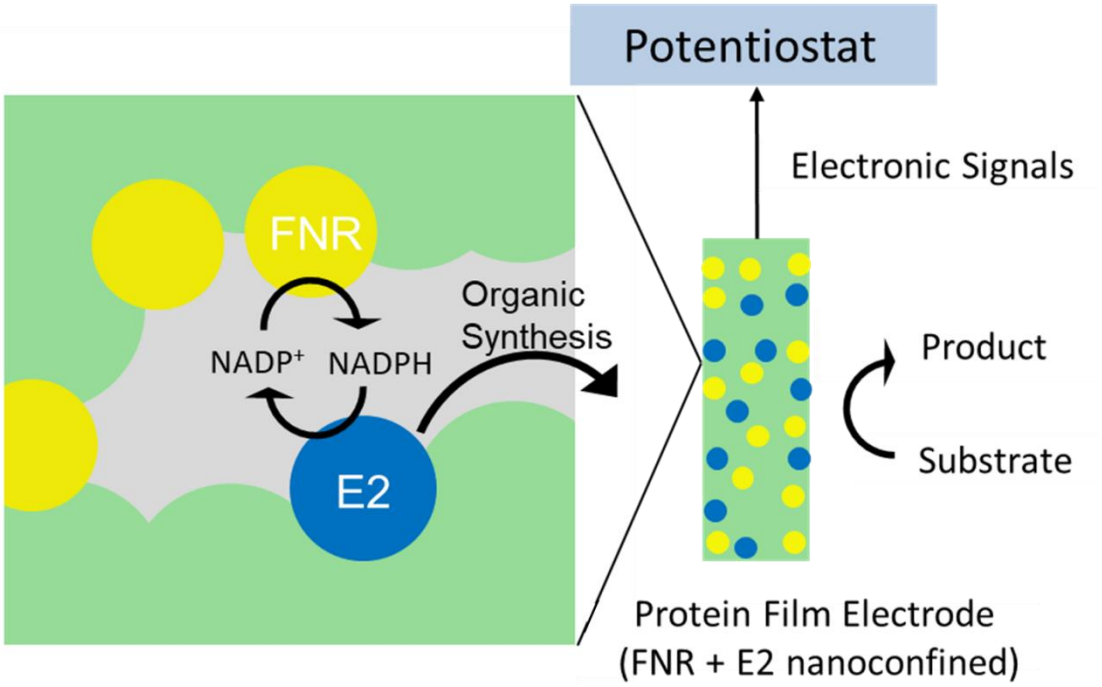


Figure 1.1. Concept of the e-Leaf biocatalytic cascade

1.2. Biocatalysis: Enzyme Catalysed Reactions

Enzymes are biocatalysts; in almost all metabolic processes in living cells they speed up the rates fast enough to sustain life.[2] With advantages over traditional chemical catalysis in terms of rates, selectivity of the substrate, and stereo- and regio-specificity of the substrates and product, biocatalysis using enzymes is widely recognized as a clean, efficient, and highly-selective approach for producing high-value products.[3–5] Biocatalysts have been increasingly employed in chemical processes in various industrial productions such as foods, fine and bulk chemicals, biofuels and pharmaceuticals.[6] With the maturing of protein engineering and genetic technologies such as directed evolution, rational, and de novo design, enzymes are subjected to manual improvement and optimisation in search of their better performance and are becoming more powerful in chemical production.[3,7] Platform technologies focusing on techniques and methods to exploit the catalytic feature of enzymes and applying enzymes in more efficient ways are being developed fast in past years. Research groups such as Minteer, Parkin and Vincent have done valuable work of electrochemical

biocatalysts.[8–10] The ‘electrochemical leaf’ is one of the representatives. Building upon the basis of enzymology, these techniques are discovering further potentials and versatility in the application of enzymes.

1.3. Nicotinamide Cofactor

(1) Structure and function

NADP and NAD

Cofactors are vital participants in enzyme-catalysed reactions in living systems. Nicotinamide adenine dinucleotide (NAD) and nicotinamide adenine dinucleotide phosphate (NADP) are the two ubiquitous ones that are required by a large number of oxidoreductase-catalysed reactions. The oxidoreductase class, which require cofactors stoichiometrically to supply redox equivalents, represents over 17% of all classified enzymes.[11] NADP(H) and NAD(H) are hydride carriers that can accept and donate hydride to/from the substrate reversibly, therefore they play essential roles in the charge-transfer reactions.[12] Typical examples are the involvement of NADH in the respiratory chain in mitochondria, and NADP(H) in the photosynthetic process.

Molecular structures of the two nicotinamide cofactors are shown in figure 1.2. The two cofactors are similar in structure, with the difference that NADP(H) has a phosphate group attached to the 2’ position of the ribose moiety. Even though the redox factors are similar chemically, they play distinct roles in biological functions. In general, NAD(H) are involved in the catabolism and while NADP(H) are involved in anabolism.[13]

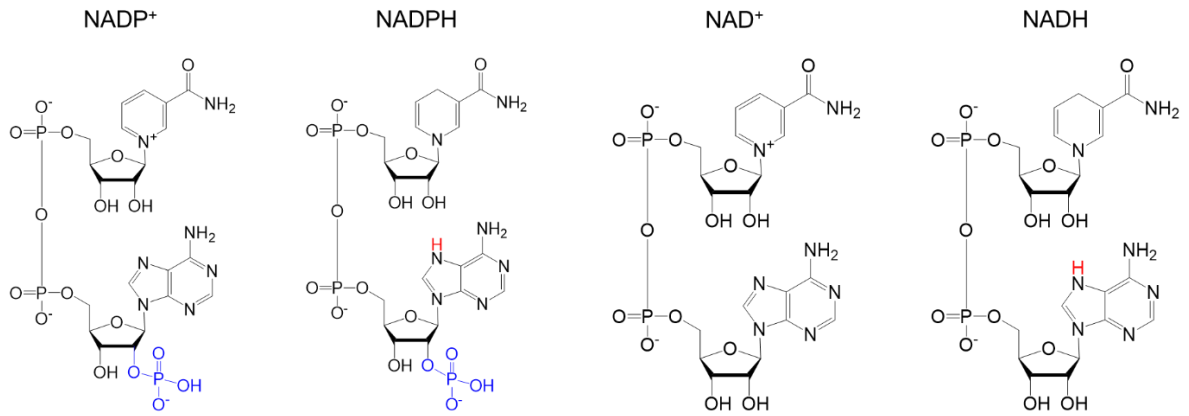


Figure 1.2. Molecular structure of nicotinamide cofactors NADP(H) and NAD(H)

Involved in hundreds of biochemical reactions, particularly those catalysed by oxidoreductases, the nicotinamide cofactors NADP(H) and NAD(H) are highly valued in industrial biocatalysis. Nicotinamide cofactors are expensive thus cannot be used stoichiometrically in the practical-scale synthesis. According to Sigma-Aldrich Co. Ltd. (as of September 2022) the cost of NADPH is £1220 /g (tetrasodium salt hydrate) and NADH is £165 /g (disodium salt hydrate). Enzymes that are NAD(P)(H)-dependent make a large enzyme class catalysing reactions such as dehydrogenase-catalysed reduction and oxidation of alcohols, aldehydes, acids, as well as amines and phenols, monooxygenase-catalysed hydroxylation-, epoxidation- Baeyer-Villiger-, or heteroatom oxidation reactions.[14,15] Regeneration methods for the cofactors are critical for the purpose of using nicotinamide cofactor-dependent enzymes in both small and large scale biocatalysis.

(2) Regeneration methods

The regeneration methods for NAD(P)(H) can be generally divided into four categories: enzymatic, chemical, electrochemical and photochemical methods.[4,16–19] The advantages and disadvantages are listed in table 1.1.

Table 1.1. Common methods for NAD(P)(H) regeneration

Method	Advantages	Disadvantages
Enzymatic	High selectivity	High cost for enzyme
	High rate	Enzyme stability
		Product separation
Chemical	Low cost	Low selectivity
	Simple substrate	Low rate
		Potential pollutions
Electrochemical	Clean and renewable electrical energy	Low selectivity
	Low voltage	Mediator
	Open access to other techniques	
Photochemical	Clean and cheap solar energy	Low efficiency
	Open access to other techniques	Photosensitizer needed

The performance of cofactor regeneration is usually evaluated by the total turnover number (TTN), which is defined as the amount of product formed divided by the amount of cofactor applied in a complete course of reaction. This number reflects how many cycles a cofactor has been regenerated/reused on average, and it is used in subsequent chapters as an indicator of the performance in an experiment.

Enzymatic method

In the enzymatic method, a regeneration cycle is established with a second enzyme that uses the opposite redox form of cofactor with its own substrate, usually a cheap sacrificial co-substrate. The hydride is transferring direction between enzymes without mediators involved. In addition, the feature of high selectivity and efficiency enables milder reaction conditions for the process. Two typical examples are shown in figure 1.3. Fumarate Dehydrogenase (FDH)-catalysed NADH regeneration is driven by oxidation of fumarate, and the NADH is used in the dehydrogenase-catalysed D-lactate synthesis

from pyruvate reaction.[20] Glucose Dehydrogenase (GDH) using glucose as the substrate, can regenerate both NADH and NADPH. The GDH regeneration system can be coupled to many biocatalysts like alcohol dehydrogenase, transaminase, levodione reductase reactions.[21–23] The drawbacks of such regeneration methods are that it requires a fair amount of addition of co-substrate. Final product separated from overdosed co-substrates could have challenges in separation process and impurity issues. Extra cost of time and efforts from co-substrate usage and the complexity of product separation is unavoidable.

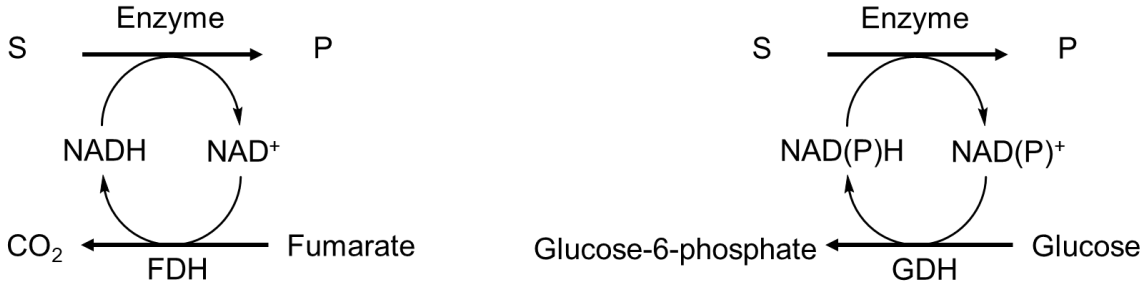


Figure 1.3. Example of enzymatic method for cofactor regeneration

Chemical method

In direct chemical regeneration methods, inorganic salts as strong reducing or oxidising agents is added. Such salts include sodium dithionite ($Na_2S_2O_4$) and sodium borohydride ($NaBH_4$), which are commonly used at high concentration to create a strong reducing environment for the cofactors.[24] The disadvantages of using large amount of salts are high cost, environmental unfriendly, and without recycling process. In addition, chemical method for cofactor regeneration is less selective and fast than the enzymatic method. Therefore overdosed chemicals and the formation of non-catalytic forms of cofactors are the main issue with this method. Based on the conventional chemical method, organometallic complex approach and coenzyme analogue-enabled biomimetic approach are explored by scientists as eco-friendly methods.[17,25–27] These methods are of high stereoselectivity and simpler process, potentially feasible for application.

Electrochemical method

Several electrochemical regeneration processes are depicted in figure 1.4. The electrode surface could be optimised or modified with nanostructured materials and mediators for certain regeneration procedure. The electrochemical approach is a powerful technique with great potential. Electricity as the driving force is clean, convenient and of low cost. By introducing the electrochemical tools, the regeneration process can be controlled and monitored.[18] The four approaches have their merits and limits. a) The direct electrochemical regeneration (typical electrode material such as Ti, Ni and Co)[28] is simple and straightforward. The process does not need much modification of the electrode. However this process forms the non-catalytic NAD(P) radicals, 1,6-NAD(P)H and NAD(P)-dimers resulting in a loss of the cofactor after each regeneration cycle.[12] b) In the indirect electrochemical method, mediator helps to lower the overpotential required for NAD(P)(H) reduction and oxidation at an electrode surface. It may also help to avoid the formation of cofactor radicals the indirect electrochemical method under the assist of mediators.[29] c) and d) are electroenzymatic methods. As mentioned in enzymatic regeneration method, enzymes regenerate cofactors in the presence of sacrificial co-substrate. In the electrochemical method, electricity is the source of electron transfer (on the working electrode), the counterpart of co-substrate in enzymatic methods, with on the counter electrode water splitting reaction. c) and d) differs in the presence of mediators. Some oxidoreductase can achieve direct electron transfer with their redox-active centres like ferredoxin adenine dinucleotide (FAD). Other oxidoreductases not able to achieve such electron transfer but can use mediators such as methyl viologen (MV) and neutral red (NR).[30] The mediator serves as an exogenous electron shuttle to help electron transfer between the electrode and enzymes.

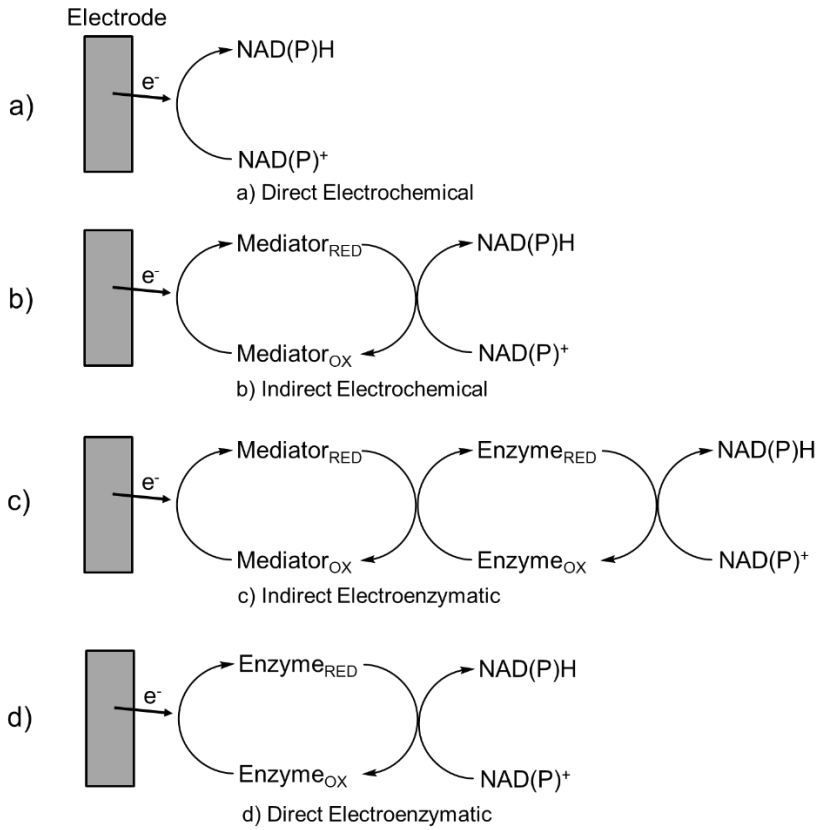


Figure 1.4. Four types of electrochemical methods of cofactor regeneration

Photochemical Methods

Photochemical methods take advantage of the cheap and clean solar energy, mimicking the nature's regeneration cycle of photosynthesis system in green plants during the synthesis of carbohydrates. The electron is excited in photosensitiser by light and then transferred to cofactor $NAD(P)^+$, with mediator often needed for the electron transferring process. Rh-based complex is currently the widely used electron mediator.[31] The challenges for the photochemical regeneration method are finding an efficient and stable photosensitizer with efficient electron mediator.[32]

1.4. Ferredoxin-NADP+ Reductase (FNR)

(1) flavoenzyme and flavin group

Flavoenzymes are a group of enzymes containing an FMN (Flavin mononucleotide) or FAD (Flavin adenine dinucleotide) cofactors. The flavin group itself is a redox agent with different redox states, which enables the mediating of one and two-electron reactions.[33] Three redox states of flavin are shown in figure 1.5: fully oxidized (quinone), one-electron reduced (semiquinone), and fully reduced (hydroquinone). Flavin serves as a relay in flavoenzymes and is essential for its function of electron transfer.

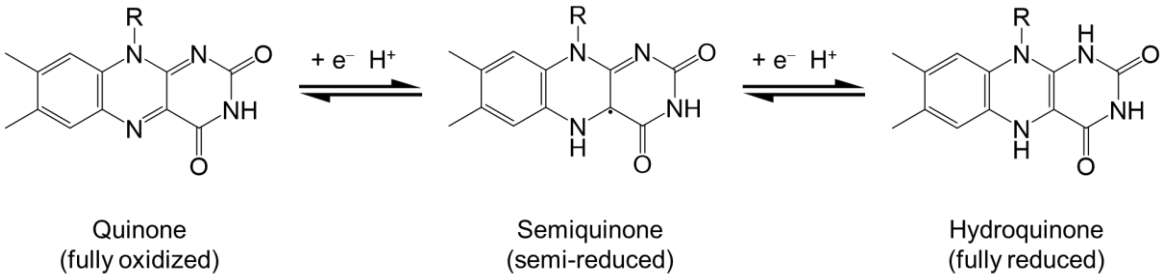


Figure 1.5. Three redox states of the flavin group

(2) FNR structure and role in electron transfer

Ferredoxin $NADP^+$ Reductase (FNR) is a flavoenzyme that catalyses the reduction of $NADP^+$ cofactor in nature. FNR in nature plays the role of a transducer, together with NADP(H) cofactors, to facilitate the photosynthesis process by chloroplast.[2] The earliest report of it is about extraction from the lysed spinach chloroplasts.[34]

Figure 1.6 shows the structure of FNR (PEA FNR from *Escherichia coli*, PDB 1QFZ) (panel (a)), with FAD and $NADP^+$ (panel (b)).[35] The FNR used in experiments for this thesis was from *Chlamydomonas reinhardtii*, and the structure has not been published. The structure is similar to that of PEA FNR because they have similar gene sequences. The production of enzyme for experiments is via the heterologous overexpression (see details in chapter 7) from *E. coli.*

FNR is highly selective towards $NADP^+$ rather than NAD^+, with the only structural difference of the two cofactors being a phosphate group connected to the adenine. The specificity is thousands times higher towards $NADP^+$ than NAD^+.[36] Recent research with FNR has discovered an enzyme variant that is highly selective towards NAD(H). Research has discovered that by replacing the C-terminal tyrosine by a serine, the specificity of FNR can be switched to NAD^+.[36,37]

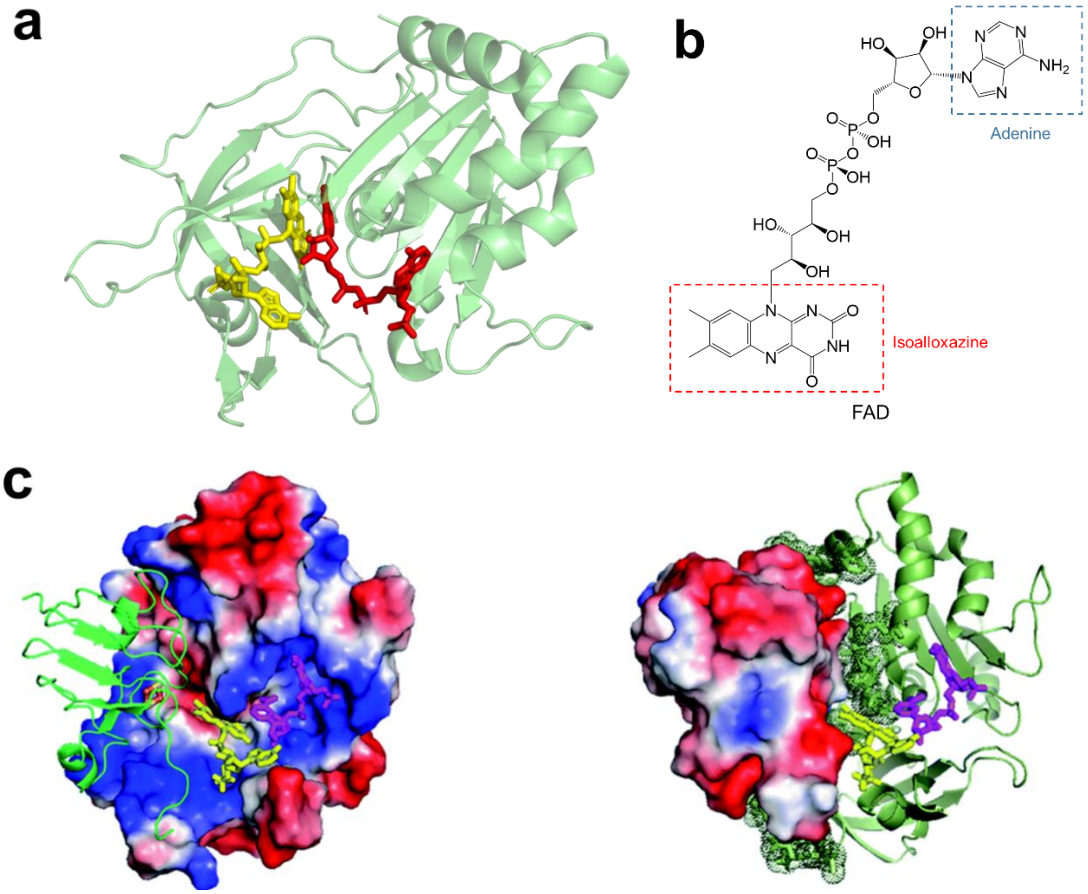


Figure 1.6. a) Structure of FNR (from *Escherichia coli*, PDB 1QFZ), with the FAD group (yellow) and $NADP^+$ (red) highlighted. **b)** Structure of FAD (Flavin adenine dinucleotide) group. **c)** Left: projection in which FNR is shown as a charge-smoothed surface (red and blue represent negative and positive charges, respectively) and bound ferredoxin is shown in green, as cartoon main chain. Right: projection in which ferredoxin is shown as a charge-smoothed surface and FNR is shown as cartoon main chain in green. In both projections, FAD is represented as yellow sticks, and NADP+ is represented as mauve sticks. Reproduced with permission from the Royal Society of Chemistry.[1]

The mechanism of FNR from many species have been investigated by multiple researchers.[38–42] There are three critical steps of FNR regenerating the $NADP^+$.

1) The $NADP^+$ cofactor binds to FNR. As shown in figure 1.6, the adenine moiety of $NADP^+$ is linked to the sugar moiety of FAD by an electrostatic attraction, the negative charge of the cofactor interacts with positively charged amino acids. The selectivity rises from the electrostatic attraction between the 2'-phosphate group of $NADP^+$ and positively charged residues of FNR, which adds to the binding.

2) The electrons are transferred from Photosystems I to ferredoxin (Fd) (a 1-electron carrier), then to FNR sequentially. The FAD group on FNR turns from fully oxidized form to reduced form, using 2 equivalents of Fd. As shown in panel (c), the interaction between FNR and Fd is mainly electrostatic attractions, between the regions of positive charge (blue) on FNR and negative charges (red) on ferredoxin.[43] The shortest distance between the [2Fe-2S] cluster of ferredoxin and the FAD group on FNR (approximately 6 Å) enables direct electron transfer.

3) Hydride is transferred from flavin group to $NADP^+$, from N_5 of the reduced $FADH_2$ to C_4 of the nicotinamide of $NADP^+$. The regeneration is finished. The electron transfer process is shown in figure 1.7.

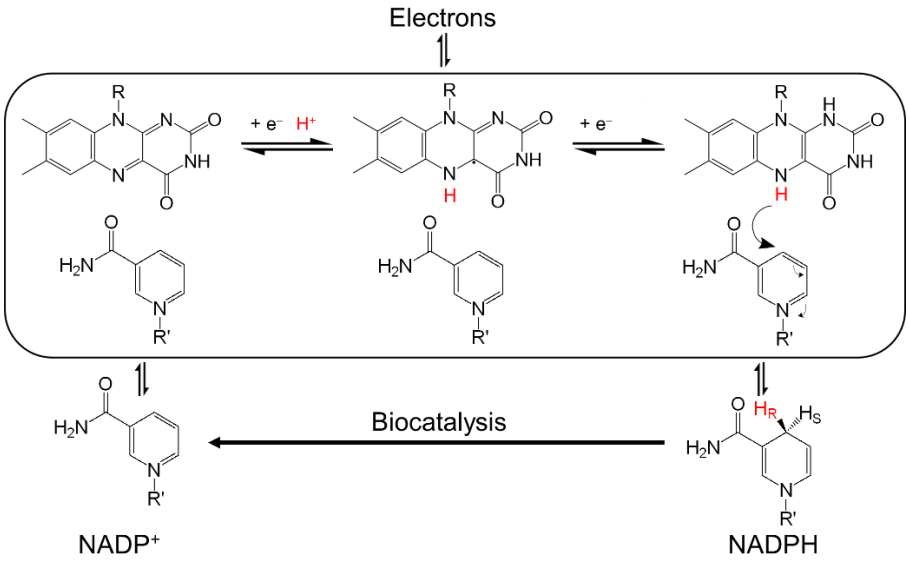


Figure 1.7. The electron transfer between flavin in FNR and the $NADP^+$ molecule in the regeneration process. (R is the nucleotide side chain of the flavin group. R' is the nucleotide side chain that contains an additional phosphate group in NADP(H).) Reprinted with permission from *C. F. Megarity et al. J. Chem. Phys. 153, 225101 (2020)*.[44]

1.5. The Electrochemical Leaf

1.5.1. E-Leaf basics: from the Nature Leaf to the E-Leaf

Protein film electrochemistry (PFE) is a subject that combines electrochemistry and biocatalysts and it is capable of providing cutting-edge insight into the chemical and biological behaviours of biocatalysts.[45,46] With enzyme immobilised on the electrode forming a protein film, the electron transfer between enzyme and electrode is facilitated without extra mediator. The controlling and monitoring of bioelectrical behaviour can be easily addressed at the touch of a button.[47]

The idea of 'electrochemical leaf'(e-Leaf) is inspired from the biological leaf. Figure 1.8 shows the concept of this bio-inspired system. In the natural leaf, FNR accepts electrons from Fd and Photosystem I to regenerate NADPH, which is used in the photosynthesis to produce carbohydrates for sustaining life. In the 'electrochemical leaf' the electron supply is the electrode instead of photosystem. The electrode support material (usually titanium foil) is coated with a thin layer of ITO nanoparticles which forms a porous structure on the electrode and entraps enzymes including FNR and downstream NADP(H)-dependent enzyme(s). Driven by electricity controlled by a potentiostat, the FNR on the ITO/Ti electrode can regenerate both $NADP^+$ and NADPH in a reversible style. With the cofactor regeneration coupled to an NADP(H)-dependent downstream single enzymatic reaction or enzyme cascades, swift cofactor and intermediate channelling within the nanopores on the electrode will be realised and thus an efficient conversion is achieved.

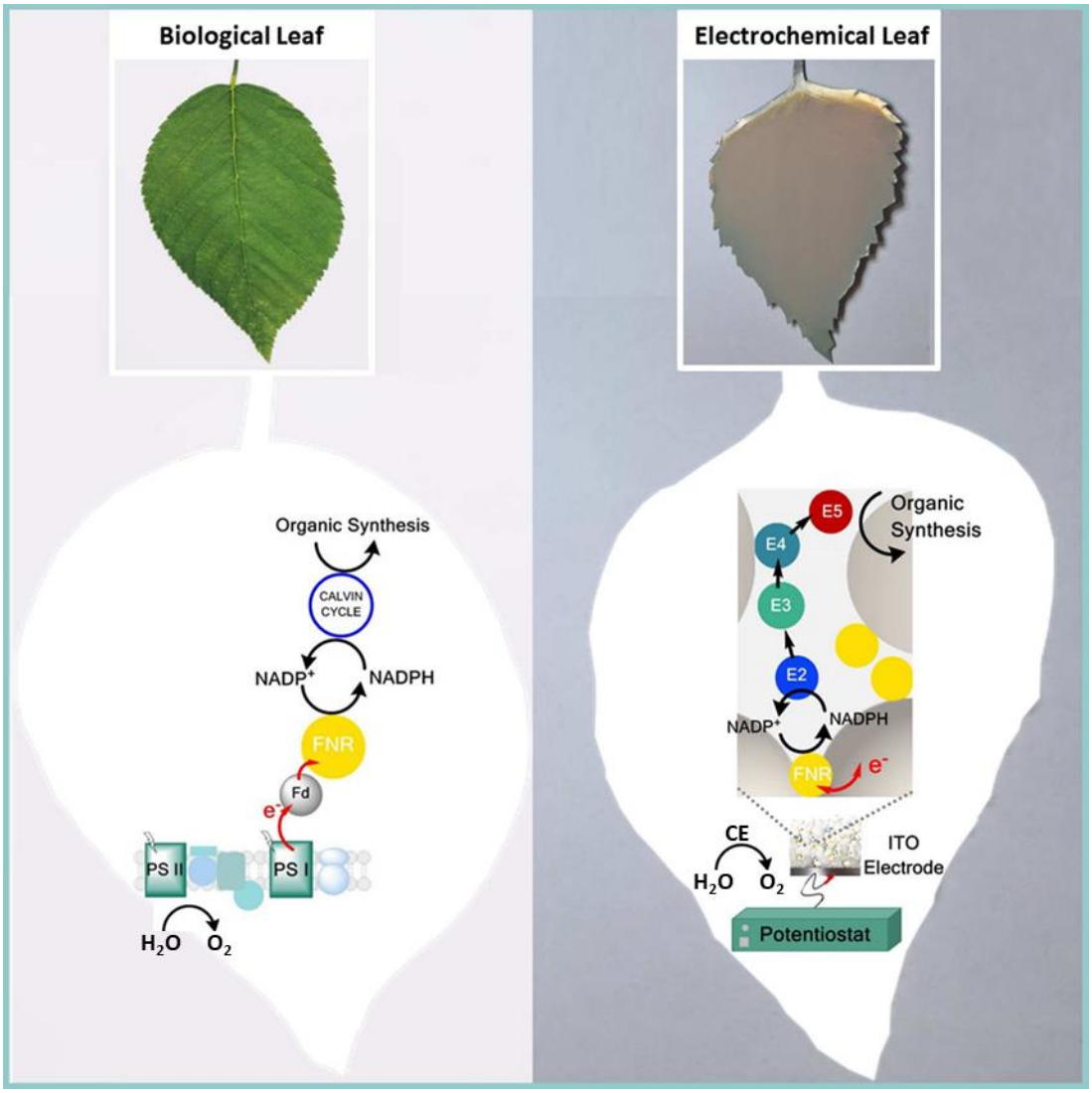


Figure 1.8. The e-Leaf (right) comparing to biological leaf (leaf) as an enzymatic cascades system. Reprinted with permission from C. F. Megarity *et al*. Copyright 2019, Wiley.[48]

The nanoporous layer formed from deposition of ITO nanoparticles (diameter < 50 nm) is filled with entrapped enzymes, resulting in an extremely high local concentrations and minimal inter-site diffusion distances for cofactor and intermediate molecules. The NADP(H) is shuttled between the enzyme pairs rapidly and a high catalytic rate is realised. The computer-controlled potentiostat is energising, controlling and monitoring the catalytic process in real-time. The first successful experiment was conducted in the Armstrong group using the e-Leaf was glutamate dehydrogenase (GLDH)-catalysed synthesis of L-glutamate from 2-oxoglutarate.[1] In more recent work, the e-Leaf has been

coupled to reactions with more complex enzyme cascades and other regeneration systems, in which at least one enzyme is NADP(H)-dependent.[49,50] Table 1.2 shows the important discoveries and development of the e-Leaf since its origination. The e-Leaf has three main features. 1) The e-Leaf is a platform technology to which downstream biocatalytic process is easy to couple. 2) Nanoconfinement facilitates biocatalytic cascades by concentrating enzyme and intermediates and boost the substance channelling within the nanopores similar to the biological cell condition. 3) As an electrochemical system, the e-Leaf holds the advantages of real-time monitoring and controlling, allowing for more data collection and possible live operations, which makes it a powerful tool in enzymology researching and process optimisation.

Table 1.2. Milestones in the development of the e-Leaf

Year	Important discoveries
2017	The invention of the 'Electrochemical Leaf'.[1]
2019	Discovery and understanding of 'nanoconfinement' in the e-Leaf.[51]
2020	Understanding the electron tunnelling effect within the e-Leaf.[44]
	Application and versatility
2018	E-leaf coupled with hydrogen fuel cell.[52]
2019	E-leaf coupled with photosensitive material.[53]
2020	Scaling up of the e-Leaf from 4 millilitre to 0.5 litre scale.[54]
2021	E-Leaf with extended multi-enzyme cascades (5 enzymes).[49]
2021	E-leaf as an in-situ analytic tool in drug development.[55]
2021, 2022	E-leaf as a one-pot enantioselective deracemiser and inverter.[56,57]
2022	E-leaf coupled to ATP regeneration system.[50]

1.5.2. Features of the E-Leaf

An excellent regeneration system with nanoconfinement

The e-Leaf was developed with its basic function as a cofactor regeneration system, with immobilised FNR coupling to downstream biocatalysts. Comparing to conventional regeneration methods (electrical, enzymatic, chemical, etc.), it holds several advantages. 1) High rate and selectivity empowered by the enzyme FNR, recycling NADP(H) with high turnover and no loss of cofactor activity. 2) 'Green' reaction conditions and low costing process. The electricity, as the driving force, is cheap, clean and stable. The reaction system is free of mediator and other additional substrates (e.g. glucose + GDH system with high concentration). This avoids the potential generation of carbon-based waste, and the toxicity from some mediators. 3) A higher efficiency of cofactor and enzyme. This is realised by the nanoconfinement of the e-Leaf.

The idea of nanoconfinement in the e-Leaf was inspired from the living cell of the leaf. Cells tends to have tiny enclosures for effective metabolism, such as the mitochondrial matrix and the chloroplast stroma, in which enzymes are concentrated and within short distances of each other. Enzymes have evolved to function in such a 'compact' state, which is different from common biocatalytic process investigated in the lab.[58–60] The distance for which cofactors and intermediates must diffuse is extremely close.[51] In the e-Leaf, enzymes are confined within the nanopores (pore size approximately 5 - 100 nm), formed by deposition of Indium Tin Oxide (ITO) nanoparticles. An estimation is made based on the sizes of enzymes and of nanopores, that the local concentration of enzyme and the average center-to-center distance are both similar to those in a living cell.[50,60] The isoelectric point of ITO is pH 6,[61] therefor at the pH normally used in reaction (pH 7.5 - 9), the ITO surface would be negatively charged. This is similar to the situation in the cell where the negatively charged Fd group as a redox partner connecting to FNR. Other nanoencapsulation for enzyme cascades includes the use of

metal−organic and covalent-organic frameworks (MOFs and COFs), protein cages, droplet encapsulation and particles confinement.[62–67]

The high local concentration of biocatalytic factors (enzymes, cofactors, intermediates) and the minimised distance between enzymes are the two important merits brought by the nanoconfinement. In such a situation, substrates, cofactors, and enzymes are less likely to diffuse out of pore, and there is more chance of them interacting with each other, which is like the channelling in nature.[68] A good example is the 5-enzyme cascade on the e-Leaf for the production of aspartic acid from pyruvic acid.[49] Multiple enzymes are entrapped on the e-Leaf and work in concert to achieve the multi-step cascade synthesis.

Monitoring and bidirectional controlling

Based on electrochemical method, the e-Leaf can be controlled manually. The electrochemical analysis allows a direct measurement of the reaction, with electronic signals sent to computer. Real-time reaction data such as reaction rate (electrical current), estimation of yields (charge passed), and other status are visualised and readily available. In addition, the e-Leaf is driven by electrical potential, which is manually controlled and can be switched to drive an enzyme cascade in either redox direction. Potential applications of the e-Leaf taking advantages of this feature can be versatile. For example, robotic-controlled biosynthesis is achievable. With programmed commands and real-time data feedbacks, the e-Leaf is under precise adjustment and automatic control for complicated biocatalytic processes. The e-Leaf is also a powerful tool for biocatalyst researching. Scientists would be able to interrogate the activity of target enzyme in action and obtain live and immediate reaction data. The usage of enzymes and cofactors are also at lower amount. Bidirectionality makes it possible for some conversion routes that are not applicable in traditional biocatalytic ways, which is discussed in detail in chapter 4 about the deracemisation of racemic enantiomers.

1.6. Downstream Enzyme (E2) Reactions

1.6.1. Glutamate Dehydrogenase (GLDH)

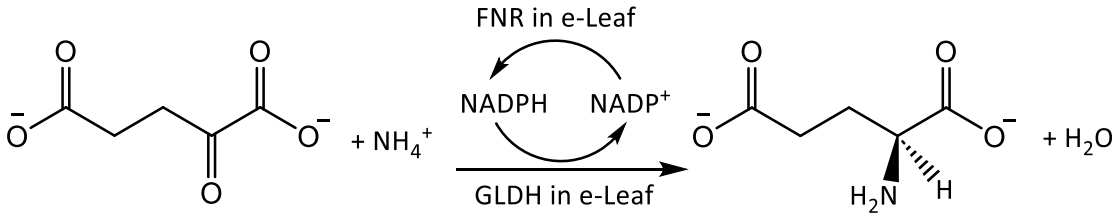


Figure 1.9. The reductive amination of α-ketoglutarate catalysed by GLDH

GLDH catalyses the conversion of 2-oxoglutarate (aka. α-ketoglutarate) to L-glutamate in the presence of NH_4^+ and NADPH (figure 1.9).[69] The GLDH-catalysed reductive amination of a-ketoglutarate is the model reaction in the scaling-up of the e-Leaf in chapter 3 and flow reactor design in chapter 6. GLDH-catalysed reaction is adopted as a model downstream reaction in the initial development of the e-Leaf and works out as a satisfactory choice. The enzyme and reaction are well-characterised. The substrates are accessible and soluble in water; the enzyme stability is excellent; and the product is easy to be detected and quantified by NMR. Strong coupling reaction of GLDH to NADPH recycling by the FNR on ITO/Ti electrode is directly observable by chronoamperometry and cyclic voltammetry (electrochemical analytical methods introduced in section 1.8).

1.6.2. Alcohol Dehydrogenase (ADH)

ADH catalyses the interconversion between alcohols and ketones or aldehydes with NADP(H) (figure 1.10).[70] This model reaction uses 4-phenyl-2-butanol as the substrate. The bidirectionality of the e-Leaf has been exploited as an invertor and deracemiser for enantiomeric alcohols (in chapter 4). According to Santa Cruz (as of September 2022) the price of racemic 4-phenyl-2-butanol is £6 /g and enantiomer is £110 /g. so the reaction is a typical value-adding process. Chiral alcohols are important intermediate in the synthesis of pharmaceutical. For example, 4-phenyl-2-butanol is an intermediate for chiral amines, key synthetic block in the making of a plethora of active pharmaceutical

ingredients (APIs).[6,71,72] The industrial synthesis of chiral intermediates was mainly developed to be conducted through metal-catalysed processes, most of which requires transition metal complexes.[73]

Ketone and alcohol as substrate in the model reaction, are hydrophobic with low solubility in water,[74] therefore an organic phase can be useful for the e-Leaf. There has been previous works involving organic stability of ADH and bi-phasic system reaction,[75] which inspires the introduction of a bi-phasic system to the e-Leaf (in chapter 5), bridging the gap between organic synthesis and bio-electrochemistry.

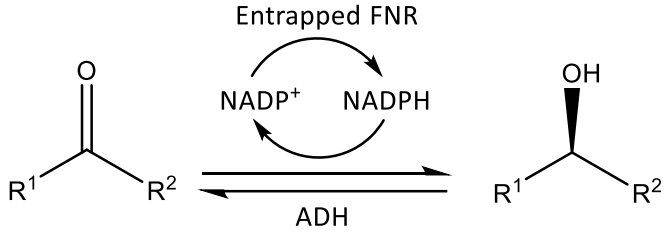


Figure 1.10. Interconversion between ketone and ethanol catalysed by ADH

1.7. Construction of the E-Leaf

1.7.1. Electrode Manufacturing: ITO Coating

Indium tin oxide is coated to created nanoporous surface on the electrode support. The (FNR+E2+...) on ITO/Ti electrode is made in several steps. The electrode support is coated with a layer of ITO nanoparticles using the electrophoretic deposition (EPD) method, then the enzymes are loaded in the electrode before the electrode is put into use in an electrochemical system. Electrophoretic deposition (EPD) was originally studied as a practical technique by Hamaker in 1940,[76] and has been developed in to an efficient tool in various field of processing. In the making of the e-Leaf, ITO nanopowder is suspended in a solution of I_2 in acetone. The suspension is then sonicated before the EPD process. During the sonication, the following reaction between iodine and ketone happens:

$$CH_3—CO—CH_3 + 2I_2 \Leftrightarrow ICH_2—CO—CH_2I + 2H^+ + 2I^- \qquad (1.1)$$

The protons formed are adsorbed onto the suspended ITO nanoparticles, making them positively charged. Under the DC field applied, the positively-charged ITO particles move towards the cathode and deposit on the surface.[77] The binding of ITO in the EPD process is based on the electrostatic interaction therefore the long-term stability may be affected by the pH conditions of the reaction solution in an experiment.

The EPD method works particularly well for Ti foil which has a flat face and is easily performed in the lab. The average loading of ITO on Ti foil is approximately 1 mg / cm^2 based on the experiment (shown in section 2.3.2 table 2.2). Previous investigation has revealed that the pore size has a significant distribution of 10-50 nm particle diameter by the scanning electron microscopy (SEM), and the void ratio of the ITO layer by simulation being 0.44-0.60.[60] Figure 1.11 shows the SEM images of ITO layer from the previous work of the group. The porous structure formed by ITO on the Ti electrode is observed in the images.

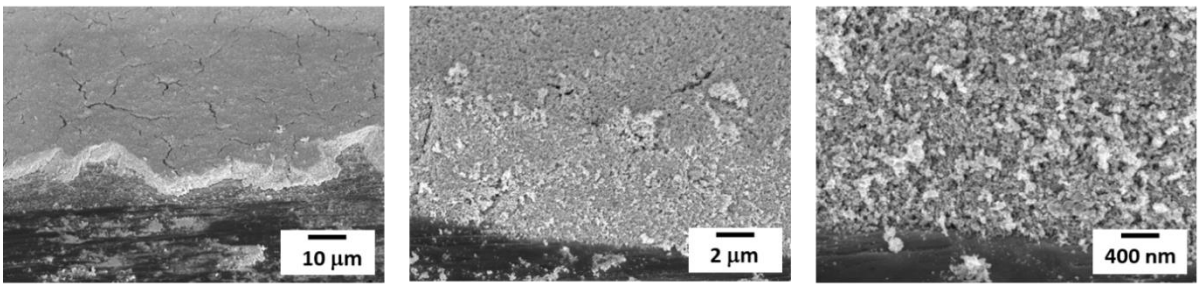


Figure 1.11. SEM image of an ITO nanoporous layer on the Ti foil

1.7.2. Enzyme Loading

Enzymes involved in an e-Leaf usually include FNR and downstream enzymes (E2, E3, E4 and more). There are two common practices for enzyme loading, stir-loading method and drop-cast method. In the drop-casting, the enzyme(s) solution (at microlitre level) is dropped directly onto the surface of the electrode and incubated for a period of time before being rinsed and put into use. This method is applicable for electrode that has regular shape and structure such as Ti foil. In the stir-loading, enzyme(s) are diluted in buffer (at mL level) in which electrode is held and the solution is stirred for a long time.

The concentration of enzyme in dilute solution is at micromolar level. Stir-loading is more universal and can apply to electrodes of different geometries. It is important to note that ‘amount used (or applied)’ in loading enzyme stated in the thesis experiments is the amount of enzyme used in the loading process. This amount is more than the final amount of enzyme adsorbed in the electrode, since the electrode is rinsed by buffer after loading process to get rid of unadsorbed enzymes. The amount of electroactive enzyme on an electrode is estimated by the non-turnover peak of FNR. However, except for FNR, other enzymes loaded cannot be directly quantified and specific inter-enzyme distances are not well-defined.[60]

In addition, the order of loading multiple enzymes is flexible. Multiple enzymes can be loaded simultaneously by making a mixture of enzyme solution, or in sequence using same or different methods. The common practice is to load FNR first by drop-casting and then E2. The optimisation of different loading methods and loading orders are conducted is shown in chapter 2.

1.7.3. Electrochemical Cell

The classic three-electrode system (details in the experimental methods in chapter 7) used in the e-Leaf is shown in figure 1.12, which consists of three compartments. The compartment in the middle is the working electrode chamber where the conversion of interest processes. The solution is stirred by a stirring flea, and argon is purging in the headspace to keep an oxygen-free environment. Two side arms are connected to the main part. The one on the left houses the Pt mesh as the counter electrode (auxilliary electrode). A glass frit junction is in between this part and the main chamber, reducing the substance crossover between the two parts, while allowing the charges (ions) to pass. The other side arm connects to the main chamber with a Luggin capillary. This part holds the reference electrode (Ag/AgCl electrode in 3 M KCl). Luggin capillary is effective in holding back the mass transfer throughout when allowing the the electrical

connection. The solution for the referece electrode holder is 0.1 M NaCl whereas the counter electrode is in the same buffer as the main chamber reaction solution.

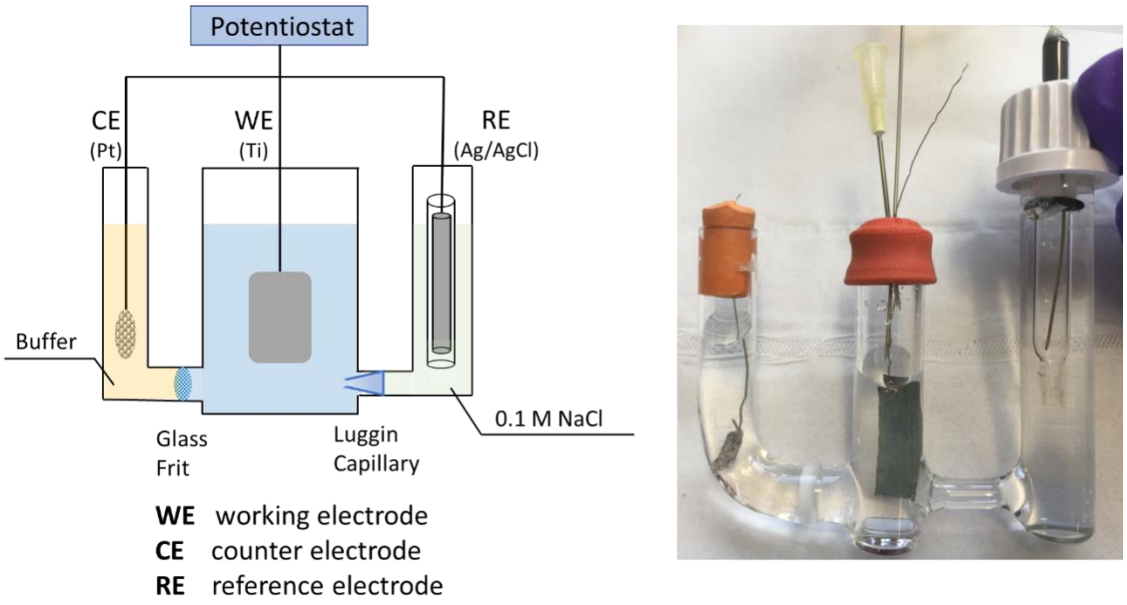


Figure 1.12. Sketch and photo of the initial electrochemical cell for the e-Leaf

Overall cell reaction

During an electrochemical process, a potential is applied to the working electrode, on which the oxidation of NADPH or the reduction of $NADP^+$ is catalysed by FNR, coupled to downstream biocatalytc processes. On the counter electrode, mutiple reactions are happening to complete the overall cell reaction (shown in equation 1.2 and 1.3). For example, when the WE is driving reduction reaction, the CE is at a oxidative potential and oxygen evolution is happening. The oxygen(or hydrogen) produced on the CE, when diffuse to the WE, can contribute to the current monitored in chronoamperometry, leading to overestimation of the charge passed attribute to substrate conversion (details in section 1.8.2).

WE: $$\mathrm{NADP^+ + H^+ + 2e^- \rightarrow NADPH} \quad (1.2)$$

CE: $$\mathrm{H_2O \rightarrow 0.5O_2 + 2H^+ + 2e^-} \quad (1.3)$$

There are other side reactions on the CE, including the decomposing of buffer salt, substrate and product, which produces unwanted impurities that may interfere the main compartment reaction. Some of the byproducts could also interfere or even poison the enzymes in the main compartment. The crossover of product and substrate from the main compartment to side arms can also lead to errors in measruing the substrate conversion and product amount.

The presented electrochemical cell is the initial model for the e-Leaf research. This design was the starting point and a good benchmark in the scaling up.[1] New designs of the electrochemical cells are inspired and based on the same core idea: three compartments that restrict mass transfer while allow the flow of charges. This will be covered in more detail in chapter 3.

1.8. Electrochemistry Analysis Methods

1.8.1. Cyclic Voltammetry

Cyclic voltammetry (CV) is an electrochemical analysis to measure the redox current in a background of electrode capacitance with potential sweeping. CV is commonly used to study the redox property of electrochemical species (i.e. the electrode and analytes in the solution) in the system. [78] It provides an overview of the performance of the e-Leaf in regard to different potentials. It is used to test the electrochemical system before a bulk electrolysis is initiated.

In the e-Leaf, CV can be used to monitor the ‘non-turnover’ peaks attributed to FNR loaded on the e-Leaf, which arises from 2-electron oxidation and reduction of the flavin group on FNR. Such signals are called ‘non-turnover’ because the electron transfer is between FNR and the electrode without NADP(H), the substrate of FNR. Figure 1.13 panel (a) shows cyclic voltammograms with FNR (red trace) and without FNR (black trace) where the FNR peaks are distinguishable. The area of the FNR non-turnover

peak is related to the amount of FNR that is electronically connected to the electrode. The relationship can be measured by the following equation:

$$\int IdE = nFA\Gamma v \qquad (1.4)$$

where n is the number of electrons in this conversion; F is Faraday constant; A is electrode area; ν is scan rate and Γ indicates the coverage of FNR.

CV is also used in monitoring the turnover current of FNR regenerating NADP(H) with and without coupling to E2. Panel (b) shows the current of NADP(H) redox reaction catalysed by FNR only (black trace) and catalysed with FNR and E2 coupled (red trace). When FNR and E2 are coupled, the NADP(H) are shuttling and recycling in between the two enzymes like a volleyball,[51] which increases the rate of cofactor regeneration on FNR, reflected as an increased reduction current. Hence in the red trace, the reduction current increases and the oxidation peak of NADPH goes away.[48] The current observed at the reductive range is indicating the reaction driven by E2.

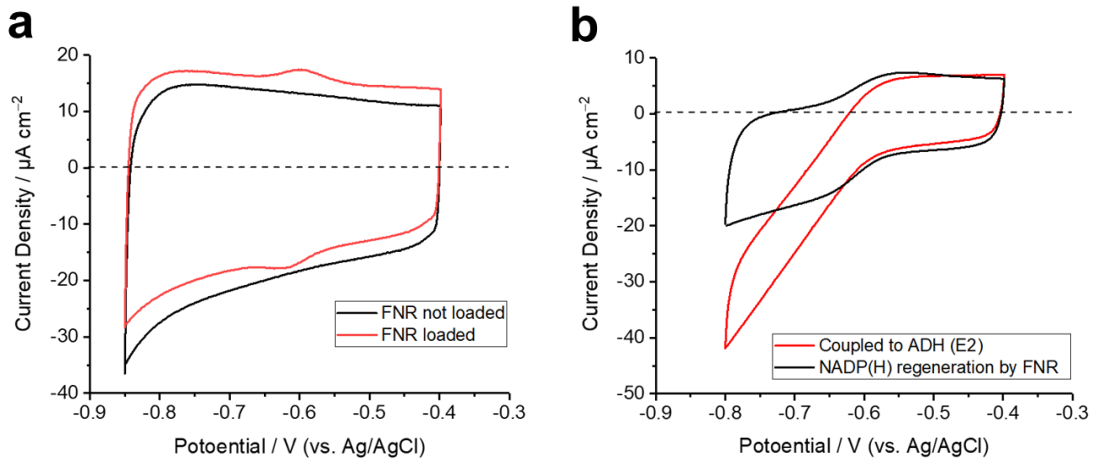


Figure 1.13. Cyclic Voltammograms of **a)** ITO/Ti electrode with (red) and without (black) FNR. and **b)** The 'Electrochemical Leaf' coupled to ADH (red) and FNR regenerating NADP(H) only (black), substrate [4-phenyl-2-butanone] = 8 mM. Experimental conditions: scan rate: 4 mV/s, buffer: 100 mM TAPS pH 8.0, temperature: 20 ℃, Adapted with permission from B. Cheng *et al*. Copyright 2020, Wiley.[54]

The rate-limiting enzyme can also be detected using cyclic voltammetry. Figure 1.14 shows the process of E2 (GLDH) loading monitored by CV. A pyrolytic graphite

electrode (PGE) was pre-loaded with FNR and the cell solution was charged with all substrates for E2 and $NADP^+$ before the measurement. The CV started with the first scan (scan 0) showing a non-coupled NADP(H) recycling by FNR. The E2 was then live injected, and the measurement continued for another 70 scans, during which the reduction current increased due to the adsorption of E2 in the electrode. It is noteworthy to compare not only the increase in current but also the shapes of the CVs over time. In the early CVs, as the potential is swept to a more reducing voltage (greater driving force), the current plateaus. Over time, this plateaued shape changes to one in which the reductive current continues to increase with increasing reductive potentials. The plateaued shape indicates that even with a greater driving force there is no significant increase in current which means that the system is not limited by FNR but rather by E2. When the shape is no longer plateaued and the current continues to increase as the potential (driving force) is increased, then the system has switched from being limited by E2 to being limited by FNR, as more E2 has entered the pores over time.

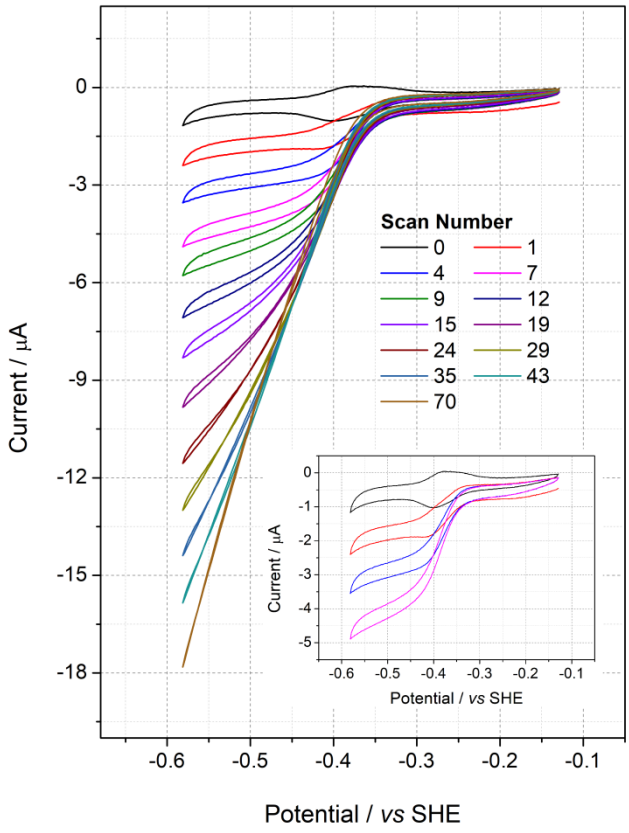


Figure 1.14. GLDH loading process monitored by cyclic voltammetry on the (FNR + GLDH) on ITO/PGE electrode. Scan rate: 3 mV/s and measurement last for 70 scans (selective ones shown in the diagram). Experimental conditions: cell volume 3 mL, buffer: 50 mM TAPS pH 8.0, substrate [a-ketoglutarate] = 20 mM, [$NADP^+$] = 20 μM., temperature: 20 °C. Enzyme loading: FNR preloaded by drop-casting; GLDH was lived-injected to a final concentration of 0.87 mM in the cell solution. Adapted with permission from B. Cheng *et al*. Copyright 2020, Wiley.[54]

1.8.2. Chronoamperometry

Chronoamperometry is a key analytical tool to monitor the biocatalytic process on the e-Leaf. In chronoamperometry, the potential of the working electrode is held constant and the current from faradaic processes occurring at the electrode is monitored as a function of time.[79] The current directly reflects the conversion rate of $NADP^+$ to NADPH and therefore overall coupled reaction rate.

One example shown in figure 1.15 is the chronoamperogram of the conversion of 4-phenyl-2-butaone to 4-phenyl-2-butanol catalysed by ADH. The electrode was loaded with FNR loaded by drop-casting, and the substrate for ADH was in the cell solution before the reaction. Upon applying potential, the current was approximately zero (with

minor residual current) indicating no reaction occurring. At the injection of $NADP^+$, an increase of current showed up, which was attribute to $NADP^+$ being reduced to NADPH by FNR. Another sharp current spike appeared upon E2 injection, indicating the loading of E2 in the electrode and the coupling of ketone reduction (catalysed by E2) to the NADPH regeneration (catalysed by FNR), powered by electricity. The current slowly grew to its peak remained steady for 4 hours at which point it dropped swiftly due to the depletion of substrate, reaching zero after approximately 8 hours upon complete substrate depletion.

Coulometric conversion and assumption of faradaic efficiency

The coulometric conversion is calculated by converting the charge passed over the process to the amount of substrates consumed as shown in the equations:

$$q = \int I \, dt \qquad (1.5)$$

$$q = nFX \qquad (1.6)$$

where q is the charge pass, which is calculated by the integration of current I over time t; n is the number of electrons per reaction; F is the Faraday's constant (96485 C mol^{-1}); and X is the amount of product in moles.

It is critical to point out that the faradaic efficiency is not necessarily 100% in the chronoamperometric process. Oxygen or hydrogen of slight amount formed on the counter electrode could diffuse to the main chamber and get reduced/oxidised by the working electrode, which contributes to the current monitored and can cause the overestimation of substrate consumption based on charge passed (coulometry). The oxygen from surrounding environment can also contribute to the extra current in reduction reaction.

Results analysis of experiments in this thesis is based on the assumption that the faradaic efficiency is approximately 100%, suggesting that the charge passed is a valid indicator of substrate consumption and product yield. This assumption is made based on

large amount of experiment results showing that the post-reaction substrate and product quantification (by NMR GC) and the coulometry match each other accurately with very minor difference (within 5%). Such assumption of approximation is a reasonable one and it also helps in elaborating experiment processes.

The current growing phase depicts how E2 was adsorbed into the ITO pores where it catalysed the reduction and in doing so increased the flux of cofactor back to FNR which catalysed the regeneration of the cofactor at a higher effective concentration and gave an increased current. The final charge passed is approximately 5.6 C, indicating a 29 μmol, 90% substrate conversion. Electrochemistry analysis brings the advantages of live monitoring and control. Enzyme-catalysed reaction is controlled manually with applied potential and can be driven to either direction. The visualized reaction rate (current) can be observed in real-time.

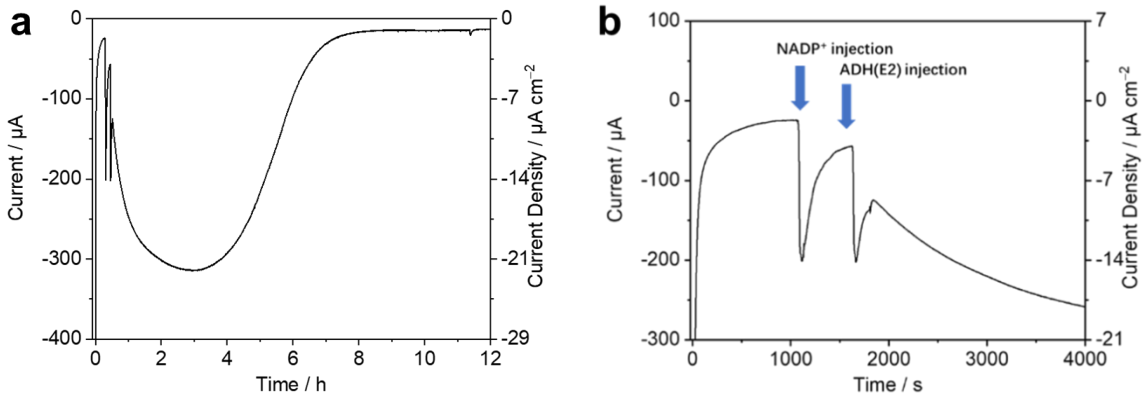


Figure 1.15. Reduction of 4-phenyl-2-butanone catalysed by ADH. Conditions: solution volume 3.5 mL; substrate [4-phenyl-2-butanone] = 8 mM, [$NADP^+$] = 20 μM, buffer 100 mM TAPS pH 8.0, temperature: 25 ℃. Potential held at -0.9 V vs. Ag/AgCl (3 M KCl) to drive reduction. Solution is purged with argon to remove O_2 before reaction and argon flow maintained in headspace thereafter. Enzyme loading: FNR loaded first by stir-loading, ADH is live injected to the final concentration of 0.63 μM in reaction solution. ITO electrode SA: 14 cm^2.

CHAPTER II

2. Optimisation of the Initial E-Leaf System

2.1. Introduction

Based on the initial setup of the electrochemical leaf as published,[1] optimisation has been conducted for the improvement before moving to the application-oriented explorations. The optimisation presented for the initial e-Leaf in this chapter includes 4 aspects, which are important steps in the process of setting up a e-Leaf: electrode support materials, ITO coating methods, enzyme loading methods and reaction conditions.

The electrode support materials tested include Ti foil, Ti mesh, Ti wire, Ti tube and carbon cloth. The ITO coating methods include electrochemical assisted deposition (EAD), Doctor's blade method, and the electrophoretic deposition (EPD). Enzyme loading methods investigation focuses on the optimisation of two types of loading orders, co-loading and stepwise loading, with the optimisation of loading amount, time, and ratio. Reaction optimisation is based on the GLDH-catalysed and ADH-catalysed reactions.

Experiments shown in this section are not chronological and may cross-reference each other. Some results are the optimisation work for topics in subsequent chapters. Even though this could mean that some optimisation is case-specific for certain situation, the optimised conditions from these experiments remains consistent and the results can shed some enlightenment into the work with similar setups and conditions.

The optimisation process is almost a direct 'input to output' test, in which the final outputs (i.e. peak current and its stability) in a reaction under different 'input variables' (i.e. conditions to be optimised) are compared and the best one is selected. It is empirical research with reliability based on the test data. The optimised condition is likely to yield better performance (higher rate, better stability, etc.) of a reaction. The biggest issue, however, is that such test is like a 'black box'. Given its convenience and efficiency in finding the optimised conditions, the whole process sometimes is hardly explainable how exactly one factor contributes to the mechanism. More speculation and

inference were made based on test results in following sections. Non-empirical hypothesis and deeper-level investigation are needed as supplement to fully elaborate the true nature of a process.

2.2. Electrode Support Material

The frequently used working electrode supports for the electrochemical leaf are carbon rotating disk electrode (RDE) and titanium foil electrode, onto which ITO particles are deposited as a porous layer. These two electrode types have been used for the mechanism test and proof of principle tests since they are convenient to handle and have an experimental condition closer to an ideal electrochemical situation. Based on these basic type of electrode, various types of support materials have been explored during the research for application-oriented test and potential improvement of the e-Leaf. The goal here is to compare the performance of potential support materials and to find the material that can fit various working conditions. With Ti foil as the benchmark, other electrode support materials were tested and compared by chronoamperometry and cyclic voltammetry, including Ti tube, Ti foam and Ti wire. Carbon cloths as a non-metal material has also been tested (details in appendix).

For clarifying purposes, the experiments presented in the followings are conducted at different time points, thus they have slightly different electrode fabrication conditions (ITO coating, enzyme loading methods) and the E2 reactions coupled (ADH or GLDH). Those results are valid solely in demonstrating the availability of materials as a working electrode, but they may be less comparable to each other.

2.2.1. Titanium Tube

Titanium tube has a rigid and regular structure and can serve as a modular unit for close-packing particularly in cylindrical space of an electrochemical cell, which is a convenient way of increasing the ‘electrode to space’ ratio, making the most use of an

electrochemical cell. The Ti tubes have been tested and used in the flow reactor in chapter 6. In the experiment (figure 2.1), four Ti tubes were coated with ITO by the doctor's blade method (introduced in section 2.3) and were packed in the cell cylindrical space as depicted in the sketch. FNR was stir-loaded before the reaction. Cofactor ($NADP^+$) and all substrates were in the cell solution before the reaction was initiated by the live injection of E2 (GLDH). The initial current was high and steady for 2 hours at which point it dropped swiftly due to the depletion of substrate, reaching zero after approximately 4 hours upon complete substrate depletion. The coulometric conversion is 90% of 032 mmol substrate in 4 hours' time. The Ti tubes proves to be a workable support material for the e-Leaf.

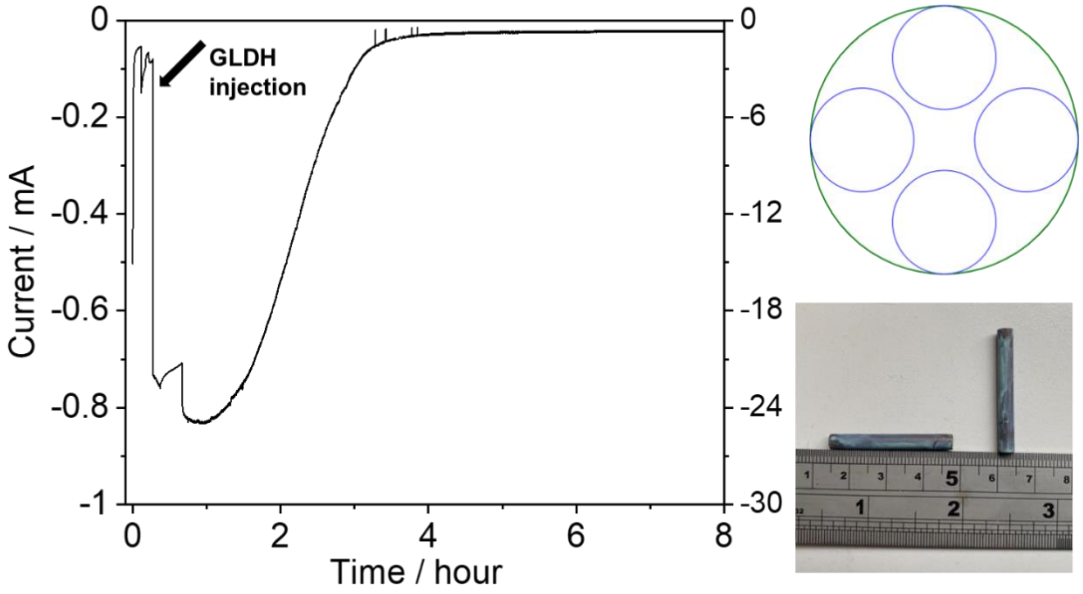


Figure 2.1. Chronoamperogram of GLDH-catalysed reductive amination with Ti tube as working electrode. Conditions: solution volume 4 mL, buffer: 100 mM TAPS pH 8.0; temperature: 25 ℃, solution is purged with argon to remove O_2 and argon flow maintained in headspace thereafter; substrate [α-ketoglutarate] = 8 mM, [NH_4Cl] = 16 mM, [$NADP^+$] = 100 µM; Potential held at -0.68 V vs. Ag/AgCl (3 M KCl) to drive reduction. ITO coated by pasting. Enzyme loading: FNR loaded first by stir-loading, GLDH is live injected to the final concentration of 1.3 µM in reaction solution. Electrode surface area: 33.2 cm^2. Tube dimensions: outer diameter 4.25 mm, inner diameter 3.75 mm, length 33 mm.

2.2.2. Titanium Foam

The porosity of ITO-coated surface is key in nanoconfinement of the e-Leaf and a higher loading amount of enzyme is desired for faster conversion rate. This inspired the use of Ti foam as the electrode. Its porous structure brings the potential of loading more enzyme in the space comparing to other materials. In the experiment (chronoamperogram shown in figure 2.2), Ti foam was coated with ITO by EPD (introduced in section 2.3). FNR was stir-loaded before reaction. Cofactor ($NADP^+$) and all substrates were in the cell solution before the reaction was initiated by the live injection of E2(ADH). The current increased to its peak and then decreased swiftly due to the depletion of substrate. 0.028 mmol of substrate was fully converted (coulometry) within 18 hours.

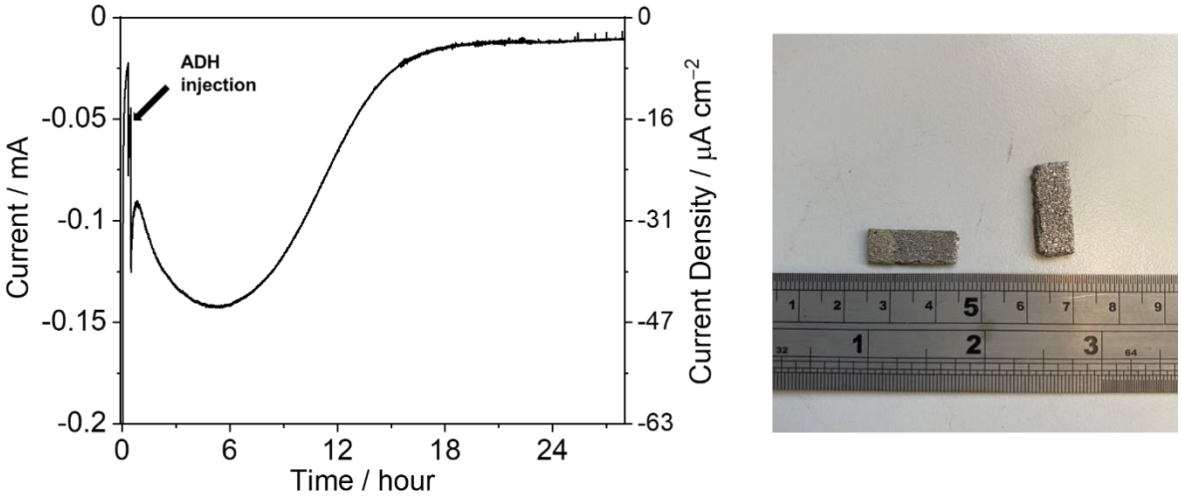


Figure 2.2. Chronoamperogram of reduction of 4-phenyl-2-butanone catalysed by TesADH W110A with Ti foam as working electrode. Conditions: solution volume 3.5 mL; substrate [4-phenyl-2-butanone] = 8 mM, [$NADP^+$] = 20 μM, buffer 50 mM TAPS pH 8.0, temperature: 25 ℃. Potential held at -0.9 V for reduction. Solution is purged with argon to remove O_2 and argon flow maintained in headspace thereafter. Enzyme loading: FNR loaded first by stir-loading, ADH is live injected to the final concentration of 0.63 μM in reaction solution. ITO coated by EPD. ITO SA: 3.2 cm^2, dimensions: 20 mm * 7 mm* 1.5 mm.

This result shows that Ti foam proves to be a workable support material for the e-Leaf with stable current and decent current density (SA calculated based on the geometric

sizes). However, it is more difficult to use since the foam structure is rigid. Ti foam is less convenient to be cut, shaped, or bent to fit in reactors.

2.2.3. Titanium Mesh

Comparing to the Ti foam, the Ti mesh is more flexible for tailoring, while still has higher surface area. ITO can be easily coated by EPD. For enzyme loading, the Ti mesh is available for drop-casting and stir-loading. In the experiment (chronoamperogram shown in figure 2.3), FNR and E2 (GLDH) were loaded by drop-casting before reaction. The reaction was initiated by $NADP^+$ live-injection, and the immediate current after $NADP^+$ injection became noisy for a while and returned to stable after approximately 2 hours. This noise has been observed in multiple repeats, and could be due to the air bubbles introduced from live-injection and trapped on the porous structure of the mesh. The current then slowly decreased due to the depletion of substrate. The coulometric conversion is 94% of 0.44 mmol of substrate within 30 hours.

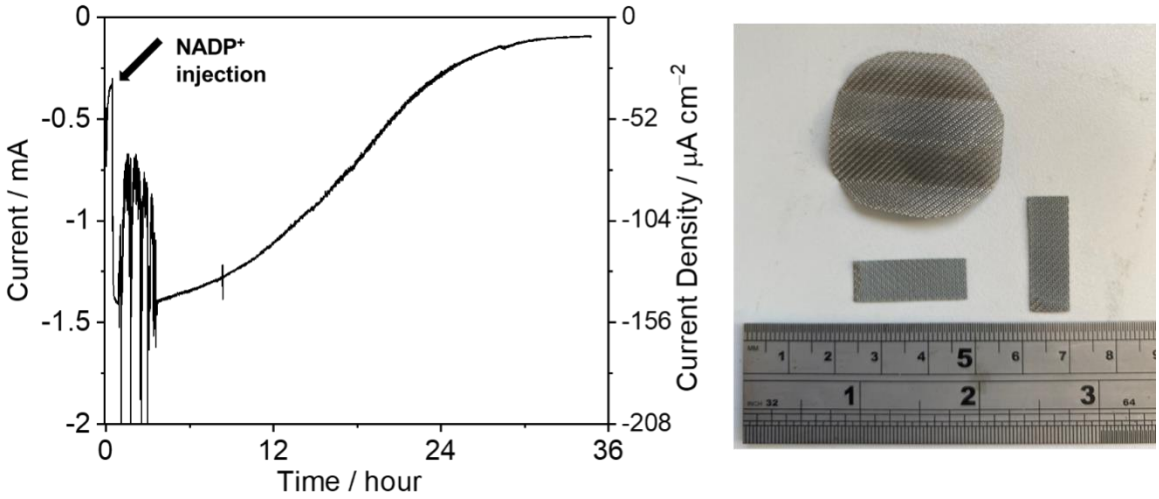


Figure 2.3. Chronoamperogram of GLDH-catalysed reductive amination with Ti mesh as working electrode. Conditions: solution volume 44 mL, buffer: 50 mM HEPES pH 7.5; temperature: 25 ℃, solution is purged with argon to remove O_2 and argon flow maintained in headspace thereafter; substrate [-ketoglutarate] = 10 mM, [NH_4Cl] = 20 mM, [$NADP^+$] = 10 µM; Potential held at -0.8 V vs. Ag/AgCl (3 M KCl) to drive reduction. ITO coated by EPD. Enzyme loading: 80 nmol FNR + 8 nmol GLDH (10:1) are mixed and loaded by drop-casting. Ti mesh geometric area: 19.2 cm^2, diameter: 3.5 cm, mesh open area: 20%.

Ti mesh proved to be an excellent alternative for the support material for the e-Leaf. Despite the starting phase with noises (confirmed to be a common issue by repeated tests), the current density is at the top tier among all the materials tested (based on dimension sizes rather than actual surface area; details shown in chapter 7 section 7.3.1). For electrodes with same surface area, Ti mesh requires approximately 3 times the volume of enzyme solution for drop-casting comparing to Ti foil material. Although the volume of drop-casting solution may not directly indicate a corresponding amount of enzyme loaded, but it still shows the capability of Ti mesh to be loaded with more enzymes. Ti mesh is not frequently used in experiments presented in this thesis since it has similar features as the Ti foil. Ti mesh can be explored in the future in an application-oriented direction to achieve higher catalytic rate with its high enzyme load on unit material.

2.2.4. Titanium Wire and Titanium Foil (twisted)

Two more hand-made Ti materials were tested, which were the Ti wire loop and the twisted foil. The photos are shown in figure 2.4 and 2.5 with the chronoamperograms of reactions. Comparing to Ti foam, both Ti wire and the twisted Ti foil are extremely ‘customizable'. Due to irregular structure, ITO coating was conducted by the doctor’s blade method and enzymes were loaded by stirring in solution. In both experiments, FNR was stir-loaded before reaction, and E2 (ADH) was live injected as the initiating of the reaction. The current was rapidly increasing to its peak at the loading of E2. The current then decreased swiftly due to the depletion of substrate. The conversion of 0.032 mmol substrate were 90% within 8 hours for the twisted foil, and 85% within 12 hours for the Ti wire loop, respectively.

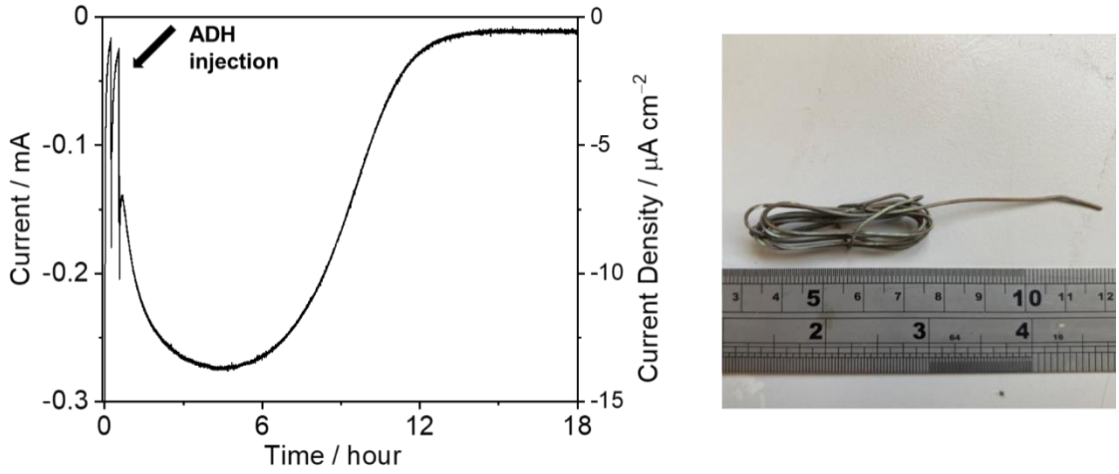


Figure 2.4. Chronoamperogram of reduction of 4-phenyl-2-butanone catalysed by ADH with folded Ti wire as working electrode. Conditions: solution volume 4 mL; substrate [4-phenyl-2-butanone] = 8 mM, [$NADP^+$] = 20 μM, buffer 50 mM TAPS pH 8.0, temperature: 25 ℃. Potential held at −0.9 V vs. Ag/AgCl (3 M KCl) for reduction. Solution is purged with argon to remove O_2 and argon flow maintained in headspace thereafter. Enzyme loading: FNR loaded first by stir-loading, ADH is live injected to the final concentration of 0.24 μM in reaction solution. ITO coated by pasting method. Ti wire SA: 20 cm^2, length 85 cm, diameter: 0.7 mm.

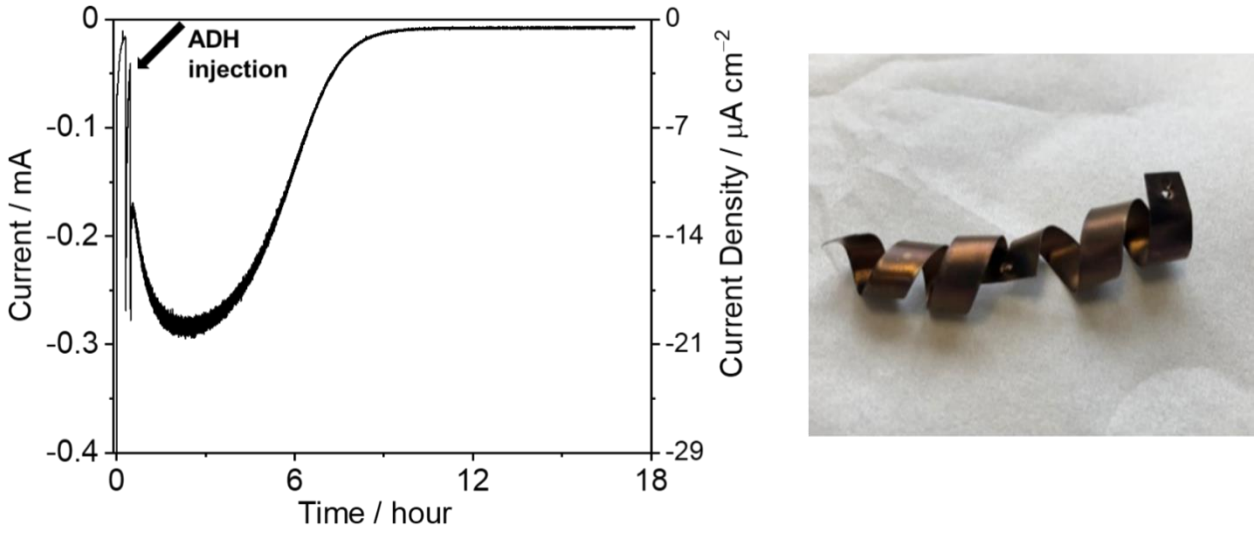


Figure 2.5. Chronoamperogram of reduction of 4-phenyl-2-butanone catalysed by ADH with twisted Ti foil as working electrode. Conditions: solution volume 6 mL; substrate [4-phenyl-2-butanone] = 8 mM, [$NADP^+$] = 20 μM, buffer 100 mM TAPS pH 8.0, temperature: 25 ℃. Potential held at −0.9 V vs. Ag/AgCl (3 M KCl) for reduction. Solution is purged with argon to remove O_2 and argon flow maintained in headspace thereafter. Enzyme loading: FNR loaded first by stir-loading, ADH is live injected to the final concentration of 0.24 μM in reaction solution. ITO coated by pasting method. Electrode SA: 14 cm^2.

For the Ti wire and twisted foil, the opportunity for customisation is great but is less needed for the specific research in this thesis. The irregular shape requires extra operations before use and also brings challenges in the repeatability. The homemade support electrode may not be the ideal electrode material for now, but it reveals the fact that how versatile the e-Leaf can be transformed in terms of the electrode design. As previously stated, an e-Leaf should be ready for action after simple operations as a few minutes' of ITO-coating followed by drop casting enzyme loading.

In addition to the Ti electrode, In summary, the ideal choice for the exploration of the e-Leaf in this thesis is the Ti foil. Ti foil has balanced flexibility and convenience. It can be customised into different shapes and be made into standard pieces. The flat surface of Ti foil is simple for EPD and enzyme loading, as well as subsequent the calculation and modelling. Further, Ti foil has been used since the initial e-Leaf setup and this means that the data is comparable. On the other hand, different forms of support materials are still potential options with simplified manufacturing methods. For instance, Ti wires are especially flexible for its shape to fill space in a reactor. Ti tubes have a rigid and modular structure and can serve as units for close packing in the cylindrical space of the electrochemical cell, which plays an important role in the design of a flow reactor.

2.3. Indium Tin Oxide (ITO) Coating

This section includes the alternative ITO coating methods, and investigation to the electrophoretic deposition (EPD) process. As mentioned in the introduction, in the initial construction of the e-Leaf, the coating of ITO on Ti foil electrode is conducted by EPD, which is the most used coating process for the experiments in this thesis. However, EPD may not be the most efficient coating method for some electrodes. For example, the Ti tube has a cylindric shape and its inner side is hard to face the counter electrode in parallel. The doctor's blade method has been tested in order to widen the scope of

available electrode materials. In addition, the electrical assisted deposition (EAD) method has also been attempted for potential use (details in the appendix A2.2).

2.3.1. Alternative ITO coating - Doctor's Blade Pasting method

Pasting method, also called 'doctor's blade' method, is widely used in the preparation of photosensitive material such as TiO_2 coating.[80,81] The process includes making of coating paste, dip-coating or painting the paste onto the support material, and finally calcination to remove the solvent. Two different pastes recipes were tested, both of which are from well-established TiO_2 pasting methods.[80,81] 1.ITO powder in ethanol with acetic acid, α-terpineol and ethylcellulose; 2.ITO powder in aqueous polyethelene glycol.

Cyclic voltammograms in figure 2.6 shows the capacitance changes by EPD and pasting methods. For Ti foil, the capacitance increased for both as expected, suggesting that the pasting method is as satisfactory in coating as the EPD method. For Ti tube, however, only pasting method had a huge increase of capacitance. The EPD method could hardly coat ITO on the Ti tube due to the shape of such electrode. It is difficult to have a counter electrode placed in parallel to the tube's surface, both outside and inner side.

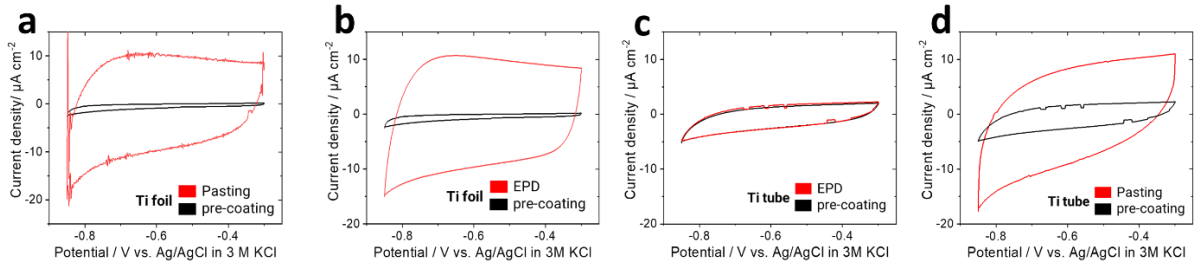


Figure 2.6 Cyclic voltammetry showing the capacitance change of **(a)** Ti foil coated by EPD and **(b)** Ti foil coated by pasting **(c)** Ti tube coated by EPD **(d)** Ti tube coated pasting. conditions: scan rate = 4 mV/s; electrode surface area: 14 cm^2, scan rate: 5 mV/s; buffer: 100 mM TAPS pH 8.0, temperature: 20 °C.

To confirm the viability of ITO/Ti tube in the electrochemical process, the electrodes are tested in the electrochemical cell for reaction. Figure 1.23 shows the chronoamperograms of a series of GLDH-catalysed reductions with different ITO coating methods and enzyme loading methods on foils or tubes of same surface area. FNR

loading methods are discussed in section 1.8.3. The loading methods and electrode types are presented in table 2.1. In general, each electrode was electrochemically active and generates similar levels of current. The pasting method is as a good a way of ITO coating as EPD. The reaction 3 has the highest current among others, where ITO is coated by EPD and FNR is loaded by drop-casting.

Table 2.1. EPD method and enzyme loading method for figure 2.7

No.	Electrode	ITO coating	FNR loading
1	Ti Foil	pasting	Drop-casting
2	Ti Foil	pasting	Stirring
3	Ti Foil	EPD	Drop-casting
4	Ti Foil	EPD	Stirring
5	Ti Tube	pasting	Drop-casting
6	Ti Tube	pasting	Stirring

* FNR is preloaded before reaction and GLDH is live injected at the start of each reaction.

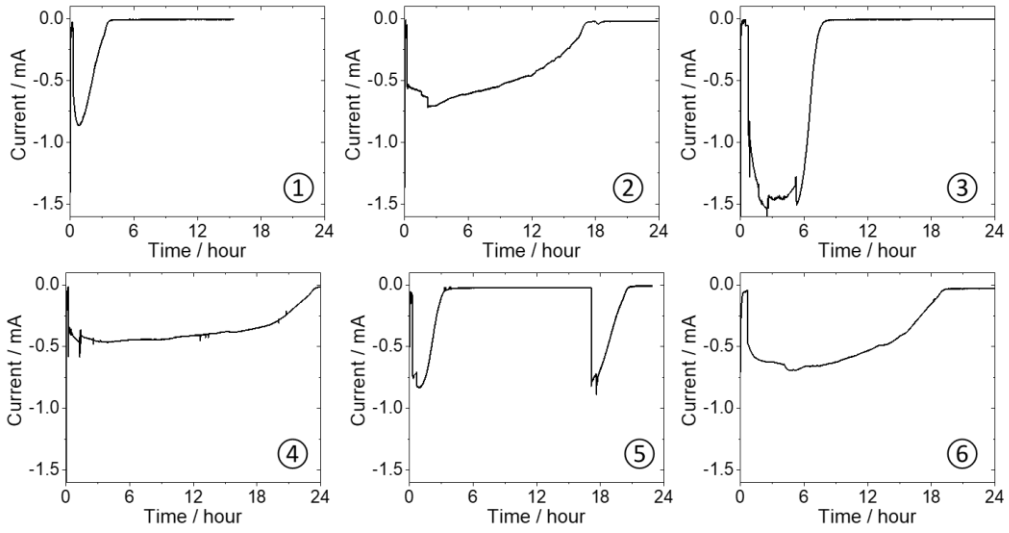


Figure 2.7. Chronoamperograms of GLDH-catalysed reduction with electrodes of different ITO coating methods and enzyme loading methods. Conditions: solution volume 45 mL, buffer: 100 mM TAPS pH 8.0; temperature: 25 ℃, solution is purged with argon to remove O_2 and argon flow maintained in headspace thereafter; substrate [α-ketoglutarate] = 8 mM, [NH_4Cl] = 16 mM for a) and e), [a-ketoglutarate] = 40 mM, [NH_4Cl] = 80 mM for b), c), d), f); [$NADP^+$] = 100 µM; Potential held at -0.69 V vs. Ag/AgCl (3 M KCl) to drive reduction. Enzyme loading: FNR preloaded and GLDH is live injected to the final concentration of 0.21 mg/mL in reaction solution. SA: 35 cm^2(foils), 33.2 cm^2 (tubes).

The disadvantages of the Doctor's Blade method is that it is less precise with the amount of ITO coated on the surface, due to the operation errors in the painting and subsequent steps. Figure 2.8 shows the photos of EPD-coated and pasting-coated electrodes and it is clear to see a less uniform ITO coverage on the pasted electrode. EPD suits particularly well for Ti foil with a flat surface, giving a regular and highly repeatable layer of ITO, while pasting can handle electrodes of irregular forms such as Ti tubes, wires, and wools.

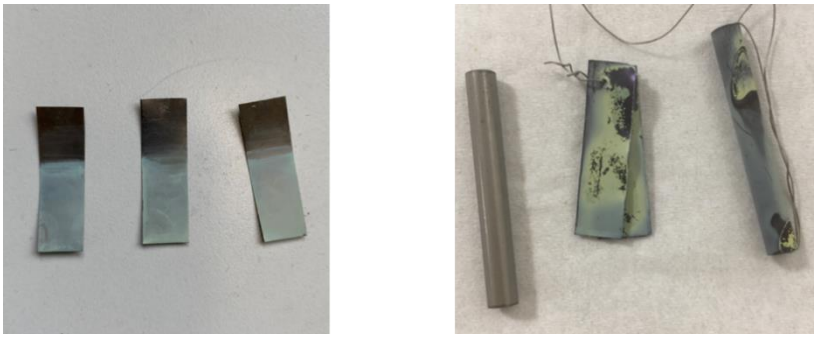


Figure 2.8 Photos of electrode with ITO coated by EPD (left) and by pasting (right)

2.3.2. Deposition Time and ITO Amount in EPD

It is desirable to investigate the effect of the EPD loading time on the amount of ITO coated, since EPD is the main way of coating ITO. Experiments were conducted to test the weight change of electrode at different EPD times. For systems with different setup from this one (i.e. electrode shape, reactor design, coupled E2s, scales and reaction conditions and etc), the loading process may have a different effect on the performance in the electrochemical process.

In this test, multiple Ti foils with the size of 4 cm * 3.5 cm (28 cm^2) were weighed before and after EPD loading. The loading time per side of electrode was between 15 seconds to 7 minutes. After ITO coating, the electrodes were loaded with enzymes (FNR and GLDH) with identical process and tested in the electrochemical cell. Capacitance difference and FNR non-turnover peak were detected by cyclic voltammetry. Then the catalytic activity was compared with chronoamperometry monitoring the reduction of

alpha-ketoglutarate in the same reaction conditions. Table 2.2 shows the weights of ITO coated, the FNR coverages calculated form FNR non-turnover peaks, and the widths of the capacitance current (double-layer capacitive current from electrochemical analysis shown in figure 2.10 panel (b)). Data from the table are plotted in figure 2.9 to show the trend. The diagrams in panel (a) (b) and (c) all show apparent linear relationships. ITO loading amount is highly related to EPD time and reflects the space available for enzyme loading. This trend has been confirmed by repeat experiments.

Table 2.2. Electrode weight increase and FNR coverage with different EPD time

	EPD time per side / min	ITO weight / mg	FNR coverage / pmol FNR cm^{-2} Ti	Capacitance current width*/ mA
1	7	25.2	110.6	0.577
2	4	14.6	80.5	0.325
3	2	9.5	47.7	0.230
4	1	5.1	13.1	0.130
5	0.5	3.8	11.8	0.047
6	0.25	2.3	1.5	0.036

*The width of capacitance current was calculated by taking current difference at -0.65 V from data in figure 2.10 panel (b) showing the capacitance current change with different EPD time.

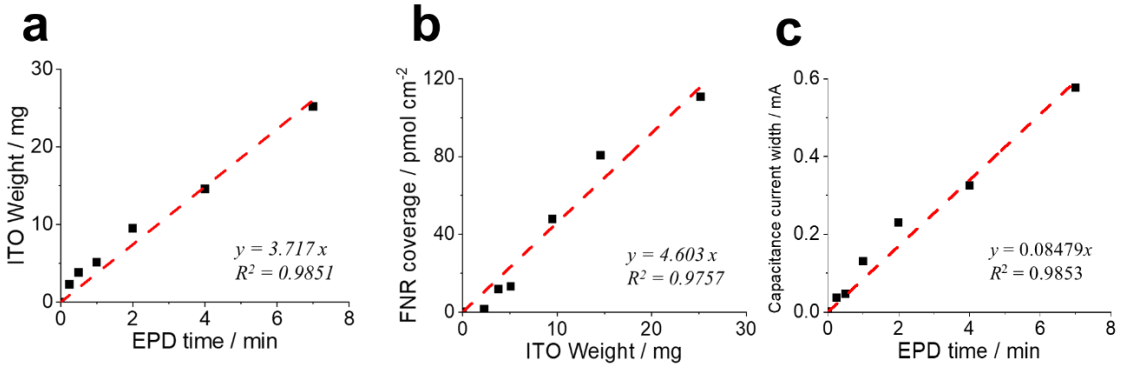


Figure 2.9 Plots of **a)** Weight of ITO loaded vs. EPD time, **b)** FNR coverage after enzyme loading vs. weight of ITO loaded. **c)** Capacitance current width change vs. EPD time. Conditions: EPD solution: 50 mg ITO + 25 mg I_2 in 50 mL acetone, solution stirred throughout using a magnetic flea; potential held at 10 V, 1.5 cm distance between two electrodes. Enzyme loading: FNR and GLDH are loaded together by drop-casting. 37.8 nmol FNR and 3.86 nmol GLDH are mixed and diluted to 192 μL by 100 mM TAPS pH 9.0, buffer and applied to electrode for 20 minutes before rinsed off by the buffer. Electrode (Ti foil) SA: 28 cm^2.

The goal of optimisation is to improve the electrochemical performance and therefore the achievable coupled current was measured for each different EPD loading time. Chronoamperometry was conducted with reduction catalysed by these electrodes with FNR and GLDH loaded to evaluate the overall performance (Figure 2.10 panel (a)). The chronoamperogram shows a clear comparison of electrochemical activity among these electrodes with different ITO amount. Electrodes with 0.25 – 1-minute EPD time hardly have any activity. Electrode with 2-minute, 4-minute, and 7-minutes EPD time showed a trend of current increase with the EPD time, but the relationship is not linear. For the electrode with 7-minute EPD time, the current level is higher by a larger scale. Among all the electrodes, only the 7-minute coating electrode yielded a current high enough to reach a substrate depletion, leading to a sharp decrease of current after 12 hours.

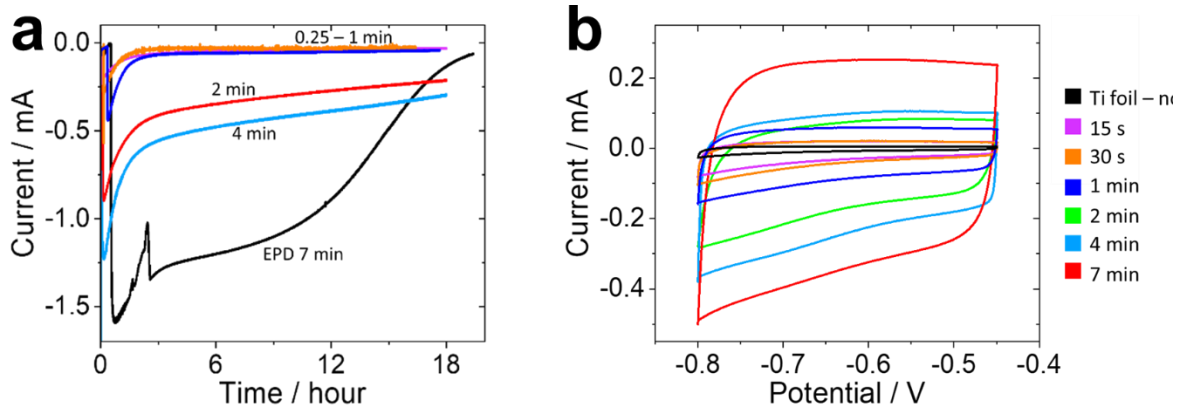


Figure 2.10. a) Chronoamperograms of GLDH-catalysed reduction and **b)** Cyclic Voltammograms with electrode of different EPD loading times. Conditions: solution volume 45 mL, buffer: 100 mM TAPS pH 8.0; temperature: 25 ℃, solution is purged with argon to remove O_2 and argon flow maintained in headspace thereafter. CV scan rate = 2 mV/s; chronoamperometry conditions: substrate [α-ketoglutarate] = 8 mM, [NH_4Cl] = 16 mM, [$NADP^+$] = 10 µM; Potential held at -0.70 V vs. Ag/AgCl (3 M KCl) to drive reduction. Electrode (Ti foil) SA: 28 cm^2.

Capacitance changes related with EPD times are shown in figure 2.10 panel (b). Like the FNR coverage, the capacitance is linear with the EPD time (as shown in figure 2.9 panel (c)). The non-linear relation between EPD time and reaction rate is possibly from the non-linear increase of the complexity of ITO layer structure. At early stage of an EPD process, the ITO layer is only formed with shallowness. It takes a threshold of time for a three-dimensional nanoporous structure to be established, before which the space in

nanostructure is little and the attachment of enzyme to nanopore is poor due to the level structure it holds. With more ITO coated on the electrode, thicker layer is formed. While the amount of ITO deposited is increasing linearly with time, the complexity of nanopore structure is upgrading even faster, creating much more space and porosity for enzymes to be adsorbed. The 7 minutes loading time worked the best and was adopted for the rest experiments in the thesis.

2.4. Enzyme Loading Optimisation with FNR Preloaded

As shown in most of the experiment above, at the early stage of the e-Leaf optimisation, E2 was loaded by live injection rather than co-loaded with FNR before reaction. At this stage of research, E2 is viewed as one of the external factors coupled to the FNR on ITO/Ti electrode though E2 is gradually adsorbed into the pores of electrochemical leaf. This section shows the optimisation with such loading methods, including FNR loading methods exploration, E2 titration, membrane-confinement test. The E2-live injection loading method was replaced by preloading both FNR and E2(s) before reaction, which is more convenient and yields highly repeatable performance.

2.4.1. FNR Loading Method: Stir-loading and Drop-casting

FNR loading is the essential part of the electrochemical leaf construction. Two FNR loading methods were tested. The loading method at the invention of the e-Leaf is to load FNR by stirring the ITO/Ti foil electrode in enzyme dilute solution for at least 5 hours. The other method is to drop-cast FNR directly on the electrode and rinse it off with buffer after 5 to 30 minutes. The performance with the two FNR loading methods is tested with GLDH-coupled system, with results shown in previous section figure 2.7. By comparing the reaction rate with electrode made from same ITO loading method but different FNR loading method, it is apparent that drop-casting method yields higher current rates. In addition, drop-casting takes much shorter time than stir-loading method,

providing convenience in electrode manufacturing. The drop-casting method is employed in the experiments in the subsequent chapters.

2.4.2. Live Injection Amount of E2

The early version of the e-Leaf has E2 loaded by live injection. Experiment of E2 injection is shown in figure 2.11 panel (a) in search for an optimal amount of E2 to be applied (from 0 to 6.1 nmol of GLDH). This test was specific to GLDH-catalysed glutamic acid production, in which FNR is preloaded by drop-casting, and $NADP^+$ and substrate are added before GLDH is injected to initiate the reaction. GLDH was live injected into the solution stepwise up to 70 μL (final concentration in solution 1.52 μM). After each injection there is a span of time for the current to reach a steady plateau. The reaction current vs. GLDH amount injected are plotted in figure 2.11 panel (b) and a trend curve is plotted. The diagram shows the loading trend of the E2 with live injection. At lower concentration, GLDH amount to the reaction rate is more linear and as the amount went up, the current no longer increased. The hypothesised loading process is that at the start of loading, the vacancy in the nanopores on the electrode was sufficient, therefore the E2 injected easily adsorbed in the electrode and contributed to the increase in current. A linear relation between E2 amount and current increase shows the fast loading. At later stage of the loading, few space was left for new-coming E2s and the enzymes is therefore slower to get adsorbed to contribute to the current increase, therefore a more flat current shape was observed, indicating a slow adsorbing of E2. The GLDH injection amount was chosen to be approximately 20 – 30 mL (final concentration of 0.43 nM to 0.65 nM) as the optimal, for both reaction rate and efficiency of enzyme (reaction rate per unit of enzyme applied). This test can be potentially improved by using CV monitoring over the process to ensure the rate-limiting enzyme at different stages, as described in section 1.8.1.

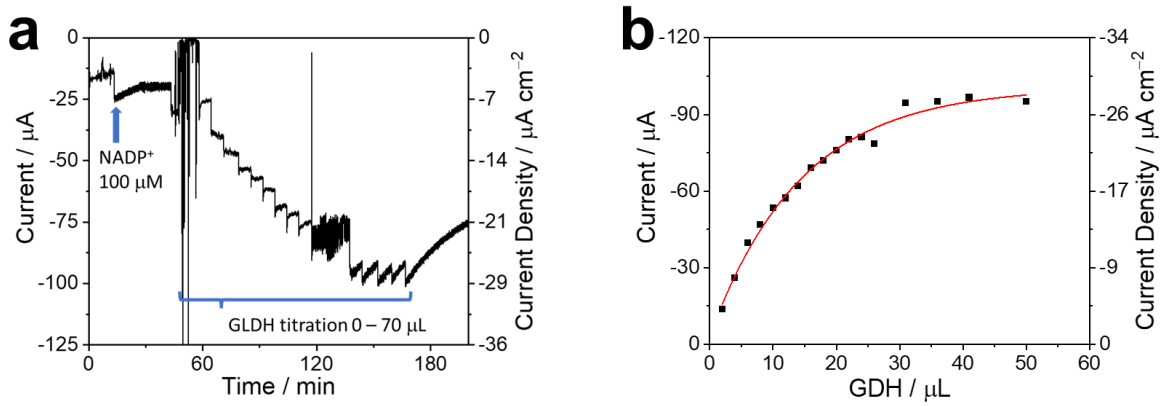


Figure 2.11. a) GLDH titration for α-ketoglutarate reductive amination. **b)** Fitting curve of reaction current vs. GLDH injected amount. Condition: solution volume 4 mL, buffer: 100 mM TAPS pH 8.0; temperature: 25 °C; solution is purged with argon to remove O_2 and argon flow maintained in headspace thereafter; substrate [α-ketoglutarate] = 250 mM, [NH_4Cl] = 500 mM, [$NADP^+$] = 100 μM; Potential held at -0.65 V vs. Ag/AgCl (3 M KCl) to drive reduction. Enzyme loading: 21.6 nmol FNR (final concentration 10.8 μM) preloaded by stirring in 2 mL buffer (pH 8.0 25 mM TAPS + 25 mM MES). GLDH (storage concentration 0.087 mM) is live injected from 0 to 70 μL; electrode SA: 33.6 cm^2.

2.4.3. Membrane for Enzyme Confining with E2 Live Injection

When it comes to scaling up the electrochemical leaf, one of the challenges is optimising the amount of E2 for live injection to avoid unnecessary waste of enzyme. One attempt was to use a dialysis membrane holding the electrode to confine E2 in a smaller volume in order to keep a high regional concentration at the electrode surface as in small-sized cell. The principal idea is shown as a sketch in figure 2.12. The membrane used has a molecular weight cut-off of 12 – 14 kDa, which is much smaller than GLDH and FNR, therefore is able to confine the enzymes within the membrane meanwhile allowing substrate and cofactors to travel through.

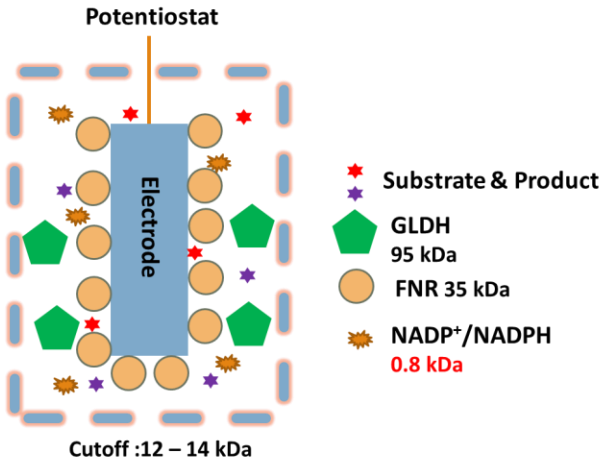


Figure 2.12. Dialysis membrane confinement for the e-Leaf

Figure 2.13 shows the chronoamperograms of experiments with membrane confinement, setup parameters listed in table 2.3. Reaction 1 was conducted in a scaled-up cell with GLDH amount increased to the same ratio. 200 μL GLDH was injected in 50 mL solution. As a comparison, reaction 2 was conducted in the same cell but with a membrane containing the electrode and GLDH. The GLDH used in membrane was only 3.5 μL and this system even achieved higher current than reaction 1. Membrane confinement gave a higher effective GLDH concentration with less amount used. Reaction 3 and reaction 4 presented the comparison between small cell no-membrane setup and the large cell with membrane. With the membrane, less amount of E2 used on the same sized electrode generated comparable current level in a large cell as the small cell.

Table 2.3. Setup of membrane test experiment in figure 2.13

	Reactor Volume / mL	Electrode Surface Area / cm^2	Membrane Volume / μL	GLDH injected / μL	Effective GLDH concentration / g mL^{-1}
1	50	8.5	No	200	168
2	50	8.5	700	3.5	210
3	4	35	No	20	210
4	50	35	1100	5.5	210

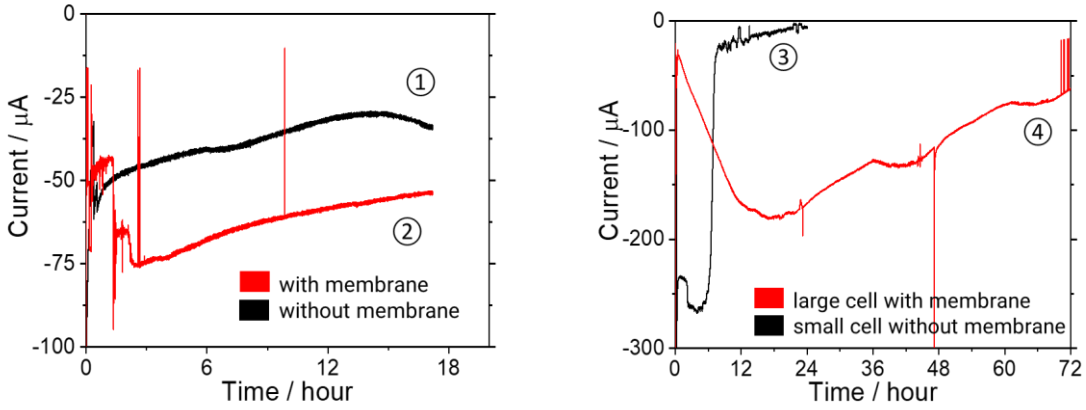


Figure 2.13. a) GLDH-catalysed reduction in 50 mL cells with and without membrane, with GLDH live injection amount 200 uL(without membrane) and 3.5 μL (with membrane) **b)** GLDH-catalysed reduction in 4 mL cell with 20 uL GLDH injection and in 50 mL cell with 5.5 uL GLDH injection (with membrane). Condition: buffer: 100 mM TAPS pH 8.0; temperature: 25 ℃; solution is purged with argon to remove O_2 and argon flow maintained in headspace thereafter; substrate [α-ketoglutarate] = 8 mM, [NH_4Cl] = 16 mM, [$NADP^+$] = a) 100 μM and b) 20 μM. Potential held at -0.68 V vs. Ag/AgCl (3 M KCl) to drive reduction. Enzyme loading: FNR is preloaded by drop-casting and GLDH is live injected. electrode SA: a) 8.5 cm^2. B) 35 cm^2.

The membrane holds the advantages of avoiding the large use of E2 in the live-injection loading method, which benefits the scaling up of the e-Leaf. The drawbacks are also obvious. First, a membrane-covered electrode system is less convenient to set up. It requires extra operations, such as pre-treatment of membrane, size tuning, loading electrode and E2 into the membrane and avoiding membrane from drying. In addition, observation from multiple experiments with membrane shows signals with more noises when comparing to non-membrane system. This may be due to the touches and hit between membrane and electrode. Also, the stirring of the solution is conducted by a stirring flea in the bulk solution outside the membrane, so the solution in the membrane is less agitated. Research on the electrochemical leaf has proved the entrapment of enzymes on the nanopores on ITO cavities is strong enough that enzymes are nanoconfined and remain stable in the electrode without excess enzymes in bulk solution.[51] The membrane served only as one step on the way of discovering nanoconfinement.

2.5. Enzyme Loading Optimisation: Stepwise Loading

As introduced in chapter 1, the ITO nanopores on the surface of electrode surface area has created a nanoconfinement environment for FNR, downstream enzymes and cofactors. This was not recognized when the early-stage experiments were conducted (some experiments in chapter 3 and 5 have E2 live-injected). Adsorbed on the inner walls of the nanopores, FNR and downstream enzymes can work in concert and remain steady for a long time. Within the 5 – 100 nm pores, enzymes are juxtaposed and $NADP^+$ and NADPH are cycled rapidly between FNR and downstream enzymes.[51] Since enzymes are highly concentrated, the distances among active sites across which intermediates and cofactors must diffuse may be tiny as well.[48] With the discovery of nanoconfinement, live injection of E2 with redundant enzyme in the solution is found not to be the key factor for the electrochemical leaf to remain stable and function properly.[51] Enzymes preloaded before reaction can remain active and stable throughout the reaction process.

The enzymes (FNR and E2) are loaded in the electrode, by the either drop-casting or stir-loading. The loading order can be simultaneous or stepwise. Therefore, there are several main loading patterns involved in the following experiments. (1) FNR and E2(s) loaded together by drop-casting (2) FNR loaded by drop-casting then E2 loaded by stirring (3) FNR and E2 loaded together by stirring. Pattern (1) is mainly used in basic optimisation test and scaling-up experiment where GLDH is involved. Pattern (2) and (3) are mostly used in deracemisation experiment where two ADHs with different affinity towards electrode are involved. The stir-loading takes 5-18 hours and drop-casting only takes approximately 30 minutes. Loading process optimisation is presented for specific situations in corresponding sections. In this chapter, the optimisation of pattern (1) drop-casting co-loading is chosen as an exemplar case to demonstrate the optimisation process of enzyme loading.

2.6. Enzyme Co-loading by Drop-casting

In the co-loading, FNR and E2 are mixed and loaded together. The enzymes are loaded by stirring in solution or by drop-casting. This method is used in most of the experiments including (FNR + GLDH) loading in the scaling up experiment in chapter 3, (FNR + LK + W110A) loading in deracemiser and inverter in chapter 4 and (FNR + ADH) loading in bi-phasic system in chapter 5. The advantage of enzyme loading for the e-Leaf is that the amount and ratio of FNR and E2 in nanoconfinement is adjustable to compensate for inherently slow enzymes. This can be utilised in the search for an optimal loading condition that allows the best reaction performance for the e-Leaf. Results presented here take the co-loading of FNR and GLDH on Ti foil(s) as an example to show the optimisation for enzyme loading process, which includes the loading ratio of enzyme, the enzyme usage, the drop volume and the incubation time.

2.6.1. Enzyme Loading Ratio (FNR to GLDH)

Experiments here investigate how the change of enzyme ratio in drop-casting affects the final catalytic performance. With other conditions being constant, three different ratios of FNR to GLDH enzyme loading were tested (FNR : GLDH = 10:1, 1:1, and 1:10). Figure 2.14 shows the reaction process with these three electrodes. The three curves show similar timecourses. The reaction rate remained steady from the initiation of reaction for a long time, and finally dropped sharply due to the depletion of the substrate. It is distinguishable that the 10:1 ratio for FNR:GLDH has the best catalytic activity, for the peak current is the highest and the reaction achieves the depletion of substrate in the shortest time.

This experiment demonstrates how the ratio in enzyme loading can be tailored for each E2 enzyme. For example the ratio of E2:FNR could be increased for a particularly slow E2 to compensate for its low rate. The 10:1 ratio of FNR to GLDH is applied in the scaling up of e-Leaf in chapter 3 and the flow reactor in chapter 5. For other

experimental situations when a different combination of enzymes is applied, similar principles of finding the optimal ratios between/among enzymes are applied.

It is noteworthy that the 10:1 ratio is probably not the optimal ratio for a highest rate, as more FNR applied could possibly further increase the overall performance based on the trend. The decision of using 10:1 ratio for subsequent experiments was based on the limitation of actual operations. The purified enzyme solution of FNR is not concentrated enough to provide a high enzyme amount within a controllable volume. The operation of drop-casting becomes inconvenient when the drop volume is increasing. Therefore, the ratio 10:1 with satisfactory reaction rate was selected.

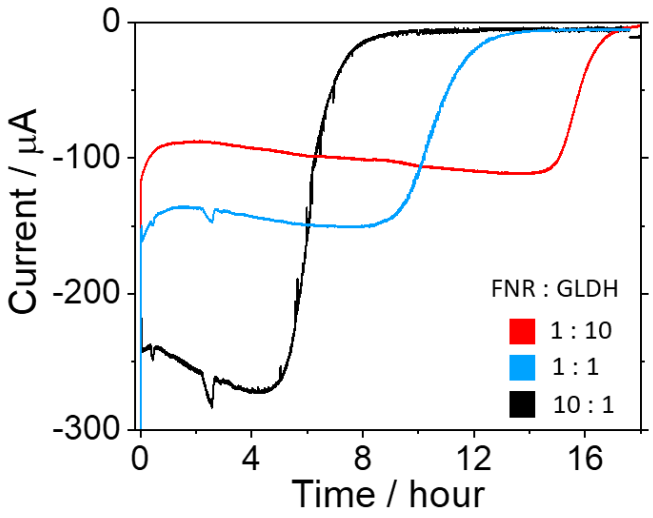


Figure 2.14. Chronoamperograms of GLDH-catalysed reduction with enzyme loading of different FNR to GLDH ratios. Conditions: solution volume 4 mL, buffer: 100 mM TAPS pH 8.0; temperature: 25 °C, solution is purged with argon to remove O_2 and argon flow maintained in headspace thereafter. substrate [α-ketoglutarate] = 8 mM, [NH_4Cl] = 16 mM, [$NADP^+$] = 10 μM; Potential held at -0.69 V vs. Ag/AgCl (3 M KCl) to drive reduction. Electrode SA = 3.5 cm^2; enzyme amounts applied: 17.02 nmol FNR + 1.70 nmol GLDH (10:1); 9.35 nmol FNR + 9.35 nmol GLDH (1:1); 1.70 nmol FNR + 17.02 nmol GLDH (1:10); Adapted with permission from B. Cheng et al. Copyright 2020, Wiley.[54]

2.6.2. Enzyme Usage in Loading

Enzyme amount applied in drop-casting was optimised by testing the catalytic performance with the rest of conditions being constant. EPD time (7 minutes per side), enzymes applied ratio (FNR:GLDH = 10:1), drop-cast volume (24 μL for 3.5 cm^2

electrode) and incubation time (20 minutes) were the same in the experiments. Figure 2.15 shows the reaction current change during the process with different enzyme applied amounts (FNR+ GLDH 8.05 nmol, 5.25 nmol, 3.5 nmol and 1.75 nmol) on electrodes of same size (data shown in table 2.4). Electrodes with higher amounts of enzymes (2.3 and 1.5 nmol cm^{-2}) shows higher current and stability while when the enzyme amount is low it shows slightly decreased stability (1.0 nmol cm^{-2}) and even lower reaction activity (0.5 nmol cm^{-2}).

Considering the surface area of electrode and the highest amount of enzyme that can be adsorbed in the pores (in the next section), the amount applied is far more than the electrode can take, which explains why the current from the 2.3 nmol loading is not increased from 1.5 nmol (approximately 130 μA). The difference among reaction performance is attributed to the concentration of enzymes in drop-casting, leading to experiments described in the next section. As a conclusion, 1.5 nmol cm^{-2} is the amount selected for most of the experiments in the thesis.

Table 2.4. Different enzyme amounts used in the experiment in figure 2.15

	Enzyme amount (FNR + GLDH) / nmol	Enzyme amount to SA / nmol cm^{-2}	Peak current / μA	Total charge passed / C
1	8.05	2.3	152	5.4
2	5.25	1.5	145	5.4
3	3.5	1.0	142	5.4
4	1.75	0.5	75	2.2

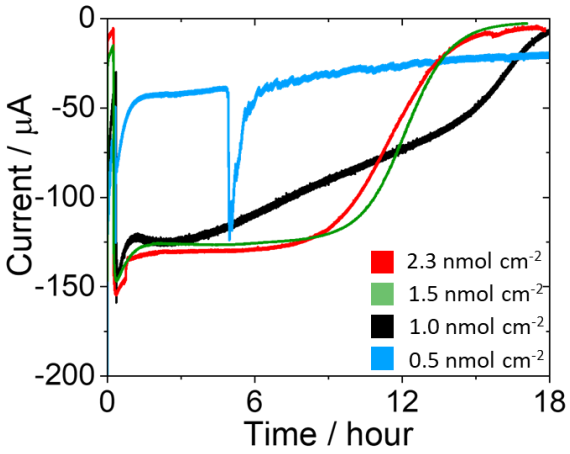


Figure 2.15. Chronoamperograms of GLDH-catalysed reduction with electrodes of different enzyme amount applied in loading. Conditions: solution volume 4 mL, buffer: 100 mM TAPS pH 8.0; temperature: 25 ℃, solution is purged with argon to remove O_2 and argon flow maintained in headspace thereafter. substrate [α-ketoglutarate] = 8 mM, [NH_4Cl] = 16 mM, [$NADP^+$] = 10 μM; Potential held at -0.70 V vs. Ag/AgCl (3 M KCl) to drive reduction. Electrode SA = 3.5 cm^2

2.6.3. Drop-casting Volume (Drop Concentration)

Drop-cast volume optimisation was conducted based on the optimised enzyme amount. With the same EPD time (7 minutes per side), enzymes applied ratio (FNR:GLDH = 10:1), enzyme amount (1.5 nmol / cm^2 electrode) and the incubation time (20 minutes), performances were measured with enzyme loadings with different drop-cast volumes. Data are shown below in table 2.5 and figure 2.16.

It is intuitive that a smaller drop volume has better performance due to the higher concentration of enzymes. Yet the results have shown an exception that when the volume of drop went too low (12 μL), the reaction performance was worse than the 24 μL run. The reason probably lies in the process of drop-casting. 12 μL drop was not enough to fully cover a 3.5 cm Ti foil and during the incubation time, water was evaporating fast and part of the electrode became dry and the enzyme lose activity. Operational restrictions are an important factor to be considered when making an electrode.

In addition, the 4000 μL test suggests the connection between drop-casting and stir-loading. Drop-casting, as the ‘drop’ becomes large enough to millilitre scales, was

actually a dilute solution loading process except that no stirring was applied. This also reveals the advantage of drop-casting that it takes less time for incubation due to the high concentration in the drop. In conclusion, a 1.5 nmol enzyme in 7 μL drop per square centimetre of electrode is selected for drop-casting of FNR and GLDH on Ti foil.

Table 2.5. Different drop-casting volume used in the experiment in figure 2.16

	Drop-cast Volume / μL	Drop concentration* / μM	Peak current / μA	Total charge passed / C
1	12	438	161	4.9
2	24	219	105	5.9
3	50	105	54	5.2
4	4000*	1.31	15	0.5

*When the drop volume increases to 4 mL, the loading methods becomes no difference to co stir-loading except that there is no stirring applied in the drop(solution).
* Drop concentration = enzyme amount / drop-cast volume, where enzymes applied include FNR and GLDH applied in a ratio of 10 : 1 on the electrode of 3.5 cm^2.

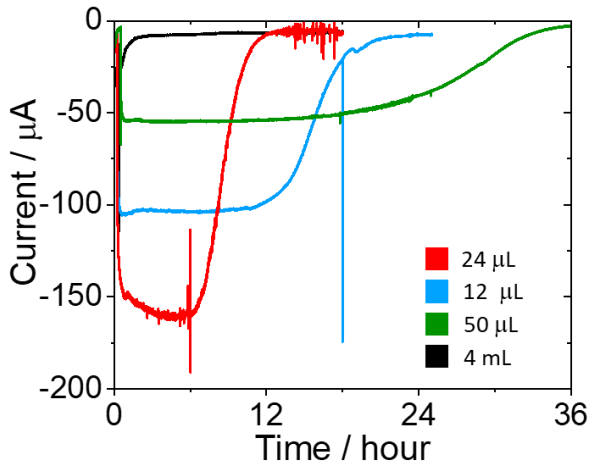


Figure 2.16. Chronoamperograms of GLDH-catalysed reduction with electrodes of different drop-cast volume in enzyme loading. Conditions: solution volume 4 mL, buffer: 100 mM TAPS pH 8.0; temperature: 25 ℃, solution is purged with argon to remove O_2 and argon flow maintained in headspace thereafter. substrate [α-ketoglutarate] = 8 mM, [NH_4Cl] = 16 mM, [$NADP^+$] = 10 μM; Potential held at -0.70 V vs. Ag/AgCl (3 M KCl) to drive reduction. Electrode SA = 3.5 cm^2

2.6.4. Incubation Time

The enzyme incubation time is the final variable in reaction conditions optimised for enzyme loading. This was explored using the same EPD time (7 minutes per side), applied enzymes ratio (FNR:GLDH = 10:1), enzyme amount (1.5 nmol / cm^2 electrode) and drop-cast volume (24 μL) as shown in figure 2.17. It is concluded that a 20-minute incubation time threshold should be met for the electrode to have an active and steady performance in reaction.

The incompleteness of the test is that more repeats could be conducted to to check the loading time range between 10 - 20 minutes and over 20 minutes. In addition, the time required for enzyme entrapment into nanopores is related to the concentration of enzyme drops, therefore the more precise optimisation would be varying enzyme amount, drop volume and incubation time all together in search for an optimal combination of these factors.

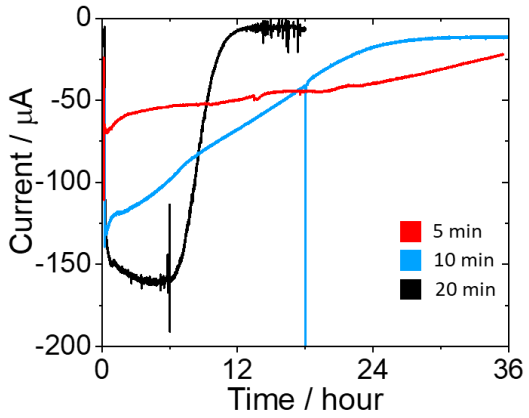


Figure 2.17. Chronoamperograms of GLDH-catalysed reduction with electrodes of different enzyme loading incubation time. Conditions: solution volume 4 mL, buffer: 100 mM TAPS pH 8.0; temperature: 25 °C, solution is purged with argon to remove O_2 and argon flow maintained in headspace thereafter. substrate [α-ketoglutarate] = 8 mM, [NH_4Cl] = 16 mM, [$NADP^+$] = 10 μM; Potential held at -0.70 V vs. Ag/AgCl (3 M KCl) to drive reduction. Electrode SA = 3.5 cm^2

2.7. Reaction Optimisation

2.7.1. Reactor

The classic design used most commonly in the e-Leaf experiments has been shown in chapter 1. Different reactor designs are shown in subsequent chapters. In the scaling up of the e-Leaf in chapter 3, several new designs of the electrochemical cell are developed to meet the requirement of larger-scaled reaction, with shifted chemical and electrical environment in the cell. The reaction scale increases from 4 mL to 0.5 L, and the large-scale setup has acquired the potential to further increase to litres scale. Another design is the flow reactor shown in chapter 6 for the application of introducing flowing system to the e-Leaf. This electrochemical cell is designed with multiple openings for coupling to the flowing solution driven by a peristaltic pump and for pressure release.

2.7.2. Cofactor NADP(H) Concentration in Bulk Solution

Reaction condition optimisation is a highly case-by-case situation considering the different nature of different enzymes. Cofactor NADP(H) is the only universal factor among the coupled enzyme-catalysed reactions. Therefore, this section of reaction optimisation shows solely the NADP(H) titration, taking GLDH-catalysed and ADH-catalysed conversion as examples.

$NADP^+$ titration in GLDH-catalysed reduction

Figure 2.18 shows the chronoamperogram of $NADP^+$ titration in the GLDH-catalysed reduction of α-ketoglutarate to determine the optimal NADP(H) concentration in bulk solution for the reaction. $NADP^+$ was live injected into the reaction solution stepwise up to 25 μM. Equal periods of time was given after each injection to allow the current to reach a new steady level.

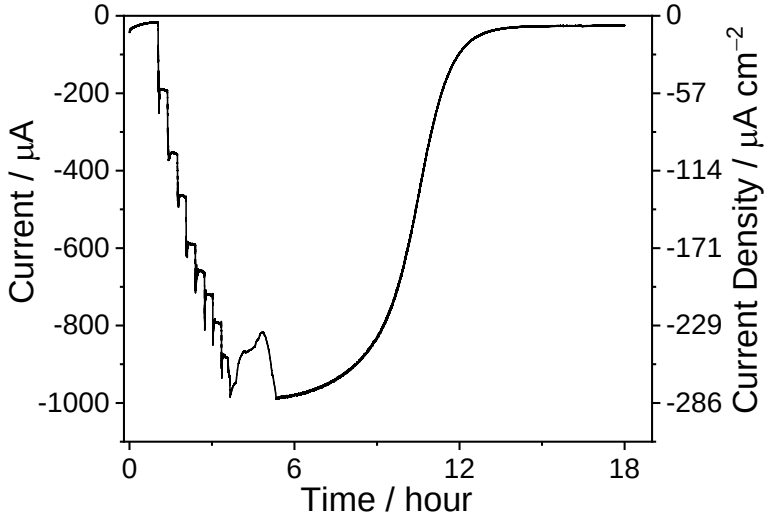


Figure 2.18. $NADP^+$ titration for GLDH-catalysed reductive amination. Conditions: solution volume 4 mL, buffer: 100 mM TAPS pH 8.0; temperature: 25 ℃, solution is purged with argon to remove O_2 and argon flow maintained in headspace thereafter; substrate [α-ketoglutarate] = 40 mM, [NH_4Cl] = 80 mM, [$NADP^+$] = 0 - 25 μM; Potential held at -0.8 V vs. Ag/AgCl (3 M KCl) to drive reduction. Enzyme loading: 17 nmol FNR + 1.7 nmol GLDH (10:1) are mixed and loaded by drop-casting electrode SA: 3.5 cm^2.

Data from the chronoamperogram is shown in table 2.6. To better characterise the efficiency of $NADP^+$ regeneration two new indicators are defined. The NADP efficiency is defined the reaction current per unit of $NADP^+$ and denoted as α. It is intrinsically similar to the turnover efficiency of the cofactor. The normalised α is normalised to the value at median concentration (10 μM) for better comparison.

The data of the table is depicted in figure 2.19, where the current as a function of $NADP^+$ concentration shown as blue bars, along with $NADP^+$ efficiency shown as the red line. From the trend shown in the figure, the overall performance when considering both NADP efficiency and reaction rate (current), is satisfying at the $NADP^+$ concentration between 5 to 12 μM. There is a trade-off between $NADP^+$ efficiency and the reaction rate. A suitable concentration should fit well with the requirement and purpose of specific experiments, i.e. whether the efficiency of cofactor or the overall reaction rate is preferred.

Table 2.6. Efficiency characterisation with different $NADP^+$ concentration

NADP concentration /μM	**Current /μA**	**NADP efficiency = I/NADP**	
		raw value	normalised
0	0	0	0
1	190	190.0	2.89
3	352	117.3	1.78
5	465	93.0	1.41
8	589	73.6	1.12
10	658	65.8	1.00
12	720	60.0	0.91
15	790	52.7	0.80
20	881	44.1	0.67
25	988	39.5	0.60

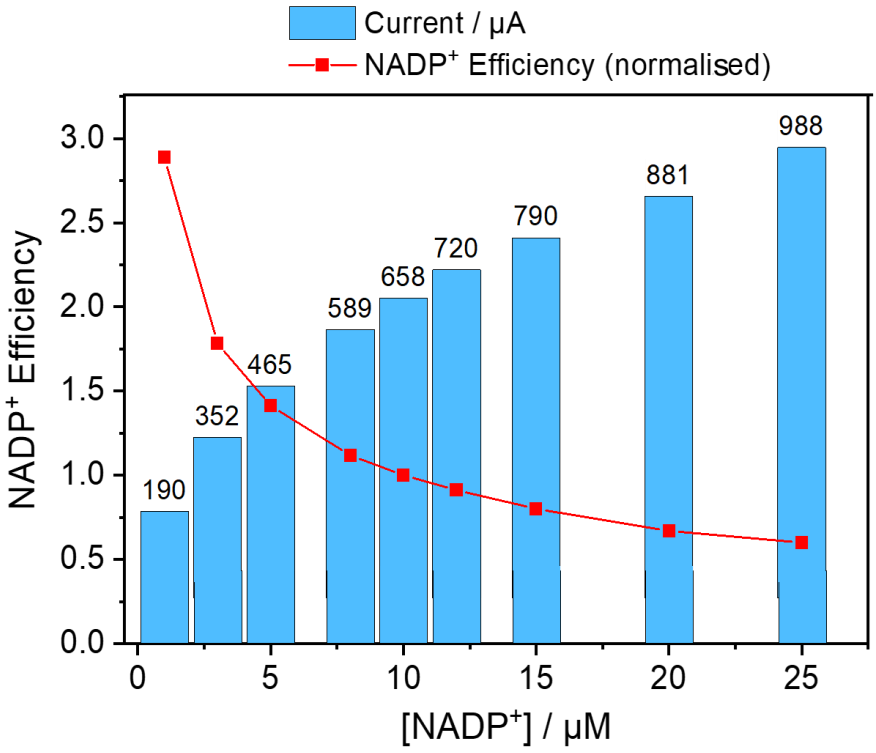


Figure 2.19. $NADP^+$ efficiency with different concentration of $NADP^+$ from figure 2.18. Adapted with permission from B. Cheng *et al*. Copyright 2020, Wiley.[54]

NADP$^+$ titration in ADH-catalysed reduction

The NADP$^+$ titration experiment was carried out with ADH-catalysed reduction as well. Figure 2.20 shows the chronoamperogram of the process. NADP$^+$ is live injected into the reaction solution stepwise up to 100 μM. Data from the chronoamperogram is shown in table 2.7. The current density in ADH reduction is lower comparing to GLDH-catalysed reduction. A relatively higher reaction rate is desired hence the weight parameter in the overall performance β is adjusted to 2. The data of table 2.7 is plotted in figure 2.21, and the trend tells that the overall performance is optimised at a NADP$^+$ concentration between 15 to 30 μM.

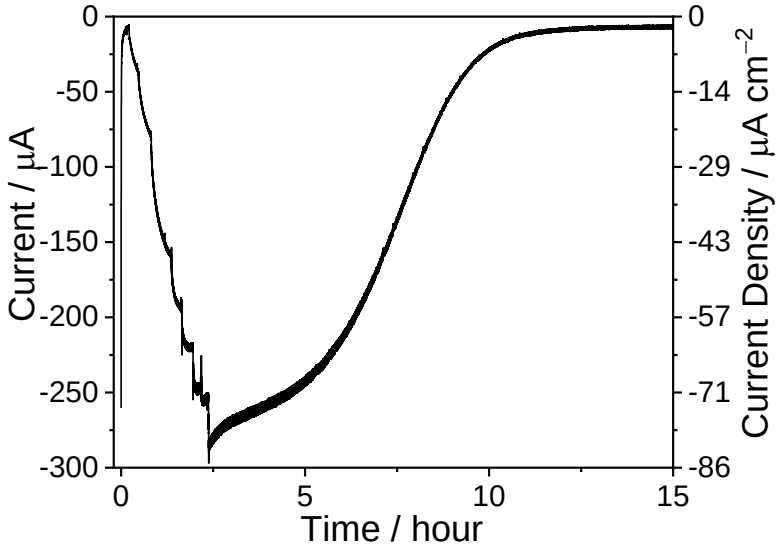


Figure 2.20. NADP$^+$ titration for ADH-catalysed reductive amination. Conditions: solution volume 4 mL, buffer: 50 mM HEPES pH 7.5; temperature: 25 ℃, solution is purged with argon to remove O_2 and argon flow maintained in headspace thereafter; substrate [4-phenyl-2-butanone] = 8 mM, [NADP$^+$] = 0 - 100 μM; Potential held at -0.85 V vs. Ag/AgCl (3 M KCl) to drive reduction. Enzyme loading: 11.4 nmol FNR + 5.7 nmol W110A are stirred together in a 2.5 mL pH 9.0 TAPS solution. electrode SA: 7 cm^2.

Table 2.7. Efficiency characterization with different $NADP^+$ concentration

NADP concentration /μM	**Current /μA**	**NADP efficiency I/NADP**	
		raw value	normalised
0	0	0	0
3	36.4	12.13	1.11
5	79.1	15.82	1.45
10	158.3	15.83	1.45
15	195.9	13.06	1.20
20	17.7	10.89	1.00
30	249	8.30	0.76
50	255.2	5.10	0.47
100	285.1	2.85	0.26

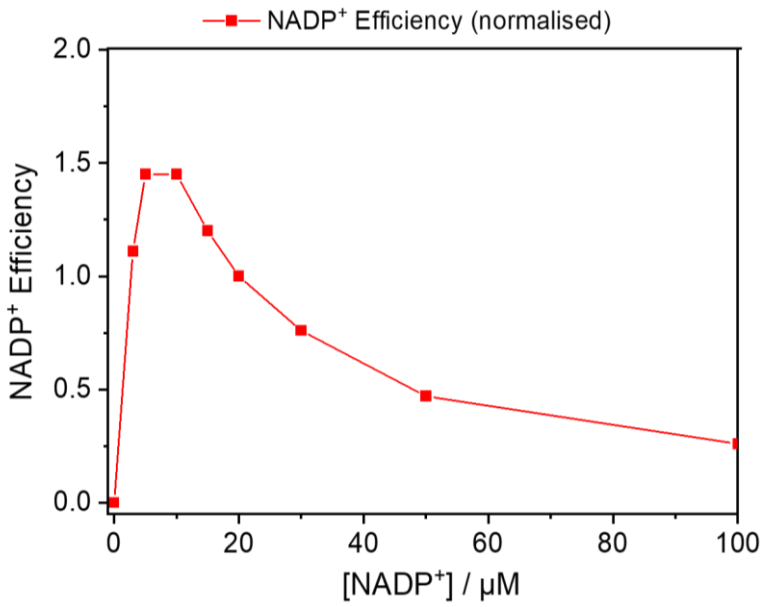


Figure 2.21. $NADP^+$ efficiency with different concentration of $NADP^+$ from figure 2.20.

2.8. Summary

The e-Leaf optimisations presented here are typical ones illustrating the principles used to optimise the system described in subsequent chapters.

The optimisation has covered the electrode support material, ITO coating methods, enzyme loading methods and reaction conditions. Titanium foil proves to be an appropriate support material for the convenience and flexibility. Other materials such as Ti tube and Ti mesh also have the potential to be used for certain circumstances. For ITO coating, EPD is preferred for its efficiency and good reproducibility. Doctor's blade method is also critical in coating electrode with an irregular shape like Ti tube. For enzyme loading, drop-casting and stir-loading are complementary to each other to cope with enzymes of different types with different loading speed to the ITO layer. Pre-loading enzyme before a reaction is preferred since it keeps a cleaner solution condition without redundant enzymes present. Live injection of E2 is also useful in monitoring the loading process and determining the loading time needed for stir-loading. The concentration of cofactor NADP(H) is chosen to be 10 – 20 μM for the experiments in following investigations, which is enough to yield a decent reaction rate while maintaining a good efficiency (total turnover number). The basic construction of the e-Leaf has been explored and initially optimised in preparation for scaling up.

The Design of Experiments (DOE) method can be an effective tool for further experiment optimisation. Design of Experiments is a method that involves the manual selection of variables and the designing of the experiment under statistically optimal conditions given the constraints of available resources.[82] As mentioned in the introduction, optimisation conducted here is a basic 'input to output' test, in which each condition is tested individually. This situation is not identical to the state in the e-Leaf reaction. DOE is a structured statistical approach for collecting data and making discoveries. The use of DOE software can be of great help for future work involving the application-oriented development of the e-Leaf.

CHAPTER III

3. Scaling-up of the Electrochemical Leaf for Biocatalytic Synthesis

3.1. Abstract

This chapter presents the scaling up of the e-Leaf from the initial volume of 4 mL to a 500 mL batch reactor. The model reaction used throughout this chapter is the L-glutamate dehydrogenase (GLDH)-catalysed reductive amination of a-ketoglutarate to L-glutamate, which is well-characterised, and its substrate and product are easily obtained. This work investigates the performance of the e-Leaf and potential challenges in scaling up to identify both advantages and disadvantages of the electrochemical biocatalytic system compared to currently used biocatalytic methods.

Previous e-Leaf work in the group focused on e-Leaf kinetics and the nanoconfinement within the ITO/Ti electrode. The e-Leaf has been coupled with photosensitive material, a fuel cell configuration, developed for deracemisation and with extended biocatalytic cascades.[48,49,51–53,56] These research were typically conducted on a laboratory scale (within 10 mL). It is important to establish the feasibility of scaling up the existing electrochemical leaf system considering its potential application for synthesis of pharmaceuticals. The e-Leaf on a large scale can benefit complex biocatalysis of high-value chemicals that otherwise require separate multiple steps in conventional biocatalytic process.[60]

The work described includes optimisation of electrode construction and reaction condition, the design of a large-scaled electrochemical cell and scaling up of the e-Leaf electrode. The key steps are the design of electrochemical cells for larger scale and the construction of working electrodes with high geometric surface area. Results show that the e-Leaf has been successfully scaled up to 0.5 L with an electrode surface area of 525 cm^2. The experiment converted >99% of 20 mmol of alpha-ketoglutarate (close to 3 grams) to L-glutamic acid with TTN of NADP(H) being 4000 within 1.5 days. The L-glutamic acid crystals were separated with a purity of >99%. The highest TTN of 10,800 was achieved in a 40 mL model reaction. The results prove the feasibility of scaling up

the e-Leaf for industrial level synthesis. The potential application (product separation, cost calculation) and challenges (limitations and improvements) are also discussed.

3.2. GLDH-catalysed Reaction

3.2.1. GLDH: The Model Reaction

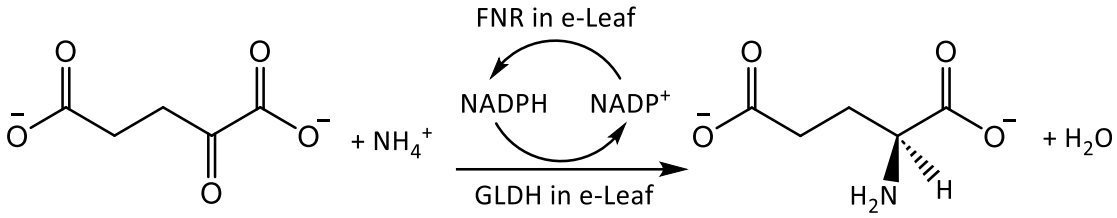


Figure 3.1. The reductive amination of α-ketoglutarate catalysed by GLDH

As mentioned in chapter1, GLDH catalyses the conversion of α-ketoglutarate to L-glutamate in the presence of NH_4^+ and NADPH (figure 3.1). This reaction is chosen as the model reaction because the substrate and product are easily detected and quantified and are commercially available. The solubility of the substrate (disodium 2-ketoglutarate dihydrate) in water is high at 1 M, which allows a batch reaction investigation with a longer reaction time thus also informing on the stability of the system. In addition, GLDH is a well-characterised enzyme, and its mechanism and kinetics are established. The enzyme has K_m values of 2.4 ± 0.8 mM, 6.5 ± 1.8 mM and 0.022 ± 0.007 mM for 2-oxoglutarate, NH_4^+ and NADPH respectively.[69] Robustness and efficiency make GLDH and its reaction a suitable test model for scale up work. Published kinetic data for GLDH measured by conventional means can vary greatly with conditions, so solution assay tests were conducted under conditions close to the electrochemical experiments.[69,83,84]

3.2.2. Kinetics by Solution Assay

The activity of GLDH has been measured by traditional solution assay (data plot is shown in figure 3.2 panel (a)). Tests were conducted at a steady-state approximation condition, as the enzyme concentration was relatively low with a high substrate

concentration (detailed data in figure 3.2 reaction conditions). Data points of reaction rate vs. substrate concentration were fitted to equation 3.1.

$$v = \frac{v_{max}[s]}{Km+[s]+\frac{[s]^2}{K_i}} \qquad (3.1)$$

where v is the reaction velocity, v_{max} is the maximum reaction velocity, K_m is the Michaelis constant, $[s]$ is the concentration of the substrate, and K_i is the substrate inhibition constant. This equation was chosen because based on initial results, it was clear that GLDH exhibited substrate inhibition. The fitted result gives k_{cat} (v_{max} / [GLDH]) 68.7 s^{-1}, K_m 0.5 mM and K_i 6.3 mM, respectively. Figure 3.2 panel (b) shows a comparison with limited cofactor concentration. The v / [GLDH] is defined as normalised k term in order to compare with the data shown in panel (a). The overlaid data points show that at lower values of [NADPH] (approx. 20 μM), the rates are similar to those measured with [NADPH] = 300 μM. The lower value of cofactor concentration is close to the actual experimental conditions in scaling up tests.

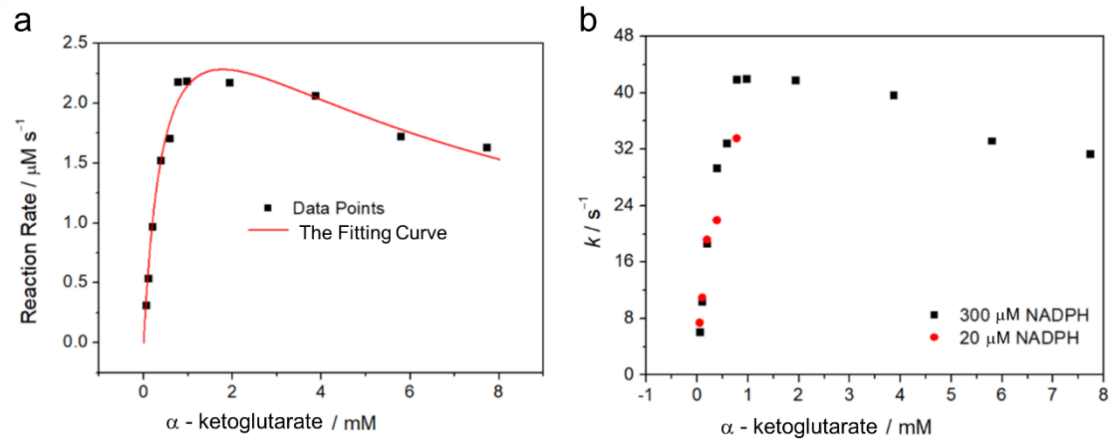


Figure 3.2. GLDH-catalysed reductive amination of α-ketoglutarate monitored in solution by UV-VIS spectroscopy. Initial reaction rates were calculated as the rate of change in A_{340} attributable to the consumption of NADPH (using the 'Timedrive' mode of the Perkin-Elmer Lambda UV-vis spectrometer). **a)** Measurements carried out with [NADPH] = 300 μM and [GLDH] = 52 nM and fitted to equation 1.1 **b)** Comparison experiment from a more cofactor-limited solution assay. Results plotted in red obtained with [NADPH] = 20 μM and [GDLH] = 26 nM. Experimental conditions: temperature: 22℃, [NH_4Cl] = 19.3 mM, cuvette cell volume = 400 μL, 100 mM TAPS pH 8.0. Adapted with permission from B. Cheng *et al*. Copyright 2020, Wiley.[54]

3.3. Optimisation Before Scaling-up

In the process of scaling up the e-Leaf, there are many conditions which need to be considered in addition to the obvious parameters of electrode size and reactor design, such as reaction conditions and enzyme loading method. These conditions were optimised before scaling up as this was more convenient than carrying out on a large scale. In previous chapter, different electrode supporting materials, ITO coating methods and enzyme loading methods have been tested and compared. This section shows the optimisation specific to e-Leaf scaling-up of this chapter, including electrodes in larger sizes, enzyme loading amount and ratio, and pH buffering.

3.3.1. Electrode Design and Scale with Enzyme Loading methods – Ti foil

Among all the accessible supportive material (Ti foil, Ti tube, Ti mesh, Ti foam, Ti wire and carbon cloth), Ti foil stands out as the best choice for scaling up due to its regular shape, high customisability, ease of ITO coating and enzyme loading and convenience in positioning in larger cells. Several typical standard Ti foil designs made during the trial of scaling up are shown in figure 3.3. with corresponding enzyme loading methods shown in figure 3.4.

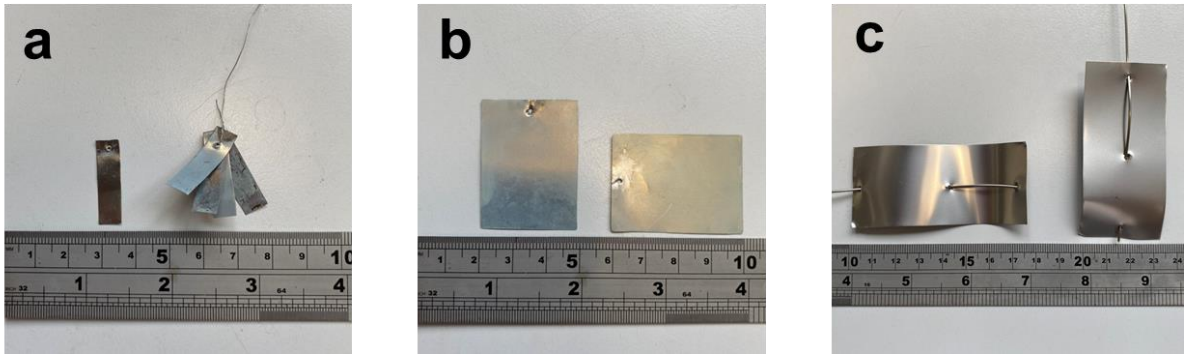


Figure 3.3. Photos of three typical Ti foil configurations of different sizes. **a)** 2.5 cm * 0.7 cm Ti foil. **b)** 3.5 cm * 3.5 cm Ti foil. **c)** 7.5 cm * 3.5 cm Ti foil.

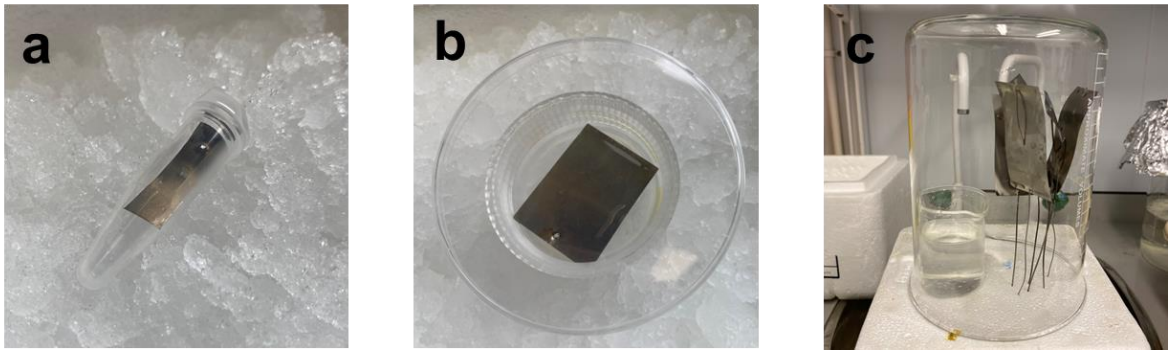


Figure 3.4. Enzyme loading methods based on electrode shapes and sizes. **a)** Holding in Eppendorf tube (2.5 cm * 0.7 cm Ti foil). **b)** Holding in a plastic cap covered by a plate (3.5 cm * 3.5 cm Ti foil). **c)** Fixing in isolated space at 4 ℃ (7.5 cm * 3.5 cm Ti foil).

1) A 2.5 cm * 0.7 cm Ti foil with geometric SA of 3.5 cm^2 is shown in figure 3.3 panel (a); an electrode of this size is used in the original electrochemical cell with a reaction volume of 4 mL. Multiple Ti foils can be wired together as a 'booklet' to increase the total surface area, making good use of the space of the cell. The length of 2.5 cm was decided based on the height of 4 mL solution in the 4 mL cell and the width was decided based on the diameter of the cell's main compartment. The ITO covered part of the electrode is able to be submerged under the solution level in the cell. Electrophoretic deposition is used for ITO coating on this Ti foil, and multiple (up to 7) pieces of foil can be coated at the same time. For enzyme loading, both drop-casting and stir-loading are available for this electrode. In stir-loading, Ti foils are submerged in a stirred solution containing enzyme(s) at the desired concentration and ratio, typically a small glass tube with 2.5 mL enzyme solution. For drop-casting (figure 3.4 panel (a)), typically 5 - 15 μL of enzyme solution is dropped on both sides of the foil, and the foil size is well suited for it to be held in an Eppendorf tube on ice, which is to prevent the enzyme solution from drying out by water evaporation.

2) A 3.5 cm * 3.5 cm Ti foil with SA of 24.5 cm^2 is shown in Figure 3.3 panel (b). Electrode of such size is used in the moderate-sized electrochemical cell with a volume of 50 mL. Up to 4 pieces of such Ti foil can be well arranged in the cell to achieve good mass transfer which does not limit the current. The length of 3.5 cm was decided based

on the diameter of the cell's main compartment. Electrophoretic deposition is also used for ITO coating on this Ti foil. Even though multiple (up to 4) pieces of such foils can be coated at the same time, the coating is often one at a time for precision and consistency. For enzyme loading, Ti foil with a larger surface area is optimally loaded by drop-casting rather than stir-loading since the loading solution volume would increase a lot more in order to cover the increased surface area of electrode. For drop-casting (Figure 3.4 panel (b)), 84 μL of enzyme solution is dropped on both sides of the foil, and this foil size fits well in a shallow cap placed on ice and covered by a plastic plate to prevent drying out by water evaporation.

3) A 7.5 cm * 3.5 cm Ti foil with SA of 52.5 cm^2 is shown in figure 3.3 panel (c). This electrode is the largest and was used in the 0.5 L electrochemical cell. In the final experiment of 0.5 L reaction, 10 pieces of this foil were used but there is still space for the arrangement of more electrodes to achieve a higher reaction rate. The length and width were decided based on the size of the 0.5 L reactor. Electrophoretic deposition was used for ITO coating on this Ti foil. Drop-casting was the chosen method for enzyme loading on these large-scale electrodes; 180 μL of enzyme solution was dropped on both sides of the foil. The foils were held in an isolated space at 4 ℃ to prevent electrode drying during enzyme loading from water evaporation (figure 3.4 panel (c)).

3.3.2. Enzyme Ratios (FNR to GLDH), $NADP^+$ and pH

(1) FNR to GLDH Enzyme Ratio

The optimisation of loading ratio of FNR to GLDH and loading amount has been described in chapter 2 (section 2.6). The corresponding cyclic voltammograms are shown in figure 3.5. The red and blue traces show the turnover current when GLDH and FNR are coupled through the interconversion of NADP(H). It is noteworthy that a 10:1 ratio for FNR:GLDH has the best catalytic activity for reduction. This ratio gave the highest peak currents in both stationary and stirring conditions. This is thought to be due

to the fact that GLDH is a 'fast' enzyme, so more FNR is needed to match its catalytic speed.[1,85] The shape of the CV curves also confirmed that the reactions were FNR-limited since the current did not plateau at the negative end of the scans. The reaction was still FNR-limited even at 10:1 ratio, which indicates that there was still potential to improve the peak current with a higher FNR to GLDH ratio.

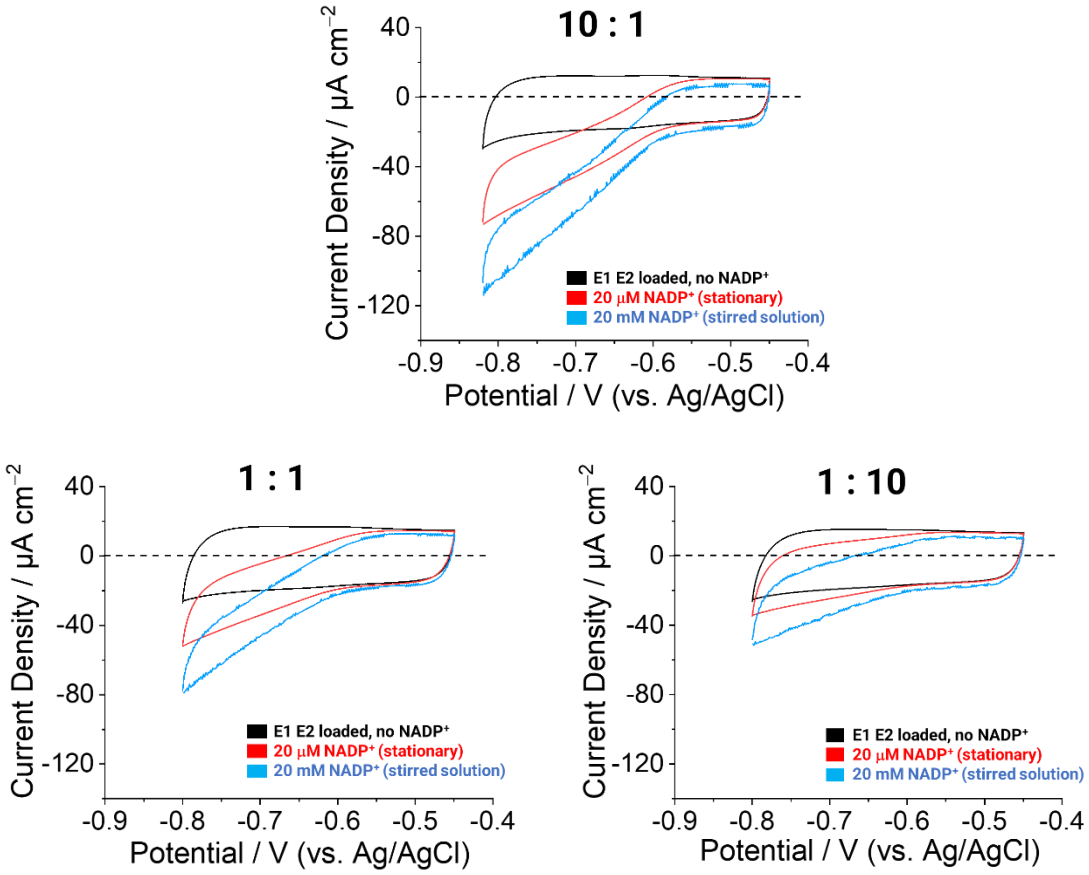


Figure 3.5. FNR:GLDH ratio investigated by cyclic Voltammetry. Three different FNR to GLDH ratios (10:1, 1:1, 1:10) corresponding to the chronoamperograms shown in figure 2.14, recorded independently. **Conditions:** solution volume 4 mL, buffer: 100 mM TAPS pH 8.0; temperature: 25 ℃, before measurement, solution was purged with argon to remove O_2 and argon flow maintained in headspace thereafter. substrate [α-ketoglutarate] = 8 mM, [NH_4Cl] = 16 mM, [$NADP^+$] = 20 µM. Electrode SA = 3.5 cm^2; enzyme amounts applied: 7.3 nmol FNR + 0.73 nmol GLDH (10:1); 4.02 nmol FNR + 4.02 nmol GLDH (1:1); 0.73 nmol FNR + 7.3 nmol GLDH (1:10); scan rate: 4 mV/s; solution stirred using a magnetic flea (400 rpm). Adapted with permission from B. Cheng et al. Copyright 2020, Wiley.[54]

(2) NADP(H) concentration in reaction

The optimisation of NADP(H) concentration for the GLDH-catalysed reduction has been described in chapter 2 (section 2.7.2). With the trade-off between current per unit $NADP^+$ and overall reaction rate considered, the optimal range for cofactor concentration is approximately 5 to 20 μM. The high efficiency due to the nanoconfined regeneration system and its requirement for very low concentrations of cofactor (uM levels) are advantages in scaling up, as the cost of cofactor can be a limiting issue for scaling up without efficient regeneration or under a bulk amount use in batch reactions.

(3) Reaction pH

The pH of the reaction can directly affect the activity of the enzymes and therefore the overall performance. Based on previous work, the reductive animation catalysed by GLDH works efficiently at pH 7 to 9.[69] Buffer used in the scaling up experiments are mostly HEPES, which has a buffering range of pH 6.8 to pH 8.2, a pH of 7.5 was chosen for the following tests. Interestingly, a unbuffered reaction has been trialled in the later 0.5 L reaction work to facilitate better product separation. The post reaction solution was less coloured, and the product separation was easier. Details are shown in later section on product separation.

3.4. Cell Design and Reactions in Scaling-up

3.4.1. 4 mL Prototype Cell Design and Reaction

Cell design

The 4 mL cell setup is shown in Figure 3.6. It is the classic cell design for the three-electrode system described in chapter 1. As mentioned, it is the starting point and benchmark for subsequent reactors of larger sizes and reactions in those cells. The typical Ti foil electrode used in this cell has a size of 0.7 cm * 2.5 cm.

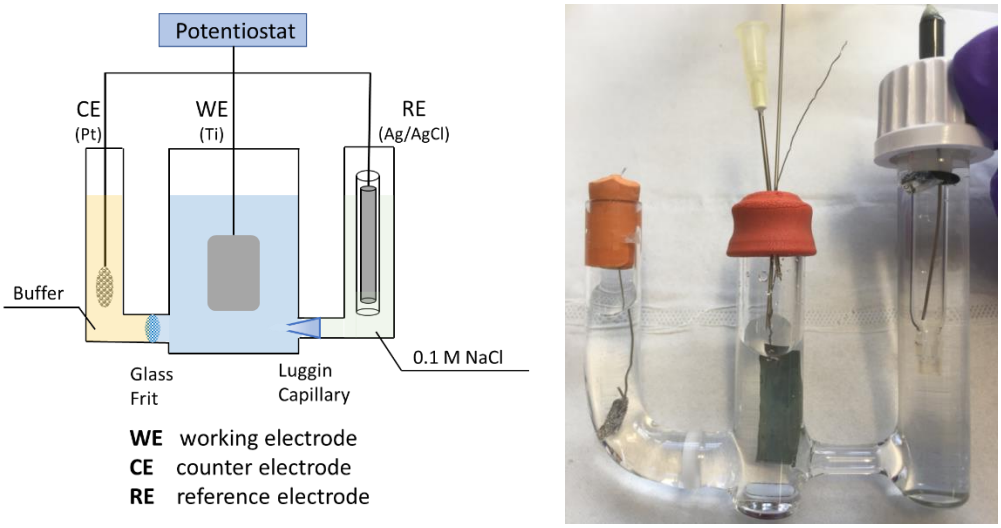


Figure 3.6. Sketch for the three-electrode system (left) and photo of the electrochemical cell (right).

Reaction

The chronoamperogram of the conversion of a-ketoglutarate to L-glutamate catalysed by GLDH in the 4 mL cell is shown in figure 3.7. Enzymes (FNR+GLDH) were loaded by drop-casting. Cofactor ($NADP^+$) and all substrates for GLDH are in the cell solution before the reaction is initiated by applying a potential of -0.82 V vs Ag/AgCl (3 M KCl). The initial current was high and remained steady for approximately 5 hours at which point it dropped swiftly due to the depletion of substrate, reaching zero after approximately 9-10 hours upon complete substrate depletion.

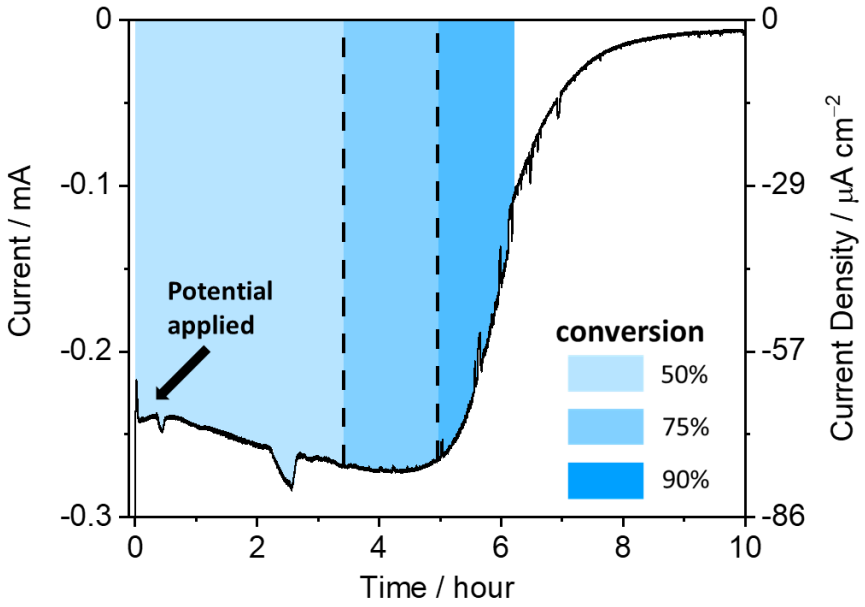


Figure 3.7. Reductive amination of α-ketoglutarate catalysed by GLDH in a 4 mL cell, with the percentage conversion marked based on charge pass. Conditions: solution volume 4 mL, buffer: 100 mM TAPS pH 8.0; temperature: 25 ℃, solution is purged with argon to remove O_2 and argon flow maintained in headspace thereafter; substrate [α-ketoglutarate] = 8 mM, [NH_4Cl] = 16 mM, [$NADP^+$] = 20 μM; Potential held at -0.82 V vs. Ag/AgCl (3 M KCl) to drive reduction. Enzyme loading: 7.3 nmol FNR + 0.73 nmol GLDH (10:1), mixed and loaded by drop-casting; electrode SA: 3.5 cm^2. Adapted with permission from B. Cheng *et al*. Copyright 2020, Wiley.[54]

The charge passed was used to estimate the change of product and substrate. In the ^1H NMR, the characteristic peaks of L-glutamate are masked by peaks attribute to TAPS buffer salt. The final conversion is 94.0% by coulometry (5.8 C charge pass). The peak current density is 84 mA cm^{-2}; 32 μmol substrate is converted within 10 hours and 90% is consumed in 6 hours. The total turnover number (TTN) of $NADP^+$ cofactor is 396. The TTN of cofactor was calculated as:

$$\text{TTN of cofactor (NADP(H))} = \frac{[\text{Product yield}]}{[NADP(H)]} \quad (3.2)$$

The amount of working enzyme on the electrode is estimated on the assumption that the enzyme per surface area of electrode is 110 pmol cm^{-2}. This number is determined in chapter 2 (section 2.3.2), where the amount of FNR loaded on electrodes with different ITO loading times are calculated from non-turnover peaks assuming the nanopores on the electrode are saturated with enzyme molecules. Since the ratio of FNR to GLDH is

10:1, the working amount of loaded FNR is estimated to be 100 pmol cm^{-2} and GLDH 10 pmol cm^{-2} assuming that the enzyme ratio present in the loading solution is the same as in the pores.[48] The estimation is based on the assumption though, it is accurate in regard to magnitude and the total turnover numbers of the two enzymes. The TTN for GLDH is 8.2 * 10^5 and the TTN for FNR is 8.2*10^4. These very high TTN values demonstrate the benefit of the nanoconfined system where low amounts of enzymes used are present at very high local concentration in the pores making the system highly efficient. This 4 mL reaction is a good benchmark and starting point for the scale up work.

3.4.2. Intermediate 40 mL Cell Design and Reaction

Monolith Cell design

This design of the intermediate-sized reactor is the first attempt in making a larger-scaled electrochemical cell for the e-Leaf. Intuitively, a conservative design was adopted such that the cell was made as an enlarged replicated version of the 4 mL cell with little change in the configuration of the key parts. The sketch and photo are shown in figure 3.8.

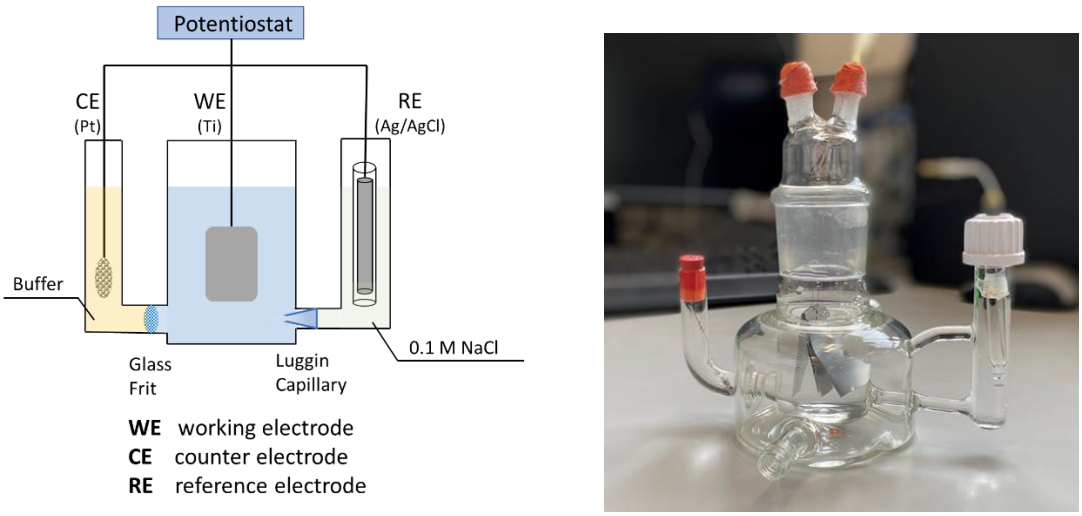


Figure 3.8. Sketch and photo of the moderate-sized electrochemical cell

The main chamber is connected by two side arms which are holding counter electrode and reference electrode separately. A glass frit is used to partition the counter electrode (Pt mesh) side arm separating it from the bulk solution because the crossing-over of substrate from the bulk solution can cause inaccuracy in quantifying the composite of reaction solution. The Pt mesh has a large surface area to ensure CE is not limiting the current. A Luggin capillary is used to electrically connect the reference electrode (Ag/AgCl) side arm with the bulk solution. A water jacket around the main compartment controls the temperature by connection to a circulating water bath. Comparing to the 4 mL cell, this enlarged version has side arms of similar sizes but the main compartment is larger and can hold up to approximately 55 mL and electrodes in a larger number and of a higher surface area. The reaction solution can be agitatated by a stirring flea, and argon purging in the head space is still an option in this cell. This design was focused on making a larger reaction chamber, the core part of a cell, assuming that the working situation in CE and RE parts will not differ a lot from that in small scale cell.

Problems and challenges

The cell worked satisfactorily when the reaction current was relatively low, with an electrode of 3.5 cm^2 for instance. As shown in figure 3.9, in experiments with high current, a flat current occurs when the counter electrode and working electrode are in separate compartments (black trace). The coupled current returned to the expected value after the working and counter electrode were put in the same chamber. The current flow between the counter electrode and the working electrode was limited in such cell configuration where the two electrodes are separated. This limitation could be related to the counter electrode, where counter reaction (H^+ production) is not efficient enough to balance the reduction on the WE. The pH of the solution was set to favour the WE reaction (reduction), which could also slow down the oxidation on the CE. This problem could be solved by increasing the SA of counter electrode and adjust the pH in the compartment to favour the oxidation. Another possible cause for the current

limitation could be the distant position between CE and WE, which could be solved by bringing closer the two electrodes. The increase of scale from 4 mL to 40 mL suggests that the scaling up of an electrochemical cell was more complex than a direct enlargement of each compartment, with challenges involving the configuration of the three-electrode system. Further improvement is discussed in following sections.

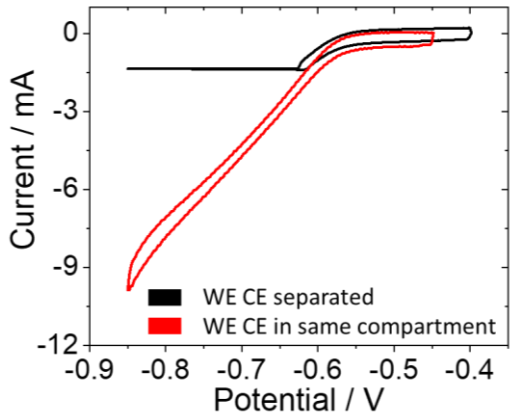


Figure 3.9. Cyclic voltammograms when CE and WE are separated vs. in the same compartment. Conditions: cell volume: 40 mL; 100 mM TAPS pH 8.0; temperature: 25 °C, [α-ketoglutarate] = 40 mM, [NH_4Cl] = 80 mM, [$NADP^+$] = 20 µM; CV Scan rate: 4 mV/s; Electrode SA = 38.5 cm^2; enzyme amounts applied in loading: 186 nmol FNR + 18.6 nmol GLDH. Agitation by stirring at 400 rpm.

40 mL Reactor with modular compartment

To address the limiting current issue, a modular approach was designed where a holder for the counter electrodes was introduced to the cell. As shown in figure 3.10 panel (a), an interchangeable glass holder was designed, which was a glass tube with one end sealed with glass frit. It is a replacement for the CE side arm. The cell configuration is shown as figure 3.10 panel (b), unlike in the initial monolith cell, the interchangeable holder for counter electrode is placed in the main chamber, allowing the counter electrode to be placed very close to the working electrode while maintaining the separation from the bulk solution.

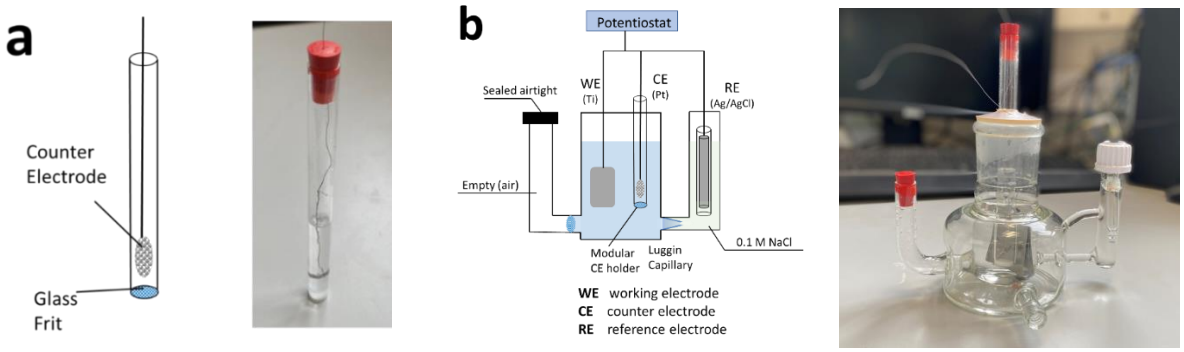


Figure 3.10. Sketch (left) and photo (right) of **a)** the modular holder for counter electrode and **b)** moderate-sized electrochemical cell with modular counter electrode holder.

The chronoamperogram for the GLDH-catalysed reaction using the moderate-scale reactor (40 mL) is shown in figure 3.11. Enzymes (FNR+GLDH) were loaded by drop-casting. All substrates for GLDH are in the cell solution before the reaction was initiated by a live injection of 10 μM of $NADP^+$. The initial current was high and remained steady for approximately 6 hours at which point it dropped swiftly due to the depletion of substrate, reaching zero after approximately 9-10 hours upon complete substrate depletion.

The coulometry shows a conversion >99%. Comparing to the benchmark reaction in the 4 mL cell, the experiment in the moderate-sized reactor has achieved a similar current density 93 μA cm^{-2}, and a higher TTN of cofactor of 1000 (comparison of experiments at different scales is listed in table 3.1). The TTN for GLDH is $1.4 * 10^6$ and the TTN for FNR is $1.4*10^5$. The result proved the feasibility of scaling up the e-Leaf from a 4 mL reactor to 40 mL.

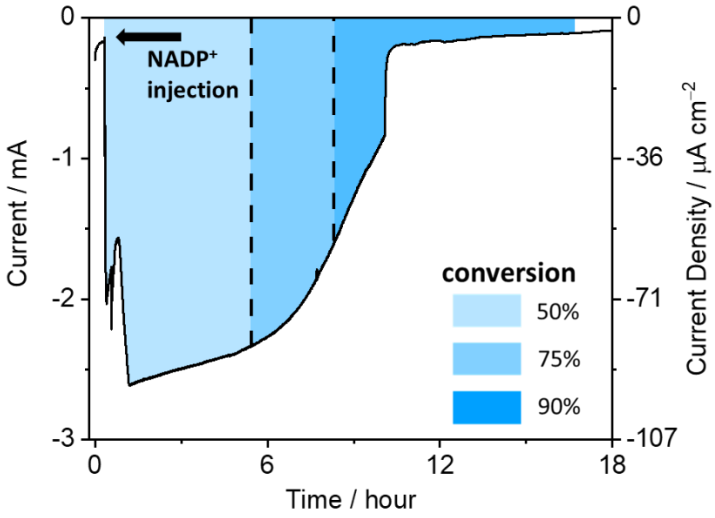


Figure 3.11. Reductive amination of α-ketoglutarate catalysed by GLDH in a 40 mL cell, with the percentage conversion marked based on charge passed. Conditions: solution volume 40 mL, buffer: 100 mM TAPS pH 8.0; temperature: 25 ℃, solution is purged with argon to remove O_2 and argon flow maintained in headspace thereafter; substrate [α-ketoglutarate] = 10 mM, [NH_4Cl] = 20 mM, [$NADP^+$] = 10 µM; Potential held at -0.8 V vs. Ag/AgCl (3 M KCl) to drive reduction. Enzyme loading: 58.7 nmol FNR + 5.9 nmol GLDH (10:1), mixed and loaded by drop-casting electrode SA: 28 cm^2.

Residual Current

A new issue was also observed from this chronoamperogram (figure 3.11): the current did not return to zero at the end of the reaction. There was a residual current which may be the baseline current throughout the whole process of reaction. This baseline current is caused by any oxygen present being reduced at the electrode which would contribute to the coulometry causing an overestimation of conversion. The faradaic efficiency becomes lower in this case. The oxygen could come from the (now empty) side arm which was used to hold counter electrode or simply from surrounding space due to poor sealing. With reactor size being scaled-up and a modular compartment used, the air-tight sealing becomes challenging and the previous argon-purging method for smaller cells may not keep an oxygen free condition in the larger cell thus longer purging time and better sealing methods were applied in subsequent work.

Reaction with highest TTN of $NADP^+$

Figure 3.12 shows another experiment in the moderate 40 mL reactor, which gave a TTN of $NADP^+$ of 10,800. This TTN is one of the highest ever achieved in this nanoconfined cofactor regeneration system: 2.38 mmol (0.45 g) of product L-glutamate was produced in 22 hours catalysed with only 5 μM $NADP^+$ in the bulk solution. The charge passed shows a conversion of 94.7%. Previous work reached a similar TTN (12,000) in small-scale reactor of 4 mL when coupling the e-Leaf in a hydrogen fuel cell configuration.[52] The results shows that the high efficiency of the e-Leaf in regenerating cofactor was maintained in its scaled-up version.

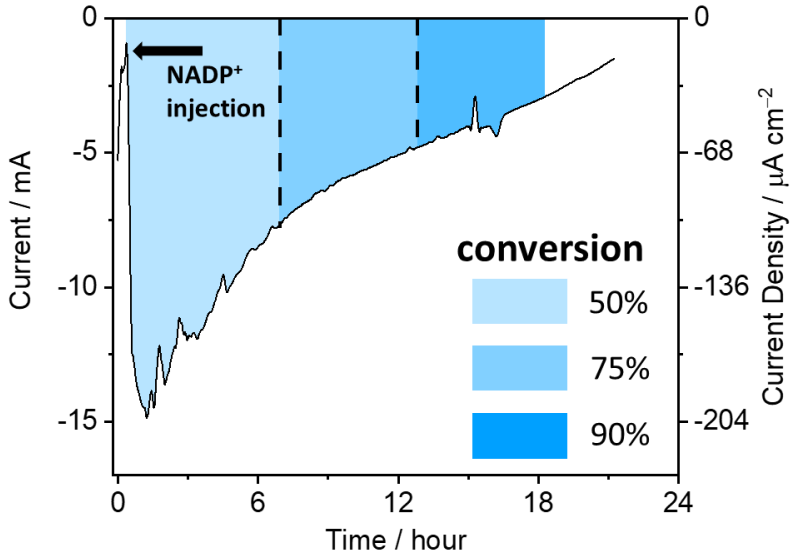


Figure 3.12. Reductive amination of α-ketoglutarate catalysed by GLDH in a 40 mL cell, with the percentage conversion marked based on charge pass. Conditions: solution volume 44 mL, buffer: 100 mM TAPS pH 8.0; temperature: 25 ℃, solution is purged with argon to remove O_2 and argon flow maintained in headspace thereafter; substrate [α-ketoglutarate] = 60 mM, [NH_4Cl] = 120 mM, [$NADP^+$] = 5 μM; Potential held at -0.82 V vs. Ag/AgCl (3 M KCl) to drive reduction. Enzyme loading: 355 nmol FNR + 35.5 nmol GLDH (10:1), mixed and loaded by drop-casting electrode SA: 73.5 cm^2.

Unstable current

The timecourse in this experiment differs from the previous two reactions. Instead of being steady before a sharp decrease caused by substrate depletion, the current starts from a peak value and keeps decreasing steadily as the reaction proceeds; there was

no sharp decrease upon depletion. The first possible cause could be related to the concentration of cofactor. The reactions shown in figure 3.7 and 3.11 used 20 and 10 μM $NADP^+$ respectively whereas the reaction presented here in figure 3.12 used 5 μM $NADP^+$. Mass transfer could be insufficient in a larger reactor with lower concentration of cofactor if the stirring is not enough. In addition, $NADP^+$ may degrade over the reaction course. This can be more obvious when it is of a lower amount that the reaction can become cofactor-limiting.

3.4.3. Large-scale Modular Cell Configuration (80 mL)

One of the challenges to scale up an electrochemical cell is the cost and inconvenience of making a new cell (which requires specialist glass blowing) of different volume size each time a new scale is to be investigated. This becomes less practical and economical when the cell size is larger. A flexible and economical way of inventing and investigating larger electrochemical cells is therefore required.

Modular electrochemical cell design is a feasible way to move forward. Inspired by the modular compartment made for the moderate-sized cell (40 mL), a new electrochemical cell was designed by combining separate interchangeable compartments. The configuration is shown in figure 3.13. The same interchangeable container was used for the counter electrode. The container served the same purpose as the side arms on the initial cell design. The CE is held in a glass tube with glass frit on the top allowing ion interchange for current to pass. The main compartment holding the working electrode and reactants is also interchangeable. Vessels of different shapes and sizes can serve as the reactor with the condition that the CE and RE containers fit well to avoid O_2 entry.

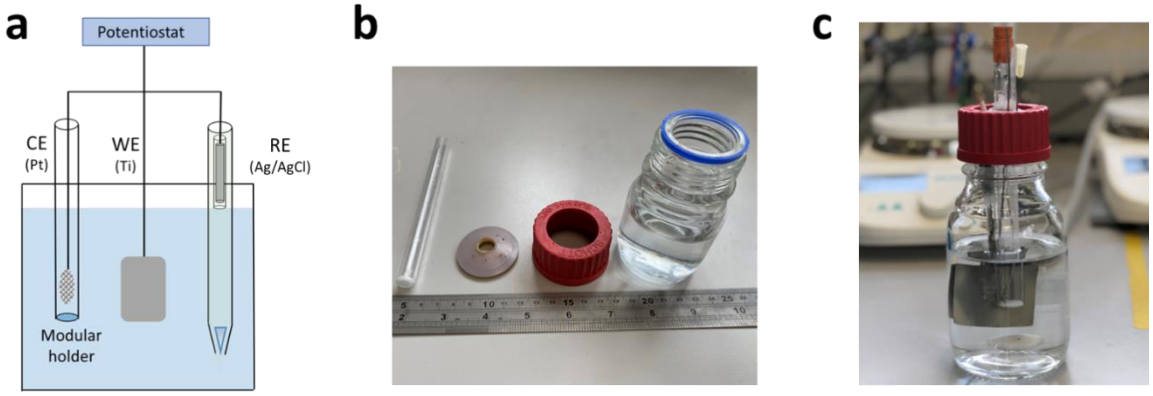


Figure 3.13. Schott bottle Modular Reactor **a)** configuration sketch **b)** cell compartments (from left: CE holder, silicone septa for sealing, bottle cap with opening, a Schott bottle as the main body of the reactor). **c)** Photo of assembled reactor

Modular design does not require manufacturing a customised cell, but only two modular containers. They can be easily forged and integrated to any vessel to work as an electrochemical cell. For instance, these modular compartments can be integrated with 50 – 500 mL Schott bottles, beakers, and other larger containers like coffee jars (500 mL reaction in section 3.4.4). These readily acquirable modular parts have opened the gate towards e-chem reactors of different sizes and for diversified purposes.

80 mL Reaction

One of the experiments conducted in the modular cell (80 mL) is shown in figure 3.14, again using the test reaction catalysed by GLDH. Substrates at 40 mM and 10 μM $NADP^+$ were present in the solution of 80 mL before the reaction was initiated. The current is at a high level and remains steady from the start and throughout the reaction progress, and eventually drops sharply due to the depletion of substrates. The charge passed shows a conversion of >99% and 98.4% respectively. By comparing with the benchmark reaction in the 4 mL cell, this 80 mL experiment in the modular reactor has achieved a slightly higher steady current density at approximately 100 μA cm^{-2}. The TTN of $NADP^+$ being 1970. The TTN of GLDH is 4.5 $*10^6$ and the TTN of FNR is 4.5 $*10^5$, which proves the reliability and consistency of this modular cell and the feasibility of scaling up the e-Leaf from 4 mL to 80 mL. It is worth pointing out that this reaction has a

relatively steady current at similar low cofactor concentration (10 μM) and high substrate concentration (40 mM) comparing with the previous reaction with decreasing activity in figure 3.12. The hypothesis on the cause for unstable timecourse is improved based on this result. The cause then could be more of an unrepeatable artificial one, such as poor ITO coating on the electrode causing the ITO falling off, or the poor quality of enzyme batch, or a poor enzyme loading process.

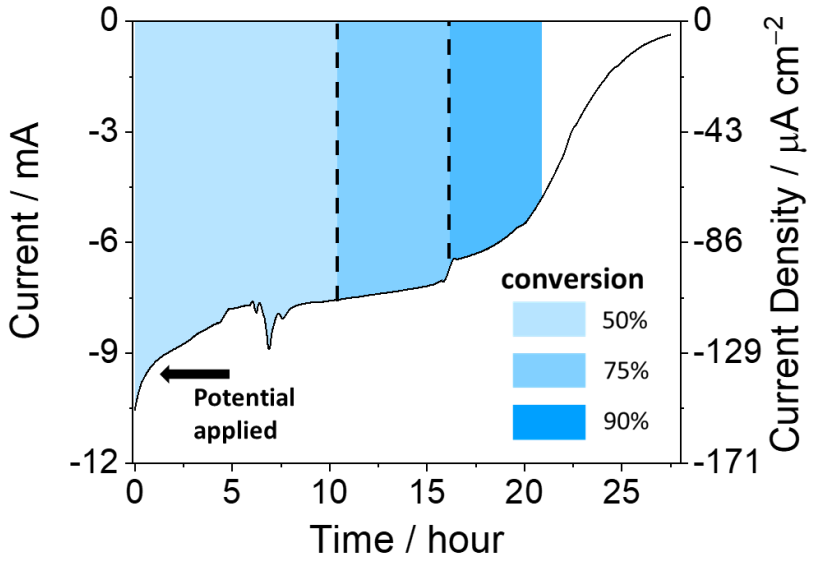


Figure 3.14. Reductive amination of α-ketoglutarate catalysed by GLDH in an 80mL cell, with the percentage conversion marked based on charge pass. Conditions: solution volume 80 mL, buffer: 100 mM TAPS pH 8.0; temperature: 25 ℃, solution is purged with argon to remove O_2 before reaction and argon flow maintained in headspace thereafter; substrate [α-ketoglutarate] = 40 mM, [NH_4Cl] = 80 mM, [$NADP^+$] = 10 μM; Potential held at -0.82 V vs. Ag/AgCl (3 M KCl) to drive reduction. Enzyme loading: 348 nmol FNR + 34.8 nmol GLDH (10:1), mixed and loaded by drop-casting electrode SA: 70 cm^2. Adapted with permission from B. Cheng *et al*. Copyright 2020, Wiley.[54]

3.4.4. Large-scale Bulk Synthesis in a 0.5 Litre Reaction

The target of scaling up the e-Leaf at the research lab level is to make it a successful 'pilot' experiment for the industrial level. This final section is a scaled-up e-Leaf to 0.5 L with modular cell configuration and electrode with increased surface area. As shown in figure 3.15, the open glass frit side of the CE holder has been increased in area to avoid possible current limitation between CE and WE as the working electrode surface area was further increased. This glass frit was changed to Nafion membrane (details in

chapter 7) after the first trial experiment which used a glass frit (shown below); Nafion membrane has a small molecular cut-off and can serve as a partition allowing only H^+ exchange without limiting the increased current, which is effective in preventing product from going into the side arm and being lost reactin g on the CE. The membrane also prevents impurities formed on counter electrode transferring to the main compartment. The RE holder was designed to be a glass tube holding the electrode, with a Luggin capillary on the top, allowing extremely low current pass and prevent most mass interchanges whilst maintaining conductivity.

A new electrochemical cell was designed and made by repurposing a coffee jar. The jar holds a volume of approximately 1L which is suitable for holding 500 mL of solution. Holes were drilled in the cap to fit multiple glass joints as openings which are to fix modular holders and electrical wires in use. The homemade coffee jar reactor is a typical case showing the flexibility of modular cells. The Ti foil electrodes used in this cell can have a surface area of up to 52.5 cm^2 as shown in the photo. Oxygen evolution, as one of the half reaction happening on the counter electrode, starts to become an issue in the large-sized reactor. In a small electrochemical cell, gas forming on the counter electrode (hydrogen or oxygen evolution) is slight, but it becomes observable in the larger-sized cells with reactions of higher currents. The counter electrode, usually of a large surface area in order to support the current generated for the working electrode, has the equally high current as the working electrode, producing the gas at a much higher rate. The liquid level in the counter electrode is dropping at approximately 0.5 mL/hour. The percentage of the current through counter electrode attribute to the electrolysis of water is less than 2% based on estimation. The CE holder therefore is usually replenished with buffer every 12 hours to prevent disconnection caused by liquid level drop.

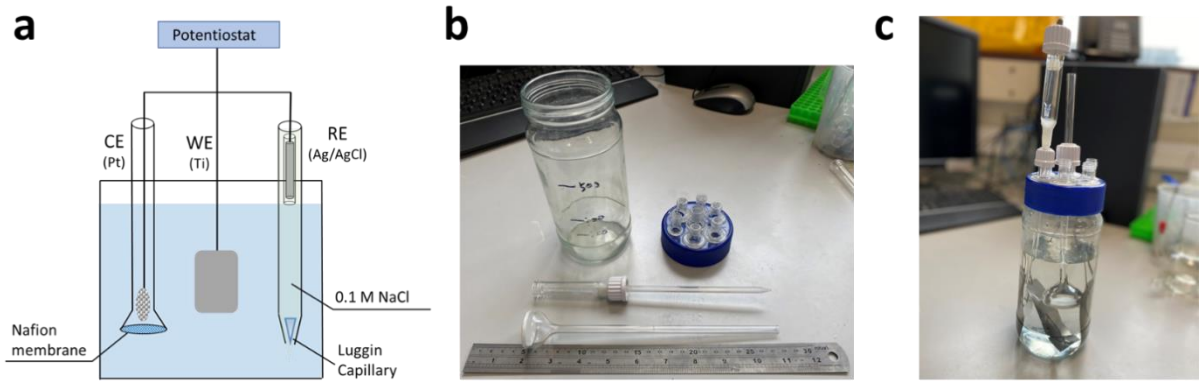


Figure 3.15. Modular coffee jar reactor 0.5 L **a)** configuration sketch **b)** cell compartments (from top: the jar (left), cap attached with glass joints(right), RE holder, CE holder). **c)** Photo of assembled reactor

First trial: problems and troubleshooting

The first pilot attempt in the 0.5 L reactor without much refinement had issues throughout the process though a good conversion was achieved. Figure 3.16 shows the entire timecourse of the reaction recorded by chronoamperometry. The current was unstable and this is attributed to temperature control failure, and signal noises caused from loose connection to the working electrode and the stirrer hitting off the working electrode. The final conversion is >99% of 16.7 mmols α-ketoglutarate, with the TTN of $NADP^+$ being 3340. The TTN of GLDH is 8.6 $*10^6$ and the TTN of FNR is 8.6 $*10^5$. The crystalline product was separated by recrystallisation, and it was pale yellow in colour due to an impurity formed at the counter electrode (likely from buffer salt) during the reaction diffusing through the glass frit to the main compartment. (photo of product shown in figure 3.19)

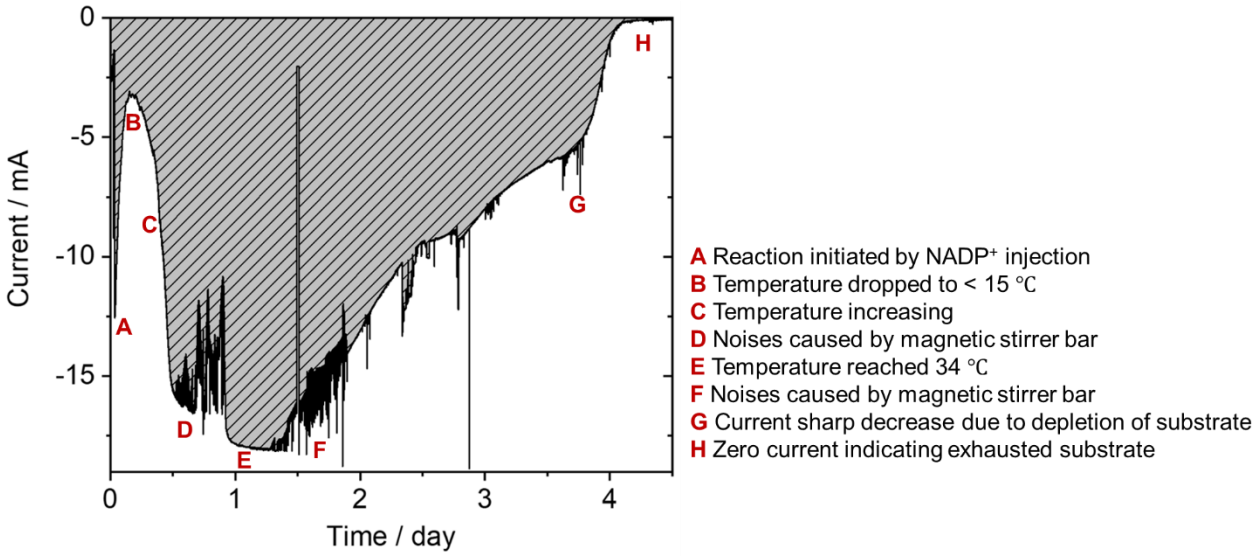


Figure 3.16. Chronoamperogram of GLDH-catalysed reductive amination in 80 mL cell. Conditions: solution volume 500 mL, buffer: 100 mM HEPES pH 7.5; temperature control failed, solution is purged with argon to remove O_2 and argon flow maintained in headspace thereafter; substrate [α-ketoglutarate] = 33.4 mM, [NH_4Cl] = 70 mM, [$NADP^+$] = 10 µM; Potential held at -0.8 V vs. Ag/AgCl (3 M KCl) to drive reduction. Enzyme loading: 949 nmol FNR + 94.9 nmol GLDH (10:1) are mixed and loaded by drop-casting electrode SA: 192 cm^2. Adapted with permission from Megarity *et al*. Copyright 2019, ChemCatChem.[48]

The time course of the reaction process is informative as any minor malfunction causing current change was recorded. Several improvements were made based on this test run. First, the buffer salt was removed from the reaction solution (in later experiment in figure 3.17). This approach was taken because in the test reaction of small scale (4 mL), it has been observed that the CE side arm solution turns brown over time when HEPES buffer is used. This was also observed in the 0.5 L reaction, the CE holder solution got dark as the reaction proceeded and the solution in the main compartment also turned to a slight yellow colour as the impurities transferred back to the main reaction solution. The colour became even darker (brown) when the solution was concentrated by rotary-evaporation. This finally caused the product colour to be yellow. The no-buffer reaction was tested by small-scale reaction and over a pH range 7.5 to 8.0, in which the viability and activity of the enzymes involved are still well-protected. Removal of buffer salt also allows the quantification of product by NMR as explained previously.

Second, small amount of buffer was still used in the counter electrode holder in the no-buffer reaction. To better prevent the impurity going into the main compartment, the partition for the counter electrode holder was changed from a glass frit to Nafion membrane. Nafion membrane as an ion-exchange membrane, is more effective in preventing the diffusion through of impurities and the flowing through of bulk solution.[86] With no solution and impurity crossing-over, the reaction solution was easy to maintain colourless and pure.

Third, the connection wire and clip for the working electrode were optimised with a more stable configuration, which helps avoiding random minor movement of working electrode under stirring causing unwanted noisy electrical signals in chronoamperometry.

Optimised bulk synthesis in the 500 mL reactor:

The e-Leaf has achieved a successful run at a large scale, after these improvements. In the 0.5 L batch reactor with 525 cm^2 electrode surface area, the experiment converted >99% (by ^1H NMR) of 20 mmols of alpha-ketoglutarate (2.92 grams) to L-glutamic acid with a TTN of 3960 within 1.5 days. The L-glutamic acid crystals were separated with a purity of >99%. The experiment process was monitored by chronoamperometry shown in the following figure 3.17. The peak current is approximately 40 mA which is equal to a rate of 1.8 mg of product converted per minute. The current is stable at a high level throughout the reaction progress and eventually drops sharply due to the depletion of substrates. The final product, L-glutamic acid has been separated by recrystallisation method with high product purity and clean appearance.

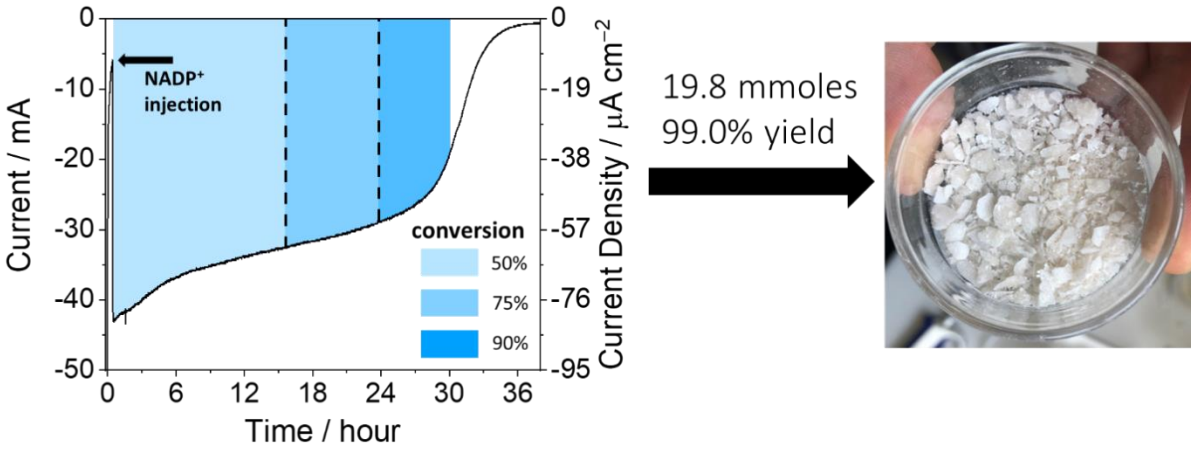


Figure 3.17. Reductive amination of α-ketoglutarate catalysed by GLDH in a 500 mL cell, with the percentage conversion marked based on charge pass. Conditions: solution volume 500 mL, No buffer, starting pH 7.5; temperature: 25 ℃, solution is purged with argon to remove O_2 and argon flow maintained in headspace thereafter; substrate [α-ketoglutarate] = 40 mM, [NH_4Cl] = 70 mM, [$NADP^+$] = 10 μM; Potential held at -0.8 V vs. Ag/AgCl (3 M KCl) to drive reduction. Enzyme loading: 1092 nmol FNR + 109 nmol GLDH (10:1) are mixed and loaded by drop-casting electrode SA: 525 cm^2. Adapted with permission from B. Cheng *et al*. Copyright 2020, Wiley.[54]

By comparing to the benchmark reaction, the 0.5 L reaction in the modular reactor has a similar steady current density at approximately 80 μA cm^{-2}. The TTN of $NADP^+$ is 3960. The TTN of GLDH is 3.8 *10^6 and the TTN of FNR is 3.8 *10^5. The 500 mL experiment is a successful case of a buffer-free reaction. The pH of solution was adjusted to 7.5 before reaction and was detected to be 7.8 when the process was finished. The pH changes could be due to the consumption of large amount (70 mM) of cosubstrate NH_4Cl which is an acidic salt, in the reaction solution without any buffer. Enzyme proved to remain robust in such pH range during the 48-hour reaction. The buffer-free condition helps product characterisation. As mentioned in section 3.4.1, buffer salt (TAPS and HEPES) in the solution will give multiple irregular peaks in ^1H NMR spectrum for the reaction solution, which makes it harder to distinguish product and substrate peaks. In the buffer-free test, the post-reaction solution has a more distinguishable NMR spectrum without peaks attributed to the buffer salt. Removal of buffer allows for clean L-glutamic acid peaks (figure 3.18).

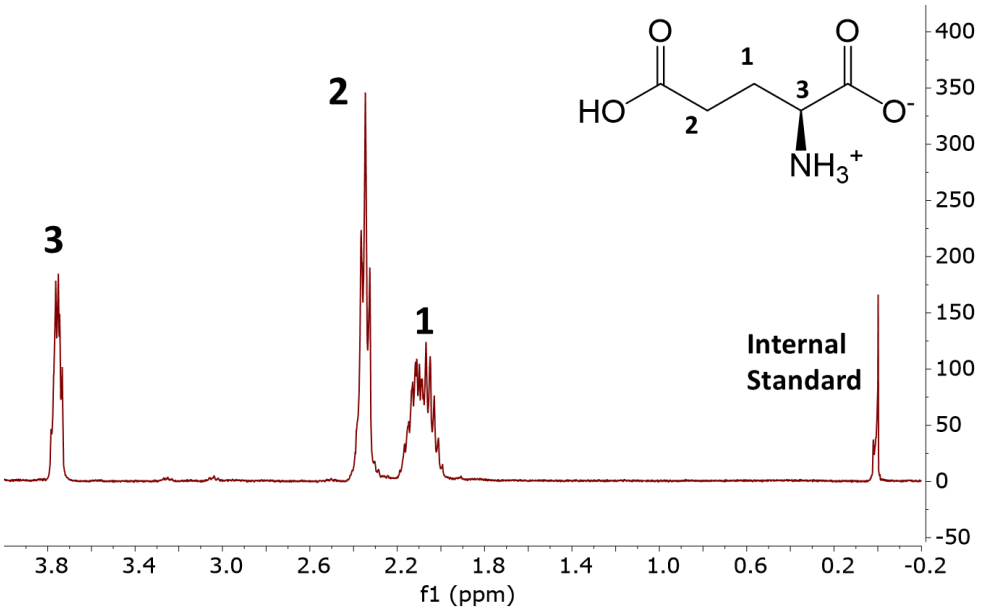


Figure 3.18. ^{1}H NMR spectra of post-reaction solution of L-glutamate in the 500 mL buffer-free reaction. Three L-glutamate characteristic peaks are indicated by the number (δ 2.11 ppm, 2.35 ppm and 3.76 ppm). Three peaks are clearly distinguishable in buffer-free sample and only one peak is clear in buffer solution. Product amount was determined by either standard curve method or internal standard.

Removal of buffer also helps to improve the product separation. As mentioned earlier, HEPES salt can yield coloured impurities on the Pt counter electrode during the reaction, which gives yellow colour to the solution (figure 3.19). The buffer-free condition will be beneficial at the industrial level, as the removal of buffer salts can simplify the purification process, lower the cost, and yield final product with higher purity, making the reaction 'green' and eco-friendly. The process is a low-voltage electrical process with low power consumption. The power consumption in the 36-hour process is approximately 0.86 watt hours (3.08 kJ).



with buffer buffer-free

Figure 3.19. Final product L-glutamic acid separated from buffered process and buffer-free process.

Milestone results compared and discussed

Data from previous experiments are listed in table 3.1. They represent the steps of scaling up the e-Leaf from 4 mL to 0.5 L. With the 4 mL reactor as a benchmark, the cell volume and electrode size have been scaled up almost linearly. Current density is the critical indicator in comparing the catalytic efficiency of reactions on different scales since it is a normalised parameter. The current density remains at a similar level, approximately 75 μA cm^{-2} indicating a successful linear upscale for electrode activity without loss of catalytic efficiency.

The optimised concentration of cofactor is at 5, 10, 20 μM for the e-Leaf reactions. The micromolar level is excellent for further scaling up, with lower usage of NADP(H) than some conventional biocatalytic systems in which cofactor concentration is at millimolar level.[87,88] All conversions are close to 100% with high TTNs of GLDH at the magnitude of 10^6. The TTN of $NADP^+$ is in the thousands level and has the potential of reaching ten thousand as demonstrated by the 44 mL reaction. The electrochemical cell design has been evolved from small to large scale and from monolith to modular configuration to address the challenges and break the limits in the scaling up of an electrochemical system. This series of successful scaling up the e-Leaf to a pilot level has made the first step in channelling laboratory-scale electrochemistry towards application-oriented

industrial use, which brings the potential of using bio-electrochemical technique and device to produce complex fine chemicals as in biotech and pharmaceutical areas.

Table 3.1. Data of milestone experiments from 4 mL to 0.5 L

Cell Volume /mL	Surface Area / cm^2	Enzyme applied[1] /nmol FNR : nmol GLDH	[$NADP^+$] / μM	Yield (conversion rate)	TTN of $NADP^+$	TTN of GLDH /10^5	Stable Current Density[2] /μA cm^{-2}
4	3.5	7.3 : 0.73	20	30.2 μmol (94%)	396	8	72
40	28	58.7 : 5.9	10	400 μmol (>99%)	1,000	14	85
44	73.5	355 : 35.5	5	2.27 mmol (95%)	10,800	31	/
80	70	348 : 34.8	20	3.15 mmol (98%)	1,970	45	110
500 (1)	192	949 : 94.9	10	16.7 mmol (>99%)	3,340	86	/
500 (2)	525	1,092 : 109	10	20 mmol (>99%)	3,960	38	75

*Enzyme amount indicates the enzymes used in loading incubation; the loading solution is fully rinsed off after incubation;

*Stable current density is the average current density at the starting phase and steady phase of the chronoamperometry, indicating the steady working efficiency of the system.

3.4.5. Product Separation of L-glutamic Acid

Product separation with re-crystallisation following the 500 mL reaction finished the complete production process. The solutes in the post-reaction solution include target product L-Glutamic acid (salt at pH 8.0), remaining substrate NH_4Cl and a minor amount of NaCl from the reference electrode side-arm solution. Insoluble impurities remaining in the solution are mainly ITO falling from the electrode over the 2-day continuous stirring.

In the re-crystallisation method, the decisive factor is the solubility of the chemicals involved. L-glutamic acid has two acidic carboxylate and one basic amine group, and in aqueous solution it can have four different charged species in different pHs, as shown in figure 3.20.[89] The solubility of L-glutamate is high in its salt form Glu^- at post-reaction pH 7.5. The acid form, L-glutamic acid however, has a solubility in aqueous solution that

varies massively with temperature, 0.0240 mol L^{-1} at 5.5 ℃, 0.2929 mol L^{-1} at 69 ℃ and 0.8346 mol L^{-1} at 100 ℃.[90,91] There is a >10-times difference of solubility between high (close to 100 ℃) and low temperature (4 ℃). While NH_4Cl is extremely soluble in water even when the temperature is low (294 g L^{-1} at 0 ℃), recrystallisation is thus well-suited for the separation of L-glutamic acid. The pH of the post-reaction solution must be brought down from 7.8 to 3.08 to ensure that L-glutamate is in its less-soluble form.

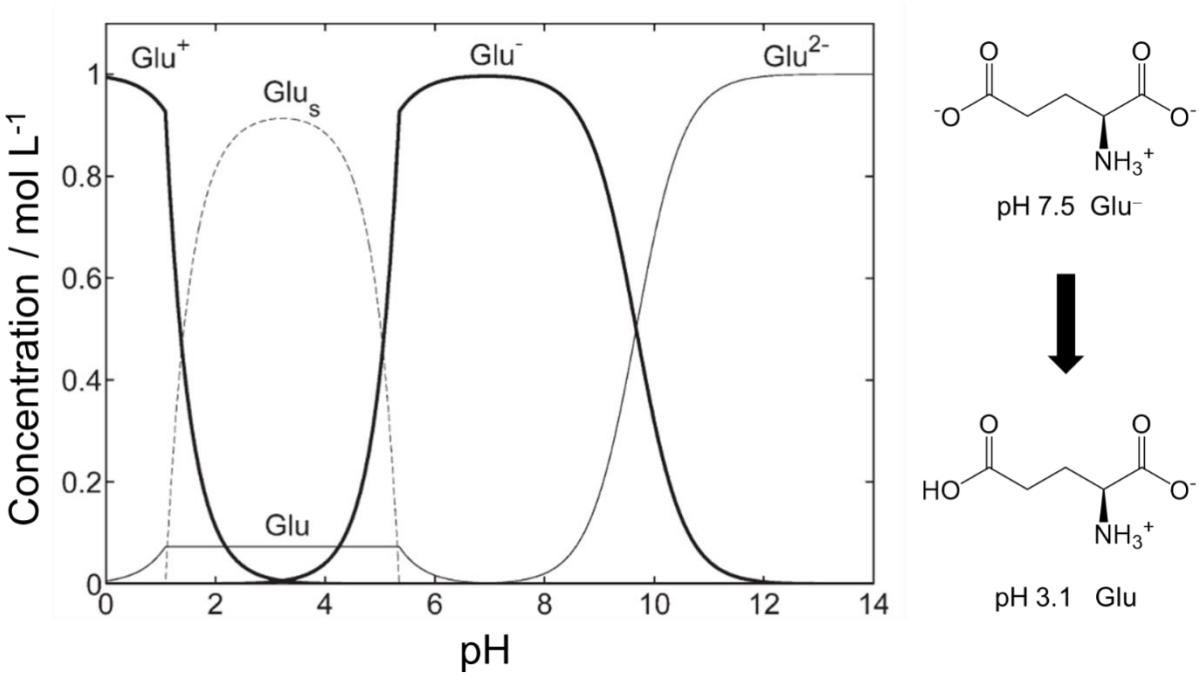


Figure 3.20. NMR spectra speciation of 1 mol/L L-glutamic acid as a function of pH (taking into account the precipitation of a-L-glutamic acid. Glu_s represents the concentration of precipitated free acid). Adapted with permission from Jochen Scholl et al.*Precipitation of L-Glutamic Acid: Determination of Nucleation Kinetics*[89]

Separation process

1) Post-reaction solution is mixed with 5 gram of activated charcoal and stirred for half hour to remove coloured impurities. Then the solution is filtered first by paper filter and then by 0.22 mm PES filter. The solution becomes colourless and free of solid impurities.

2) The solution is put in a rotary-evaporator to bring down the volume from 500 mL to 5 mL. The final solution is still colourless, transparent and with no precipitation. This step is to concentrate the solution.

3) Adjust the pH of concentrated solution in a beaker to pH 3.2. The solution is stirred while titrated with dilute HCl solution. White solid precipitates when the solution reaches the target pH. This step is to lower the pH for the product to get in the isoelectronic acid form which has a much larger solubility difference with temperature than its salt form.

4) The recrystallisation starts by heating the solution to 80 ℃ with an oil bath under stirring. All precipitated solid re-dissolves and the solution is colourless and transparent.

5) Heating is stopped after all solid has been dissolved. The solution is then slowly cooled down from 80 ℃ to 4 ℃. This is carried out by putting the beaker into a 2 L water bath at 80 ℃ and let it naturally cool down to room temperature. Then the solution beaker and the water bath are transferred to the 4℃ cold room to be further cooled to 4℃. The large-volume water bath provides higher heat capacity to increase the time length of the cooling process, which helps to yield more regular crystals and less impurities.

6) The crystalline product is filtered from the mother liquor at 4 ℃, rinsed by cold pH 3.2 MQ water and then dried in the oven. The pure product is acquired.

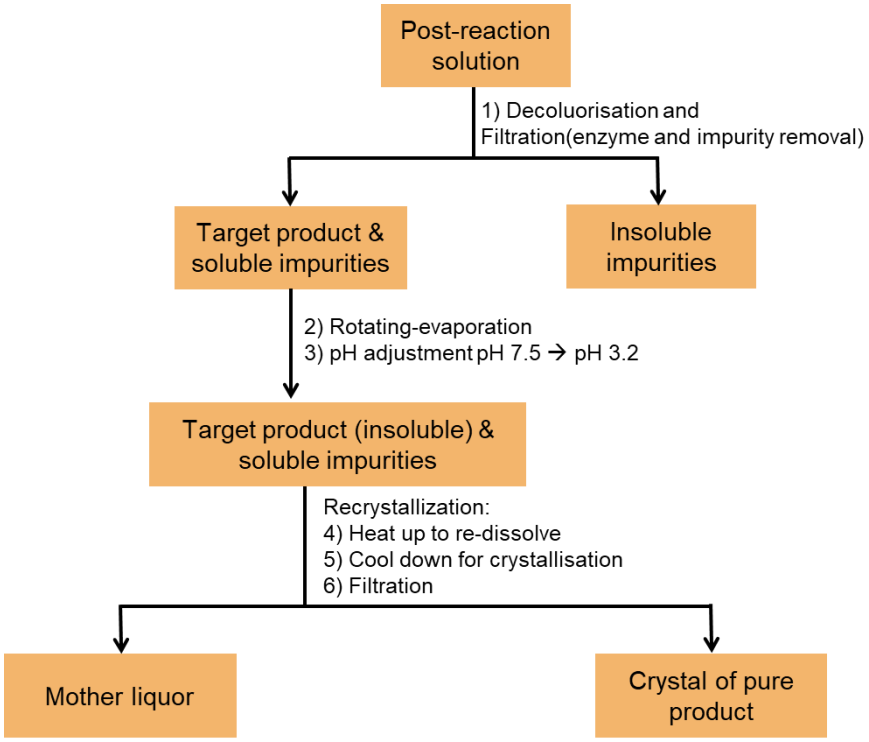


Figure 3.21. Flowchart of L-glutamic acid product separation

The product crystals are shown in following figure 3.22. The purity is tested by ^{1}H NMR to be >99%. The weight is 1.86 g, with a recovery rate of 66% (out of 2.83 g for theoretical full recovery)

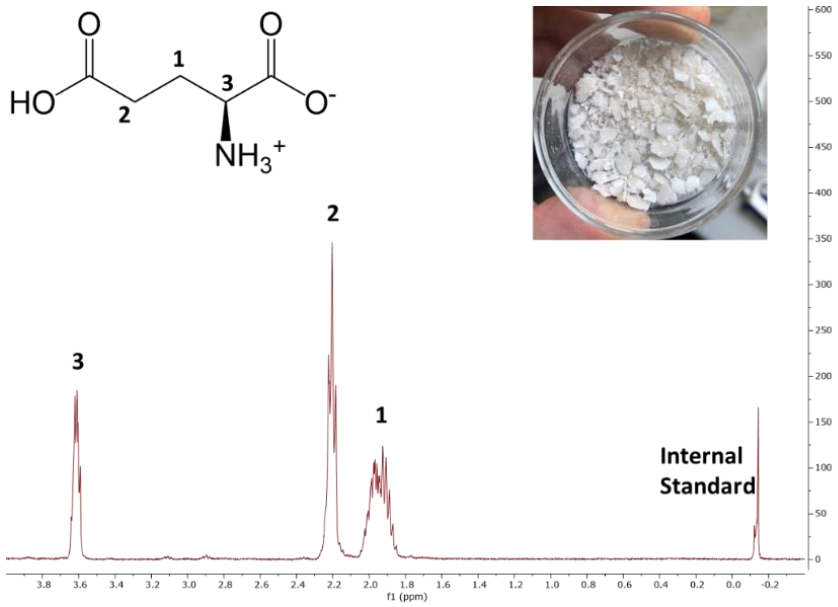


Figure 3.22. ^{1}H NMR spectrum of crystalline product L-glutamic acid produced in experiment shown in figure 3.17, dissolved in water.

3.5. Conclusion and Possibilities of the E-Leaf

This chapter has demonstrated the main work of a linear scale-up of the electrochemical leaf from a 4 mL lab-scale reactor to a 500 mL pilot-size reactor, with increased electrode size from 14 cm^2 to over 500 cm^2. The e-Leaf in a large scale has an excellent performance as in its small-scale prototype. With condition optimisation, reactor design have product separation conducted, the exploration shows the potential of the e-Leaf to become a powerful tool in producing valuable chemicals.

1) Increasing usage of enzyme and cofactor

An inevitable issue in enlarging a biocatalytic process is the increasing amount of enzyme and cofactors. It is typical in conventional biocatalytic process that the enzyme and cofactor usage increase in scale with the volume size, so the cost increases. For huge scale production, industrial enzymes with high efficiency and low cost may still be available but high-value enzymes may face barriers due to their requirement in high quantities. Fortunately, enzyme nanoconfinement in the e-Leaf has eased this issue with enzyme use. With e-Leaf used in a biocatalytic process, the enzymes are entrapped in the e-Leaf and are no longer required to scale with the size of reaction volume but only with the size of electrode. Even though the scaling relation remains between enzyme amount and the electrode size, the enzyme needed per unit electrode surface area (with e-Leaf) can be decreased comparing to enzyme usage in bulk solution biocatalysis to achieve comparable catalytic efficiency.[49]

The NADP(H) usage in experiments in this thesis is not decoupled from the reaction volume. The latest research has discovered that the e-Leaf can confine the NADPH copurified with E2 much better with minor loss to the bulk solution. The copurified cofactor is used and regenerated in the e-Leaf to sustain efficient biocatalytic process. The TTN of NADPH in this process reaches a high magnitude (160,000) with good stability in 5 days, suggesting that the e-Leaf is potential to be developed into a ‘cofactor built-in’ devices.[50,92]

2) Scaling up an electrochemical system

Electrochemistry, upon bringing its advantages to biocatalytic process, introduces features that may cause limitation when it comes to scaling up. Using larger electrodes requires a suitable electrochemical cell, ITO coating methods and enzyme loading methods, which is hugely different from the initial lab-level design. The conventional solution biocatalytic process, when being scaled up without an electrode system, focuses more on the pot size and enzyme usage and the work is more predictable and straightforward. To scale up an electrochemical system with enzymes loaded has more factors involved and requires an excellent combination of reactor design and electrochemical system design. Factors as current limits, mass transfer and stability of the enzyme need to be considered carefully.

The scaling up of e-Leaf in this chapter has provided an excellent example of enlarging a bio-electrochemical system. The 0.5 L e-Leaf is able to retain a similar current density as the initial 4 mL prototype, and there is still potential for further scaling up to higher limits until the optimised maximum scale. This challenge is addressable by further cell and electrode engineering. In addition, at the industrial level, modular and standardised electrochemical cells will be more versatile in function and more accessible to couple with other technologies, such as robotic control, continuous reaction blocks, and in-situ sampling and separation.

3) Different perspective of 'Scaling up'

There are some successful cases in scaling up electrical systems like fuel cells and electrochemical systems which has proved the feasibility of a bio-electrochemical system being scaled up.[15,93,94] Improvement from various perspectives could be introduced to the e-Leaf.

An alternative to directly scaling up the reactor size might be to increase the number of basic cell units which would also increase the overall productivity.[95,96] Such e-Leaf units

could be stacked in series or parallel to accommodate different application scenarios. Another way to boost the efficiency is to optimise the space usage of the e-Leaf. In the 500 mL reactor presented, electrodes only take a minor portion of the total space in the reactor, while the bulk solution is too much, beyond the requirement for the electrochemical reactions. To fill the reactor space with more electrode and increase the conversion rate of unit volume of the reactor is a possible optimisation. The e-Leaf could also be made into a packed-bed reactor with electrochemical system. A successful example of combining an electrochemical system and packed reactor has given a huge boost in the conversion rate.[97] In regard to the functionality of the e-Leaf, the core function of NADP(H) regeneration can be widened to the regeneration of other co-factors such as NAD(H), ATP and so on, expanding the scope even further.

CHAPTER IV

4. Dual Control of a Bidirectional Nanoconfined Enzyme Cascade: A Novel Approach for Deracemisation and Inversion

4.1. Introduction

Enantiopure chemicals for pharmaceutical and biotechnological purposes are increasingly produced with biocatalysts. The importance of obtaining enantiopure compounds is exemplified in the classic example, the story of the drug Thalidomide, and there are numerous other chiral drugs that must be enantiopure. Some drugs only work if it is a specific enantiomer – their target doesn't recognise the other enantiomer. The wrong enantiomer could even be harmful.[98]

There are two main approaches in biocatalytic deracemisation which are the one-pot multi-step biocatalytic cascade and the dynamic kinetic resolution (DKR) method. The one-pot multi-step deracemisation typically starts with a non-enantioselective step that convert the racemic mixtures to a pre-chiral intermediate. The second step is a biocatalytic process catalysed by enantioselective enzyme(s). The approach has at least two enzymes, one of which is enantioselectivity. It also requires the addition and adjustment of extra co-substrate to controller the selectivities in both steps.[99]

Dynamic kinetic resolution (DKR) approach takes advantages of the equilibrium between the two enantiomers under resolution process (different reaction rates). The process includes a high-speed resolution step and a racemisation step coupled. When the enantiomer with the higher resolution speed is consumed, the equilibrium between the two enantiomers is moving towards the conversion from the slower enantiomer to the faster enantiomer via the racemisation. Biocatalysts are commonly involved in the DKR solely or with chemical catalysts.[100]

Methods outside biocatalysis for deracemisation have also been researched and developed including crystallization, photocatalysis, and post-reaction enantiomer separation.[101–103] The use of enzymes in biosynthesis allows for built-in deracemisation since biocatalysts themselves are chiral and therefore can catalyse with high enantioselectivity and conversion rates.[104,105]

In the electrochemical leaf, as introduced in previous chapters, enzyme cascades are nanoconfined in tiny enclosures of a highly porous indium tin oxide electrode where they are driven by electricity, via the quasi-reversible interconversion of NADP/NADPH catalysed by FNR, controlled by the potential applied, and monitored live as current.[1,48] By extension, whole cascades can also be driven via this control point (from FNR to NADP(H)), and the only requirement is that one downstream enzyme in the cascade is NADP(H)-dependent. In addition to the ability to drive and control enzyme cascades using electricity, the nanoconfinement (as occurs in living cells) of the enzymes is also key to this system. Under nanoconfinement, enzyme catalysis is enhanced since enzymes are trapped at very high local concentration in the electrode pores thus increasing efficiency.[60] The distance between different catalytic sites the substrate, cofactors, and intermediate (which may be unstable) must travel is extremely shortened, enabling the cluster channelling which keeps the small molecules retained in the nanopores and increases the efficiency of the reaction.

A previous deracemisation strategy using the e-Leaf involved the use of separate electrodes loaded with dehydrogenases of different enantioselectivities, in sequence with each completing a half cycle for deracemisation (similar experiment performed shown in section 4.5.1).[56] Inspired by the unusual fact that despite many alcohol dehydrogenases having tightly-bound Zn at catalytic sites, some alcohol dehydrogenases, such as the ADH from *L. Kefir* used in this study, are dependent on non-catalytic Mg^{2+} ions. The removal of Mg^{2+} will cause the loss of catalytic activity of this type of alcohol dehydrogenase and it is therefore possible to exploit this feature to make an on/off 'switch' for such a dehydrogenase. [106,107] The role Mg^{2+} plays in the *LK* ADH is hypothesized as either (1) having indirect effect on the substrate binding and product release or (2) assisting in maintaining the binding pocket of the enzyme and its unique charge distribution on the active site.[107,108]

In this chapter, an electrochemically controlled bidirectional alcohol deracemiser is presented (Figure 4.1). By using two alcohol dehydrogenases of opposing enantioselectivities (LK which is R-specific and W110A or W110V which are S-specific) with the ability to selectively switch off one of these enzymes, a one electrode, one pot deracemiser has been developed. In the process, starting with a racemic mixture of alcohols, both alcohol dehydrogenases are driven to oxidise their specific alcohol enantiomer to ketone at which point the applied potential is changed to a reducing voltage and the Mg-dependent enzyme is switched off by adding ethylenediaminetetraacetic acid disodium salt dihydrate (EDTA) to chelate the Mg^{2+}. The Zn-dependent S-specific enzyme remains active and is then driven to reduce all of the ketone produced during the oxidation stage, to (*S*)-alcohol, thus deracemising the starting racemic mixture. The EDTA chelation process was confirmed by the control experiment that the Mg^{2+}-binding LK was deactivated while Zn^{2+}-binding W110V remained active. This is also backed by the seminal work on the binding of catalytic zinc to ADH enzymes.[109] The deracemiser successfully transformed the racemic 4-phenyl-2-butanol into S-enantiomer under electrochemical control, resulting in an enantiomeric excess (ee%) of 82% in 50 hours. The design was then extended to an enantiomer inverter and a larger scale deracemiser.

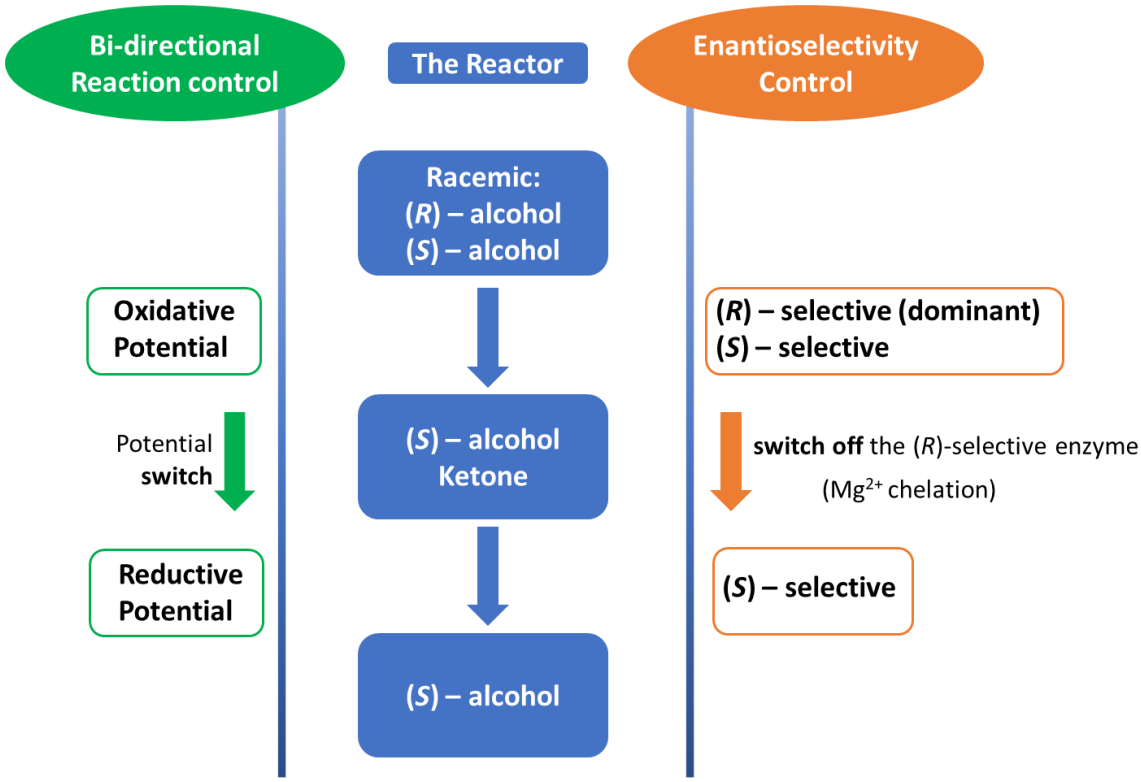


Figure 4.1 The process of the dual-controlled (catalytic directional control and enantioselectivity control) bidirectional deracemiser.

4.2. Characteristics of Three Alcohol Dehydrogenases

In this chapter, three alcohol dehydrogenases are involved in the deracemisation and inversion process in which (*R*)-4-phenyl-2-butanol (referred to as (*R*)-alcohol in this chapter) or a racemic mixture is turned into (*S*)-4-phenyl-2-butanol (referred to as (*S*)-alcohol). The (*S*)-selective variants are from *Thermoanaerobacter ethanolicus* 39E,[87,110] where a tryptophan at position 110 has been changed to an alanine or a valine and are referred to as W110A and W110V and the (*R*)-selective enzyme is from *Lactobacillus kefir* and is referred to as LK.[107,108,111]

The enantioselectivity for these enzymes was previously investigated by conventional solution assay which confirmed that W110A and W110V were selective for (*S*)-alcohol with the latter variant having improved (*S*)-selectivity (and no activity on (*R*)-alcohol) but with lower activity (W110A k_{cat} (*S*) = 29.8 s^{-1} and W110V k_{cat}(*S*) = 6.2 s^{-1}). LK was also confirmed as being exclusive for R (k_{cat}(*R*) = 29 s^{-1}) [56].

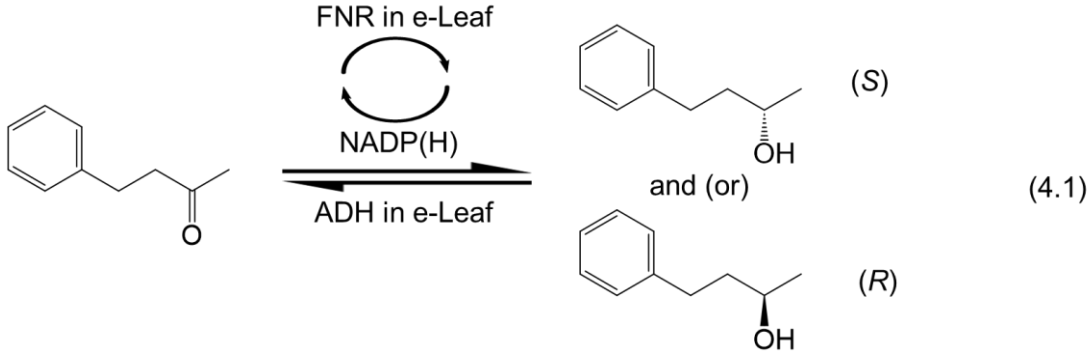
The substrate alcohol is 4-phenyl-2-butanol which has (*R*) and (*S*) enantiomers and the substrate ketone is 4-phenyl-2-butanone. The majority of this work was carried out using LK and W110A. And in later course of this project, the system was improved by the use of W110V which has enhanced enantioselectivity for S (in section 4.6).

4.2.1. Enantioselectivity

4.2.1.1. Cyclic Voltammetry of W110A and LK

The interconversion of alcohol and ketone catalysed by ADH (equation 4.1) can be demonstrated in a more direct view by cyclic voltammetry (figure 4.2). The CV shows the coupling effect of E2 with NADP(H) interconversion catalysed by FNR. Figure 3.1 panel (a) shows W110A high selectivity towards the (*S*)-alcohol (red trace) and slight selectivity towards (*R*)-alcohol (blue trace), as can be seen by the increase in positive current in the oxidising potential region of the voltammogram.

In contrast, LK (shown in panel (b)) is solely selectivity towards (*R*)-alcohol (blue trace) and no activity in (*S*)-alcohol solution (red trace) which shows only the redox peaks (since the electrode is stationary) for the interconversion of NADP(H) by FNR. The CVs also show that both LK and W110V can be bi-directionally controlled for oxidation (blue and red traces) or reduction (black traces) depending on the potentials applied.



(4.1)

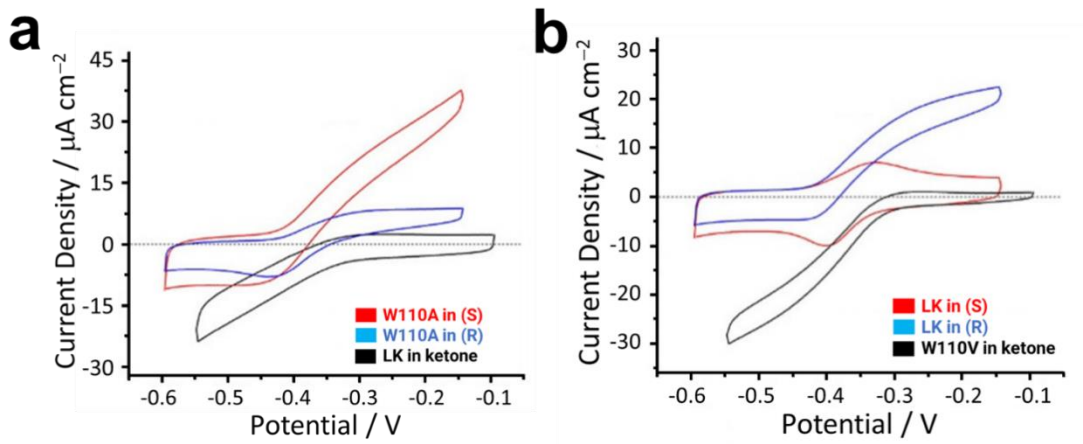


Figure 4.2 The enantioselectivity of ADHs (W110A and LK) and for the LK enzyme monitored by cyclic voltammetry. **a)** cyclic voltammograms of coupling effect of NADP(H) interconversion to W110A in the presence of (*S*)-alcohol(red), (*R*)-alcohol(blue) at pH 9.0 (50 mM TAPS + 1 mM $MgCl_2$ buffer) and to LK in the presence of ketone (black) at pH 7.5 (50 mM TAPS + 1 mM $MgCl_2$ + 25 mM NaCl buffer). **b)** cyclic voltammograms of coupling effect of NADP(H) cycling to LK in the presence of (*S*)-alcohol (red), (*R*)-alcohol (blue) at pH 9.0 (50 mM TAPS + 1 mM $MgCl_2$ buffer) and to W110V in the presence of ketone at pH 7.5 (50 mM TAPS + 1 mM $MgCl_2$ + 25 mM NaCl buffer). Conditions: cell volume 8 mL; substrate [4-phenyl-2-butanone] = 5 mM, [Mg^{2+}] = 5 mM, [NADPH] = 50 µM; temperature: 25 °C; scan rate = 2 mV/s. Headspace purged with Ar. Adapted with permission from L. Wan *et al*. Copyright 2021, ACS Catal.[56]

4.2.1.2. Chronoamperometry of the Enantiomer-specific Conversion Catalysed by W110A, LK and W110V

In addition to the CVs above, chronoamperometry is another way of showing enantioselectivity of ADHs. It is the real-time monitoring and tracking of the actual process of conversion, showing the change of the reaction rate (current) over time. while CV shows potential-dependent data, a chronoamperogram shows time-dependent data held at a fixed potential. The charge passed during chronoamperometry equates to the amount of product, and the post-reaction solution can also be analysed afterwards by gas chromatography (GC, detailed settings in chapter 7 experimental methods) to verify this and quantify specific components of enantiomers. The following results are the chronoamperograms for oxidation and reduction catalysed by different E2s (W110A, LK and W110V).

(1) W110A

Figure 4.3 shows chronoamperograms for a bulk oxidation (panel (a)) and reduction (panel (b)) catalysed by W110A. Enzymes (FNR+W110A) were loaded by stir-loading. All substrates were in the cell solution before the reaction. The oxidation was initiated by live injection of $NADP^+$ after the applying of a potential of 0 V vs Ag/AgCl (3 M KCl). The reduction solution contained $NADP^+$ and the reaction was initiated by applying a potential of -0.85 V. The initial current was high and gradually decreased to the depletion of substrates, reaching zero after approximately 18 hours in both timecourses. The coulometric conversion is 47.9% in the oxidation of racemic alcohol, and 92.1% in the reduction of ketone. Since W110A is a (*S*)-alcohol specific enzyme, a conversion close to 50% for racemic substrate can be viewed as complete. This experiment using W110A shows the potential capability of achieving a close-to-complete conversion in a one-pot reaction.

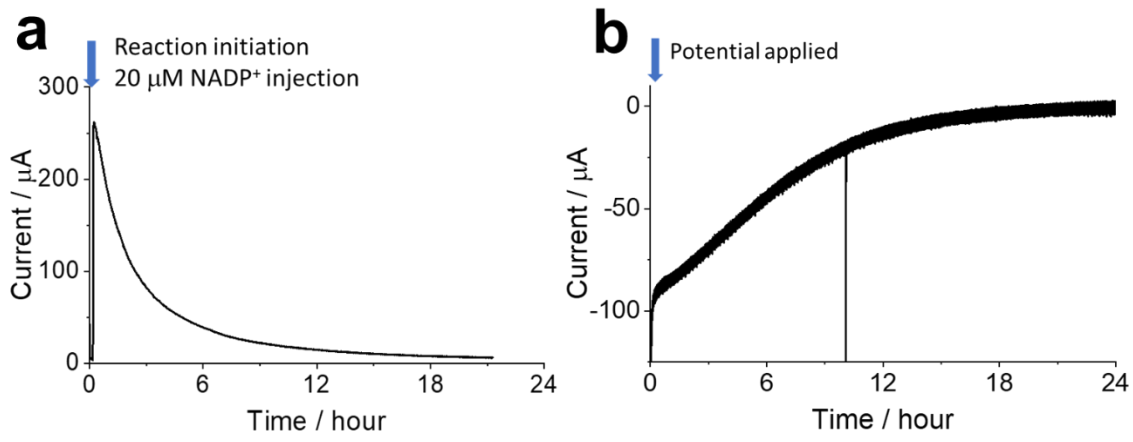


Figure 4.3. The timecourses for **a)** the oxidation of racemic alcohol and **b)** the reduction of ketone catalysed by W110A. Conditions: cell volume 4 mL, solution stirred throughout using a magnetic flea; substrate in oxidation [(±)-4-phenyl-2-butanol] = 8 mM; substrate in reduction [4-phenyl-2-butanone] = 4 mM [$NADP^+$] = 20 µM, buffer: 50 mM TAPS pH 9.0; temperature: 25 ℃, Potential held at 0 V vs. Ag/AgCl (3 M KCl) to drive oxidation and –0.85 V for reduction. Solution purged with argon to remove O_2; argon flow maintained in headspace thereafter. Enzyme loading (oxidation and reduction): FNR and W110A are loaded together by stirring in a 2.5 mL solution containing 11.5 nmols of FNR and 5.7 nmols of W110A in 50 mM TAPS buffer pH 9.0; electrode (Ti foil) SA: 7 cm^2.

The enantioselectivity of W110A towards (*S*)-alcohol was confirmed by the GC analysis of post-reaction solution. The result of post-reduction solution is shown in table 4.1. Ketone is reduced to mainly (*S*)-alcohol and a small ratio of (*R*)-alcohol.

Table 4.1. GC Enantiomer analysis (Red)

	[S]/mM	[R]/mM	[ketone]/mM	ketone%	S%	R%	ee%(*S*)
Starting	4.05	0.00	3.95	49.4	50.6	0.0	>99.9
Post-reduction	6.95	0.83	0.22	2.7	86.9	10.4	78.7

(2) LK

Figure 4.4 shows chronoamperograms monitoring the activity of LK for an oxidation (panel (a)) and reduction (panel (b)). The coulometric conversion is 48% in oxidation of racemic alcohol and 97.2% in reduction of ketone. This experiment has shown the catalytic capability of LK in both oxidation and reduction directions to achieve a close-to-complete conversion in a one-pot reaction as well.

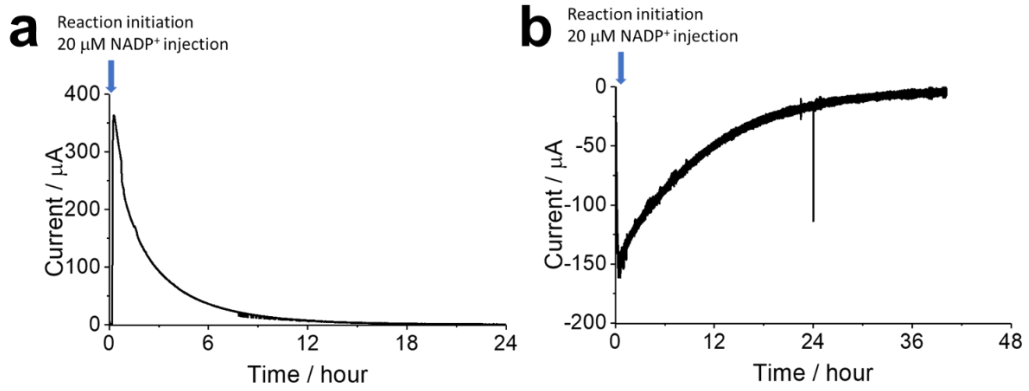


Figure 4.4. The timecourses for **a)** the oxidation of racemic alcohol and **b)** the reduction of ketone catalysed by LK. Conditions: cell volume 4 mL, solution stirred throughout using a magnetic flea; substrate in oxidation [(±)-4-phenyl-2-butanol] = 8 mM, substrate in reduction [4-phenyl-2-butanone] = 6 mM, [$NADP^+$] = 20 μM, [Mg^{2+}] = 5 mM; buffer: 50 mM TAPS pH 9.0; temperature: 25 ℃, Potential held at 0 V vs. Ag/AgCl (3 M KCl) to drive oxidation and −0.74 V for reduction. Experiments performed in an anaerobic glovebox to avoid any contribution to the current form the reduction of O_2. Enzyme loading (oxidation): FNR loaded first by drop-casting, LK loaded after FNR, by stirring in a 2.5 mL solution containing 4.96 nmols of LK in 50 mM TAPS buffer pH 9.0; electrode (Ti foil) SA: 7 cm^2. Enzyme loading (reduction): FNR loaded first by drop-casting, LK loaded after FNR, by stirring in a 2.5 mL solution containing 3.28 nmols of LK in 50 mM TAPS buffer pH 9.0; electrode (Ti foil) SA: 7 cm^2.

The enantioselectivity of LK towards (*R*)-alcohol was confirmed by the GC analysis of post-reaction solution. Results are shown in table 4.2 and table 4.3. All of (*R*)-alcohol has been converted into ketone during oxidation and in the reduction, ketone is reduced to only (*R*)-alcohol. There are several possible sources of error which are outlined in the appendix.

Table 4.2. GC Enantiomer analysis (OX)

	[S]/mM	**[R]/mM**	**[ketone]/mM**	**ketone%**	**S%**	**R%**	**ee%(*S*)**
Starting	3.40	4.24	0.36	4.5	0.0	52.9	-10.9
Post-oxidation	4.22	0.00	3.78	47.2	1.2	0.0	100.0

Table 4.3. GC Enantiomer analysis (Red)

	[S]/mM	**[R]/mM**	**[ketone]/mM**	**ketone%**	**S%**	**R%**	**ee%(*S*)**
Starting	0.00	0.00	6.00	100.0	0.0	0.0	
Post-reduction	0.00	4.52	0.14	2.9	0.0	97.1	-100.0
Side-arm	0.00	1.06	0.28	21.2	0.0	78.8	-100.0

(3) W110V

Figure 4.5 shows chronoamperograms of W110V for the oxidation (panel (a)) and reduction (panel (b)) for a bulk conversion. The coulometric conversion is 45.0% in oxidation of racemic alcohol and 95.3% in reduction of ketone. The activity of W110V has shown by oxidation and reduction that the capability of achieving a close-to-complete conversion in a one-pot reaction is possible.

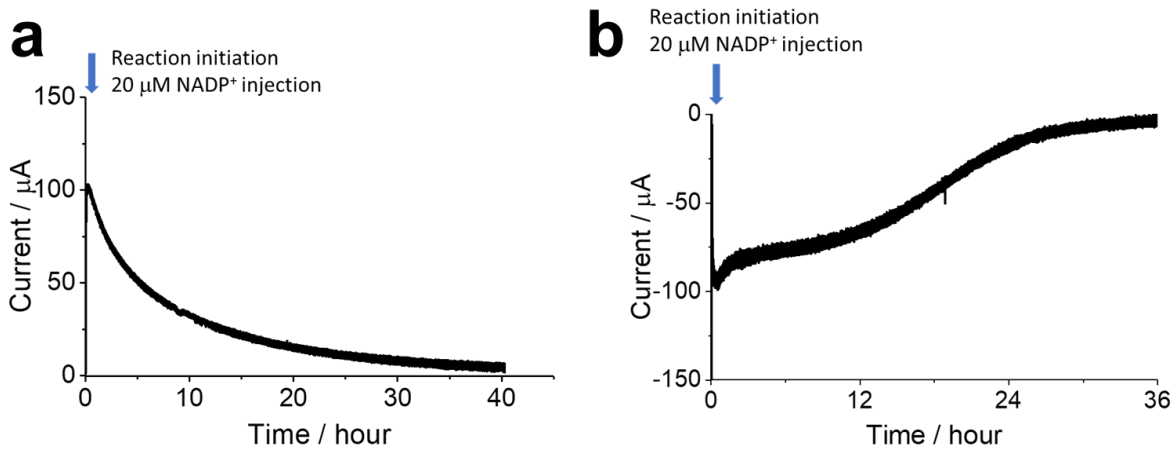


Figure 4.5. The timecourses for **a)** the oxidation of racemic alcohol and **b)** the reduction of ketone catalysed by W110V. Conditions: cell volume 5 mL, solution stirred throughout using a magnetic flea; substrate in oxidation [(±)-4-phenyl-2-butanol] = 8 mM, substrate in reduction [4-phenyl-2-butanone] = 6 mM, [$NADP^+$] = 20 μM, [Mg^{2+}] = 5 mM; buffer: 50 mM TAPS pH 9.0 for oxidation and pH 8.0 for reduction; temperature: 25 ℃, Potential held at 0 V vs. Ag/AgCl (3 M KCl) to drive oxidation and –0.74 V for reduction. Experiments performed in an anaerobic glovebox to avoid any contribution to the current form the reduction of O_2. Enzyme loading (oxidation and reduction): FNR loaded first by drop-casting, LK loaded after FNR, by stirring in a 2.5 mL solution containing 3.28 nmols of W110V in 50 mM TAPS buffer pH 9.0; electrode (Ti foil) SA: 7 cm^2.

The enantioselectivity of W110V towards (*S*)-alcohol was confirmed by GC analysis. Results are shown in table 4.4 and table 4.5. (*S*)-alcohol has been converted into ketone during oxidation and in reduction, ketone was reduced to mainly (*S*)-alcohol. W110V is more selective for (*S*) comparing to W110A. As mentioned earlier, W110V was used in the later stage of this research as a replacement for W110A to increase the final enantiomeric purity.

Table 4.4. GC Enantiomer analysis (Ox)

	[S]/mM	[R]/mM	[ketone]/mM	ketone%	S%	R%	ee%(*S*)
Starting	3.92	4.08	0.00	0.0	49.0	51.0	-2.0
Post-oxidation	0.16	3.23	2.73	44.7	2.6	52.7	-90.6
Side-arm	0.23	0.97	0.69	36.7	11.9	51.3	-62.2

Table 4.5. GC Enantiomer analysis (Red)

	[S]/mM	[R]/mM	[ketone]/mM	ketone%	S%	R%	ee%(*S*)
Starting	0.00	0.00	6.00	100.0	0.0	0.0	
Post-reduction	4.15	0.00	0.11	2.7	97.3	0.0	100.0
Side-arm	1.28	0.00	0.46	26.4	73.6	0.0	100.0

4.2.2. Product-inhibition in ADH-Catalysed Oxidation

Product inhibition for the oxidation catalysed by W110A and W110V has previously been observed.[112,113] A test for product inhibition monitored by chronoamperometry was performed using a rotating disk working electrode coated with ITO and pre-loaded FNR by drop-casting. As shown in figure 4.6, LK was injected into the bulk solution right at the start of the reaction and after approximately 50 minutes during which LK adsorbed into the electrode pores, a buffer exchange was carried out to remove the excess LK in solution. After the buffer exchange, the reaction was left running for 10 minutes and current was steady since only the enzymes nanoconfined in the electrode were presented. The product ketone was live injected into the solution which caused a sharp decrease in current. Another 4 mM product injection was carried out after a few more minutes which also gave a sharp decrease in current (injection marked by red arrows).

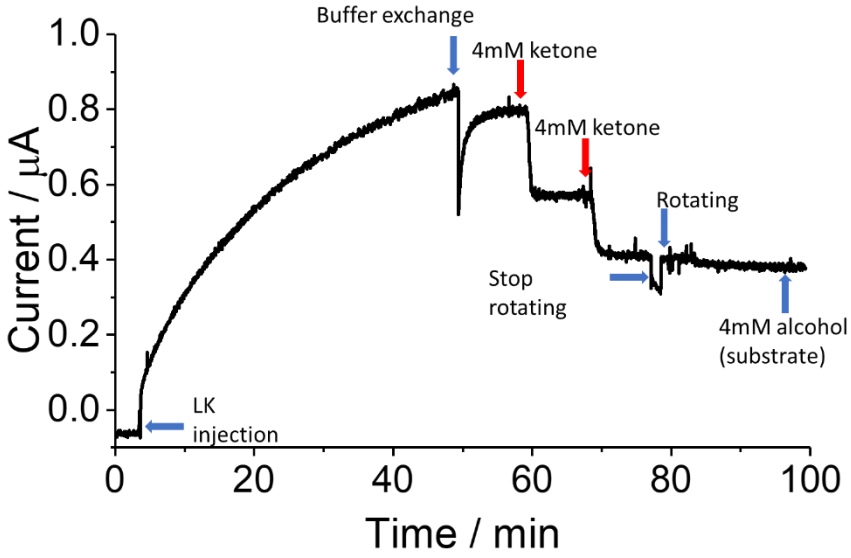


Figure 4.6. Product inhibition test for the LK-catalysed oxidation via product titration. Conditions: cell volume 4 mL; substrate [(±)-4-phenyl-2-butanol] = 8 mM, [$NADP^+$] = 20 µM, [Mg^{2+}] = 5 mM buffer: 50 mM TAPS pH 9.0; temperature: 25 ℃, Potential held at −0.175 V vs. SCE to drive oxidation. Solution purged with argon to remove O_2; argon flow maintained in headspace thereafter. Rotating disk electrode (RDE) SA: 0.07 cm^2, 1000 rpm. Enzyme loading: FNR loaded by drop-casting before the experiment; LK are loaded during the experiment as shown in graphs.

Later during this timecourse, the rotation was switched off for a brief period to test the effect of mass transport (the current decreased). At the end of the experiment, another 4 mM substrate (alcohol) was injected, which had no effect on the reaction current as expected, since the substrate concentration already is far higher than the Km value. The effect of excess substrate is later discussed in chapter 5 about biphasic reaction.

4.3. LK and W110A Nanoconfined Together in a Single Electrode: Real-time Investigative Experiments.

4.3.1. The Effect of Changing Enantiomers and the Addition of EDTA in Real-time, on each Enzyme Separately.

The key idea of the deracemiser/inverter is to utilize the opposite selectivity of two ADHs (W110A + LK) and the ability to switch off one of them (LK) to achieve a controlled selective conversion. To test the selectivity and also the switching off effect of EDTA, a

few trial experiments were carried out on a small-scale with an rotating disk electrode (RDE). Tests using single-E2 systems were carried out as simplified cases and controls for the later two-E2 tests which are closer to the final design. The electrochemistry method shines in its ability to monitor live intervention experiments and its ability to show signal in real time. The first two single-E2 tests for W110A and LK are shown in the following figure 4.7.

FNR was pre-loaded by drop-casting and to initiate the coupled reaction, E2 (W110A or LK) was injected into the bulk solution and the current grew indicating the loading of E2 from the solution into the nanoporouselectrode. After the loading phase, a buffer exchange was carried out to remove the enzyme remaining in the solution and also to change the 8 mM racemic alcohol to 4 mM (*R*)-alcohol. For W110A (panel (a)), the activity rapidly decreased to a very low level due to its high selectivity towards (*S*)-alcohol (active before buffer exchange) and low activity with (*R*)-alcohol. For LK (panel (b)), the current level remains unchanged because the buffer exchange retained the same concentration of 4 mM (*R*)-alcohol. Then the second buffer exchange replaces the (*R*)-alcohol by 4 mM (*S*)-alcohol, in which W110A recovers a high level current even higher than the current at then end of the loading phase while, as expected, the LK electrode loses all the catalytic activity.

It is noteworthy that the electrode with W110A has a higher reaction rate in pure (*S*)-alcohol than in racemic alcohol. The reason could be that the W110A is able to bind and convert a minor amount of (*R*)-alcohol, which contributes to the lower rate compared to (*S*)-alcohol. In contrast, LK has low affinity for the (*S*)-alcohol so the current does not change whether it is in racemic substrate or (*R*)-alcohol solution. Another reason is probably from the removal of product. Product may have contributed to the inhibition effect to W110A, while LK has no obvious product-inhibition.

The LK system was then buffer exchanged back to (*R*)-alcohol to recover the current for further live interventions. In both the systems, a CV was taken (as indicted on the

timecourse) to check the coupling situation and to check which enzyme (E1 or E2) was limiting (introduced in chapter 1; CVs not shown). The measurement was restarted and FNR was injected; the current did not change in response to the FNR injection, suggesting that FNR was not the limiting factor in the system. Further investigation about three enzymes' interaction is show in the appendix (section A4.3.3). Following a buffer exchange to remove the excess FNR in solution, a 25 mM EDTA injection to chelate the Mg^{2+} ions in the solution, immediately inactivated the LK system while no effect on the current in the W110A system was observed. These two experiments clearly show the activity of each E2 with each alcohol and the inactivating effect of Mg^{2+} ion chelation by EDTA.

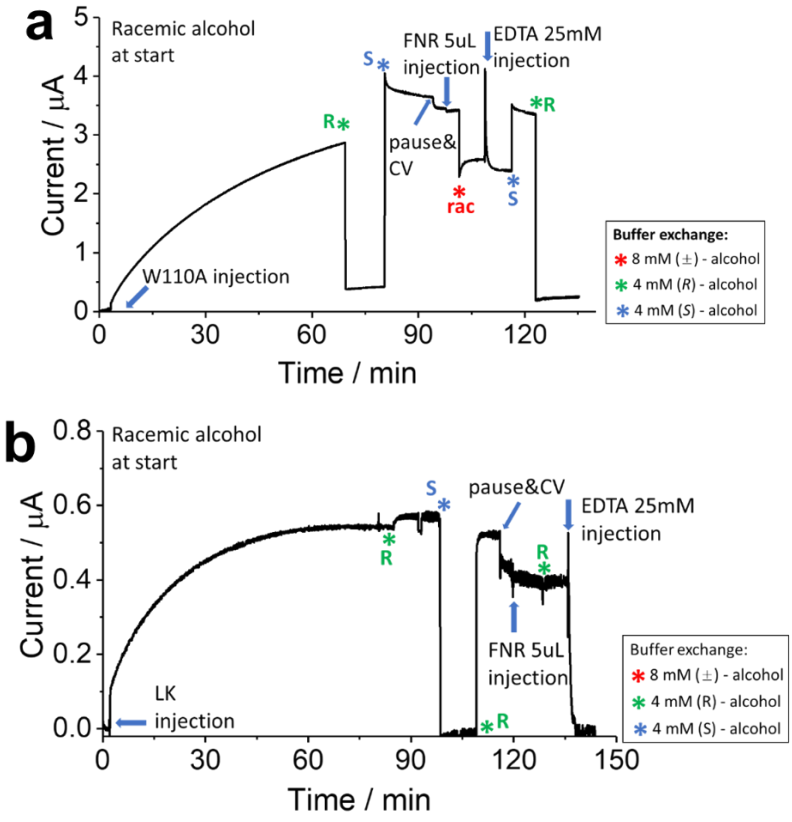


Figure 4.7. Chronoamperograms investigating substrate buffer exchange and EDTA effect on single-E2 system. **a)** W110A **b)** LK. Conditions: cell volume 4 mL; substrate [(±)-4-phenyl-2-butanol] = 8 mM, [$NADP^+$] = 10 µM, [Mg^{2+}] = 5 mM buffer: 50 mM TAPS pH 9.0; temperature: 25 ℃, Potential held at -0.175 V vs. SCE to drive oxidation. Solution purged with argon to remove O_2; argon flow maintained in headspace thereafter. Rotating disk electrode (RDE) SA: 0.07 cm^2, 1000 rpm. Enzyme loading: FNR loaded by drop-casting before the experiment; E2s are loaded during the experiment as shown in graphs.

4.3.2. Investigating the Effect of Changing the Alcohol and the Addition of EDTA in Real-time on LK and W110A Co-entrapped in One Electrode

Based on the separate single-E2 experiments in the last section, the system in which both enzymes are co-entrapped in the pores was then investigated. The chronoamperograms are shown in figure 4.8; FNR was pre-loaded and sequential loading was then used for each E2. After each loading process, a buffer exchange was carried out to remove enzyme from the bulk solution. Buffer switches between racemic, (*S*) and (*R*) show the attribution of current to each enzyme and injection of EDTA confirms the inactivation of LK and the subsequent 'shutting-off' of current attributed to LK. Loading two enzymes can be complex because they could possibly displace each other from the pores.

Figure 4.8 panel (a) shows a timecourse in which the coupled reaction was initiated by the addition of LK into the bulk solution (racemic alcohol substrate and cofactor present from the start, FNR preloaded in the pores). When the current reached a maximum level, a buffer exchange was carried out to remove excess LK from the solution, replacing it with buffer containing the same concentration of all substrates and cofactor. A real-time injection of W110A was then carried out and the current again increased gradually due to its adsorption into the pores, reaching a maximum at approximately 1.5 hours. A second buffer exchange was carried out to remove enzyme from bulk solution but this time replacing the solution with the (*R*) enantiomer (4 mM). The current decreased to a value lower than the original activity of LK with 4 mM R (in 8 mM racemic) which may be due to the displacement of LK by W110A during the latter's loading phase. The buffer was then exchanged to (*S*)-alcohol and the current increased to similar level as the current at the end of the W110A loading phase, which was because the buffer exchange retaind the same concentration of 4 mM (*S*)-alcohol and the product inhibition was not limiting the current. An FNR live injection was carried out,

and the current did not change in response to the FNR injection, suggesting that FNR was not the limiting factor in the system. A buffer exchange to racemic alcohol was conducted to remove the excess FNR in solution. A 25 mM EDTA injection was carried out to chelate the Mg^{2+} ions in the solution, which immediately decreased the current by a large level. This was due to the inactivation of the LK in the electrode on the chelation of Mg^{2+} ions. The buffer was exchanged to (*S*)-alcohol with a slightly higher current and then exchanged to (*R*)-alcohols to almost no current, showing again the inactivating effect of Mg^{2+} ion chelation on the LK while W110A remained unaffected.

Figure 4.8 panel (b) shows a similar experiment in which the time allowed for enzyme adsorption was much shorter (3.5 minutes for LK and W110A). The loading phases were interrupted by buffer exchanges when the current was showing a sharp increasing trend. The rest of the interventions were similar to the experiment in panel (a).

The difference between the two experiments is the time length of loading phase. Experiment in panel (a) has enough time for enzyme loading process so that the current finally became a plateau. The nanopores were well occupied by enzymes (FNR, LK, W110A). In the W110A loading phase, the W110A of an excess amount was probably displacing the LK already adsorbed in the electrode, since there were few empty sites for enzymes to attach to after a long-time loading phase of LK that ended with a plateau current. The displacement was confirmed by fact that the current level immediately after LK loading phase was higher than the current in the (*R*)-alcohol buffer after W110A loading.

As a comparison, the experiment in panel (b) had a loading phase of W110A interrupted by buffer exchange after a very short loading time (3.5 minutes), to avoid the saturation of the pores by the first enzyme (W110A) so that there was space for the second enzyme (LK) to be adsorbed. The increased scale of current in the LK loading phase was close to (slightly larger than) the current after buffer exchange to (*R*)-alcohol which

represents the current due to LK-catalysed reaction alone. And the current growth during W110A loading is slightly lower than current in (*S*)-alcohol as expected.

It is an interesting fact that since there is competitive displacement in the pores among enzymes, there will be an optimal ratio of all three enzymes in nanopores. At this specific loading points (enzyme ratio and amount), the three enzymes should occupy all the empty sites in the electrode and any shift from the specific ratio/amount of the three enzymes would cause a decrease in the overall catalytic rate (further discussion is in the appendix A4.3.3). This optimal point hypothesis also explains that in figure 4.7, due to the limit of the full occupation of the electrode nanopores, the current achieved with the racemic alcohol is similar to that with (*S*)-alcohol after buffer exchange.

The conclusion from this set of experiments is that the loading of two E2s in an optimal and controllable way is possible. The ADHs can be loaded together in the same electrode and can turnover separate enantiomers at the same time. Chelation of Mg^{2+} by EDTA titration can effectively shut off the conversion catalysed by LK whilst W110A and W110V remain active. The Mg^{2+} effect is discussed in the following section.

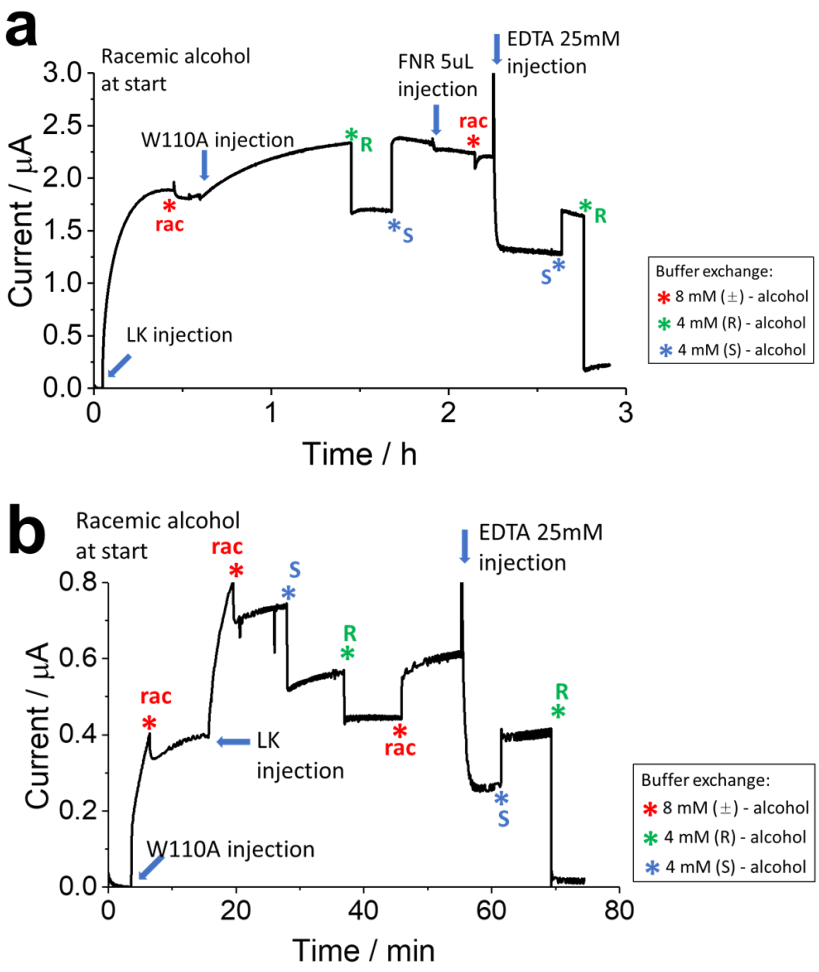


Figure 4.8. Chronoamperograms investigating substrate buffer exchange and EDTA effect on two-E2 system with **a)** a long time period loading phase **b)** a short time period loading phase. Conditions: cell volume 4 mL; substrate [(±)-4-phenyl-2-butanol] = 8 mM, [$NADP^+$] = 10 µM, [Mg^{2+}] = 5 mM buffer: 50 mM TAPS pH 9.0; temperature: 25 ℃, Potential held at –0.175 V vs. SCE to drive oxidation. Solution purged with argon to remove O_2; argon flow maintained in headspace thereafter. Rotating disk electrode (RDE) SA: 0.07 cm^2, 1000 rpm. Enzyme loading: FNR loaded by drop-casting before the experiment; E2s are loaded during the experiment as shown in graphs.

4.4. The Magnesium Effect

As mentioned in early sections, Mg^{2+} ions play an important role in maintaining the viability of LK. EDTA chelation of Mg^{2+} shuts down the LK-catalysed conversion and in this section, the effect of Mg^{2+} and its chelation by EDTA on the ADHs is investigated more thoroughly. The real-time response live-intervention takes advantages of the chronoamperometry.

4.4.1. W110A: A Mg^{2+} Titration

An Mg^{2+} titration with W110A as E2 is shown in figure 4.9. The chronoamperometry starts with a W110A injection into the bulk solution (FNR was already preloaded in the electrode pores). After 2 hours of loading, W110A in the solution was removed by buffer exchange (as described previously) and the titration began afterwards. Two 2.5 mM Mg^{2+} injections and one 5 mM Mg^{2+} injection were carried out sequentially (the amounts shown in the figure are cumulative concentrations), and followed by a 10 mM EDTA injection.

According to the figure, Mg^{2+} within the range of 0 – 5 mM can slightly boost the rate of the W110A-catalysed oxidation; approximately 15-20% increase on the oxidation current. When the concentration of Mg^{2+} rises to between 5 mM to 10 mM, there is no further boost to the rate. This is a control experiment to check the effect of Mg^{2+} and its removal by EDTA on the activity of W110A.

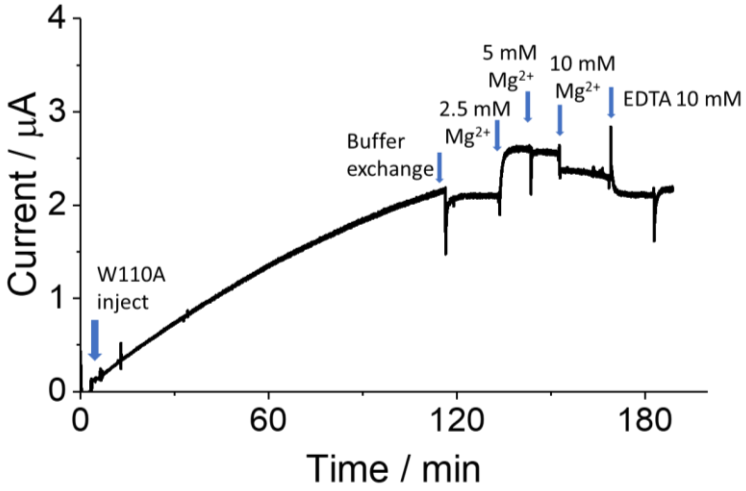


Figure 4.9. The effect of an Mg^{2+} titration on the W110A-catalysed oxidation; EDTA chelation also shown. Conditions: cell volume 4 mL; substrate [(±)-4-phenyl-2-butanol] = 8 mM, [$NADP^+$] = 10 µM, [Mg^{2+}] = 5 mM buffer: 50 mM TAPS pH 9.0; temperature: 25 ℃, Potential held at 0.175 V vs. SCE to drive oxidation. Solution purged with argon to remove O_2; argon flow maintained in headspace thereafter. Rotating disk electrode (RDE) SA: 0.07 cm^2, 1000 rpm. Enzyme loading: FNR loaded by drop-casting before the experiment; W110A 4.89 nmol live injected during the experiment as indicated by arrows in graph.

4.4.2. Further Investigations of the Mg^{2+} effect by EDTA Titration on LK and W110A

As a supplement and further extension to the Mg^{2+} titration, an EDTA titration experiment can give more comprehensive information. The first experiments presented were conducted with a small scale rotating disk electrode for simple initial trials and later were conducted with Ti foil electrodes since this is what was to be used for the deracemiser and inverter bulk conversion reactions.

4.4.2.1. Small Scale EDTA Titration with Rotating Disk Electrode

(1) W110A oxidation using a rotating disk electrode

The effect of the addition of EDTA for a W110A oxidation in the presence and absence of Mg^{2+} is shown in figure 4.10. In the experiment in panel (a), FNR and W110A were pre-loaded to the electrode before the reaction. With all of substrate presented with 5 mM Mg^{2+} in the cell, the electrode was applied a potential of -0.175 V vs. SCE and the reaction was initiated by the live injection of $NADP^+$. The EDTA injection was carried out and caused an immediate decrease of the current by approximately 20%, which suggests that Mg^{2+} must also enhance the activity of this variant in oxidation, since its chelation has caused this decrease. This matches the observation shown in figure 4.9, which is discussed in later section (4.4.2.2). There is potential enzyme structural and catalytic enhancement that Mg^{2+} ions may have on the W110A.

Panel (b) shows the control experiment without Mg^{2+}. FNR was pre-loaded to the electrode before the reaction. With all of substrate including $NADP^+$ presented with no Mg^{2+} in the cell, the same potential was applied, followed by the injection of W110A to initiate a loading process. A buffer exchange was conducted after the enzyme loading to remove excess W110A in the solution. The titration of EDTA was then carried out. And itself (from 1 mM to 10 mm) has no effect on the current, thus it can be concluded that the decrease of current caused was due to the chelation of the Mg^{2+}.

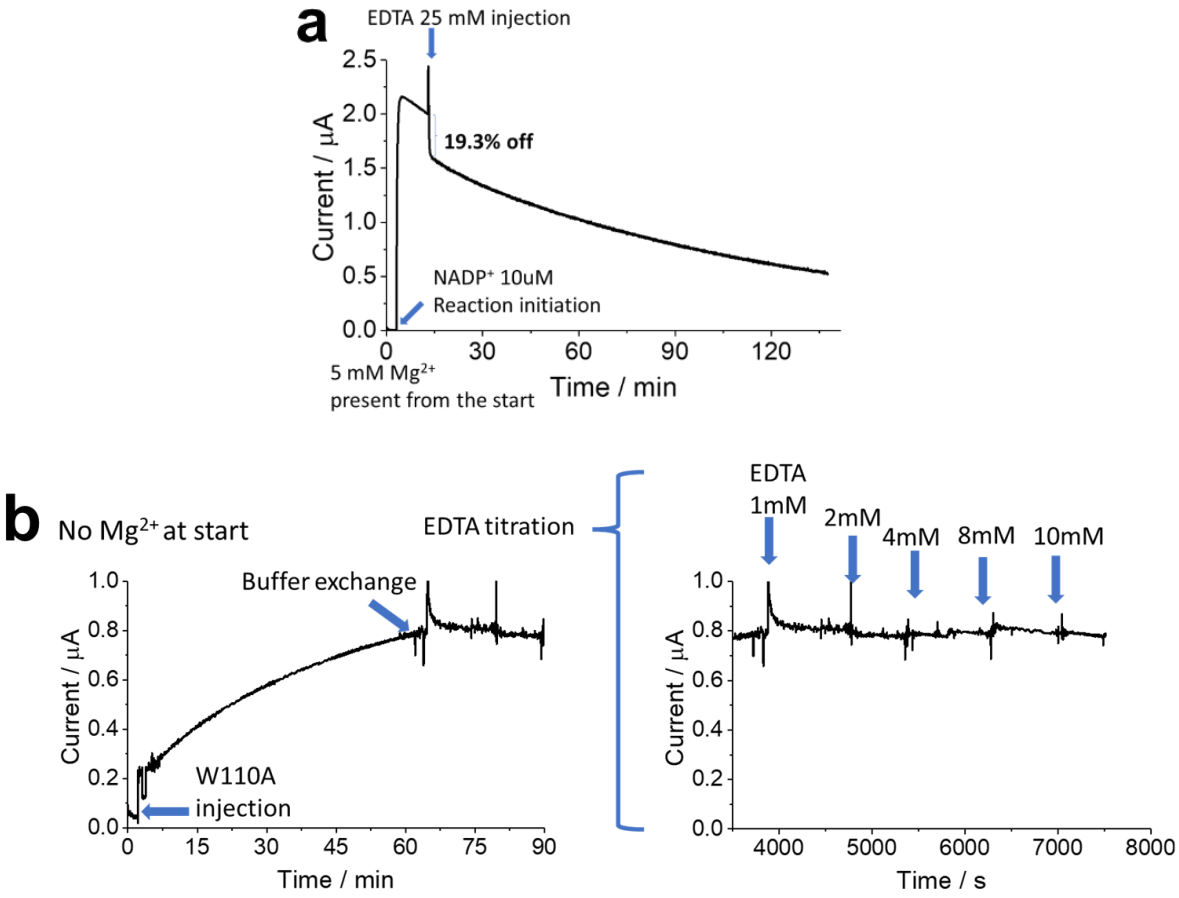


Figure 4.10. The effect of EDTA on the activity of W110A in the presence and absence of Mg^{2+}. **a)** with 5 mM Mg^{2+} present before reaction **b)** without Mg^{2+} in solution (b2 is the zoom-in of EDTA titration phase of the b1). Conditions: cell volume 4 mL; substrate [(±)-4-phenyl-2-butanol] = 8 mM, [$NADP^+$] = 10 µM, [Mg^{2+}] = 5 mM buffer: 50 mM TAPS pH 9.0; temperature: 25 ℃, Potential held at 0.175 V vs. SCE to drive oxidation. Solution purged with argon to remove O_2; argon flow maintained in headspace thereafter. Rotating disk electrode (RDE) SA: 0.07 cm^2, 1000 rpm. Enzyme loading: a) FNR 2.76 nmol + W110A 1.40 nmol applied in drop-casting together before experiment b) FNR first loaded by drop-casting, W110A is loaded by live injection 2.44 nmol during experiment.

(2) LK oxidation using a rotating disk electrode

The effect of EDTA on the oxidation reaction catalysed by LK is shown in figure 4.11. In this experiment, FNR was pre-loaded and LK was introduced into the bulk solution in real-time, allowed to adsorb and then the excess removed from solution by buffer exchange. The real-time addition of EDTA (25 mM) after this point, caused a sharp decrease to zero current, suggesting that it completely deactivated the LK.

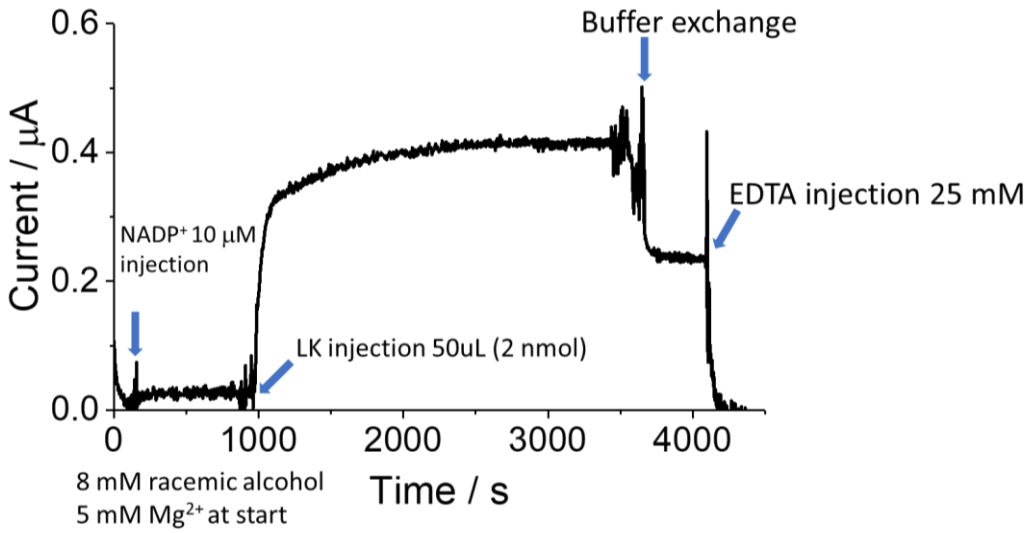


Figure 4.11. The effect of EDTA on the LK-catalysed oxidation reaction. Conditions: cell volume 4 mL; substrate [(±)-4-phenyl-2-butanol] = 8 mM, [$NADP^+$] = 10 µM, [Mg^{2+}] = 5 mM buffer: 50 mM TAPS pH 9.0; temperature: 25 ℃, Potential held at –0.175 V vs. SCE to drive oxidation. Solution purged with argon to remove O_2; argon flow maintained in headspace thereafter. Rotating disk electrode (RDE) SA: 0.07 cm^2, 1000 rpm. Enzyme loading: a) FNR 2.76 nmol + LK 0.37 nmol applied in drop-casting together before experiment

4.4.2.2. EDTA Titration with Ti Foil Electrode

This investigation on the effect of EDTA and Mg^{2+} was then carried out with a Ti foil electrode and this set of tests includes W110A, LK and W110V in both oxidation and reduction directions. In the following experiments, FNR and E2 were preloaded and each test was carried out in the following order. 1) cyclic voltammetry (CV1) is scanned first to check the amount of FNR loaded in the electrode by measuring its non-turnover peaks. 2) A second CV (CV2) was measured with 20 µM $NADP^+$ (all substrates for E2 were present from the start), showing the coupled current of oxidation or reduction. 3) A chronoamperometry experiment was then carried out with 5 mM Mg^{2+} in the solution, and 25 mM EDTA added in real-time to observe its effect on the current. 4) A third CV (CV3) is measured to show the effect of EDTA on the coupled CV shape. A comparison is made by overlapping CV2 and CV3.

(1) W110A

W110A in oxidation process

The test of W110A in the oxidation process was conducted with results shown in figure 4.12. The non-turnover peak from the CV (panel (a)) indicated a FNR loading amount of 93 pmol/cm^2. Such CV is mainly for testing the electrochemical connection and to ensure the foil electrodes are comparable to each other (enzyme amount and capacitance). The voltammetry under reaction conditions in panel (b) shows a plateaued current on the oxidation potential, indicating that the electrode was E2-limiting in the reaction. In the chronoamperometry (panel (c)), all of substrate were presented with 5 mM Mg^{2+} before the reaction. The reaction was initiated by the applying of a potential of 0 V vs. Ag/AgCl. A real-time addition of 25 mM EDTA was carried out afterwards and had no effect on the current. The overlaid CVs (panel (d)) confirms it by showing similar oxidation current level before and after the EDTA addition. The current level on the reduction side of the CV, however, were different, which could be due to the formation of ketone as a product in the oxidation process. Overall, the EDTA effect on the W110A activity in the oxidation is negligible with Ti foil electrode.

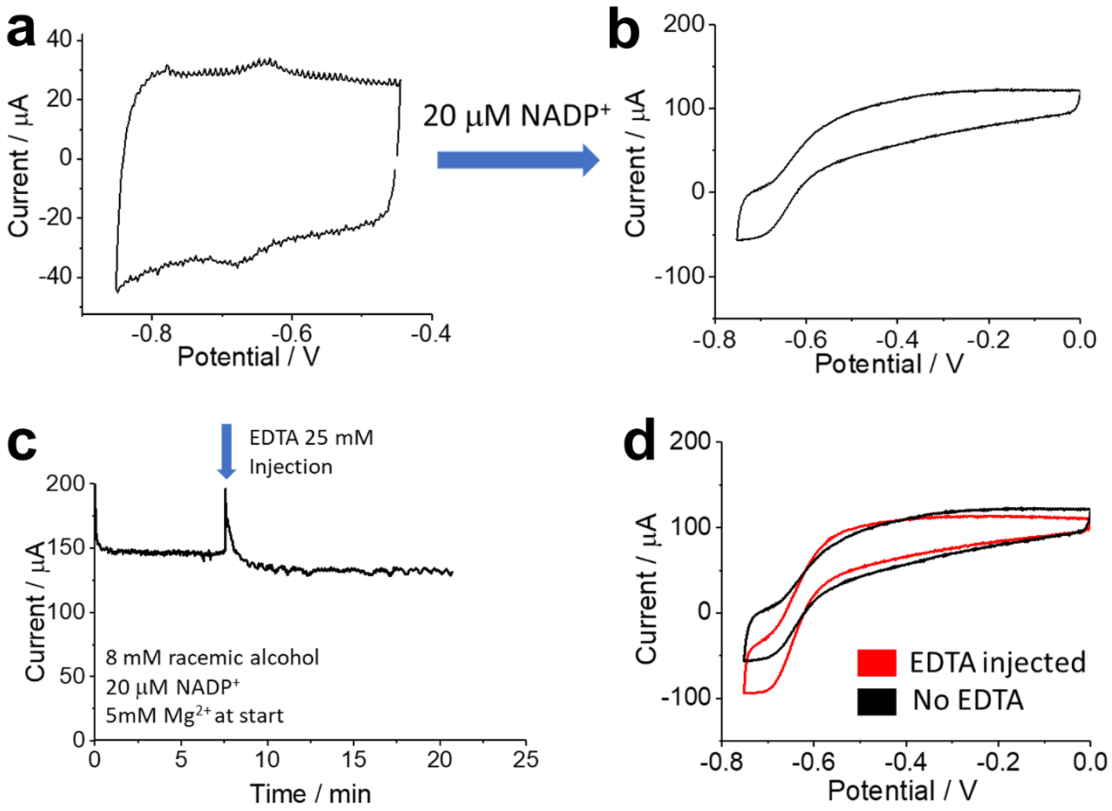


Figure 4.12. W110A-catalysed oxidation before and after EDTA injection in alcohol oxidation **(a)** cyclic voltammetry of electrode in reaction solution without $NADP^+$ showing FNR non-turnover peaks; scan rate = 4 mV/s **(b)** cyclic voltammetry of electrode in reaction solution with 20 µM $NADP^+$ showing coupled current; scan rate = 4 mV/s **(c)** chronoamperogram monitoring EDTA live injection effect on enzyme activity **(d)** cyclic voltammetry comparing coupled currents before and after EDTA injection; scan rate = 4 mV/s. Cell conditions: starting cell volume 5 mL; solution stirred throughout using a magnetic flea during chronoamperometry; substrate [(±)-4-phenyl-2-butanol] = 8 mM, [Mg^{2+}] = 5 mM buffer: 50 mM TAPS pH 9.0, [$NADP^+$] = 20 µM injected after (a); temperature: 25 ℃, Potential held at 0 V vs. Ag/AgCl (3 M KCl) to drive oxidation in chronoamperometry. All tests performed in an anaerobic glovebox to avoid any contribution to the current form the reduction of O_2. Enzyme loading: FNR loaded first by drop-casting, W110A loaded after FNR, by stirring in a 2.5 mL solution containing 2.38 nmols of W110A in 50 mM TAPS buffer pH 9.0; electrode (Ti foil) SA: 3.5 cm^2.

W110A in reduction process

A similar experiment was carried out on W110A in the reduction direction (figure 4.13). With the non-turnover voltammogram tested (panel (a)), the voltammetry under reaction conditions in panel (b) shows a non-plateaued current on the reduction potential, indicating that FNR is the limiting factor. This was different from the electrode in the experiment above which was E2-limiting. The difference may be due to irreproducibility

in electrode fabrication. It is also probably due to the different activities of the two enzymes in oxidation and reduction conditions. In the chronoamperometry (panel (c)), all of substrate were presented with 5 mM Mg^{2+} before the reaction. The reaction was initiated by the applying of a potential of 0 V vs. Ag/AgCl. Two real-time additions of 25 mM EDTA was carried out afterwards. The first addition of EDTA caused an increase of current by approximately 66% and the second one by 8%. The overlaid CVs (panel (d)) confirmed the increase in reduction currents before and after the EDTA additions. The fully active red trace is even less plateaued indicating that E2 was working at a very fast speed which the FNR cannot keep up with. There was also a slight increase on the oxidation current due to alcohol produced.

As shown in figure 4.9 And Figure 4.13, surprisingly, Mg^{2+} ion affects the oxidation activity and the reduction activity of the W110A differently. The addition of EDTA, which chelates the Mg^{2+} ions, increased the rate of the reduction reaction catalysed by W110A which suggests that the Mg ions have a deactivating effect on this enzyme's activity. The same is not true for its oxidation activity where Mg^{2+}ions in this case increase the activity. A hypothesised explanation is that the Mg^{2+}ions bind to the enzyme and cause a change in its conformation, possibly the active site geometry or charge distribution, such that the reduction of ketone becomes slower but the oxidation of alcohols, faster. The opposite effect of Mg^{2+} on W110A in different redox conditions is in fact a bonus for the designed deracemiser/inverter, in which W110A is working alone for the reduction process when LK is switched off by EDTA and the boost effect from Mg^{2+} chelation by EDTA will benefit the rate of the reduction phase.

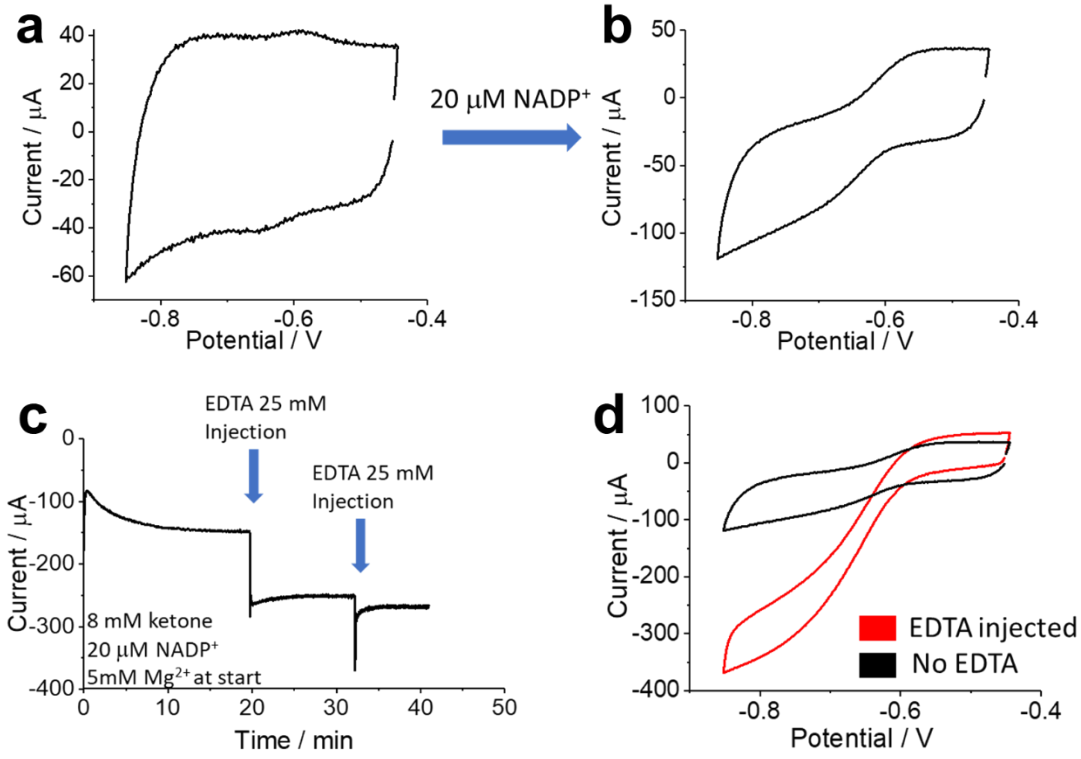


Figure 4.13. W110A-catalysed reduction before and after EDTA injection in ketone reduction process **(a)** cyclic voltammetry of electrode in reaction solution without $NADP^+$ showing FNR non-turnover peaks; scan rate = 4 mV/s **(b)** cyclic voltammetry of electrode in reaction solution with 20 µM $NADP^+$ showing coupled current; scan rate = 4 mV/s **(c)** chronoamperogram monitoring EDTA live injection effect on enzyme activity **(d)** cyclic voltammetry comparing coupled currents before and after EDTA injection; scan rate = 4 mV/s. Cell conditions: starting cell volume 5 mL; solution stirred throughout using a magnetic flea during chronoamperometry; substrate [4-phenyl-2-butanone] = 8 mM, [Mg^{2+}] = 5 mM buffer: 50 mM TAPS pH 8.0, [$NADP^+$] = 20 µM injected after (a); temperature: 25 ℃, Potential held at –0.74 V vs. Ag/AgCl (3 M KCl) to drive reduction in chronoamperometry. All tests performed in an anaerobic glovebox to avoid any contribution to the current form the reduction of O_2. Enzyme loading: FNR loaded first by drop-casting, W110A loaded after FNR, by stirring in a 2.5 mL solution containing 2.38 nmols of W110A in 50 mM TAPS buffer pH 9.0; electrode (Ti foil) SA: 3.5 cm^2.

(2) LK

LK in oxidation process

A similar experiment was carried out on LK in the oxidation direction (shown in figure 4.14). With the non-turnover voltammogram tested (panel (a)), the voltammetry under reaction conditions in panel (b) shows a plateaued current on the oxidation potential, indicating that the electrode was E2-limiting in the reaction. In the chronoamperometry (panel (c)),

all of substrate were presented with 5 mM Mg^{2+} before the reaction. The reaction was initiated by the applying of a potential of 0 V vs. Ag/AgCl. A real-time addition of 25 mM EDTA was carried out afterwards and the enzyme was inactivated immediately. The overlaid CVs (panel (d)) confirms it by showing a decrease of oxidation current to zero. The current level on the reduction side had no change, indicating a deactivation of LK.

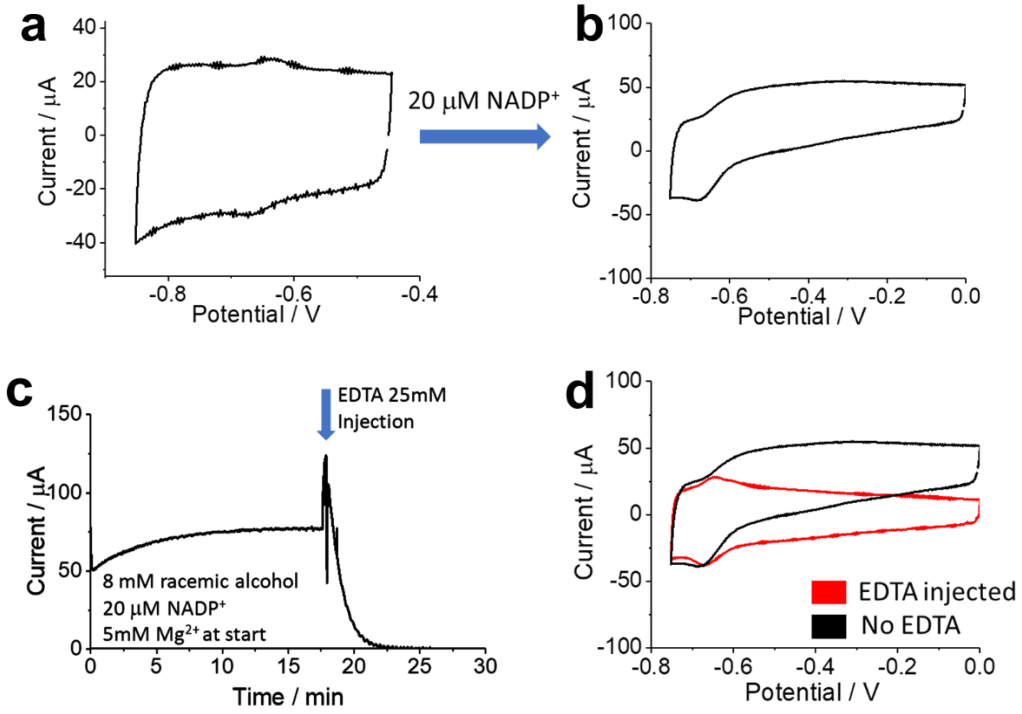


Figure 4.14. LK-catalysed oxidation before and after EDTA injection in alcohol oxidation process **(a)** cyclic voltammetry of electrode in reaction solution without $NADP^+$ showing FNR non-turnover peaks; scan rate = 4 mV/s **(b)** cyclic voltammetry of electrode in reaction solution with 20 µM $NADP^+$ showing coupled current; scan rate = 4 mV/s **(c)** chronoamperogram monitoring EDTA live injection effect on enzyme activity **(d)** cyclic voltammetry comparing coupled currents before and after EDTA injection; scan rate = 4 mV/s. Cell conditions: starting cell volume 5 mL; solution stirred throughout using a magnetic flea during chronoamperometry; substrate [(±)-4-phenyl-2-butanol] = 8 mM, [Mg^{2+}] = 5 mM buffer: 50 mM TAPS pH 9.0, [$NADP^+$] = 20 µM injected after (a); temperature: 25 ℃, Potential held at 0 V vs. Ag/AgCl (3 M KCl) to drive oxidation in chronoamperometry. All tests performed in an anaerobic glovebox to avoid any contribution to the current form the reduction of O_2. Enzyme loading: FNR loaded first by drop-casting, LK loaded after FNR, by stirring in a 2.5 mL solution containing 1.28 nmols of LK in 50 mM TAPS buffer pH 9.0; electrode (Ti foil) SA: 3.5 cm^2.

LK in reduction process

A similar experiment was carried out on LK in the reduction direction (shown in figure 4.15). With the non-turnover voltammogram tested (panel (a)), the voltammetry under reaction conditions in panel (b) shows a plateaued current on the reduction potential, indicating that the electrode was E2-limiting. In the chronoamperometry (panel (c)), all of substrate were presented with 5 mM Mg^{2+} before the reaction. The reaction was initiated by the applying of a potential of -0.74 V vs. Ag/AgCl. A real-time addition of 25 mM EDTA was carried out and the current decreased to zero at a fast rate indicating the inactivation of enzyme. The overlaid CVs (panel (d)) confirms it by showing a decrease of reduction current to zero. This experiment has confirmed the ability to rapidly switch off LK which implies it will be successful in the proposed approach for deracemisation and inversion. It is noteworthy that the decreasing of current after the EDTA addition took approximately 10 minutes in the large-scale reaction. The unwanted (*R*)-enantiomer could be produced during this period. Therefore, an addition of EDTA under zero reaction conditions could be better for the actual deracemisation/inversion process.

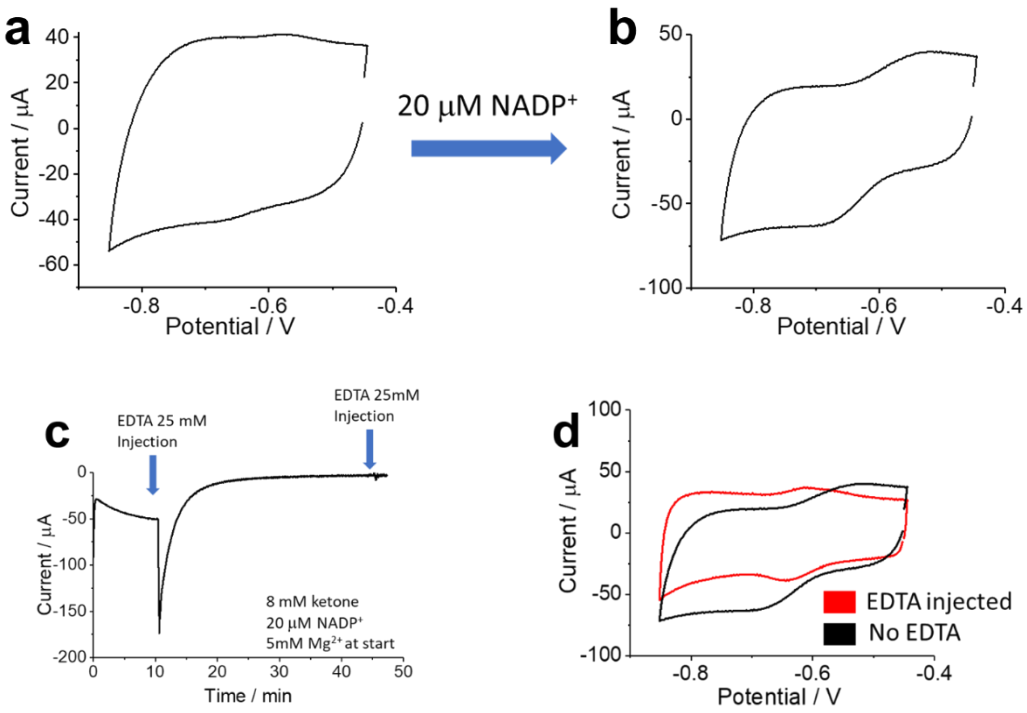


Figure 4.15. LK-catalysed reduction before and after EDTA injection in ketone reduction process **(a)** cyclic voltammetry of electrode in reaction solution without $NADP^+$ showing FNR non-turnover peaks. scan rate = 4 mV/s **(b)** cyclic voltammetry of electrode in reaction solution with 20 µM $NADP^+$ showing coupled current; scan rate = 4 mV/s **(c)** chronoamperogram monitoring EDTA live injection effect on enzyme activity **(d)** cyclic voltammetry comparing coupled currents before and after EDTA injection; scan rate = 4 mV/s. Cell conditions: starting cell volume 5 mL; solution stirred throughout using a magnetic flea during chronoamperometry; substrate [4-phenyl-2-butanone] = 8 mM, [Mg^{2+}] = 5 mM buffer: 50 mM TAPS pH 8.0, [$NADP^+$] = 20 µM injected after (a); temperature: 25 ℃, Potential held at −0.74 V vs. Ag/AgCl (3 M KCl) to drive reduction in chronoamperometry. All tests performed in an anaerobic glovebox to avoid any contribution to the current form the reduction of O_2. Enzyme loading: FNR loaded first by drop-casting, W110A loaded after FNR, by stirring in a 2.5 mL solution containing 1.28 nmols of LK in 50 mM TAPS buffer pH 9.0; electrode (Ti foil) SA: 3.5 cm^2.

(3) W110V

W110V in oxidation process

Similar tests were carried out on W110V in the oxidation direction (shown in figure 4.16). With the non-turnover voltammogram tested (panel (a)), the voltammetry under reaction conditions in panel (b) shows a plateaued current on the oxidation potential, indicating that the electrode was E2-limiting in the reaction. In the chronoamperometry (panel (c)), all of substrate were presented with 5 mM Mg^{2+} before the reaction. The reaction was initiated by the applying of a potential of 0 V vs. Ag/AgCl. A real-time addition of 25 mM

EDTA and had no effect on the current. The overlaid CVs (panel (d)) confirms it by showing similar oxidation current level before and after the EDTA addition. There was also a slight increase on the reduction current side due to ketone produced. W110V is as stable as W110A in the addition of EDTA. With a better selectivity, W110V could therefore be a good substitute for W110A.

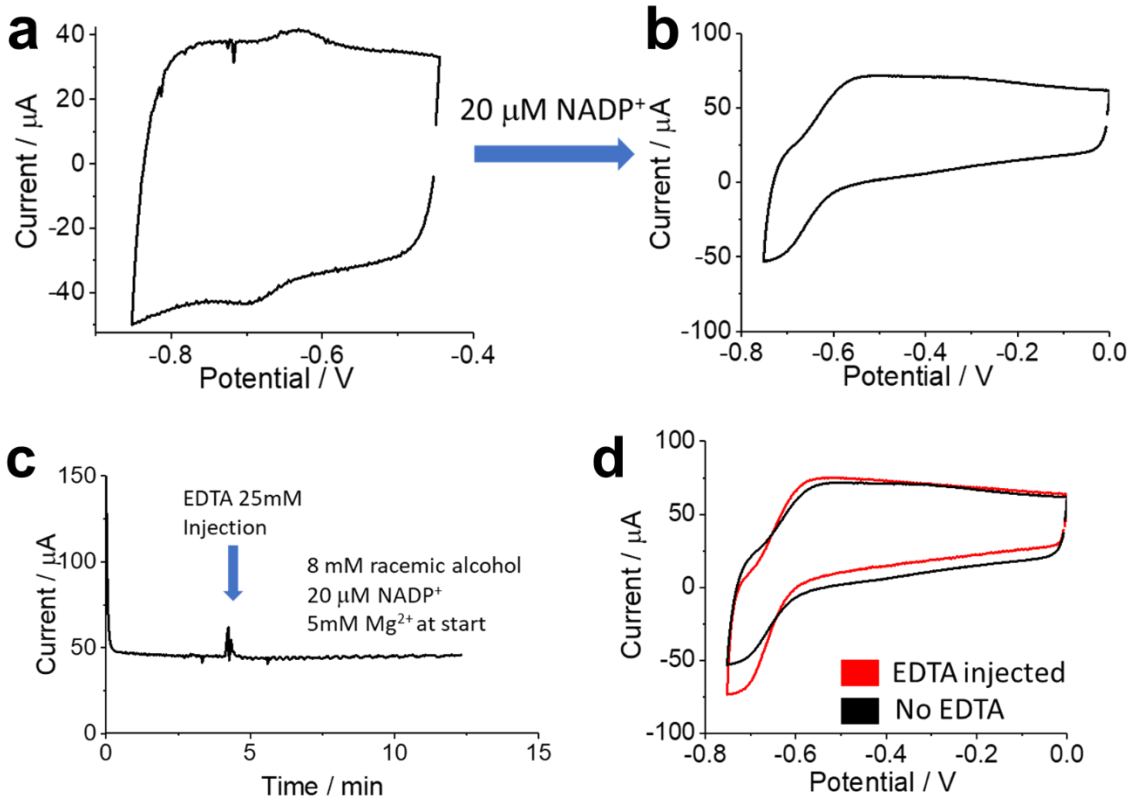


Figure 4.16. W110V-catalysed oxidation before and after EDTA injection in alcohol oxidation process **(a)** cyclic voltammetry of electrode in reaction solution without $NADP^+$ showing FNR non-turnover peaks; scan rate = 4 mV/s **(b)** cyclic voltammetry of electrode in reaction solution with 20 µM $NADP^+$ showing coupled current; scan rate = 4 mV/s **(c)** chronoamperogram monitoring EDTA live injection effect on enzyme activity **(d)** cyclic voltammetry comparing coupled currents before and after EDTA injection; scan rate = 4 mV/s. Cell conditions: starting cell volume 5 mL; solution stirred throughout using a magnetic flea during chronoamperometry; substrate [(±)-4-phenyl-2-butanol] = 8 mM, $[Mg^{2+}]$ = 5 mM buffer: 50 mM TAPS pH 9.0, $[NADP^+]$ = 20 µM injected after (a); temperature: 25 ℃, Potential held at 0 V vs. Ag/AgCl (3 M KCl) to drive oxidation in chronoamperometry. All tests performed in an anaerobic glovebox to avoid any contribution to the current form the reduction of O_2. Enzyme loading: FNR loaded first by drop-casting, LK loaded after FNR, by stirring in a 2.5 mL solution containing 3.28 nmols of W110V in 50 mM TAPS buffer pH 8.0; electrode (Ti foil) SA: 3.5 cm^2.

W110V in reduction process

A similar experiment was carried out on W110V in the reduction direction (shown in figure 4.17). With the non-turnover voltammogram tested (panel (a)), the voltammetry under reaction conditions in panel (b) shows a non-plateaued current on the reduction potential, indicating that the electrode was in FNR-limiting in the reaction. In the chronoamperometry (panel (c)), all of substrate were presented with 5 mM Mg^{2+} before the reaction. The reaction was initiated by the applying of a potential of -0.74 V vs. Ag/AgCl. Two real-time additions of 25 mM EDTA was carried out afterwards. The first addition of EDTA caused an increase of current by approximately 66% and the second one by 8%. The overlaid CVs (panel (d)) confirmed the increase in reduction currents before and after the EDTA additions. The current increased upon the additions of EDTA suggests the similar effect of Mg^{2+} of slowing down the activity of W110V in reduction as W110A.

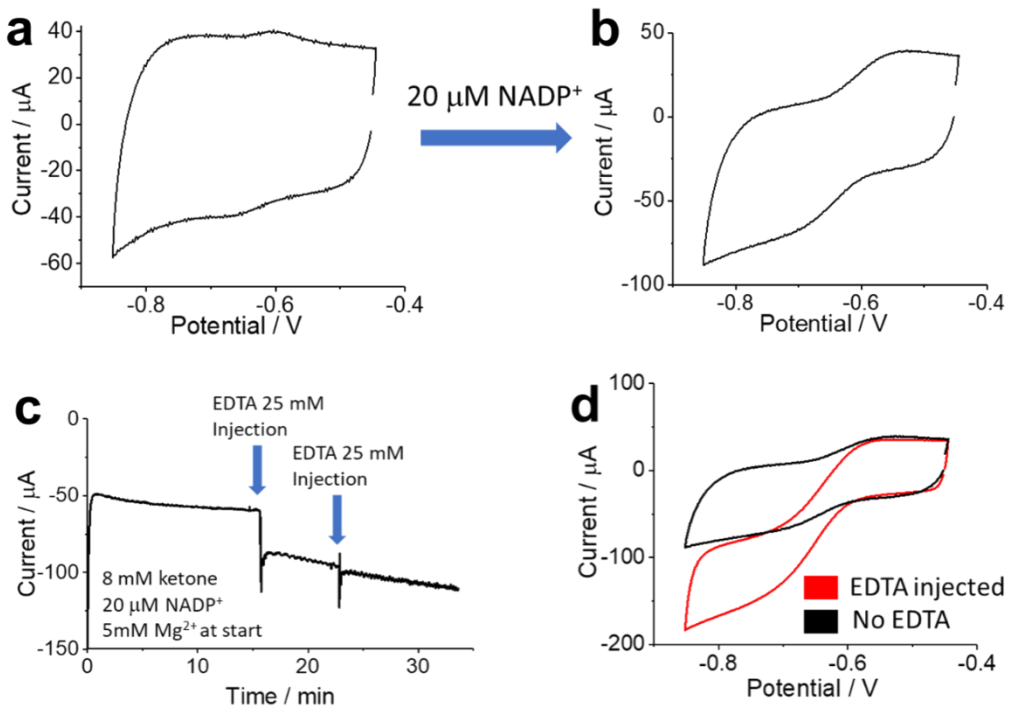


Figure 4.17. W110V-catalysed reduction before and after EDTA injection in ketone reduction process **(a)** cyclic voltammetry of electrode in reaction solution without $NADP^+$ showing FNR non-turnover peaks; scan rate = 4 mV/s **(b)** cyclic voltammetry of electrode in reaction solution with 20 µM $NADP^+$ showing coupled current; scan rate = 4 mV/s **(c)** chronoamperogram monitoring EDTA live injection effect on enzyme activity **(d)** cyclic voltammetry comparing coupled currents before and after EDTA injection; scan rate = 4 mV/s. Cell conditions: starting cell volume 5 mL; solution stirred throughout using a magnetic flea during chronoamperometry; substrate [4-phenyl-2-butanone] = 8 mM, [Mg^{2+}] = 5 mM buffer: 50 mM TAPS pH 8.0, [$NADP^+$] = 20 µM injected after (a); temperature: 25 ℃, Potential held at −0.74 V vs. Ag/AgCl (3 M KCl) to drive reduction in chronoamperometry. All tests performed in an anaerobic glovebox to avoid any contribution to the current form the reduction of O_2. Enzyme loading: FNR loaded first by drop-casting, W110A loaded after FNR, by stirring in a 2.5 mL solution containing 3.28 nmols of W110V in 50 mM TAPS buffer pH 8.0; electrode (Ti foil) SA: 3.5 cm^2.

4.5. The Electrochemical Leaf: Optimisation for Inversion and Deracemisation

This section includes the key experiments for the deracemiser and inverter, from the initial idea to an optimised version with further improvement. Enzyme loading process has been optimised for this system before the experiments (appendix A4.3). The core of the design for the deracemiser and inverter is the control of enantioselectivity through choice of nanoconfined enzyme and the ability to control the direction of the reaction by the applied potential. The primary idea is to co-load FNR and two ADHs with opposite

enantioselectivities in the same electrode, taking advantage of nanoconfinement to generate high synergy among enzyme catalysis of NADP(H) cofactor regeneration catalysed by FNR, and downstream conversion by E2. The reaction direction is manually controlled by switching the potential applied, and the enantioselectivity is also manually selected with Mg^{2+} chelation shutting off LK activity.

In the dual-control invertor, an oxidative potential is applied first, and (*R*)-alcohol is oxidised to ketone catalysed by LK, while the (*S*)-alcohol is also oxidised by W110A at the same time. Then the potential is switched from oxidative to reductive, and LK is deactivated by an injection of EDTA to chelate Mg^{2+} in solution. The ketone is then reduced to (*S*)-alcohol by W110A and the whole process is complete. The deracemiser is a similar process as an inverter except some (*S*)-alcohol will be oxidised in the first step by the S-selective enzyme. The ratio between LK and W110A needs to be carefully adjusted to favour (*R*)-alcohol selectivity in oxidation and to guarantee sufficient activity of W110A in reduction. The whole process takes normally at least 2 days, and the enzymes are stable and active enough throughout the process. The time could be shortened by an increased electrode surface area for a higher rate. Improvements made based on the basic design include pH adjustment on potential switching, W110V as a substitute with better selectivity for S compared to W110A and optimisation by higher electrode surface area and an increase of EDTA deactivating time to ensure LK is fully deactivated.

4.5.1. A Two-electrode Deracemisation System

A repeat deracemisation experiment by using two separate electrodes[56] has been conducted to outline this approach for ease of comparison to the novel system designed and used later throughout this chapter. This also serves as a test case to describe certain issues involved in the rest of experiment (performance evaluation, calculation and errors, etc.). The chronoamperogram is shown in figure 4.18; enzymes were loaded in the pores of the ITO/Ti foil electrode as follows: FNR was first loaded by drop-casting and rinsing,

LK and W110A were loaded from a stirred solution overnight (each in different separate FNR-loaded electrodes). The (FNR+LK) on ITO/Ti electrode (electrode 1) was used for the oxidation process, aiming to convert only (*R*)-alcohol to ketone. After oxidation, the working electrode was switched to electrode 2, (FNR+W110A) on ITO/Ti and a negative potential was applied to drive reduction, in order to reduce the ketone produced in oxidation, to (*S*)-alcohol.

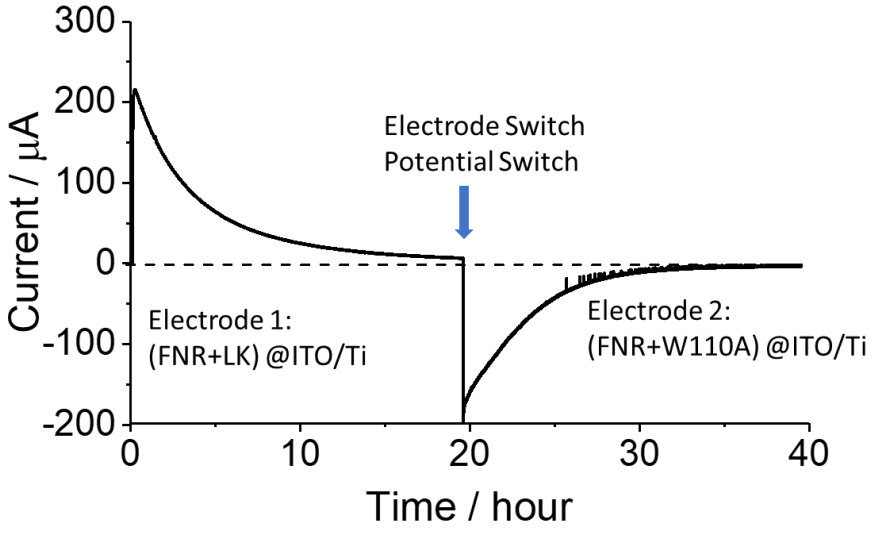


Figure 4.18. Deracemisation using a two-electrode system. Reaction monitored by chronoamperometry with the starting electrode (loaded with FNR and LK) replaced at the halfway stage with electrode 2 (loaded with FNR and W110A). Conditions: starting cell volume 5 mL and 1 mL sample is taken at potential switch; solution stirred throughout using a magnetic flea; substrate [(±)-4-phenyl-2-butanol] = 8 mM, [$NADP^+$] = 20 µM, [Mg^{2+}] = 5 mM buffer: 50 mM TAPS pH 9.0; temperature: 25 ℃, Potential held at 0 V vs. Ag/AgCl (3 M KCl) to drive oxidation and −0.85 V for reduction. Solution purged with argon to remove O_2; argon flow maintained in headspace thereafter. Enzyme loading: FNR loaded first by drop-casting, E2s loaded after FNR, by stirring in a 2.5 mL solution containing 5.12 nmols LK, or solution containing 4.85 nmols of W110A. (in 50 mM TAPS buffer pH 9.0); electrode (Ti foil) SA: 7 cm^2 for both electrodes.

The coulometric conversion from the chronoamperogram was 43.6% in oxidation and 92.1% in reduction, which are both close to full conversion assuming a 100% faradaic efficiency. The GC enantiomer analysis peak and result is shown in following table 4.6. The enantioselectivity in oxidation is excellent in that nearly all of (*R*)-alcohol is converted. In reduction, most of the ketone was converted to (*S*)-alcohol with a small amount of (*R*)-

alcohol produced since W110A has a very low selectivity towards (*R*). The overall ratio of (*S*) to (*R*) is increased by a large amount.

Table 4.6. GC Enantiomer analysis for electrode-switching deracemiser

	[S]/mM	[R]/mM	[ketone]/mM	ketone%	S%	R%	ee%(*S*)
Starting	3.40	4.24	0.36	4.5	42.6	52.9	-10.9
Post-oxidation	4.05	0.00	3.95	49.4	50.6	0.0	100.0
Post-reduction	6.95	0.83	0.22	2.7	86.9	10.4	78.7

Performance evaluation

The performance of a deracemiser or an inverter is evaluated from several dimensions:

1) The coulometric conversion is calculated from the charge passed as:

$$\mathrm{X} = \frac{\int I\, dt}{n\, F} \qquad (4.2)$$

Where X is the amount of product in moles, n is the number of electrons per reaction, F is Faraday's constant which is 96485 C mol^{-1}. The conversion is then calculated by dividing amount of product by the starting concentration of substrate. Since it is based on the real-time current, coulometric conversion throughout the timecourse gives a real indication of the reaction progress.

2) Gas chromatography (GC) analysis data is linked to the final status of the cell solution. GC peak area indicates the amount of sample present, from which the concentration and percentage of components are calculated. It is important that the protocol (especially the amount and concentration of sample used in test) is always the same among each test, so that peaks signals are comparable across all the experiments. GC analysis data and coulometric data should match if the faradaic efficiency is 100%. The actual experiments have a faradaic efficiency close to 100% (with an error of 5 - 10% tested by NMR). The data indicates not only the completeness of the process, but also the enantiomer selectivity.

3) The enantiomer excess (ee%) is calculated based on the GC result as

$$ee\%(S) = \frac{S\% - R\%}{S\% + R\%} \times 100 \qquad (4.3)$$

This number suggests to how much extent one enantiomer is over the other. Higher ee% is an indicator of high chiral purity.

Comparing to the two-electrode deracemiser, the newer design is simpler in operation with only potential switch and live interventions required with all three enzymes involved loaded together in the pores of the ITO on one Ti foil electrode with the conversion achieved in one pot. It is much more elegant in the process comparing to the two-electrode-switch design, even though with a slightly lower ee%. The optimisation and development process for the new deracemiser and inverter with the dual control, is presented in the following sections.

4.5.2. Inversion (*R* to *S*): (LK + W110A) Co-entrapped in a Single Electrode

4.5.2.1. Initial Design for Inversion

The goal of this enantiomer inverter is to convert (*R*)-alcohol to (*S*)-alcohol. Enzymes are coloaded in the pores of the ITO/Ti foil electrode; FNR is first loaded by drop-casting and LK and W110A are loaded together from solution at a ratio of 10:1. All three enzymes are loaded on the same electrode, and the (FNR+LK+W110A)@ITO/Ti electrode is used for the whole process including first oxidation and then reduction.

Figure 4.19 shows the chronoamperogram of the initial version of this inverter. To start with, the solution has 4 mM (*R*)-alcohol as substrate as well as 5 mM Mg^{2+} required for the activity of LK. The oxidation was initiated by applying a potential of 0 V (vs. Ag/AgCl in 3 M KCl) at which point the current rapidly increased (positive current since the first stage is an oxidation). The oxidation step takes 18 hours to finish (as the current approached zero), with a coulometric conversion of 88.6%. When oxidation is complete,

the potential was switched to −0.85 V. The real-time addition of 25 mM EDTA was carried out to chelate the Mg^{2+} in solution for the purpose of shutting down LK activity, making the leaf electrode (*S*)-alcohol selective only. The potential was then switched to a reductive one which yields a rapid increase in negative current indicating reduction is being catalysed. The reduction process takes approximately 18 hours to finish and the coulometric conversion is 83.1%.

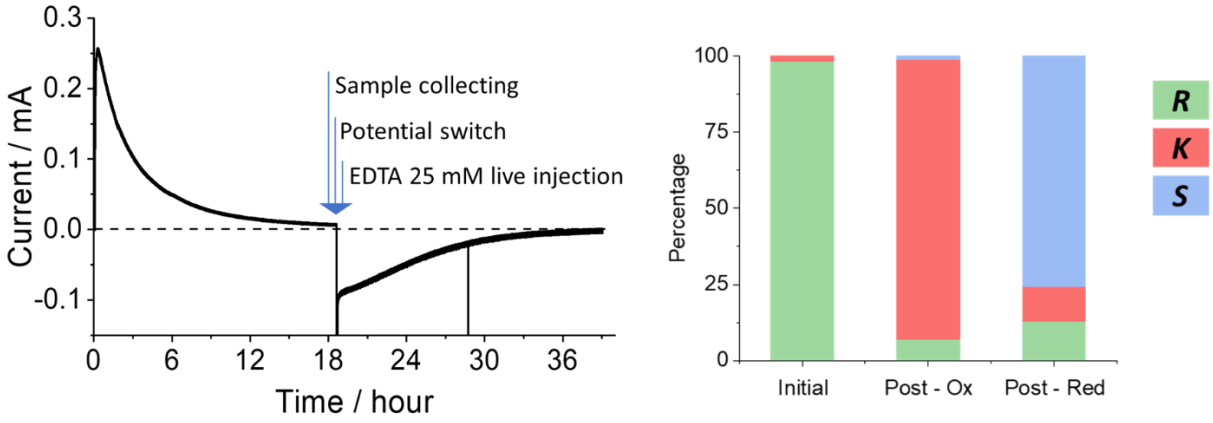


Figure 4.19. Inversion of (*R*)-4-phenyl-2-butanol catalysed by co-entrapped ADHs with bidirectional control monitored via chronoamperogram, with composite detected by GC shown in a bar chart. Conditions: starting cell volume 5 mL and 1 mL sample is taken at potential switch; solution stirred throughout using a magnetic flea; substrate [(*R*)-4-phenyl-2-butanol] = 4 mM, [$NADP^+$] = 20 µM, [Mg^{2+}] = 5 mM buffer: 50 mM TAPS pH 9.0; temperature: 25 ℃, Potential held at 0 V vs. Ag/AgCl (3 M KCl) to drive oxidation and −0.85 V for reduction. Experiments performed in an anaerobic glovebox to avoid any contribution to the current form the reduction of O_2. Enzyme loading: FNR loaded first by drop-casting, LK and W110A loaded after FNR, by stirring in a 2.5 mL solution containing 1.28 nmols of LK and 0.47 nmols of W110A in 50 mM TAPS buffer pH 9.0; electrode (Ti foil) SA: 7 cm^2. Reprinted from Cheng et al with permission from the Royal Society of Chemistry.[57]

Table 4.7 shows the analysis of solution at the start, after oxidation and after reduction which was also depicted as a bar chart in figure 4.19. The starting solution has a tiny amount of ketone impurity that can be from the oxidation of alcohol by oxygen in open air. For oxidation, the enantioselectivity and conversion are both excellent in that nearly all of (*R*)-alcohol is converted. The extent of reaction is satisfactory with 0.28 mM substrate left considering the K_m(*R*) for LK in pH 9.0 is approximately 1.57 mM and product inhibition exists. In reduction, most of the ketone is converted to (*S*)-alcohol with a small amount of (*R*)-alcohol produced. The process has an ee% of 70.4. The cell solution which initially

contained 3.93 mM (*R*)-alcohol, contained 3.02 mM (*S*)-alcohol, 0.52 mM (*R*)-alcohol and 0.45 mM ketone at the end of the experiment. It is a decent proof of concept for inversion using the electrochemical leaf that takes great advantage of controlling the reaction direction and selectivity from multiple enzymes.

Table 4.7. GC Enantiomer analysis for the initial inverter

	[S]/mM	**[R]/mM**	**[ketone]/mM**	**ketone%**	**S%**	**R%**	**ee%(*S*)**
Starting	0.00	3.93	0.07	1.7	0.0	98.3	100.0
Post-oxidation	0.05	0.28	3.67	91.7	1.2	7.1	-70.4
Post-reduction	3.02	0.52	0.45	11.3	75.5	13.1	70.4

*GC traces in appendix A4.4

4.5.2.2. Inverter Improved by pH Adjustment

A Pourbaix diagram for the $NADP^+$/NADPH couple and the alcohol/ketone couple was constructed (Figure 4.20). It can be seen that oxidation will be favoured at higher pH (pH>8.3) and the reduction favoured at lower pH. This shows that at pH 9.0 the reduction can be slowed down and the conversion would be incomplete. It has been observed from multiple repeated experiments as well, that the post-reduction usually has approximately 10% or an even higher amount ketone left. To address this problem, pH adjustment has been introduced to the process.

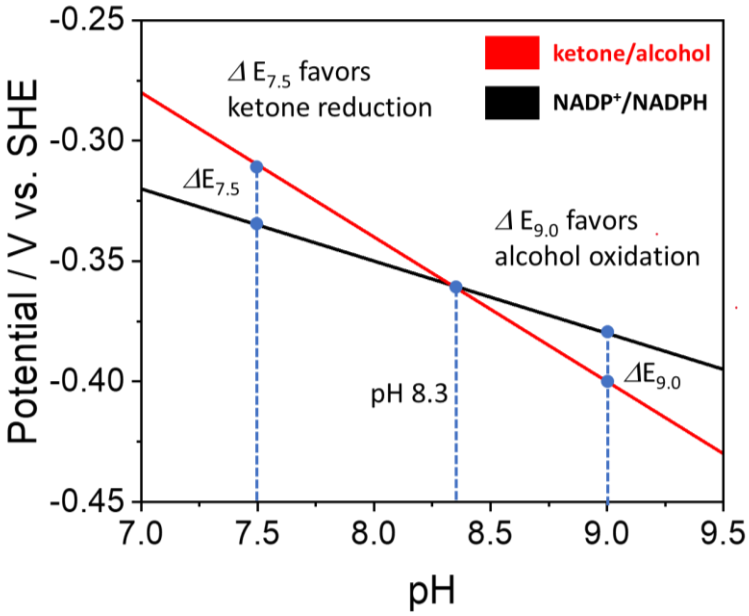


Figure 4.20. Pourbaix diagram depicting $NADP^+$/NADPH couple and 4-phenyl-2-butanone/4-phenyl-2-butanol couple. The slope of the $NADP^+$/NADPH couple is -30 mV/pH since it is a $2e^-/1H^+$ reaction. The slope of the ketone/alcohol couple is -60 mV/pH since it is a $2e^-/2H^+$ reaction, and the formal reduction potential for the couple at pH9.0 is approximately -0.4 V vs SHE.[112] The ΔE indicates the bias for ketone/alcohol redox coupled to the $NADP^+$ /NADPH cycling.

The pH adjustment is carried out by simply injecting diluted HCl solution (9.25% HCl, 4-fold dilution of 37% HCl) into the cell solution. The amount of HCl solution injected was determined by titration trials with a pH metre. It turns out to be that for the 4 mL pH 9.0 solution (50 mM TAPS buffer and 25 mM EDTA), an injection of 135 μmol HCl (45 μL in volume) will bring the pH from 9.0 to pH 7.5 – 8.0, at which reduction is favoured.

Figure 4.21 shows the chronoamperometry of the inverter with a pH adjustment improvement. The basic steps are the same as the previous inverter. The HCl addition took place at the potential switch. When oxidation was complete, the potential was switched to –0.74 V vs. Ag/AgCl (3 M KCl) and 25 mM EDTA injected, together with 105 μmol HCl to adjust the pH from 9 to approximately 8. The pH was tested after reduction and was 8.22 in the main compartment of the cell.

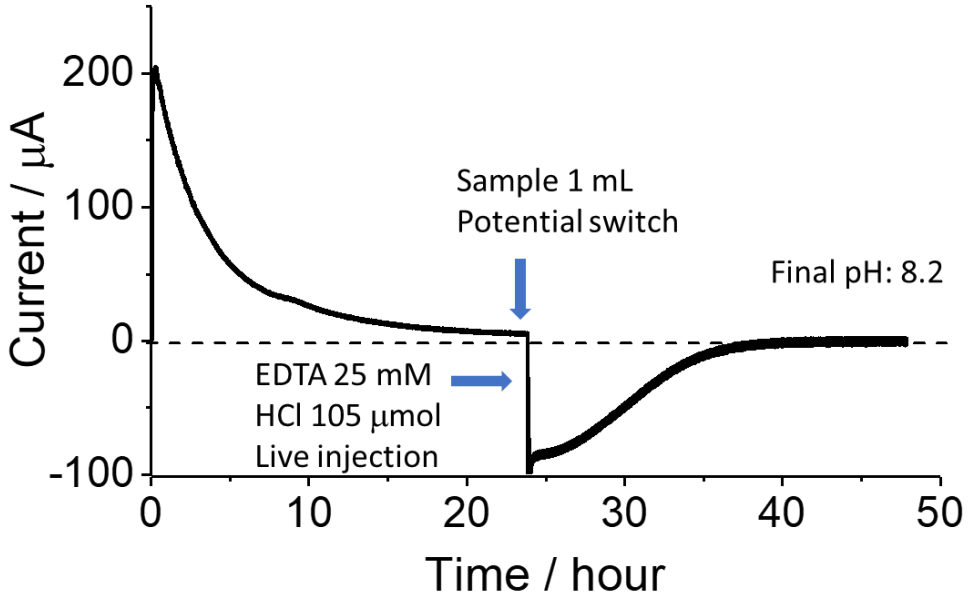


Figure 4.21. Inversion of (*R*)-4-phenyl-2-butanol catalysed by ADHs nanoconfined in a single electrode with bidirectional control with pH adjustment. Conditions: starting cell volume 5 mL and 1 mL sample is taken at potential switch; solution stirred throughout using a magnetic flea; substrate [(*R*)-4-phenyl-2-butanol] = 4 mM, [$NADP^+$] = 20 µM, [Mg^{2+}] = 5 mM buffer: 50 mM TAPS pH 9.0, pH is adjusted by HCl injection to approximately pH 8.0 at potential switch; temperature: 25 ℃, Potential held at 0 V vs. Ag/AgCl (3 M KCl) to drive oxidation and −0.74 V for reduction. Experiments performed in an anaerobic glovebox to avoid any contribution to the current form the reduction of O_2. Enzyme loading: FNR loaded first by drop-casting, LK and W110V loaded after FNR, by stirring in a 2.5 mL solution containing 1.28 nmols of LK and 0.47 nmols of W110A in 50 mM TAPS buffer pH 9.0; electrode (Ti foil) SA: 7 cm^2.

In term of the outcome from figure 4.21 and table 4.8, the oxidation process takes approximately 24 hours to finish with a coulometric conversion of 86.5%. The enantioselectivity is good but the conversion is poor. The reduction process has performed well with a coulometric conversion of 81.3%, full completion of ketone into (*S*)-alcohol. The calculation assumptions and errors caused are discussed in the appendix (A4.1).

In this experiment, in addition to the pH adjustment, a slight change was made to the enzyme ratio in order to increase activity during the reduction stage. The LK: W110A ratio was changed from 1.28 nmol: 0.47 nmol to 0.96 nmol 0.71 nmol (LK:W110A). But this change has caused the poor conversion observed in the oxidation stage as the

lower amount of LK is not enough to complete full conversion in oxidation. This is an example which shows how much the balance in enzyme ratios can affect the outcome.

Table 4.8. GC Enantiomer analysis for the inverter with pH adjustment

	[S]/mM	[R]/mM	[ketone]/mM	ketone%	S%	R%	ee%(*S*)
Starting	0.00	3.93	0.07	1.68	0.00	98.3	-100.0
Post-oxidation	0.05	0.45	3.50	87.6	1.2	11.2	-80.6
Post-reduction	2.14	0.46	0.07	2.7	80.0	17.3	64.4
Side-arm	0.76	0.27	0.29	21.9	57.8	20.3	48.0

4.5.3. Deracemisation (Racemic to S): LK + W110A Co-entrapped in a Single Electrode

This section shows the first proof of principal experiment with pH adjustment improvement for the deracemiser. The general process and operation are the same as in an inverter to convert (*R*)-alcohol to (*S*)-alcohol, with the starting substrate a racemic alcohol mixture.

4.5.3.1. Initial design for deracemisation

Figure 4.22 shows the chronoamperogram for the initial version of the deracemiser. The starting solution has 8 mM (±)-alcohol and 5 mM Mg^{2+} for LK activity. A positive potential is first applied to drive oxidation (positive current). This step takes 24 hours to finish, with a coulometric conversion of 68.9%. The gradual current drop is primarily due to product inhibition since the coulometry is not close to full completion. The oxidation process was stopped by switching the potential to −0.85 V vs. Ag/AgCl (3 M KCl) and 25 mM EDTA was injected to chelate the Mg^{2+} in solution to deactivate LK, making the leaf (*S*)-alcohol selective only. The reduction process took 46 hours to complete and achieved a conversion of 60.0%.

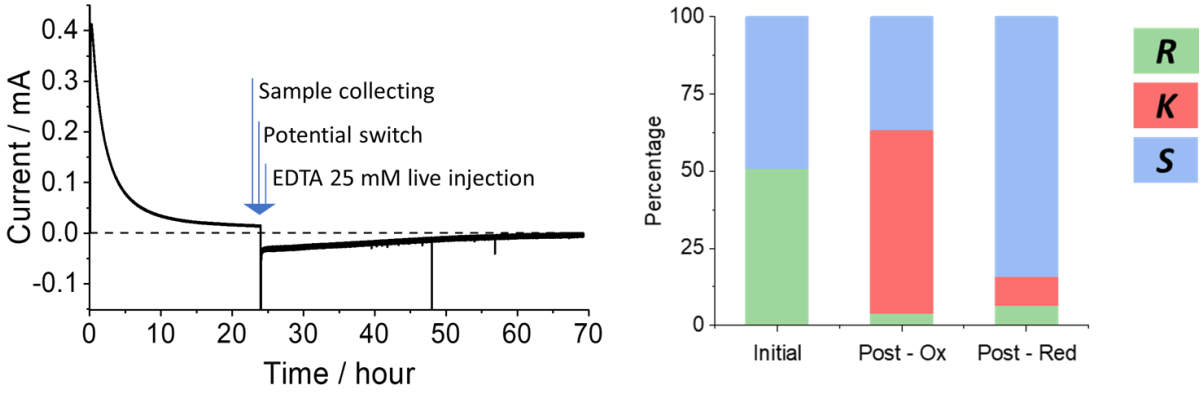


Figure 4.22. Deracemisation of (±)-4-phenyl-2-butanol catalysed by ADHs with bidirectional control monitored via chronoamperometry, with composite detected by GC shown in a bar chart. Conditions: starting cell volume 5 mL and 1 mL sample is taken at potential switch; solution stirred throughout using a magnetic flea; substrate [(±)-4-phenyl-2-butanol] = 8 mM, [$NADP^+$] = 20 µM, [Mg^{2+}] = 5 mM buffer: 50 mM TAPS pH 9.0; temperature: 25 ℃, Potential held at 0 V vs. Ag/AgCl (3 M KCl) to drive oxidation and −0.85 V for reduction. Experiments performed in an anaerobic glovebox to avoid any contribution to the current form the reduction of O_2. Enzyme loading: FNR loaded first by drop-casting, LK and W110A loaded after FNR, by stirring in a 2.5 mL solution containing 1.28 nmols of LK and 0.47 nmols of W110A in 50 mM TAPS buffer pH 9.0; electrode (Ti foil) SA: 7 cm^2. Reprinted from Cheng et al with permission from the Royal Society of Chemistry.[57]

Table 4.9 shows the solution GC analysis of the process, which was also depicted as a bar chart in figure 4.22. For oxidation, the enantioselectivity and conversion are excellent, the (*R*)-alcohol is almost fully converted from 4 mM to 0.32 mM. The conversion from solution GC analysis is 59.3%. In the reduction process (main compartment), most ketone was converted to (*S*)-alcohol and the conversion was 88.6%. The final ee% in the main compartment is 85.8. There is quite a big difference between the coulometry and GC solution analysis in this experiment. The details are discussed in appendix (section A4.2), about calculation and errors.

Table 4.9. GC Enantiomer analysis for the initial deracemiser

	[S]/mM	[R]/mM	[ketone]/mM	ketone%	S%	R%	ee%(*S*)
Starting	3.92	4.08	0.00	3.92	49.0	51.0	-2.0
Post-oxidation	2.94	0.32	4.74	2.94	36.7	4.0	80.3
Post-reduction	4.82	0.37	0.54	4.82	84.1	6.4	85.8
Side-arm	2.27	1.44	0.14	30.2	63.5	6.3	81.9

*GC traces in appendix A4.4

Trade-off between LK and W110A in deracemiser

The chronoamperogram shows a very low current in reduction. It is much trickier in a deracemiser than an inverter to balance the activity of LK and W110A: the system with racemic substrate needs higher LK activity to consume as much as possible (*R*)-alcohol in oxidation. From the observation of past experiments, the product inhibition slows down oxidation by both enzymes and the current drops rapidly to nearly zero when 4 – 6 mM product is made. This means achieving high activity with LK (which is required for conversion of (*R*)-alcohol becomes difficult. In the reduction stage however, high W110A activity is required to reduce the ketone produced in last step back to (*S*)-alcohol. When W110A loading is low or the reaction condition is not favoured, the process could take a long time and the final conversion is incomplete. As figure 4.22 shows, the reduction current is very low over the whole process and the reduction takes 46 hours. The leaf has been working for 70 hours, and the activity of enzymes decreasing over time. The current decrease can possibly be due to either the consumption of ketone or the deactivation of the system or both. Many deracemisation experiments through the course of this work have shown the trend that in the experiments with low reaction rates, the discrepancy between GC solution analysis and coulometric conversion is larger compared to experiments with higher reaction rates.

This initial deracemiser is a proof of concept for the idea of using the electrochemical leaf, and it has disclosed the possible improvements required: the reduction process can be improved by adjusting the ratio of the two ADHs and by pH adjustment.

4.5.3.2. Deracemiser Improved by pH Adjustment

As mentioned previously pH 9.0 is less favourable for reduction and the low reaction rate causes incomplete conversion and a longer reaction time. It is most important for a deracemiser to have a pH adjustment since the balance between LK and W110A is more complex. As mentioned in last section, LK selectivity needs to be dominant for a good oxidation performance, but W110A at too low amounts will cause issues in

reduction. Therefore, pH adjustment is more desired for a deracemiser to improve the reduction rate.

The pH adjusting operation was carried out in the same way as in the inverter, by injecting diluted HCl solution (9.25% HCl, 4-fold dilution of 37% HCl) into the cell solution. The pH of the post-oxidation will change from pH 9.0 to pH 7.5 – 8.0 at which the reduction is favoured. Figure 4.23 shows the chronoamperometry for the deracemiser with pH adjustment. When oxidation is finished, the potential was switched to –0.74 V vs. Ag/AgCl (3 M KCl) and 25 mM EDTA injected along with 135 μmol HCl to adjust the pH from 9 to approximate 8. The pH tested after reduction was 8.1 in the main compartment of the cell.

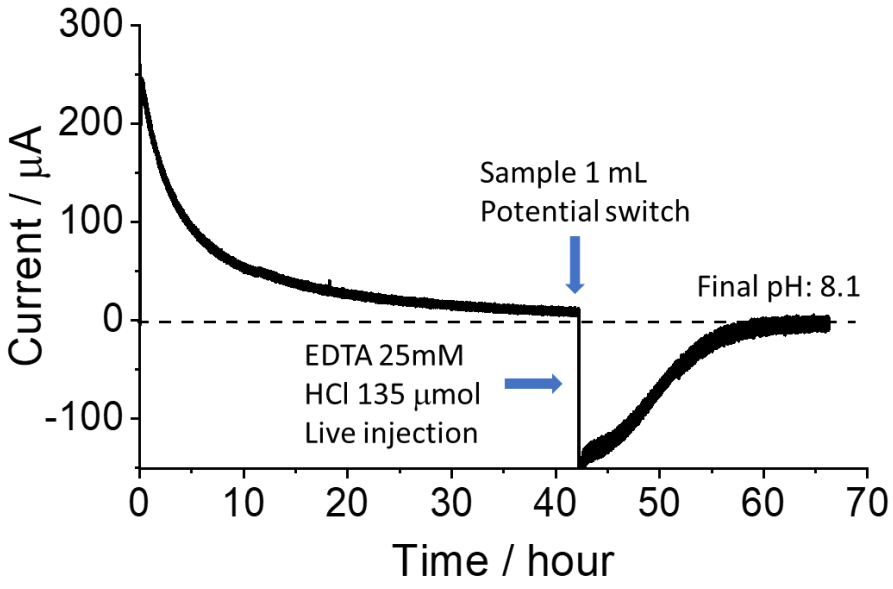


Figure 4.23. Deracemisation of (±)-4-phenyl-2-butanol catalysed by ADHs with bidirectional control and pH adjustment. Conditions: starting cell volume 5 mL and 1 mL sample is taken at potential switch; solution stirred throughout using a magnetic flea; substrate [(±)-4-phenyl-2-butanol] = 8 mM, [$NADP^+$] = 20 μM, [Mg^{2+}] = 5 mM buffer: 50 mM TAPS pH 9.0, pH is adjusted by HCl injection to approximately pH 8.0 at potential switch; temperature: 25 ℃, Potential held at 0 V vs. Ag/AgCl (3 M KCl) to drive oxidation and –0.74 V for reduction. Experiments performed in an anaerobic glovebox to avoid any contribution to the current form the reduction of O_2. Enzyme loading: FNR loaded first by drop-casting, LK and W110V loaded after FNR, by stirring in a 2.5 mL solution containing 2.56 nmols of LK and 0.95 nmols of W110A in 50 mM TAPS buffer pH 9.0; electrode (Ti foil) SA: 7 cm^2.

The 40-hours oxidation phase achieved a coulometric conversion of 85.1%. The reduction process achieved a higher current than the previous experiment without pH adjustment, and a coulometric conversion of 80.1%. Table 4.10 shows the GC analysis. The conversion of (*R*)-alcohol in oxidation is ~81.6%. The reduction has a 95.2% conversion of ketone. The final ee% is 71.9.

Table 4.10. GC Enantiomer analysis for the deracemiser with pH adjustment

	[S]/mM	[R]/mM	[ketone]/mM	ketone%	S%	R%	ee%(*S*)
Starting	3.92	4.08	0.00	0.0	49.0	51.0	-2.0
Post-oxidation	0.80	0.75	6.45	80.6	10.0	9.4	2.8
Post-reduction	4.49	0.73	0.31	5.5	81.2	13.3	71.9
Side-arm	1.06	0.45	0.96	38.9	42.8	18.4	39.9

This improved version of the deracemiser has shown better performance with good conversion rate and enantiomer selectivity. It is a successful case showing the dual-control features of electrochemical leaf. By controlling the enantiomer selectivity and reaction direction, inversion and deracemisation can be well achieved in a fast and elegant way, to give a product with good chiral purity.

4.6. A New ADH Variant: W110V

In the observation of past experiments, it was found that the percentage of (*R*)-alcohol often increases slightly in reduction, resulting in a decrease in final ee%. This is due to the fact that W110A can produce some (*R*)-alcohol since it is not extremely highly selective for (*S*)-alcohol (W110A have some activity towards (*R*)-alcohol). In addition, the nanoconfinement also adds to the issue. Under nanoconfinement some interconversion catalysed by W110A can occur without being driven via FNR, resulting in the concentrating of (*R*)-alcohol that is interconverted at extremely slow rate.[56,112] To alleviate this problem and to improve the concept of electrochemical leaf as an inverter

and deracemiser further, a new variant was chosen with superior enantioselectivity for the (*S*)-enantiomer. The W110V variant substitutes W110A in following experiments.

As shown in table 4.11, W110V is a slower variant than W110A with an extremely low k_{cat}(*R*) for the oxidation of (*R*)-alcohol. In fact, this can be used as a benefit for the system. By adjusting the loading amount of W110V, a comparable reduction rate to that achieved with W110A and a lower oxidation activity can be achieved at the same time. The optimisation of W110V loading process is discussed in the appendix (A4.5).

Table 4.11. Kinetic data by steady-state solution assays for (*S*)-selective TeSW110A, W110V and LK

Variant	k_{cat}(*S*) / s^{-1}	K_m(*S*) / mM	k_{cat}(*R*) / s^{-1}	K_m(*R*) / mM	k_{cat}(ketone) / s^{-1}	K_m(ketone) / mM
TeSW110A	29.8	0.50	0.68	0.57	48.4	0.29
TeSW110V	6.2	0.13	/	/	20.1	0.12
LK	/	/	29.0	1.58	32.8	0.13

Solution assay conditions: 25 °C, [$NADP^+$] = 300 M for alcohol oxidation, [NADPH] = 200 μM for ketone reduction; volume = 400 μL, buffer for alcohol oxidation: pH 9.0, 50 mM TAPS, 1 mM $MgCl_2$, buffer for ketone reduction: pH 7.5, 50 mM TAPS, 1 mM $MgCl_2$, 25 mM NaCl. Adapted with permission from L. Wan *et al*. Copyright 2021, ACS Catal.[56]

4.7. The Optimised Inverter and Deracemiser: with W110V Substituting W110A

This section shows experiments for the (FNR+LK+W110V) in the ITO/Ti electrode system working as a deracemiser and an inverter. The slight production of (*R*)-alcohol may also come from the LK activity. In previous experiments, the EDTA was injected in real-time when the reductive potential was applied. According to figure 4.15, even though EDTA titration can eliminate activity of LK quickly, it still takes approximately 20 – 30 minutes for the current to return to zero. Another small improvement of the system has now been applied together with the use of W110V: the EDTA addition process is no longer in real-time, and a one-hour incubation time is added after the injection, in between the oxidation and reduction steps.

Figure 4324 shows the chronoamperograms for the inverter (panel (a)) and deracemiser (panel (b)) using W110V. The process is similar to previous experiments: after oxidation, the chronoamperometry was stopped and a 1 mL sample taken from the reactor's main compartment, 25 mM EDTA with 135 mmol HCl was then injected into the solution and the solution was then stirred for 1 hour, after which the reductive potential was applied and the chronoamperometry resumed.

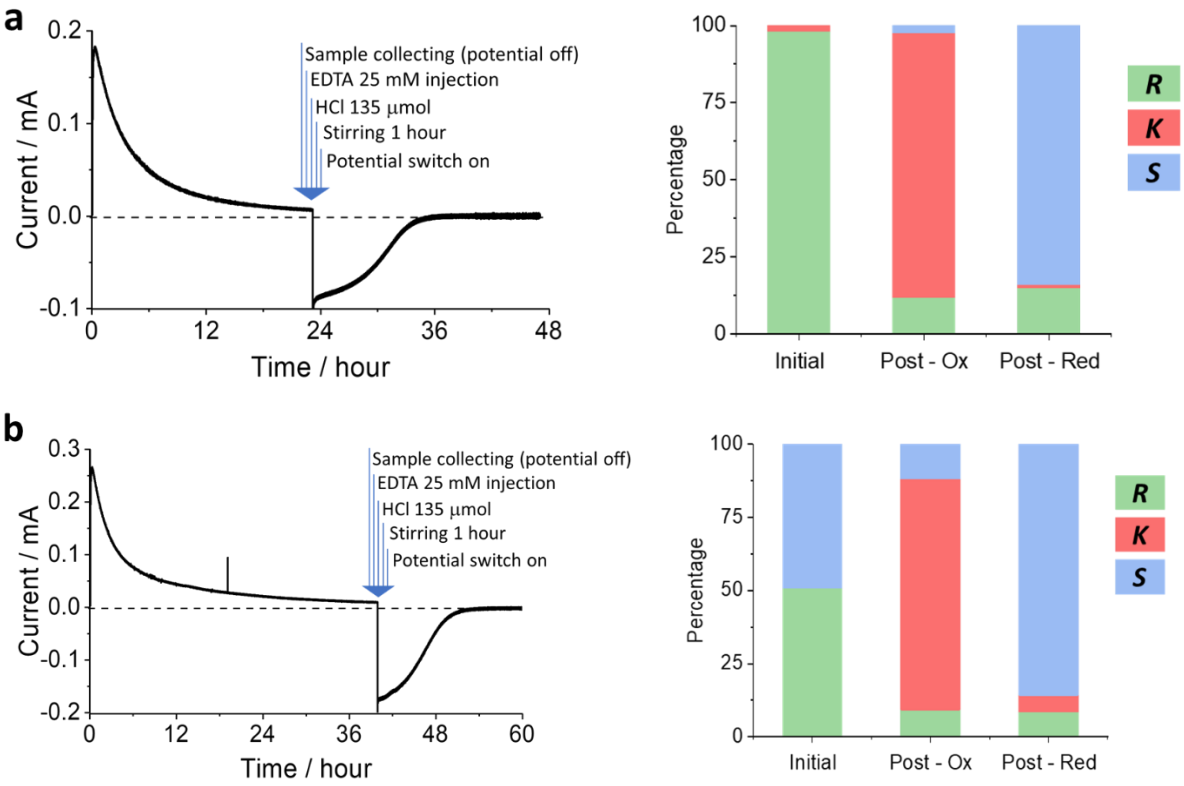


Figure 4.24. E-Leaf deracemiser and inverter with W110V**. a)** Inversion of (*R*)-4-phenyl-2-butanol **b)** deracemiser of (±)-alcohol catalysed by ADHs (W110V + LK) with bidirectional control and extra EDTA stirring time before reduction, composite detected by GC shown in bar charts.

Conditions: starting cell volume 5 mL and 1 mL sample is taken at potential switch; solution stirred throughout using a magnetic flea; substrate [(*R*)-4-phenyl-2-butanol] = 4 mM for inverter and [(±)-4-phenyl-2-butanol] = 8 mM for deracemiser, [$NADP^+$] = 20 µM, [Mg^{2+}] = 5 mM buffer: 50 mM TAPS pH 9.0, pH is adjusted by HCl injection to approximately pH 8.0 at potential switch; temperature: 25 ℃, Potential held at 0 V vs. Ag/AgCl (3 M KCl) to drive oxidation and –0.74 V for reduction. Experiments performed in an anaerobic glovebox to avoid any contribution to the current form the reduction of O_2. Enzyme loading: FNR loaded first by drop-casting, LK and W110V loaded after FNR, by stirring in a 2.5 mL solution containing 1.28 nmols of LK and 0.66 nmols of W110V in 50 mM TAPS buffer pH 9.0; electrode (Ti foil) SA: 7 cm^2. Reprinted from Cheng et al with permission from the Royal Society of Chemistry.[57]

The inverter took ~36 hours to finish and has a coulometric conversion of 85.2% in oxidation and 83.8% in reduction. The deracemiser with a longer oxidation process took ~54 hours to finish has a coulometric conversion of 83.5% in oxidation and 79.0% in reduction. It can be concluded from the trace shape that the reduction is close to a full completion in both experiments as there is quite a sharp decrease to zero.

Enantiomer analysis of the reaction solution is also depicted as bar chart in figure 4.24, with detailed data in table 4.12 and 4.13 (GC signals shown in the appendix). The (*R*)-alcohol concentration of the post-reduction solution is close to, if not less than, that of the post-oxidation solution, which suggests no (*R*)-alcohol was produced in the reduction process and nearly all ketone was converted to (*S*)-alcohol. These results have proved the success of the new improvements in limiting the production of (*R*)-alcohol in reduction. The deactivation of LK before the reduction phase to prevent(*R*)-alcohol being produced during the reduction is critical and the EDTA deactivating effect on LK became sufficient given enough incubation time.

Table 4.12. GC Enantiomer analysis for the inverter with W110V

	[S]/mM	[R]/mM	[ketone]/mM	ketone%	S%	R%	ee%(*S*)
Starting	0.00	3.93	0.07	1.7	0.0	98.3	-100.0
Post-oxidation	0.09	0.48	3.43	85.7	2.4	12.0	-67.1
Post-reduction	2.78	0.50	0.04	1.1	83.9	15.0	69.6
Side-arm	0.34	0.16	0.19	27.7	49.2	23.1	36.2

*GC traces in appendix A4.4

Table 4.13. GC Enantiomer analysis for the deracemiser with W110V

	[S]/mM	[R]/mM	[ketone]/mM	ketone%	S%	R%	ee%(*S*)
Starting	3.92	4.08	0.00	0.0	49.0	51.0	-2.0
Post-oxidation	0.95	0.73	6.31	78.9	11.9	9.2	12.9
Post-reduction	5.06	0.50	0.33	5.6	86.0	8.5	82.1
Side-arm	1.10	0.31	0.71	33.7	51.9	14.4	56.5

*GC traces in appendix A4.4

This latest design has optimised the selectivity performance in reduction and achieved a good conversion rate with acceptable ee%. The W110V + LK system also has more typically shaped (sudden depletion of substrate) chronoamperograms than W110A+LK system. It is an excellent representative design demonstrating the dual-control features of electrochemical leaf. However, the new improvement is not able to increase final ee% by much. The design is still open for further improvement since the (*R*)-alcohol after the oxidation is still present, although at a low concentration, preventing the final product to be ultra-pure.

By far, the data collected have pointed to the fact that the limit of enzyme selectivity has been reached. Most of the best oxidizing results have lowered the concentration of (*R*)-alcohol down to ~5% for deracemisation and slightly higher for inversion. The concentration after oxidation would be approximately 8 mM * 5% = 0.4 mM which is far below the K_m for this alcohol with LK (which is 1.58 mM). Thus, it is likely that the system has reached its limit for deracemising/inverting in terms of the amount of (*R*)-alcohol left after oxidation. Improvement in the future would be to use a new variant of an (*R*)-selective enzyme which has both higher selectivity and activity.

4.8. Inverter and Deracemiser: with More Substrate

From past results, it has been observed that inversion's ee% is not as high as those obtained in the deracemisation. In addition, the intrinsic nature of enzymes' selectivity and activity, the reason could also lie in the calculation. The ee%(*S*) is calculated as:

$$ee\%(S) = \frac{S\% - R\%}{S\% + R\%} \times 100 \qquad (4.4)$$

where S% and R% is the concentration percentage of (*S*) and (*R*) alcohol in the solution. For most of the inversion experiments above, the starting concentration is 4 mM (*R*)-alcohol rather than 4 mM (*R*)-alcohol plus 4 mM (*S*)-alcohol used in deracemisation. Enzymes in the system have worked to their limit so that theoretically no matter how

much substrate to start with, the end points (absolute concentration of remaining substrate) are always quite similar. In oxidation, the concentration of (*R*)-alcohol remaining afterwards is ~0.5 mM on average. The deracemisation process, with more final product (*S*)-alcohol at beginning, is likely to have a higher '(*S*) to (*R*) ratio' in the end given same amount of substrate left. The calculation favours a higher starting amount and therefore the inversion's ee% is not as high as deracemisation in general.

Several experiments are conducted with higher substrate concentration. The experiments are based on the hypothesis that since the system has reached the limit of enzyme selectivity, the same amount of substrate would be left no matter how much amount to start with. The solubility of alcohol is approximately 12 mM, and it is still good to start the conversion with 10 mM substrate instead of 8 mM or 4 mM. Increasing the concentration of starting substrate is expected to be a way to increase the final ee%.

LK +W110V Inverter and deracemiser with more substrate

Figure 4.25 shows the chronoamperograms of the inverter (a) and deracemiser (b) with (FNR+LK+W110V) on ITO/Ti electrode. The process is the same as previous experiments with only different concentration of starting substrates. The outcomes are not as good as expected. According to the solution analysis in table 4.14 and 4.15, the conversion rate of (*R*)-alcohol in oxidation is lower than usual, causing a larger amount of (*R*)-alcohol in final solution. In the reduction phase for the inverter experiment, the current is low. This could be due to the poor loading process and the low amount of W110V relative to LK.

The reason for the low conversion rate of (*R*)-alcohol in oxidation is due to product inhibition. It is the factor that has been neglected when the high substrate concentration experiment was designed. It can be observed from the chronoamperograms that at the later stage of oxidation, the current becomes extremely low and can do minimal further conversion. The ketone produced is ~6 mM which is higher than previous experiments, thus causing the stronger inhibition effect. The enzymes cannot achieve the limit of their

selectivity before the inhibition slows down their activity. Repeated experiment has been conducted with the electrode loaded with (W110A + LK), and the similar problem with product-inhibition was observed (details in the appendix A4.6).

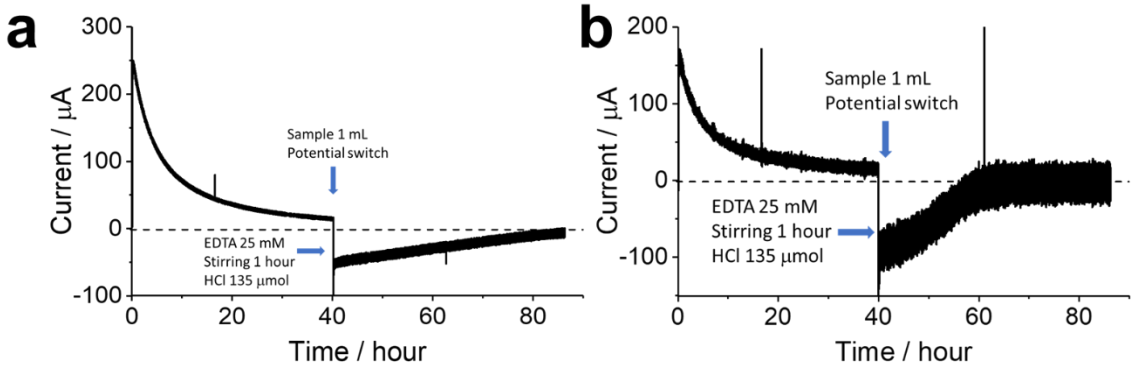


Figure 4.25. Chronoamperogram of **a)** Inversion of (*R*)-alcohol and **b)** deracemisation of (±)-alcohol catalysed by ADHs (W110V + LK) bidirectional control with 10 mM substrate at start. Conditions: starting cell volume 5 mL and 1 mL sample is taken at potential switch; solution stirred throughout using a magnetic flea; substrate [(*R*)-4-phenyl-2-butanol] = 10 mM for inverter or [(±)-4-phenyl-2-butanol] = 10 mM for deracemiser, [$NADP^+$] = 20 µM, [Mg^{2+}] = 5 mM buffer: 50 mM TAPS pH 9.0, pH is adjusted by HCl injection to approximately pH 8.0 at potential switch; temperature: 25 ℃, Potential held at 0 V vs. Ag/AgCl (3 M KCl) to drive oxidation and −0.74 V for reduction. Experiments performed in an anaerobic glovebox to avoid any contribution to the current form the reduction of O_2. Enzyme loading: FNR loaded first by drop-casting, LK and W110V loaded after FNR, by stirring in a 2.5 mL solution containing 2.56 nmols of LK and 1.31 nmols of W110V in 50 mM TAPS buffer pH 8.0; electrode (Ti foil) SA: 14 cm^2.

Table 4.14. GC Enantiomer analysis for the inverter (LK+W110V) with more substrate

	[S]/mM	[R]/mM	[ketone]/mM	ketone%	S%	R%	ee%(*S*)
Starting	0.03	9.84	0.13	1.3	0.3	98.4	-99.3
Post-oxidation	0.29	3.33	6.37	63.7	2.9	33.3	-83.9
Post-reduction	3.68	2.23	0.53	8.3	57.1	34.6	24.5
Side-arm	0.80	1.44	1.32	37.0	22.6	40.4	-28.3

Coulometric Conversion (oxidation): 84.8 % Conversion (reduction): 68.7% (produced in oxidation)

Table 4.15. GC Enantiomer analysis for the deracemiser (LK+W110V) with more substrate

	[S]/mM	[R]/mM	[ketone]/mM	ketone%	S%	R%	ee%(*S*)
Starting	4.87	5.13	0.00	0.0	48.7	51.3	-2.5
Post-oxidation	2.42	1.82	5.77	57.7	24.2	18.2	14.2
Post-reduction	5.44	1.32	0.42	5.8	75.8	18.4	61.0
Side-arm	1.50	0.56	0.77	27.3	53.1	19.6	46.0

Coulometric Conversion (oxidation): 60.2% Conversion (reduction): 92.4% (produced in oxidation)

4.9. The Electrochemical Leaf: Bulk Deracemisation

In this section, the most optimal version of the deracemiser and the inverter have been scaled up for bulk reactions. The complexity of scaling up a specific system requires substantial rationally guided trials. More adjustment is needed to perfect the design for scaling up.

The scaled-up inversion and deracemisation was conducted in a 50 mL electrochemical cell. The configuration is the same small-scale cell which is described in chapter 3, the solution volume was increased to 50 mL with the same concentrations of substrates, cofactor NADP(H) and buffer. The electrode surface area was also increased to 56 cm^2 for inversion and 86 cm^2 for deracemisation. The procedure remains the same as in small-scale reactors. Chronoamperograms in figure 4.26 (inverter) and figure 4.27 (deracemiser) show the reaction current over the process, from which it can be observed that the current did not increase linearly to surface area increased, thus yields a lower current density compared to the small-scale system.

In regard to the coulometric conversion rate, the inverter has 83.6% conversion in oxidation and 90.4% in reduction and the deracemiser has 79.3% in oxidation and 88.0% in reduction. These conversion rates are excellent, however, the solution analysis (table 4.16 and table 4.17) reveals a relatively poor enantiomeric purity. The final ee% is 55.6 in the inverter and 65.7 in deracemiser.

For the inverter, the experiment was carried out during the early work with W110A in use and without an extended incubation time after EDTA injection. LK is not fully deactivated and W110A can also produce small amount of (*R*)-alcohol. As a result, a large ratio of (*R*)-alcohol was produced during reduction by the poor overall enantioselectivity. The oxidation process also has some (*R*)-alcohol left, which is due to the product inhibition.

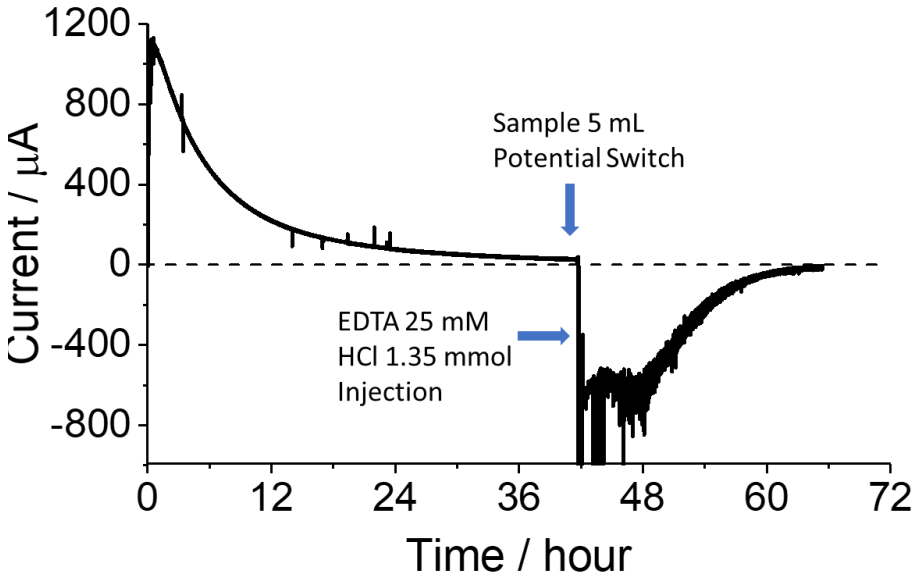


Figure 4.26. Large-scale Inverter of (*R*)-4-phenyl-2-butanol catalysed by ADHs (LK+W110A) in 50 mL cell. Conditions: starting cell volume 50 mL and 5 mL sample is taken at potential switch; solution stirred throughout using a magnetic flea; substrate [(*R*)-4-phenyl-2-butanol] = 4 mM, [$NADP^+$] = 20 µM, [Mg^{2+}] = 5 mM buffer: 50 mM TAPS pH 9.0, pH is adjusted by HCl injection to approximately pH 8.0 at potential switch; temperature: 25 ℃, Potential held at 0 V vs. Ag/AgCl (3 M KCl) to drive oxidation and −0.74 V for reduction. Experiments performed in an anaerobic glovebox to avoid any contribution to the current form the reduction of O_2. Enzyme loading: FNR loaded first by drop-casting, LK and W110A loaded after FNR, by stirring in a 40 mL solution containing 12.8 nmols of LK and 4.8 nmols of W110A in 50 mM TAPS buffer pH 9.0; electrode (Ti foil) SA: 56 cm^2.

Table 4.16. GC Enantiomer analysis for the scaled-up inverter (LK+W110A)

	[S]/mM	[R]/mM	[ketone]/mM	ketone%	S%	R%	ee%(*S*)
Starting	0.00	3.93	0.07	1.7	0.0	98.3	-100.0
Post-oxidation	0.00	0.57	3.43	85.6	0.0	14.4	-100.0
Post-reduction	2.84	0.81	0.24	6.1	73.1	20.8	55.6
Side-arm	0.05	0.03	0.04	32.5	44.2	23.3	30.9

Coulometric Conversion (oxidation): 83.6 % Conversion (reduction): 90.4% (produced in oxidation)

For the deracemiser, the new improvements of W110V and a longer incubation time for EDTA have been used. The oxidation resulted in more (*S*)-alcohol consumed than (*R*)-alcohol, suggesting that the loading ratio of two ADHs used in the small-scale electrode may not transfer and apply well to the large-scale electrode. The reduction process is more satisfying in that most of the ketone was converted to (*S*)-alcohol. The slight increase in (*R*)-alcohol concentration suggests that the LK deactivation process may not be enough and would need a longer time for the large-scale system.

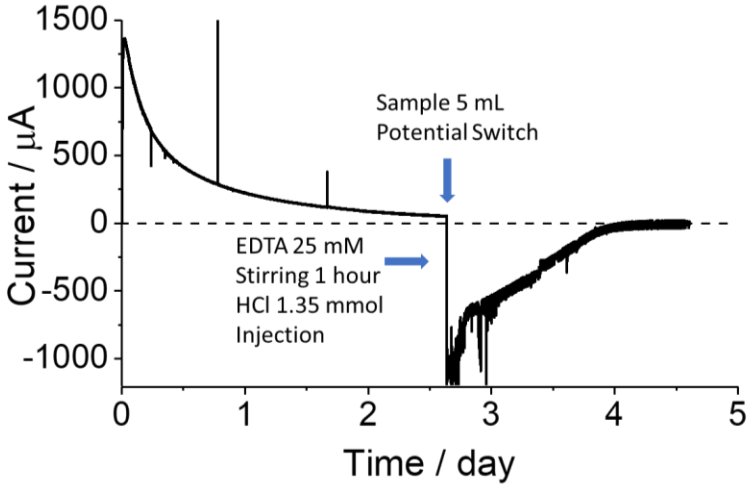


Figure 4.27. Large-scale deracemiser of (±)-4-phenyl-2-butanol catalysed by ADHs (LK+W110A) in 50 mL cell. Conditions: starting cell volume 50 mL and 5 mL sample is taken at potential switch; solution stirred throughout using a magnetic flea; substrate [(±)-4-phenyl-2-butanol] = 8 mM, [$NADP^+$] = 20 µM, [Mg^{2+}] = 5 mM buffer: 50 mM TAPS pH 9.0, pH is adjusted by HCl injection to approximately pH 8.0 at potential switch; temperature: 25 ℃, Potential held at 0 V vs. Ag/AgCl (3 M KCl) to drive oxidation and –0.74 V for reduction. Experiments performed in an anaerobic glovebox to avoid any contribution to the current form the reduction of O_2. Enzyme loading: FNR loaded first by drop-casting, LK and W110V loaded after FNR, by stirring in a 40 mL solution containing 10.2 nmols of LK and 7.9 nmols of W110V in 50 mM TAPS buffer pH 9.0; electrode (Ti foil) SA: 84 cm^2.

Table 4.17. GC Enantiomer analysis for the scaled-up inverter (LK+W110V)

	[S]/mM	[R]/mM	[ketone]/mM	ketone%	S%	R%	ee%(*S*)
Starting	3.92	4.08	0.00	0.0	49.0	51.0	-2.0
Post-oxidation	0.35	1.08	6.57	82.1	4.4	13.5	-50.7
Post-reduction	6.38	1.32	0.13	1.7	81.5	16.9	65.7
Side-arm	0.12	0.04	0.00	0.0	73.3	26.7	46.7

Coulometric Conversion (oxidation): 79.3 % Conversion (reduction): 88.0% (produced in oxidation)

In conclusion, the scaling up of with the inverter and deracemiser is feasible in principle and would be promising with further optimisation. Possible improvement includes 1) optimisation of loading process by adjusting the loading amount and ratio of enzymes, to achieve comparable current with larger electrode and to complete (*R*)-selective conversion in oxidation 2) optimisation of LK deactivation process to secure (*S*)-selectivity exclusively in reduction 3) alternative enzyme: a new (*R*)-selective ADH with lower Km towards (*R*)-alcohol in oxidation, 4) alternative reaction: a new model reaction that the interconversion between alcohol and ketone is not product-inhibited.

4.10. Conclusion and Potential Improvement

The function of a dual-controlled deracemisation and stereoinversion has been developed in the e-Leaf with several features, providing a new method for chiral synthesis. First, the nanoconfined system of the e-Leaf is capable of holding multiple enzymes, in this case, FNR and two ADHs with opposing enantioselectivities. Second, the process is dual-controlled. The redox direction of the reaction is controlled by the applied potential from the potentiostat and can be switched at ease; the enantioselectivity is controlled by the addition of EDTA chelating Mg^{2+} which is essential for the catalytic activity of the (*R*)-selective ADH. Third, the reaction is under monitoring in rea-time, with effective information to guide potential live interventions. Fourth, comparing to other deracemisation methods, the e-Leaf driven by electricity has a more elegant solution condition with no extra co-substrate. The method is also an efficient a one-pot, one-step process.

There is considerate room for potential improvement with the e-Leaf deracemiser and inverter. First, the highest enantiomer excesses achieved is approximately 85%, which is less than the numbers achieved with other methods. This is a cap caused by the slow rate of enzymes and relatively high K_m values. In addition, the inversion and deracemisation presented only convert (*R*)-alcohol to (*S*)-alcohol, since the

EDTA chelation affects only (*R*)-selective enzyme for now. To further improve this design, enzymes with better selectivity and rate are needed. More methods to deactivating and re-activating an enzyme are also worth exploring.

CHAPTER V

5. Biphasic Electrochemical Leaf for Sustainable Substrate Supply and Product-Inhibition Relief

5.1. Introduction

Combining biocatalysts and electrochemistry, bio-electrochemistry is a step forward, e-Leaf being one of the representatives. The 'audience enzyme' for the e-Leaf include oxidoreductases, such as dehydrogenases (ADH),[110,111,114] amino acid dehydrogenases,[115] amine dehydrogenases, imine reductase, glycerol dehydrogenases,[116] carbonyl reductases,[117] and many others; the reaction catalysed by those enzymes are involved with organic substrates.

E-Leaf in organic synthesis

Unlike the electrochemical and biocatalytic methods for organic synthesis, bi-phasic electroenzymatic systems have not been studied extensively. Schmid et al achieved the *Thermus* ADH-catalysed conversion of ketone to chiral alcohol((*1S,3S*)-3-methylcyclohexano) with electrochemical cofactor regeneration in biphasic solution of aqueous and octane.[118,119] Lütz and Hildebrand used the *Lactobacillus brevis* ADH to catalyse the chiral conversion of ketone to alcohol ((*R*)-phenylethanol) with electrochemical cofactor regeneration, in an organic phase of methyl tert-butyl ether (MTBE), featuring higher productivity and enantioselectivity.[88] Minteer et al achieved the production of β-hydroxy nitriles catalysed by ADH and HHDH enzymatic cascade with MTBE as the organic phase.[120] The use of an organic phase substrate reservoir and aqueous phase cofactor regeneration system decouples the cofactor and mediator concentration from the substrate concentration.[74,121] In such biphasic systems one of the issues was the use of mediators. The usage of expensive metal mediator and construction of polymer material for immobilisation can add to the complexity of the systems. In addition, the total turnover number of cofactor NAD(P)(H) and enzymes were also limited to relatively low level (<100). Polymer immobilisation also has a relatively shorter lasting time before it starts to lose the stability.[9]

A biphasic e-Leaf was therefore explored to mainly address two challenges. The first is that organic substrates and products have low solubilities in aqueous phase, which limits

the production in one batch. Reaction in a batch reactor can only be run for a short duration before a substrate replenishment is needed, resulting a low space yield. The other challenge is the product-inhibition in many biocatalytic processes, which limits the conversion rate and the purity of target product. In a biphasic reactor, substrate can be pre-dissolved in the organic phase and have a higher concentration than in aqueous phase. The organic phase can serve as a 'reservoir' and continuously supply substrate to the aqueous phase, maintaining a saturated concentration for the aqueous phase where most biocatalytic reactions are occurring. Meanwhile, products will be extracted and accumulated in the organic phase, and the product inhibition can be relieved to some extent.[122] In addition, the organic layer is easily separated from the aqueous phase and biocatalysts. The separation among organic substances are relatively easier than separate lower amount of organic product from aqueous phase, which help to minimise the efforts and cost at the application level.[123]

The features of the e-Leaf make it a promising tool for organic synthesis scenarios. First, rather than scattered in the solution in common biocatalytic process, enzymes are confined in the nanopores on the electrode. The immobilisation reduces the chance of enzymes' direct contact with organic solvent, which protects biocatalysts from accelerated deactivation due to their poor resistance to organic solvent. Nanoconfinement is applicable to different enzymes without extra pre-treatment, which brings more choices of biocatalysts and reaction routes. Further, the substrate/intermediate channelling on the e-Leaf allows the biocatalytic cascades to involve even insoluble intermediate (extremely low aqueous solubility). Within short distance and time, the insoluble intermediate is to be consumed by a second enzyme before it accumulates to its solubility limit. This feature makes some unlikely multi-step reaction routes possible. In addition, cofactor regeneration by the e-Leaf is mediator-free, fulfilled by FNR directly wired to the electrode. The cofactor regeneration is more efficient, since lower concentration of NADP(H) is needed (at μM level). Energised by

electricity, the e-Leaf has a cleaner and milder solution condition that is particularly helpful for product separation after a synthetic step.[124,125]

In this chapter, the e-Leaf has been explored to facilitate organic synthetic processing, providing an innovative perspective for organic synthetic methods. With the organic phase introduced, the e-Leaf is aiming for the catalytic process of insoluble or poorly soluble substrate and the relief of product inhibition. The conceptual setup is shown in the sketch in figure 5.1. The biphasic design is based on the conventional small-scale reactor, with an extra organic layer added on the top of the aqueous phase. The organic layer can include organic solvent (hexane, heptane, etc.) and pure substrate, solely or mixed. The working electrode loaded with FNR and E2 is kept under the interface to avoid direct contact to the organic layer. Cofactor NADP(H) is added to the aqueous solution. Substrate can be added directly to the aqueous solution or diffuses from the organic layer. The model reaction is the interconversion between 4-phenyl-2-butanol and its corresponding ketone 4-phenyl-2-butanone.

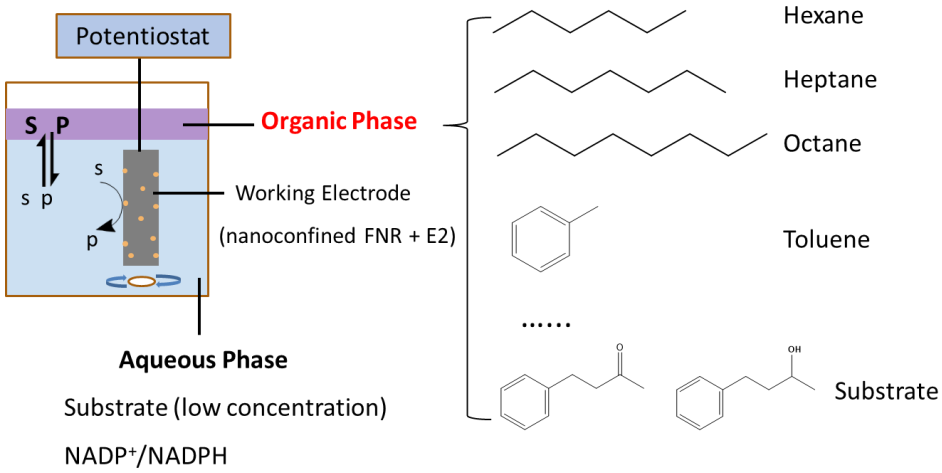


Figure 5.1. Conceptual sketch of the biphasic e-Leaf

This chapter consists of four main sections. First, the electrode construction was optimised, including enzyme loading method, loading monitoring method and enzyme loading ratio, which further completes the electrode construction optimisation conducted in previous chapters.

Then, various organic solvents were tested. The partitions of alcohol and ketone between water solution and organic solvents were tested and characterised by NMR. The stability of enzyme working in biphasic conditions was also tested using electrochemical methods.

Finally, using the optimised system, two main topics have been investigated in the biphasic e-Leaf with electrochemical analysis, substrate reservoir and product-inhibition relief. Experiments for this chapter were conducted at two different time stages therefore the results are presented in two sections (section 5.4 and 5.5). The early-stage experiments were carried out on the bench, and mostly initiated by the addition of E2 in real-time. In those reactions, argon purging was applied throughout the process to get rid of oxygen, and excess E2 was in the bulk solution all the time. The later-stage experiments were conducted in the glovebox, and the electrode was pre-loaded with FNR and E2; the results therefore are less noisy and have a better repeatability.

5.2. Enzyme and Reaction Involved

Alcohol Dehydrogenase (ADH)

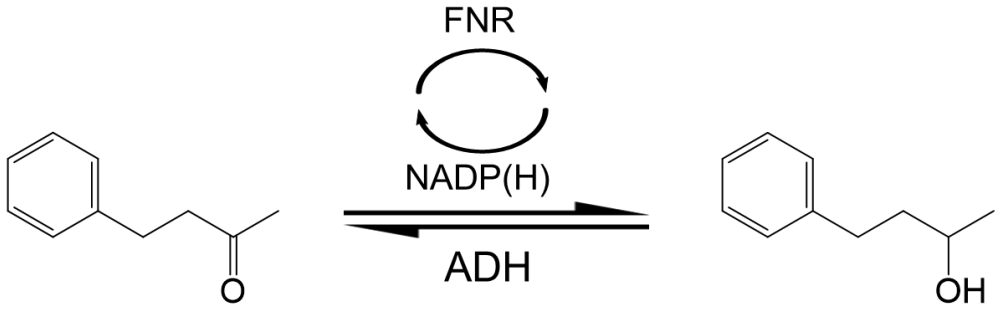


Figure 5.2. Interconversion between ketone and ethanol catalysed by secondary alcohol dehydrogenase (ADH)

The model reaction in this chapter is ADH-catalysed interconversion of ketone and alcohol for the biphasic system experiments with the e-Leaf. As introduced in chapter 4, the substrates 4-phenyl-2-butanone and 4-phenyl-2-butanol, are organic substrates which are hydrophobic with low solubility in water.[74] The solubility for 4-phenyl-2-

butanone and 4-phenyl-2-butanol are approximately 10 mM. The kinetic constants for the ADH used are shown in table 5.1. In water the three variants are all active on the (*S*)-alcohol with different K_m. [56] Enantioselectivity is not the major factor being considered in the biphasic reactor. As suggested by the solution assay data, the W110A variant is a relatively efficient enzyme with enzyme efficiency k_{cat} / k_m (*S*) = 59.6 s^{-1} mM^{-1}. The reaction process can be swift and the electronic signal is more distinguishable than slow enzymes.

Table 5.1. Kinetic Data for (*S*)-selective TeSADH W110A, W110V and W110G

Variant	k_{cat}(*S*) / s^{-1}	K_m(*S*) / mM	k_{cat}(*R*) / s^{-1}	K_m(*R*) / mM	k_{cat}(ketone) / s^{-1}	K_m(ketone) / mM	Ki (ketone) /mM
W110A	29.8	0.50	0.68	0.57	48.4	0.29	2.20
W110V	6.2	0.13	\	\	20.1	0.12	1.58
W110G	55.5	1.26	1.92	0.74	\	\	\

**S*: (+)-4-phenyl-2-butanol, *R*: (-)-4-phenyl-2-butanol. Data acquired by steady-state solution assays. Experimental conditions: 25 ℃, [$NADP^+$] = 300 μM for alcohol oxidation, [NADPH] = 200 μM for ketone reduction; volume = 400 μL, buffer for alcohol oxidation: pH 9.0, 50 mM TAPS, 1 mM $MgCl_2$, buffer for ketone reduction: pH 7.5 50 mM TAPS, 1 mM $MgCl_2$, 25 mM NaCl. [56]

The reactions were well-researched in the previous study chapter 4 with all the substrate easily characterised by NMR and GC. The e-Leaf is stable in the working conditions. More importantly, the low solubility of substrates suits well for in the exploration of biphasic system.

Product inhibition in oxidation

As introduced previously, the oxidation of 4-phenyl-2-butanol to ketone catalysed by ADH displays product inhibition. The inhibition effect is obvious even at a low concentration of product (K_i = 2.20 mM for W110A), as shown in table 5.1. A simple test is presented in figure 5.3 to show this. The reaction was initiated by live injection of ADH. The loading phase last for approximately 1 hour until the oxidation current barely increases and a buffer exchange was conducted. There is an apparent increase of

current after buffer exchange (by 0.03 mA), suggesting the product inhibition exists as the reaction goes in the loading phase. The reaction carried on and current finally reaches zero due to the depletion of substrate and product inhibition. The coulometric conversion after buffer exchange is 2.3 C, corresponding to 12 μmol substrate converted, with a conversion of 37.5%. It is worth pointing out that the alcohol used for the experiments in this chapter is the racemic mixture. Since the ADH is (*S*) - selective, 50% conversion is basically a full depletion of the substrate available.

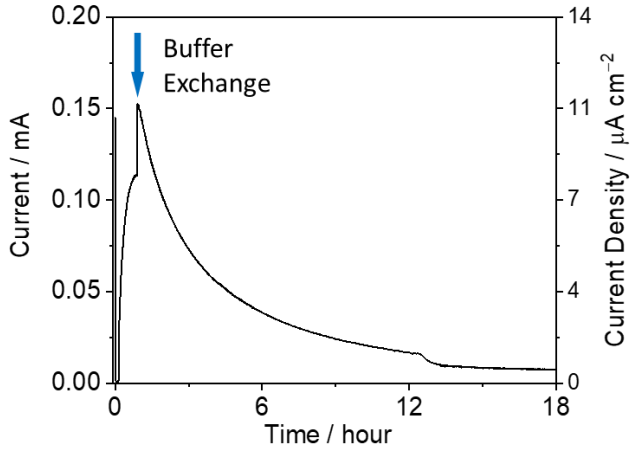


Figure 5.3. Investigation of product inhibition in the oxidation of 4-phenyl-2-butanol catalysed by W110A ADH. ADH live injected at beginning and buffer exchange after 52 minutes when peak current is reached. Conditions: volume 4 mL; solution stirred throughout using a magnetic flea; substrate [4-phenyl-2-butanol] = 8 mM, [NADPH] = 20 μM, buffer: 100 mM TAPS pH 9.0; temperature: 25 ℃, Potential held at −0.1 V vs. Ag/AgCl (3 M KCl) to drive reduction. Solution purged with argon to remove O_2; argon flow maintained in headspace thereafter. Enzyme loading: FNR loaded first by drop-casting, ADH loaded by live injection 0.96 nmol into the cell, electrode (Ti foil) SA: 14 cm^2.

5.3. Condition Optimisation

5.3.1. Enzyme Loading

The optimisation of the (FNR + ADH) enzyme loading for the biphasic system has been carried out, with details in appendix (A5.1).

FNR preloading and E2 live injection was the first loading methods frequently used in the early-stage experiments. Due to the low solubility of the substrate, the change of current monitored by chronoamperometry is often under the mixed influence of

enzyme loading (increase of current) and substrate depleting (decrease of current). Thus, the chronoamperometry cannot monitor the current from solely enzyme loading without being affected by the depletion of substrate (appendix A5.1). Different ways to monitoring the loading process has been explored, including monitoring with excess substrate by chronoamperometry, monitoring by continuous cyclic voltammetry and monitoring by intermittent chronoamperometry (appendix A5.1.1). The loading of ADH by live-injection with FNR preloaded normally takes at least 6 hours to reach the optimised loading situation.

Stepwise drop-casting loading was another way of enzyme loading tested (appendix section A5.1.2). FNR is drop-cast on the ITO/Ti electrode first, and then ADH is drop-cast on the electrode. Different incubation time combinations of the two enzymes have been tested and compared. Stepwise drop-casting is an available loading method which is potential for precise control in loading but is less convenient comparing to the co-dropcast method. Drop-casting and stir-loading (FNR+E2 simultaneously), as the most used methods in preparing the e-Leaf in thesis, have been tested as well, in comparing with other loading methods (appendix A5.1.3). They prove to be the most efficient ways to loading the enzymes.

The optimisation of the ratio of enzymes (FNR to ADH) and the applied amount (for E2 live-injection method) has been conducted. The relation of E2 loading speed to the amount of E2 in a live injection is investigated, showing that a higher addition amount could speed up the process. The drop-casting ratio of FNR to ADH has been optimised to 10:1 (appendix A5.2).

5.3.2. Scaling-up Feasibility

A simple feasibility test for scaling up was conducted for the ADH-catalysed interconversion between ketone and alcohol (e-Leaf scaling-up with GLDH-catalysed model reaction discussed in detail in chapter 3). The targeted volume is 50 mL, from the benchmark of 4 mL reactor. Figure 5.4 shows the chronoamperograms of oxidation and

reduction reaction. The surface area of electrode increases from 3.5 cm^2 to 24.5 cm^2 and the cell volume increases from 4 mL to 50 mL. Reaction conditions including substrate concentration and cofactor concentration remain the same. Detailed data are shown in table 5.2. The results show a good linearity in scaling up that the current density remains at similar levels. The peak current density in oxidation in the large cell was over twice of that in the small cell, which can be due to the different electrode batches with thicker ITO layer allowing for more enzyme adsorbed. The conversion in oxidation is at similar level that is limited due to product inhibition and the enantioselectivity of W110A. The minor issue is the low conversion in large-scale reduction reaction. The process shows a decreasing reaction rate. Improvement to achieve a more stable activity in the reductive conditions is required for the scaled-up biphasic e-Leaf.

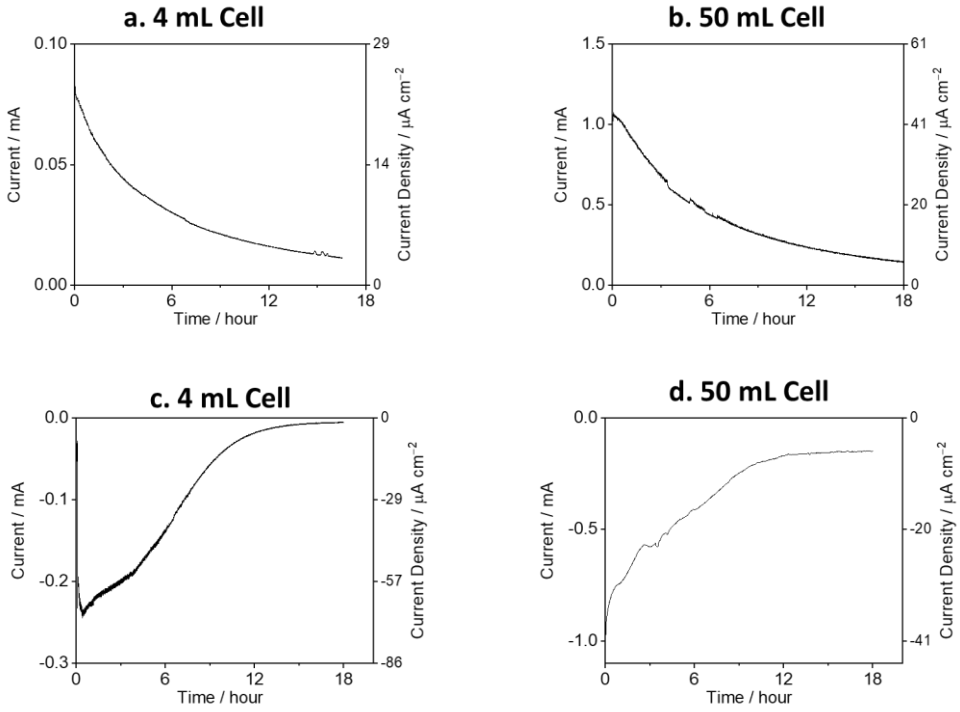


Figure 5.4. Chronoamperograms of ADH-catalysed reaction in small and larger scales. **a)** 4 mL oxidation **b)** 50 mL oxidation **c)** 4 mL reduction **b)** 50 mL reduction. Conditions: solution volume 4 mL (a) and 50 mL (b); buffer: 100 mM TAPS pH 9.0 in oxidation and pH 8.0 in reduction; temperature: 25 ℃, solution is purged with argon to remove O_2 and argon flow maintained in headspace thereafter. substrate [4-phenyl-2-butanol] = 8 mM in oxidation, [4-phenyl-2-butanone] = 8 mM in reduction, [$NADP^+$] = 20 µM; Potential held at -0.1 V vs. Ag/AgCl (3 M KCl) to drive oxidation and -0.9

V to drive reduction. Electrode SA = 3.5 cm^2 in small cell (a) (c) and 24.5 cm^2 in large cell (b) (d); enzyme amounts: (a) (c) 6.4 nmol FNR + 0.64 nmol ADH, (b) (d) 12.8 nmol FNR + 1.28 nmol ADH.

Table 5.2. Reaction data for the scaling-up feasibility test in figure 4.4

No.	Cell Volume /mL	Surface Area / cm^2	Enzyme applied[1] /nmol FNR : nmol GLDH	Yield (conversion rate)	TTN of $NADP^+$	TTN of ADH /10^4	Peak current Density /μA cm^{-2}
a	4	3.5	6.4 : 0.64	10.2 μmol (32%)	128	1.6	
b	50	24.5	12.8 :1.28	137 μmol (34%)	137	10.7	
c	4	3.5	6.4 : 0.64	30 μmol (94%)	375	4.7	
d	50	24.5	12.8 :1.28	114 μmol (29%)	114	8.9	

*Enzyme amount indicates the enzymes used in loading incubation; the loading solution is fully rinsed off after incubation;

5.4. Organic Solvent

In addition to substrate, the organic solvent also plays an important role in a biphasic e-Leaf. Pure substrate offers a concentration (for example, 6.67 M for 4-phenyl-2-butanone) that is in large excess for the aqueous phasic reaction to proceed at the typical reaction rate in a 4 mL e-Leaf.[56,57] By dissolving the substrate in organic solvent to an appropriate concentration, efficient supply of substrate can be maintained with less excess substrate. In addition, dissolving in solvent helps to slow down the evaporation of some volatile substrates. Second, organic solvent has the function of product extraction, with plenty choices for different situations. Pure substrate in theory can also have extraction effect on the product, but the restrictions are obvious; the similar structures shared by the substrate and its product would make separation difficult and the overuse of substrate for production extraction can be a waste.

In this section, the partition situation of substrates and products in different organic solvents has been tested. For an ideal solvent, the product should tend to be extracted and dissolved in the organic phase and the substrate should have decent partition in the aqueous phase. The extraction capability is especially important for the model reaction where product inhibition exists.

The stability and activity change of enzymes and the whole e-Leaf in the presence of organic phase has also been tested and discussed. The compatibility between enzyme and organic solvent needs to be considered as organic solvent is different from the aqueous environment where enzymes are normally functioning. They may have detrimental or beneficial effects on the catalytic activity of the system.[88]

5.4.1. Organic Solvent Partition Numbers Tested by NMR

The ^{1}H NMR is the method used for detecting the concentration change of ketone (4-phenyl-2-butanone) and alcohol (racemic 4-phenyl-2-butanol) in aqueous solution. The post-reaction solution is tested with 10% of D_2O at water suppression (details in chapter 7 section 7.5.2). The characteristic peaks are shown in following figure 5.5. The solution for the test has 8 mM ketone and alcohol dissolved in aqueous buffer (TAPS 100 mM), same as the reaction solution.

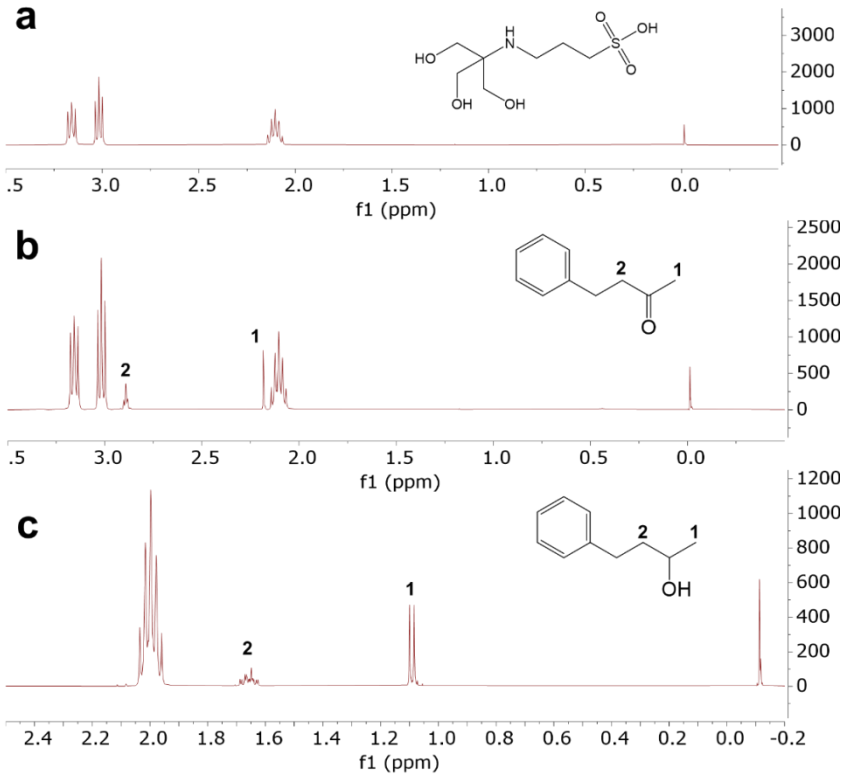


Figure 5.5. NMR spectra of chemicals involved. **a)** TAPS buffer salt 50 mM with 10% D2O, water suppression; **b)** The ketone 4-phenyl-2-butanoe 8 mM in TAPS buffer with 10% D2O, water suppression. (δ 2.18 ppm, 3H, and 2.89 ppm, 2H); **c)** the alcohol 4-phenyl-2-butanol 8 mM in TAPS

buffer with 10% D2O, water suppression. (δ 1.09 ppm,3H, and 1.65 ppm, 2H). Characteristic peaks are indicated with numbering. The absolute positions of peaks may shift yet the relative position against the buffer peak holds. Product amount was determined by internal standard method (TMSP as standard, details in chapter 7 material and methods).

Partition of substrates in organic solvents

Several organic solvents are chosen and tested based on earlier work conducted by multiple scientists.[75,126] Based on this, ADH W110A variant proved to be stable in organic solvent such as hexane, heptane and octane. Toluene is also tested as a common organic solvent other than normal alkanes.

In the test, 1 mL of TAPS buffer (aqueous) containing 8 mM of substrate ketone or alcohol is mixed with 1 mL of organic solvent. The biphasic solution is stirred by a stirring flea for 18 hours. Then the aqueous phase is tested by NMR to check the concentration of substrate left. The NMR results are shown in following figure 5.6. (alcohol) and figure 5.7 (ketone).

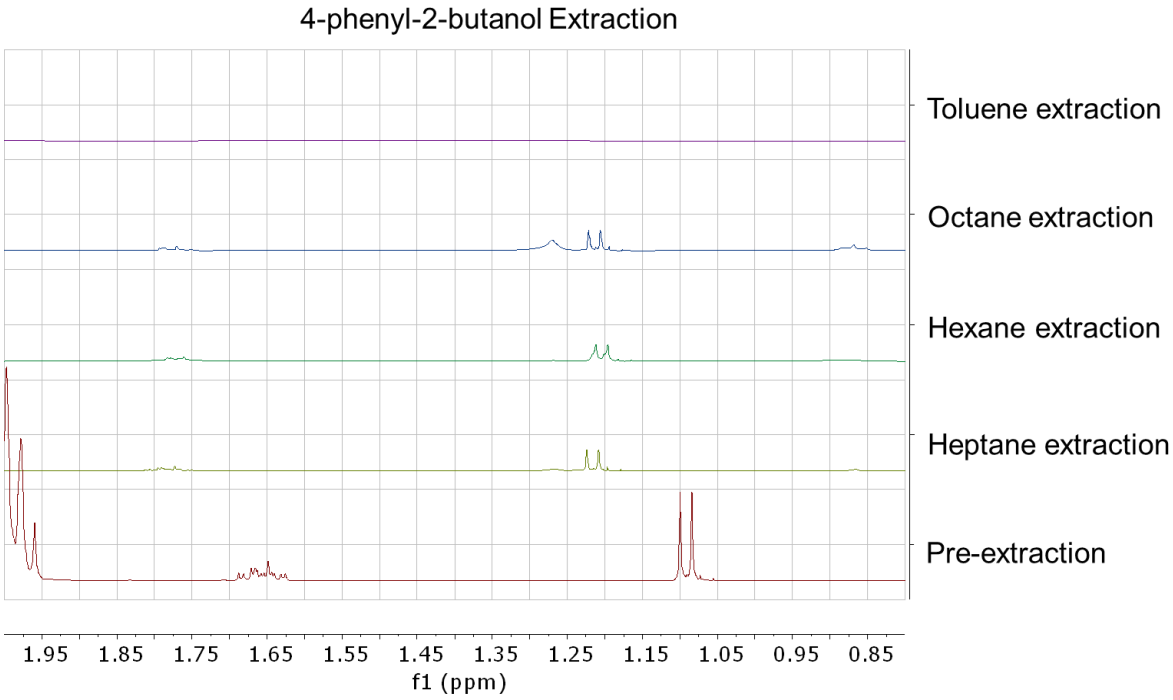


Figure 5.6. NMR spectra of 4-phenyl-2-butanol before and after extraction of different organic solvent. Extraction conditions: 1 mL organic + 1 mL substrate solution (8 mM substrate in 100 mM TAPS buffer), stirred for 18 hours before the aqueous phase is separated for NMR test.

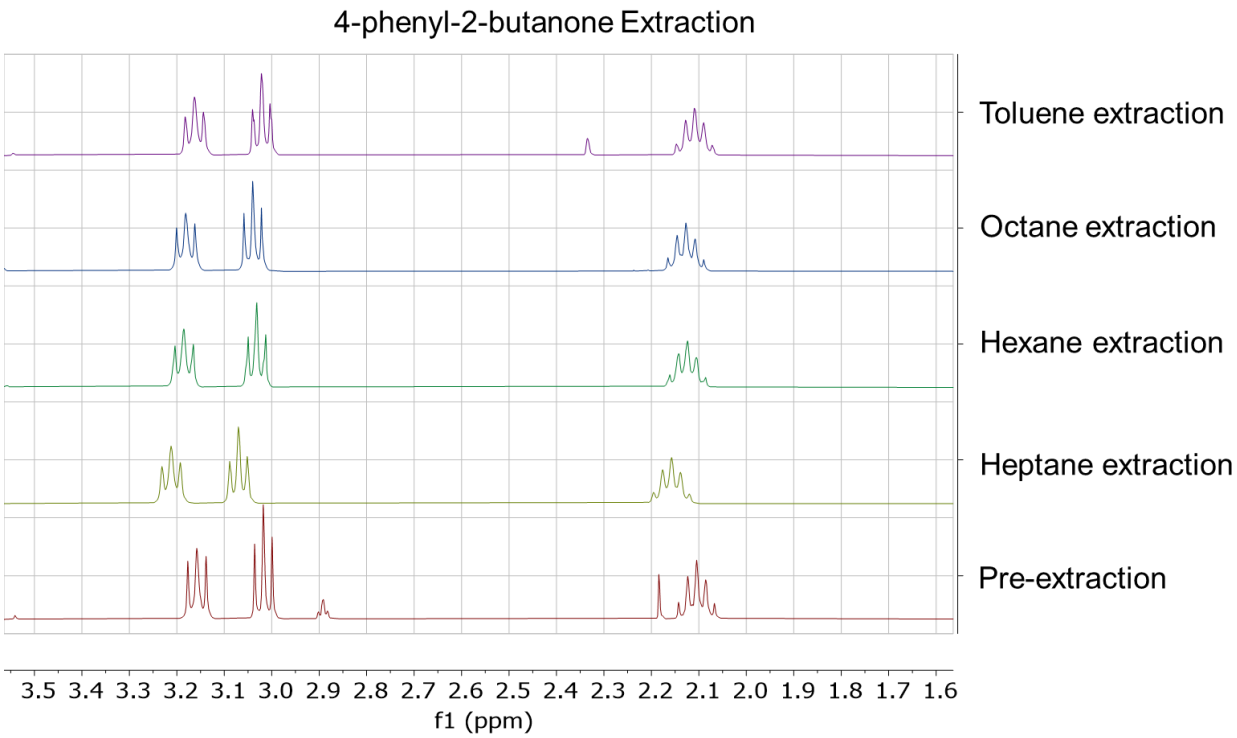


Figure 5.7. NMR spectra of 4-phenyl-2-butanone before and after extraction of different organic solvent. Extraction conditions: 1 mL organic + 1 mL substrate solution (8 mM substrate in 100 mM TAPS buffer), stirred for 18 hours before the aqueous phase is separated for NMR test.

The partitioning of substrates is calculated based on the NMR peaks and the results are shown in table 5.3. The extraction percentage is calculated as:

$$extraction\ percentage\ = \frac{[substrate\ in\ organic\ solvent]}{[substrate\ in\ total]} \qquad (5.1)$$

Ketone and alcohol dissolve more in organic solvent than aqueous phase. Hexane, heptane, and octane shares similar features in extraction that approximately 90% of ketone and 70% alcohol is dissolved in organic solvent. Toluene tends to extract more alcohol (97%) and less ketone (18%). The high partition of ketone and lower partition of alcohol favours the conversion of alcohol to ketone. Ketone that causes the inhibition can be extracted to organic solvent swiftly by alkanes. Hexane, heptane, and octane are the promising candidates for the relief of product inhibition in the oxidation.

Table 5.3. Extraction percentage of organic solvent tested by NMR

	4-phenyl-2-butanone	4-phenyl-2-butanol
Hexane	90%	65%
Heptane	93%	73%
Octane	91%	70%
Toluene	18%	97%

5.4.2. Effect of Additional Solvent Layer on Enzyme Stability

Some of the initial e-Leaf experiments include the addition of ADH in real-time to the bulk solution. The enzyme could therefore have direct contact with the organic solvent. The enzyme stability in direct contact with organic solvent has therefore been tested in this section.

(1) Test with cyclic voltammetry

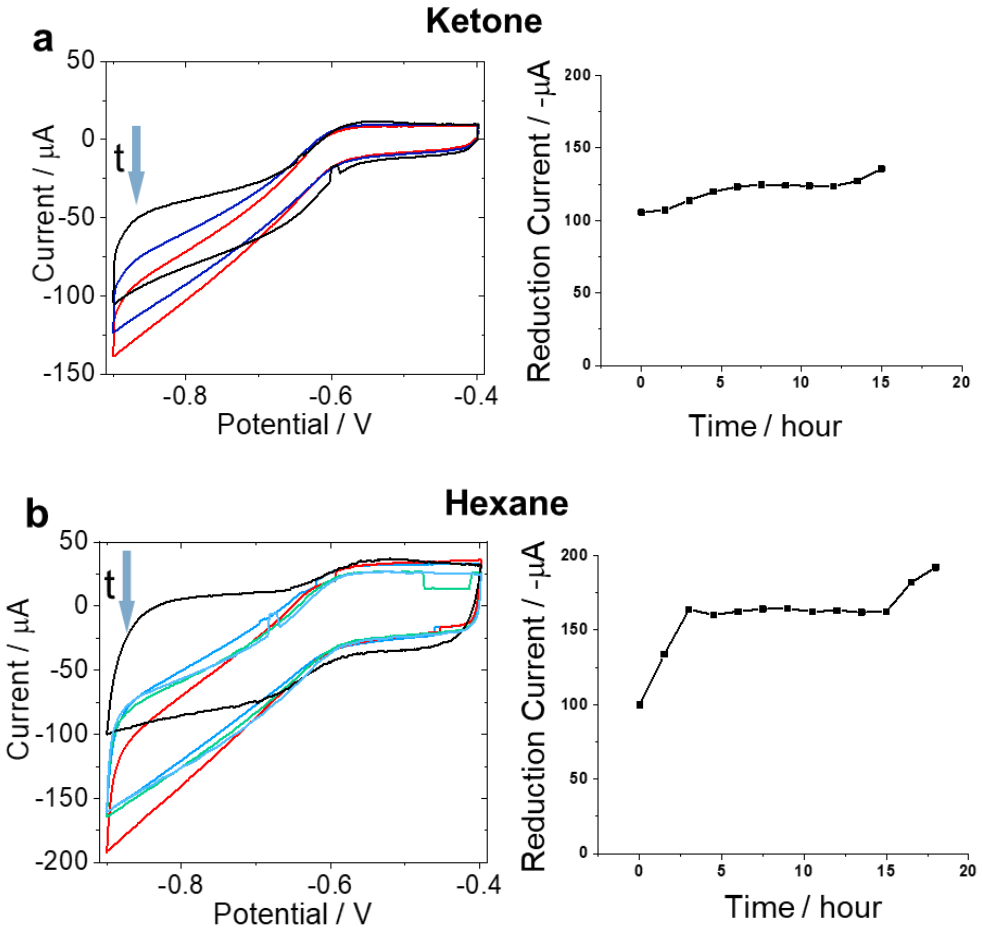
Four tests (shown in figure 5.8) are conducted to check the possible effect the organic phase has on the e-Leaf. In the experiment, the coupled current was monitored to show the change of activity in the e-Leaf. The working electrode was in the aqueous solution containing substrate, and the organic layer is on the top. The electrode was preloaded with FNR before the reaction. The monitoring started with the initiation of the reaction by the addition ADH in real-time, which gave rise to the increase of redox current.

The CVs in panel (a) and (b) monitors the reduction reaction with pure substrate ketone and organic solvent hexane as the additional layer, respectively. The CVs in panel (c) and (d) monitor the oxidation reaction with pure substrate alcohol and solvent hexane presented as the additional layer, respectively.

The current at -0.9 V (a, b) and -0.3 V (c, d) from the voltammograms are plotted as a function of time in the right figure of each panel.

The results show steady current levels within 18 hours. The system seems to be stable in sustaining the reaction rate in both redox directions in the presence of substrate and

hexane. Nevertheless, some minor issues are worth noting here. The current level of reduction in the presence of ketone is lower than that of hexane, according to (a) and (b). This could be a batch difference due to the minor difference of ITO electrode or suggest that the pure substrate ketone is detrimental to the activity of the e-Leaf with live-injected E2. More tests with different methods would be required to confirm the stability.



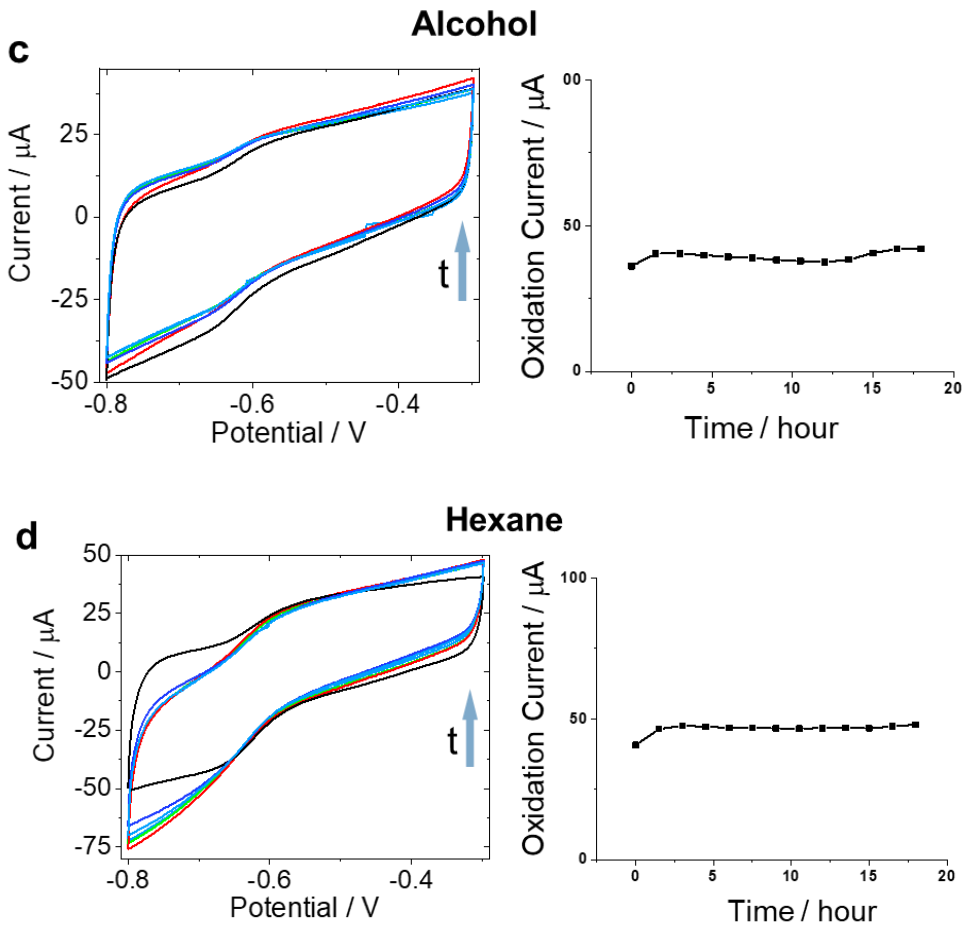


Figure 5.8. Cyclic voltammograms for ADH redox current change in the presence of organic layer. a) Reduction current monitoring with pure ketone; b) reduction current monitoring with hexane; c) oxidation current monitoring with pure alcohol; d) oxidation current monitoring with hexane. Conditions: volume 3.5 mL; solution stirred throughout using a magnetic flea; substrate [4-phenyl-2-butanone] = 8 mM for reduction (a) (b), [(±)-4-phenyl-2-butanol] = 8 mM for oxidation (c) (d), [$NADP^+$] = 20 µM, buffer:100 mM TAPS pH 8.0; temperature: 25 ℃. Solution purged with argon to remove O_2; argon flow maintained in headspace thereafter. Scan rate: 4 mV/s. Enzyme loading: FNR loaded first by stirring (15 µL in 2.5 mL TAPS buffer pH 9.0), ADH loaded by live injection 1.65 nmol, electrode (Ti foil) SA: 3.5 cm^2.

(2) Chronoamperometry test with enzyme pre-treated with hexane

In addition to previous investigation of the effect of the organic layer in live reaction condition, a direct test on how organic solvent affects the enzymes has been conducted. Separately, each enzyme is pre-treated with organic solvent before being loaded in the electrode. The pre-treatment includes dissolving FNR (or ADH) in 3.75 mL aqueous buffer (50 mM TAPS pH 9.0) with 3.75 mL of hexane added. The biphasic solution was

stirred by a stirring flea for 5 hours. After the pre-treatment, 2.5 mL of aqueous solution is injected with fresh enzyme of the other type i.e., ADH for the pre-treated FNR (or FNR for ADH). An ITO electrode was then put in the solution for the stir-loading of enzymes. The electrode activity was tested after the enzyme loading by cyclic voltammetry to check FNR coverage and chronoamperometry to detect the overall conversion rate (figure 5.9).

The electrode with pre-treated ADH (a) shows a FNR coverage of 76 pmol/cm^2. The peak current in the chronoamperogram is approximately 90 μA. The electrode with pre-treated FNR (b) shows a lower FNR coverage (32 pmol/cm^2) and the peak current is approximately 115 μA. The FNR non-turnover peaks are the direct evidence that FNR can be deactivated by the organic solvent.

The effect of organic solvent on ADH is confirmed indirectly by the chronoamperograms. Oxidation current rates are at the similar level compared to the monophasic reactor results (in previous section, figure 5.4). The difference of oxidation currents between (a) and (b) could be due to the different amount of active enzymes loaded on the electrode. Assuming hexane pre-treatment does not change the affinity of enzymes to the nanopores, the loading ratio and amount of the two enzymes (no matter dead or alive) should be the same, given no operation and batch errors in the stir-loading process. With this assumption, the electrode (b) which yielded higher current with less amount of active FNR, should have a higher amount of active ADH than the electrode in (a). Hence, some of the ADH was deactivated by the organic solvent during the pre-treatment.

Such direct contact of enzymes and organic solvent is less likely in actual reactions for electrode pre-loaded with both enzymes. Enzymes are nanoconfined in the electrode and always kept in the aqueous phase, which can enhance the stability of these enzymes on the e-Leaf to achieve better stability comparing the reaction with E2 added in real-time.

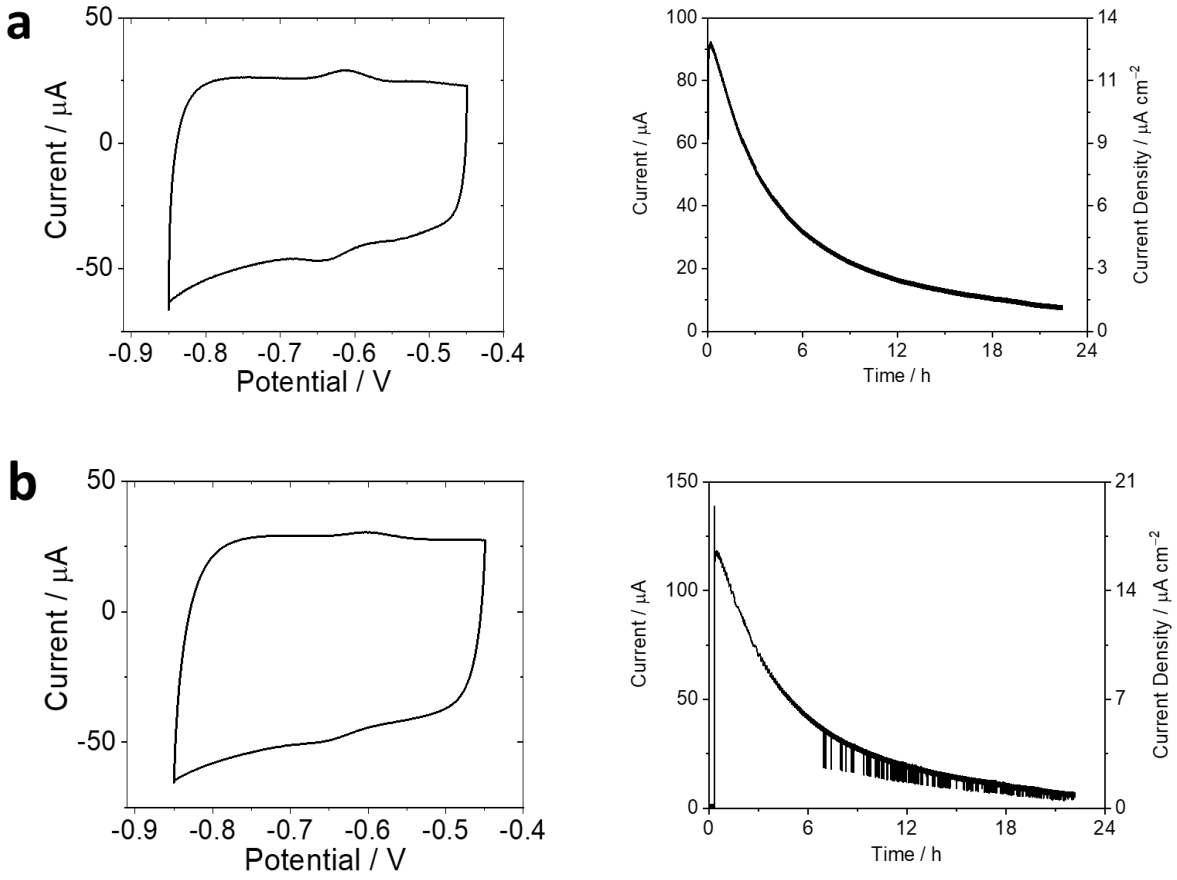


Figure 5.9. Test of enzyme activity after stirring with organic solvent heptane by cyclic voltammograms and chronoamperogram. **a)** ADH stirred with heptane **b)** FNR stirred with heptane. Enzyme pre-treatment: a) 17.2 nmol FNR in 3.75 mL pH 9.0 TAPS buffer (aq.) with 3.75 mL hexane, stirred for 5 hours. b) 8.55 nmol FNR in 3.75 mL pH 9.0 TAPS buffer (aq.) with 3.75 mL hexane, stirred for 5 hours. Experiment conditions: cell volume 4 mL; solution stirred throughout using a magnetic flea; substrate [4-phenyl-2-butanol] = 8 mM, [$NADP^+$] = 20 µM, buffer:100 mM TAPS pH 9.0; temperature: 25 ℃. Solution purged with argon to remove O_2; argon flow maintained in headspace thereafter. CV scan rate: 4 mV/s, potential for chronoamperometry held at 0 V vs. Ag/AgCl (3 M KCl) to drive oxidation. Enzymes loaded after pre-treatment by stir-loading in 2.5 mL pH 9.0 TAPS buffer containing 11.5 nmol FNR + 5.7 nmol ADH. Electrode SA: 7 cm^2

5.5. Initial Experiments with Real-time Addition of ADH

This section presents the initial experiments in which the FNR was preloaded and ADH was live injected during the reaction. The experiments were conducted on the bench and continuous argon purging is required to remove oxygen from atmosphere. The argon purging can cause accelerated evaporation of organic substrate and solvent since they are volatile. In the later-stage experiments (section 5.5), FNR and ADH were

preloaded either by drop-cast or stir-loading method. The electrochemical cell was in a glovebox to achieve the oxygen-free condition. Electronic signals are less noisy in a condition that is not affected by oxygen and gas purging.

5.5.1. The Electrochemical Leaf Setup as a Biphasic Reactor

Figure 5.10 shows the sketch of concept and photo of the e-Leaf cell with an organic layer added. Organic solvents and the pure substrates have lower density than water, therefore are added on the top after the aqueous phase is settled. The working electrode is held in the aqueous phase containing substrate and cofactors. The enzymes in action are nanoconfined in the nanopores on the electrode, well protected from direct contact with organic layer. The reference and counter electrodes and their connection to the working electrode are also in aqueous phase, which ensures the current flow and signal to be stable and free from extra interferences, with mass transfer across the interface of the two phases.

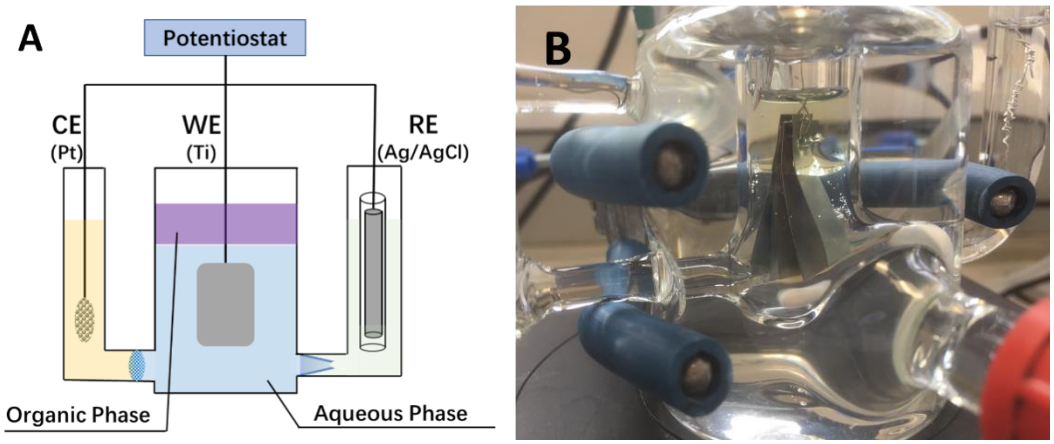


Figure 5.10. Sketch and photo showing the Configuration of biphasic reactor

5.5.2. Benchmarks and First Trials

(1) benchmark reactions with ADH live injection

Monophasic benchmark reactions of the interconversion of ketone and alcohol catalysed by ADH are shown in figure 5.11 (panel (a) for reduction of ketone, panel (b) for

oxidation of alcohol). Substrates (8 mM ketone or alcohol) were pre-dissolved in the solution before the potential was applied. An addition of 20 μM $NADP^+$ was carried out, followed by the addition of ADH in real-time, as the initiation of the reaction. The current increased as the ADH loading proceeded since more ADH were adsorbed into the electrode catalysing the conversion. The current reached the peak (3 hours for reduction, 1.5 hours for oxidation) and started to decrease right after. This turning of current change with no plateau stage was due to the mixed effect of enzyme loading, substrate limitation and product inhibition (in oxidation only). The current then decreased to almost zero indicating the depletion of substrate. The peak current is approximately 0.31 mA for reduction and 0.11 mA for oxidation. The coulometric conversion rate is 83% for reduction and 34% for oxidation.

The full conversion (50% for oxidation, 100% for reduction) is not reached due to the substrate loss from two causes. The first cause is that the continuous argon purging in the headspace over the solution takes away some volatile substrate through evaporation. The other reason is the loss from the crossover of substrate to the side-arm (as mentioned in chapter 4). A loss of approximately 15% substrate has often been observed.

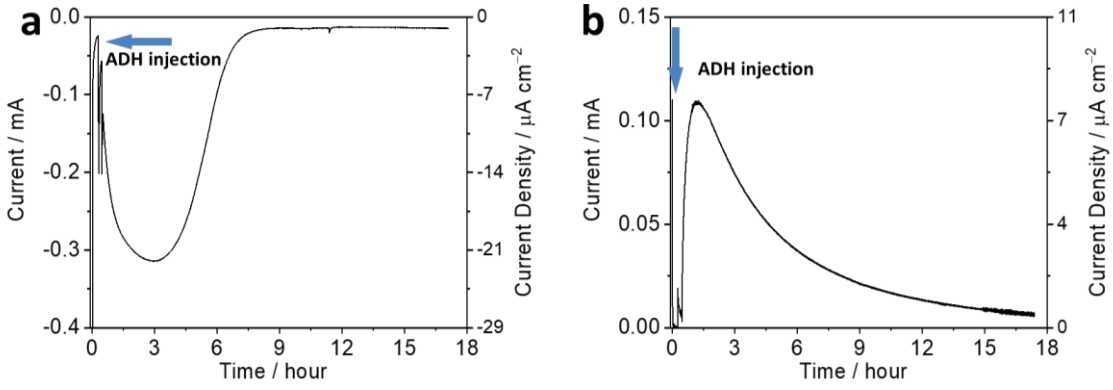


Figure 5.11. Chronoamperograms of mono-phase redox reactions catalysed by ADH as benchmarks **a)** Reduction and **b)** Oxidation. Conditions: solution volume 4 mL; buffer: 100 mM TAPS pH 8.0 for oxidation and pH 9.0 for reduction; temperature: 25 ℃, solution is purged with argon to remove O_2 and argon flow maintained in headspace thereafter. substrate [4-phenyl-2-butanone] = 8 mM for reduction and [4-phenyl-2-butanol] = 8 mM for oxidation, [$NADP^+$] = 20 μM; Potential held at -0.9 V vs. Ag/AgCl (3 M KCl) to drive reduction and -0.36 V to drive oxidation. Electrode SA = 14 cm^2. Enzyme loading: FNR pre-loaded by drop-cast, ADH loaded by live injection 2.18 nmol.

(2) First trials with organic phase (v/v 1:1 hexane and substrate)

The first trial of biphasic reduction and oxidation with the e-Leaf is shown in figure 5.12. Panel (a) shows the reduction experiment, with the purpose of using organic layer as a 'reservoir' for substrate supply. In stage 1, monophasic reaction was carried out with 8 mM substrate pre-dissolved in the solution. The reaction was initiated by the addition of ADH in real-time. The current increased to the peak current (approximately 250 μA) and then decreased due to the depletion of substrate in 18 hours. The stage 2 started with the addition of hexane and ketone of equal volume (389 μL in total) on the top of the aqueous solution as a layer. The current increased sharply at the addition of organic phase due to the replenishment of substrate and the reaction carried on for another two days with slowly decreasing activities attributed to the loss of activity of enzymes. The coulometric conversion of the monophasic stage is 68.5% of the 32 μmol substrate. The biphasic stage has a coulometric production of 110 μmol product, which is 3.9 times of the batch amount. The introduction of the second phase solution containing substrate has an excellent effect on continuous substrate supplying.

Panel (b) shows the oxidation reaction, the purpose of which is to test the possible product-inhibition relief brought by the organic phase. In stage 1, a monophasic reaction was initiated by the addition of ADH in real-time and the current increased to the peak current (approximately 80 μA) and then decreased due to the depletion of substrate and product-inhibition in 16 hours. At this point, 3.1 mM concentration of product has accumulated, which is sufficient to inhibit the oxidation rate. The stage 2 started with the addition of hexane and alcohol of equal volume (390 μL in total) on the top of the aqueous solution as a layer. The current increased sharply at the injection of organic phase and the reaction carried on for another two days with slowly decreasing activities. The signal became extremely noisy under the biphasic condition due to poor connection. This could be caused by the organic drops trapped and direct contacted to the electrode on the injection operation. The coulometric conversion of the monophasic stage is 39%

of the 32 μmol racemic substrate. The biphasic stage has a coulometric production of 38 μmol product, which is 1.4 times of the batch amount. The introduction of the second phase solution containing substrate and solvent in an oxidation process has increased the reaction current. However, it is not clear whether the increase of current is due to the supply of the substrate or the extraction of product to relieve the product inhibition. The recovered current is likely from the substrate since the conversion in stage 1 is high.

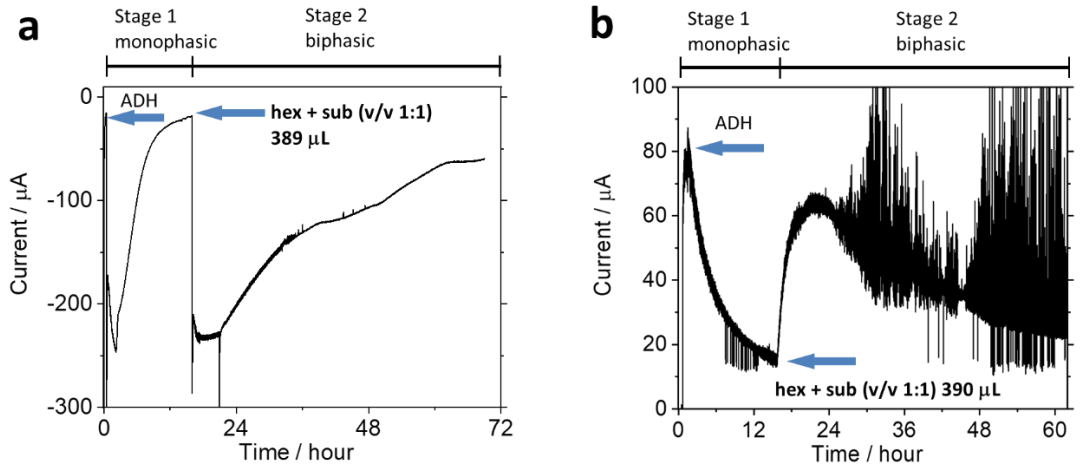
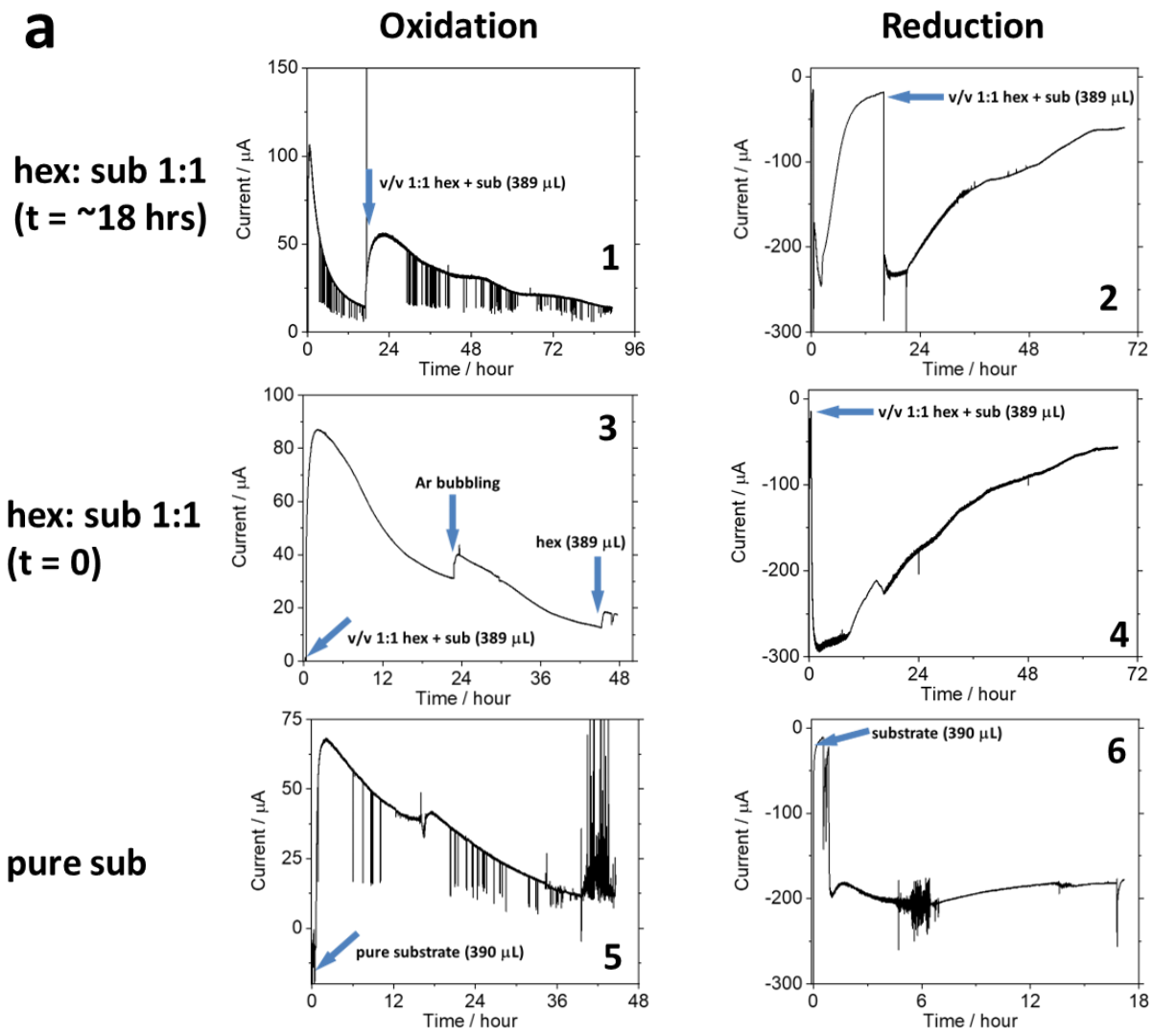


Figure 5.12. Chronoamperogram of biphasic reactions with 1:1(v/v) organic phase added. (a) reduction and (b) oxidation. Conditions: starting solution volume 3.5 mL; buffer: 100 mM TAPS pH 8.0; temperature: 25 ℃, solution is purged with argon to remove O_2 and argon flow maintained in headspace thereafter. Substrate [4-phenyl-2-butanone] = 8 mM (aq) for reduction and [4-phenyl-2-butanol] = 8 mM (aq) for oxidation, [$NADP^+$] = 20 μM; Potential held at -0.9 V vs. Ag/AgCl (3 M KCl) to drive reduction and -0.34 V to drive oxidation. Electrode SA = 14 cm^2; enzyme loading: FNR pre-loaded by drop-cast, ADH loaded by live injection 2.18 nmol.

5.5.3. Biphasic Reactions with Hexane and Pure Substrates

To investigate the effect that organic substrate and solvent have on the e-Leaf reaction, a series of tests are conducted. The experiments include oxidation and reduction processes with hexane, alcohol, and ketone as the organic phase. As shown in figure 5.13, panel (a) is the comparison experiment to investigate the substrate replenishment effect (with reaction 1 - 6) and panel (b) is to investigate the product extraction effect (with reaction 7 - 10). Organic phases were added either after one batch reaction (reaction 1, 2) or at the starting stage of reaction or later (reaction other than 1, 2) The

volume of the organic phase is 10% of the total volume (3.5 mL aqueous + 0.39 mL organic). Organic phase consists of either pure sub, pure hexane or a mixed one with 1:1 volume ratio (reaction 1, 2, 3, 4) or 80 mM substrate in the solvent (reaction 7, 8). In regard to enzyme loading, FNR was pre-loaded by drop-casting before the reaction and ADH was loaded by live injection at the starting stage of the reaction.



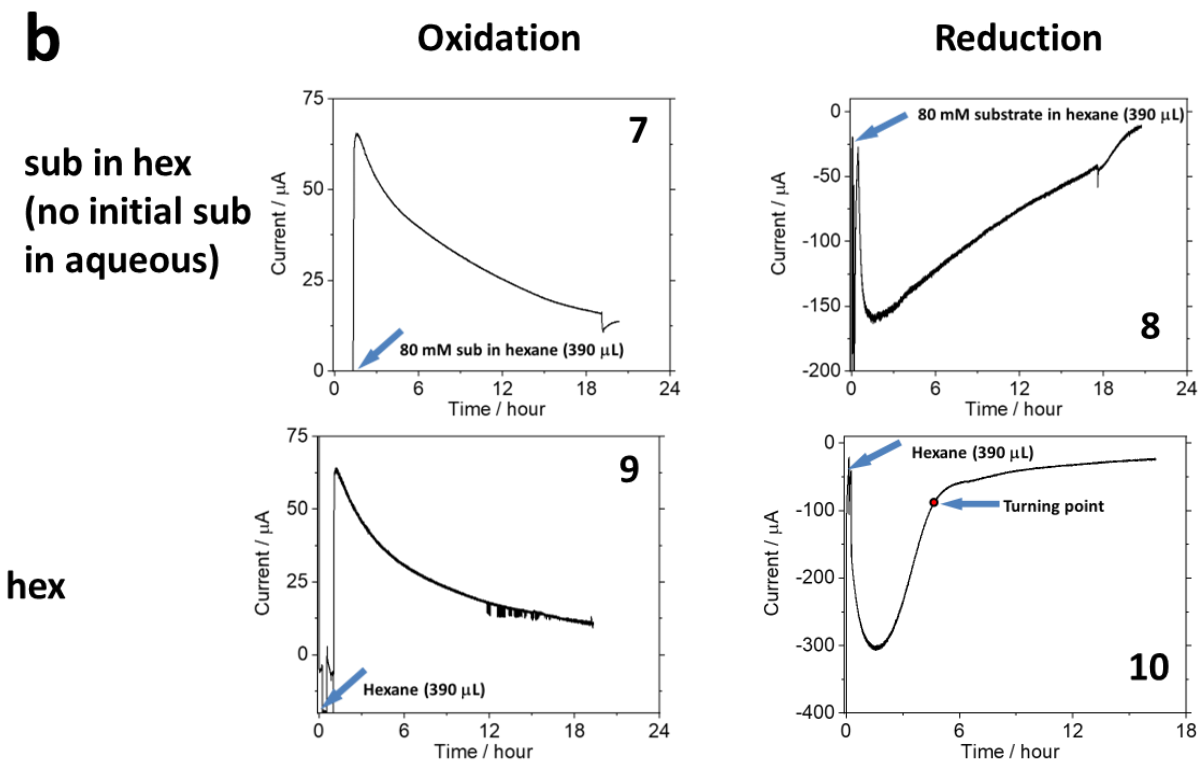


Figure 5.13. Comparison experiments of ADH-catalysed redox reaction between 4-phenyl-2-butanol and 4-phenyl-2-butanone in biphasic conditions. **(a)** Tests investigating the substrate replenishment effect. Organic phase addition: 1:1 hexane and substrate added after a monophasic reaction (reaction 1, 2); 1:1 hexane and substrate added at beginning (reaction 3, 4); pure substrate added at beginning (reaction 5, 6). **(b)** Tests investigating the product extraction effect. Organic phase addition: 80 mM substrate in hexane solvent and no substrate in aqueous phase (reaction 7, 8); pure hexane added at beginning (reaction 9, 10).

Cell conditions: solution volume 3.9 mL (3.5 mL aqueous + 390 µL organic phase); buffer: 100 mM TAPS pH 8.0 for reduction and pH 9.0 for oxidation; temperature: 25 ℃, solution is purged with argon to remove O_2 and argon flow maintained in headspace thereafter. Substrate [4-phenyl-2-butanol] = 8 mM (aq) in oxidation and [4-phenyl-2-butanone] = 8 mM (aq) in reduction, except reaction 7 and 8 where no substrate in the aqueous phase at beginning. [$NADP^+$] = 20 µM; Potential held at -0.34 V (oxidation) and -0.9 V (reduction) vs. Ag/AgCl (3 M KCl). Electrode SA = 14 cm^2; enzyme loading: FNR pre-loaded by drop-cast, 1.28 nmol ADH is loaded by live injection at initiation of the reaction.

Substrate replenishment

Test 2 is the first trial shown in figure 5.12 in previous section (reproduced here for ease of comparison). The injection of substrate and hexane recharges the depleted substrate in aqueous phase.

First, looking at the reduction direction, Test 4 and test 6 shows the reaction with substrate introduced at the start of experiment. In test 4, the reduction lasts for 3 days. Even though the current decreases over time, the peak current at the starting stage was of similar level as the benchmark reaction (figure 5.11 panel (a)). With the continuous supply of substrate, the coulometric conversion is 5.8 times as in the monophasic benchmark. Test 6 presents an ideal stability of the reaction system with almost no loss of activity over 17 hours, although the current is slightly lower than the peak current in the benchmark experiment. It converted 2.4 times substrate (62.2 μmol) versus the benchmark reaction. It is promising for longer time reaction with such stability. Optimisation work is still needed as most of the curves are showing a decreasing current in a longer time length.

The oxidation reactions also show higher conversion amount compared to the benchmark. In test 1, a live injection of substrate was conducted after 18 h when the current had decreased almost to background levels, restoring the current to approximately 50 percent of the initial peak current. Test 3 and test 5 had substrate present at beginning and have similar timecourse as the benchmark. The charge passed shows higher substrate consumptions in one batch, which are 51.1 μmol, 34.4 μmol and 27.1 μmol respectively (test1, 3, 5), versus the 11 μmol conversion in the benchmark reaction. In summary, the substrate (either in 1:1 organic solution or as pure substrate) as organic phase can sustain the supply to aqueous phase, maintaining the reaction rate and hence resulting in a higher product yield in both oxidation and reduction processes.

Product extraction by solvent

The introduction of organic solvent (hexane) is to exploit the product extraction for product inhibition relief. As an initial indication of product extraction, Test 3 shows a minor current increase upon injecting of pure hexane at approximately 44 hours. The organic solvent possibly extracts the product in aqueous phase which leads to recovery

of reaction current and the slowing down of current decrease. Test 1 shows injection of solvent and substrate together. The current recovery was good (50%) after the batch reaction, but this is convoluted with substrate recharging. In addition, the product inhibition still exists at the presence of organic solvent and cannot be fully eliminated, which is confirmed by the current decrease under sufficient supply of substrate and with the presence of organic solvent (Test 1,3 and 7).

Although the addition of organic solvent could relief product inhibition, it also has a disadvantage, since it also extracts the substrate from the aqueous solution, slowing down the reaction rate. Test 9 shows the oxidation with pure organic solvent present throughout the process. This test is meant to utilise the product extraction effect for better conversion. The conversion is lower with a decreased substrate consumption of 8.6 μmol, 78% of the benchmark after 18 hours. The extraction effect is confirmed by a slower decline rate in current comparing to the benchmark reaction (figure 5.11 panel (b)). The time for the current to decrease 50% from the peak current in this reaction is 4.6 hours, while the time is 3.5 hours for the benchmark reaction. However, the conversion is lower in this test. The possible reason is that pure solvent extracts the substrate from the aqueous phase at the early stage of the reaction and causes limited substrate supply. Test 10 confirms this effect by testing in reduction reaction that is free from product inhibition. The curve shows a turning point (abrupt change in the derivative of the current) at approximately 6 hours. Instead of decreasing to zero, the decreasing rate slowed down at the point and had a long ‘tail’. This could be the slow substrate release from the organic solvent. The mass transfer speed was too slow to match the depletion of substrate in aqueous phase, which became the rate-limiting hence at the turning point.

Next, the effect of having the substrate only initially present in the organic layer has been investigated. Test 7 and test 8 had an organic solvent with 80 mM substrate dissolved; the aqueous phase had no substrate to start with. In this case, the total

amount of substrate in the 3.9 mL solution (10%organic, 90% aqueous) is the almost the same as in test 9, where 8 mM substrate is dissolved in aqueous phase. In test 7 and test 8, substrate has to transfer from the organic solvent to the buffer where it can be converted on the working electrode. Test 7 has a curve with the same timecourse as test 9, with similar peak current (65 μA) and coulometric converted amount, indicating that the transport of the alcohol substrate from then organic layer was sufficiently fast. Interestingly, the chronoamperogram of test 8 is a lot different from test 10. The peak current of test 8 is half of test 10, also with a lower conversion. This can be explained by several factors. First, the partition of alcohol and ketone are quite different in the organic solvent. As shown in table 5.3, hexane can extract over 90% of ketone from water of the same volume, but only 70% of alcohol. Ketone extraction to the organic solvent is more favoured than alcohol. Second, in this specific ADH-catalysed redox reaction, reduction has higher reaction rate than oxidation, therefore it needs a more sufficient supply of substrate, and it is more sensitive to the lower amount of initial substrate that has transferred. Third, oxidation process has a strong product inhibition, which means the extraction effect of the solvent can have a boosting effect to the oxidation reaction, while in the reduction solvent only slows down the conversion. Therefore, in test 8, the transfer of ketone from hexane to aqueous phase is limiting, which causes much lower current compared to test 10. In test 10, the ketone was initially at the aqueous phase; the extraction of it to hexane needs some time under given agitation. The substrate was sufficient in test 10 for most of the time until 6 hours. So in this test 10, the slow mass transfer (of substrate between organic and aqueous phases) is benefiting the conversion, while in test 8 it is the opposite. The concentration of substrate in test 8 is never sufficient in this case.

In the oxidation reaction, the transfer of alcohol between the two phases is more efficient than ketone in the reduction process. The reaction rate is slow, and consumption of substrate is minor, thus the substrate is always sufficient in both tests. The reason causing test 7 and 9 to have similar timecourse while test 8 and 10 have different ones

is that the different ‘supply vs. consumption’ situations of substrate. The different partition of ketone and alcohol in organic solvents, the reaction rate in certain directions and other effect such as product inhibition are the factors contributing to this.

Summary

In summary of the hexane biphasic reaction series, some features are clear in the biphasic e-Leaf. Substrate can be kept sufficient with the organic layer containing pure substrate as a ‘reservoir’. Organic substrate with low water solubility is now available. And more product can be produced in one batch process. There is still potential improvement available in the system. First, the conversion amount is much higher comparing to monophasic batch reaction, however, only a small percentage of the pure substrate added is consumed. Second, organic phase may cause noisy signals. Third, the lifetime of e-Leaf is not long enough for an ‘endless’ supply of substrate. There are some incompleteness of the test with the hexane system. For example, there is a lack of experiment with injection of organic layer in later-stages, especially for oxidation reactions, to show the effect of organic solvent. The extraction effect has not been distinguishably shown. Tests in larger-scale cell are needed to check the feasibility of biphasic system in a larger scale.

5.5.4. Supplementary Test for Initial Experiments

Large-scale cells

Experiments in a larger scale cell (40 mL) were conducted as an extension of the biphasic system (previously all conducted on a 4 mL scale as shown in figure 5.13). Chronoamperograms are shown in figure 5.14. The oxidation is conducted with 40 mL of aqueous buffer containing 8 mM of alcohol as substrate. The electrode was preloaded with FNR before reaction and ADH was added in real-time to initiate the reaction. However, direct injection of the enzyme in a ten times larger cell while maintaining the same concentration of ADH as in the smaller cell would be inefficient and enzyme

wasting. Therefore, the working electrode is confined in a dialysis membrane separating electrode from the solution. The dialysis membrane has a cut-off of 12-14 kDa that prevents the crossing-over of ADH, but still allow the transport of substrate and product. Similar amount of ADH is injected in the membrane holding the electrode at a volume of 200 μL, with the concentration of ADH being 8 μM which is much higher than in the 4 mL cell (0.37 μM).

The purpose of both experiments is to test the effect of organic solvent heptane on the product inhibition. In both experiments, the reaction started with the ADH addition in the membrane. After the loading process of 18 hours, reaction (a) had the membrane and the ADH within it removed while reaction (b) had the membrane remaining as it was. In reaction (a), the current increases upon the removal of membrane, due to the increased mass transfer from stirred bulk solution. After another 24 hours, 4.4 mL of heptane was injected on the top of the reaction solution. The current then increased for approximately 5 hours before started to decrease again. In reaction (b), the first heptane injection caused an immediate increase of current, and the current decreased afterwards. Two more injections of heptane were conducted yet they hardly bring about any changes in the current.

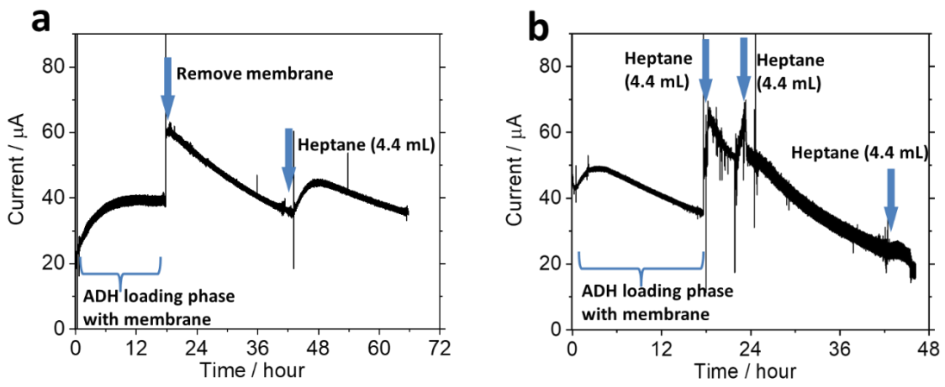


Figure 5.14. Chronoamperograms of oxidation of 4-phenyl-2-butanol in biphasic conditions in larger cell with dialysis membrane enzyme confinement. Conditions: solution volume 4.4 mL (10% organic phase); buffer: 100 mM TAPS pH 9.0; temperature: 25 ℃, solution is purged with argon to remove O_2 and argon flow maintained in headspace thereafter. Substrate [4-phenyl-2-butanol] = 8 mM (aq), [$NADP^+$] = 20 μM; Potential held at -0.1 V vs. Ag/AgCl (3 M KCl). Electrode SA = 14 cm^2; enzyme loading: FNR pre-loaded by drop-cast, 1.6 nmol ADH is loaded by live injection (in membrane with working electrode).

This experiment confirms that organic solvent (heptane) is able to increase the overall performance of the e-Leaf by extracting product and relieving product-inhibition, even though the product inhibition cannot be fully eliminated. The organic product partitions in different ratios in both phases preferring the organic phase. Organic solvent keeps removing certain percentage of product while the product accumulates at a steady rate and ratio. In addition, the product molecules that are deeply confined in the nanopores and close to the enzymes are hard to diffuse out. The concentration gradient created between the bulk solution and nanopores seems to be not enough to extract those molecules.

The scaling up of the biphasic reactor is feasible, though live injection loading of the coupled enzyme is not an appropriate loading method for such experiment. The assistance of dialysis membrane is also restricting the reaction rate, likely by a weaker agitation for the bulk solution within the membrane.

Different volume composite of substrate and solvent in organic phase

Following the discussion above, adding organic solvent does not eliminate the product inhibition but can help to relieve it to some degree. Experiments comparing different volumes of organic solvent in reaction were conducted and are shown in figure 5.15. Panel (a) shows the monophasic benchmark reaction (red trace) and the biphasic reaction with 200 μL substrate and 200 μL octane as organic solvent. Panel (b) shows the monophasic benchmark reaction (red trace) and the biphasic reaction with 100 μL substrate and 1.4 mL octane. Both reactions were initiated by the live injection of ADH. Reaction (a) a has a charge passed of 6.9 C, indicating 35 μmol substrate converted, which is 219% of a typical batch reactor (8 mM in 4 mL, racemic alcohol). Reaction (b) has a charge passed of 9.2 C, indicating 48 μmol substrate converted, which is 300% of a typical batch reactor (8 mM in 4 mL, racemic alcohol). The reaction (b) has the higher conversion, with organic phase containing more octane and less substrate. Both experiments show a higher conversion than the monophasic reaction which can be

easily quantified by the integral area of the current over time. It can be concluded that the organic solvent helps improve the conversion of alcohol oxidation catalysed by ADH by extracting product and easing the inhibition. More solvent can boost the extraction effect and further increase the substrate consumption within the same reaction time.

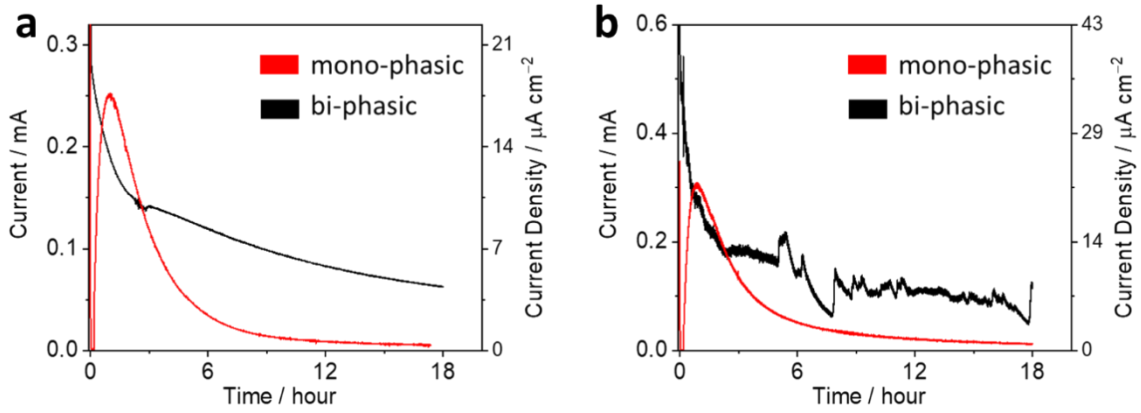


Figure 5.15. Chronoamperograms of ADH-catalysed oxidation of mono-phase system (red trace) and octane and substrate biphasic system (black trace). **a)** organic phase: 220 μL substrate + 220 μL octane, and **b)** organic phase: 100 μL substrate + 1.4 mL octane. Conditions: starting solution volume 4 mL; buffer: 100 mM TAPS pH 9.0; temperature: 25 ℃. solution is purged with argon to remove O_2 and argon flow maintained in headspace thereafter. substrate [4-phenyl-2-butanol] = 8 mM (aq.), [$NADP^+$] = 20 μM; Potential held at -0.1 V vs. Ag/AgCl (3 M KCl) to drive oxidation. Electrode SA = 14 cm^2; enzyme loading: FNR pre-loaded by drop-cast, 0.96 nmol ADH is loaded by live injection at initiation of the reaction.

5.6. Later-stage Experiments in a Glovebox with Enzyme Pre-loaded

Experiments conducted in this stage has adopted a more elegant operation compared to the former experiments in section 5.4. The main shortcoming in early-stage experiments is the enzyme loading method, with preloaded FNR and live injected ADH at the start of the reaction. Redundant ADH in the aqueous solution can have direct contact with organic phase, which may cause some undesired deactivation of enzymes (as observed in section 5.3.2) even though ADH proves to be stable with some alkanes.[70] In addition, the loading process is occurring at the same time as the reaction, thus convoluting the initial part of the chronoamperogram. The enzyme amount and composition in the nanopores is changing over time and the electrode is not working at a constant

condition. Such a loading method can add to the complexity of reaction process and make the experiments less repeatable. In the later-stage experiments, enzyme loading is conducted by co-stirred preloading of FNR and ADH, then rinsing the excess enzymes off before using. This method allows enough time for both enzymes to be loaded and no extra enzymes are introduced into reaction solution. The electrochemical cell is working in an anaerobic glovebox to avoid the undesired current from the reduction of O_2, which is likely to occur when the cell is working on the bench in open air. No more argon purging is needed and the possible loss of organic substances (substrate and organic solvent) through evaporation is decreased. Experiments in this section includes tests of different organic phase composite in oxidation process with different injection timings, and the test of pure substrate effect on reduction process.

5.6.1. Reduction with Pure Substrate: Substrate Replenishing and Deactivation

The new reduction experiment is to test the idea of an organic ‘reservoir’ for substrate supply. The chronoamperogram is shown in figure 5.16. The reaction is in similar conditions as previous ones. The first half of reaction is a monophasic batch reaction, initiated by the injection of NADPH. The current rapidly increased to the peak current 150 μA. Once the batch reaction was finished, 500 μL pure ketone was added at the top of the solution as the second layer. The current recovered to a level (145 μA) similar to the peak current in the batch reaction. The current then decreased in the following time until a low level. The charge passed in the monophasic stage is 7.0 C and the coulometric conversion is 91.3% of the 40 μmol substrate. The biphasic stage with pure substrate layer has a charge passed of 4.6 C and the coulometric production is 23.6 μmol. The extra layer of substrate could be the cause of the decrease in the activity of the system.

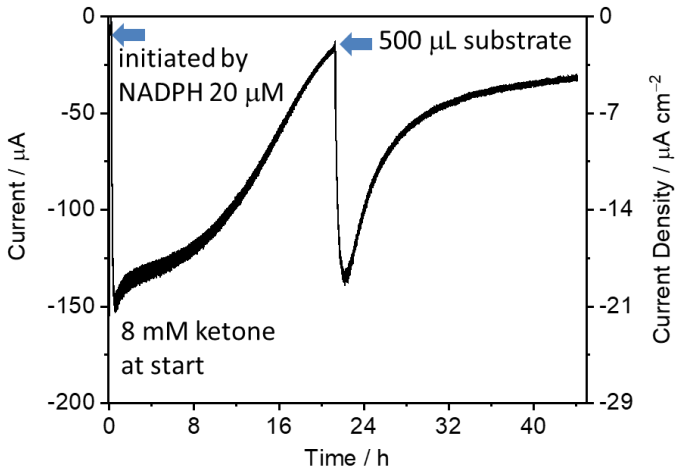


Figure 5.16. Chronoamperograms of mono-phase reduction of alcohol catalysed by ADH as benchmark with pure substrate injected after one batch. Conditions: solution starting volume 5 mL; buffer: 100 mM TAPS pH 8.0; temperature: 25 ℃. Experiments performed in an anaerobic glovebox to avoid any contribution to the current form the reduction of O_2. substrate [4-phenyl-2-butanone] = 8 mM (aq), [NADPH] = 20 μM; Potential held at -0.85 V vs. Ag/AgCl (3 M KCl) to drive reduction. Electrode SA = 7 cm^2. Enzymes loaded by stir-loading in 2.5 mL pH 9.0 TAPS buffer containing 11.5 nmol FNR + 5.7 nmol ADH.

A repeat experiment was conducted to confirm the deactivating effect brought by the pure substrate. The chronoamperogram is shown in figure 5.17 (right), with the magnified view of the starting stage (left). The aqueous phase contained no substrate at start and the reaction was initiated by the addition of pure substrate in real-time. The curve shows a similar decreasing pattern as in the previous reaction, in which the peak current was reached on the injection of substrate followed by fast decreasing over the reaction course. The reaction was manually stopped at 20 hours and a buffer exchange was conducted to move the working electrode into a monophasic aqueous solution containing 8 mM substrate and 20 μM NADPH. The system remained at the lower current after the buffer exchange, indicating an irreversible deactivation of the system.

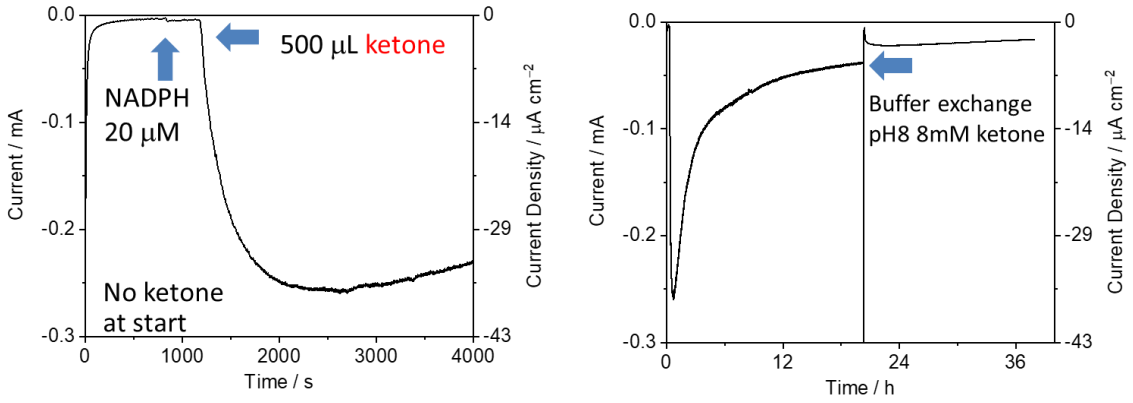


Figure 5.17. Chronoamperograms of ADH-catalysed reduction of ketone with 10% v/v pure substrate (ketone) added at beginning. Full process of the reaction (right) and the magnified starting stage (left). Conditions: starting solution volume 5 mL; buffer: 100 mM TAPS pH 8.0; temperature: 25 ℃. Experiments performed in an anaerobic glovebox to avoid any contribution to the current form the reduction of O_2. No substrate in aqueous phase at beginning, [$NADP^+$] = 20 µM; Potential held at -0.85 V vs. Ag/AgCl (3 M KCl) to drive reduction. Electrode SA = 7 cm^2. Enzymes loaded by stir-loading in 2.5 mL pH 9.0 TAPS buffer containing 23 nmol FNR + 5.7 nmol ADH.

Both experiments have shown an obvious deactivation of the system on injection of pure ketone, which is inconsistent with initial experiments (figure 5.13, test 2 and 6), where the current is sustained for a longer time with pure substrate introduced to the system. Based on the observations from experiments (section 5.3.2), ADH and FNR alone are stable in the mixture of biphasic solution. And the e-Leaf working performance is stable with the presence of pure ketone or ketone and organic solvent mixture with live-injected ADH. The hypothesis could be that the presence of pure ketone as an organic layer is detrimental to the stability of enzymes in the electrode, particularly ADH.

In addition, the excess ADH presented in the bulk solution in early-stage experiments is of a much higher amount comparing to ADH in the electrode (normally > 10 times). These ADH in aqueous phase may help to stabilise the enzymes in the electrode and ease the deactivation caused by pure ketone. In conclusion, organic phase as a 'reservoir' for substrate supplying may not apply to the system with enzyme pre-loaded in the electrode. More endeavour is needed to enhance the stability of electrode with enzyme preloaded for biphasic solution. Potential improvement includes searching for

organic solvents and enzyme loading methods that fit better for specific biocatalytic reactions.

5.6.2. Organic Phase in Oxidation for Product Inhibition relief

The following results show a series of tests with strictly controlled conditions to investigate the effect of organic phase on the oxidation process. Pure organic solvent, pure substrate and a mixture of substrate and solvent were added to the aqueous solution at the beginning or in the middle of the reaction process. Working electrodes were prepared from the same batch. The enzymes FNR and ADH were also from the same batch of enzyme production. Tests were carried out within a short length of time for similar general operation and experimental conditions.

(1) benchmark monophasic reaction

The monophasic oxidation reaction was conducted as the benchmark reaction for comparison. The chronoamperogram is shown in figure 5.18. FNR and ADH were preloaded on the ITO coated Ti foil electrode (7 cm^2). The starting solution contains 8 mM of racemic substrate 4-phenyl-2-butanol. The reaction was initiated by the addition of $NADP^+$ in real-time. The current quickly increased to the peak current (270 μA) after initiation and decreased as the reaction proceeded. The current finally reached close to zero, indicating the depletion of substrate and the domination of product inhibition. The charge passed of the process is 2.9 C, corresponding to 15 μmol product. The coulometric conversion is 47% (of total 32 μmol), which is almost a full conversion (of the (*S*)-4-phenyl-2-butanol in the racemic substrate) considering the enantioselectivity of W110A.

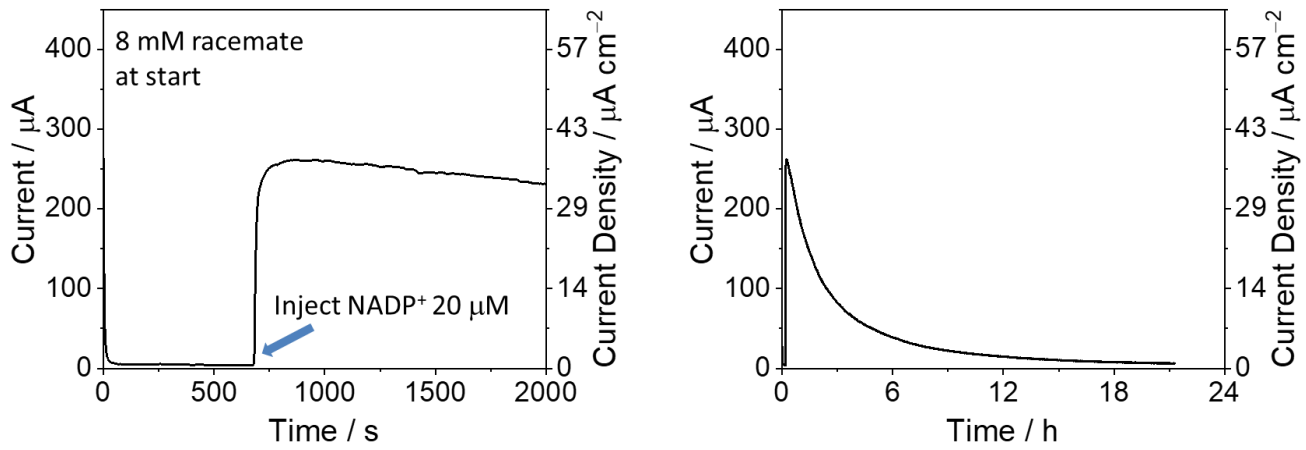


Figure 5.18. Chronoamperograms of mono-phase oxidation of alcohol catalysed by ADH as benchmark. Full process of the reaction (right) and the magnified starting stage (left). Conditions: solution volume 4 mL; buffer: 100 mM TAPS pH 9.0; temperature: 25 ℃. Experiments performed in an anaerobic glovebox to avoid any contribution to the current form the reduction of O_2. substrate [4-phenyl-2-butanol] = 8 mM, [$NADP^+$] = 20 μM; Potential held at 0 V vs. Ag/AgCl (3 M KCl) to drive oxidation. Electrode SA = 7 cm^2. Enzymes loaded by stir-loading in 2.5 mL pH 9.0 TAPS buffer containing 11.5 nmol FNR + 5.7 nmol ADH.

(2) Organic phase added at beginning

In the following tests, organic solvent and substrate were added to the reactor at the start of experiment. The chronoamperograms are shown in figure 5.19. The starting solution contained 8 mM of racemic substrate 4-phenyl-2-butanol. The reaction was initiated by the addition of $NADP^+$ in real-time. The current quickly increases to the peak current after initiation. Organic phase (alcohol, solvent, and mixture) was also added in real-time right after the initiation when the current just reached its peak. The introduction of solvent and substrate did not cause any immediate change to the current (other than some artificial noises) because the substrate supply was sufficient and not much product had been produced yet. The current gradually decreased as the reaction proceeds and finally to a low level at the end of the reaction at approximately 20 hours.

The charges passed of the three oxidation processes within 18 hours are 10.9 C, 3.9 C and 6.1 C for pure substrate, pure solvent and mixture of substrate and solvent, respectively, corresponding to 56.5 μmol, 20.2 μmol, and 31.6 μmol of product, which

are corresponding to conversion rate of 141%, 51% and 79% in a typical monophasic batch reactor (8 mM in 5 mL).

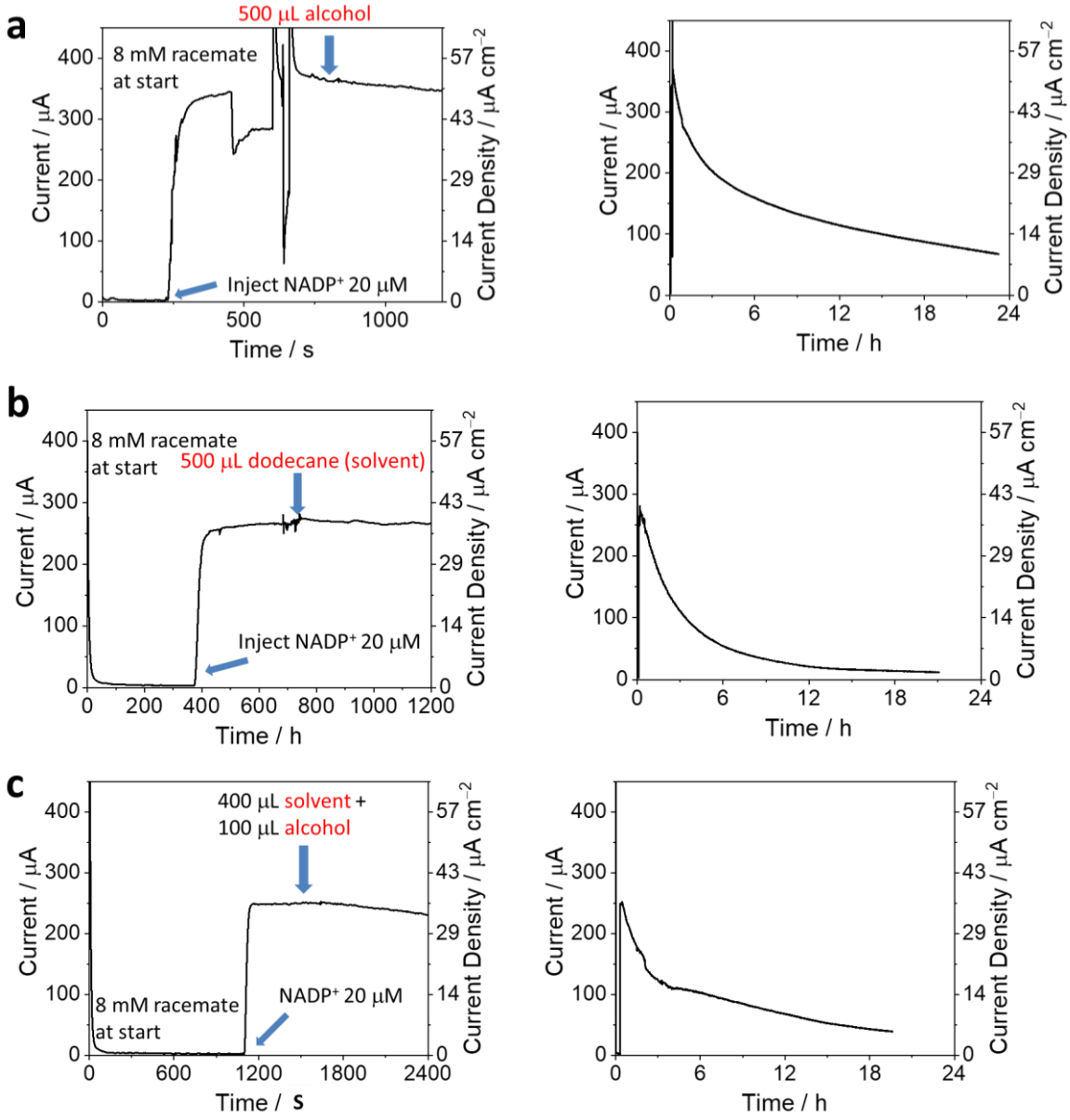


Figure 5.19. Chronoamperograms of ADH-catalysed oxidation of 4-phenyl-2-butanol with 10% v/v organic phase added at beginning. Full process of the reaction (right) and the magnified starting stage (left). Organic phase: **a)** 500 µL pure substrate **b)** 500 µL pure solvent dodecane **c)** mixture of 400 µL solvent and 100 µL substrate. Conditions: starting solution volume 5 mL; buffer: 100 mM TAPS pH 9.0; temperature: 25 ℃. Experiments performed in an anaerobic glovebox to avoid any contribution to the current form the reduction of O_2. substrate [4-phenyl-2-butanol] = 8 mM, [$NADP^+$] = 20 µM; Potential held at 0 V vs. Ag/AgCl (3 M KCl) to drive oxidation. Electrode SA = 7 cm^2. Enzymes loaded by stir-loading in 2.5 mL pH 9.0 TAPS buffer containing 11.5 nmol FNR + 5.7 nmol ADH.

For a better comparison of the three chronoamperograms, the overlaid diagram is plotted in following figure 5.20 panel (a). It can be observed that the reaction with pure substrate has the highest reaction rate and the most product converted within reaction time (18 hours). The reaction with a pure solvent layer has slightly more conversion than the benchmark reaction. The reaction with a mixture of solvent and substrate (400 μL dodecane and 100 μL substrate) has a conversion amount higher than the benchmark but lower than the reaction with pure substrate.

In addition, to exclude the influence of batch difference, as the different peak current levels, the normalised diagram is depicted as panel (b). The normalised diagram focuses on the pattern and the shape of the current over the process. It can be observed that the reactions with substrate involved have an overall higher current level and slower current decreasing rate as indicated by the dash lines. The reaction with solvent alone has a similar pattern as the benchmark. This suggests that the solvent is not contributing to the reaction in this case. It is likely that the product inhibition is not obvious in this situation, while the substrate supply is more of a rate-determining factor. This is backed by the slower decrease in reactions with substrates, and also reflected in the conversion, that both the benchmark reaction and the biphasic reaction with pure solvent has a conversion of nearly 50%, a full depletion of the target enantiomer.

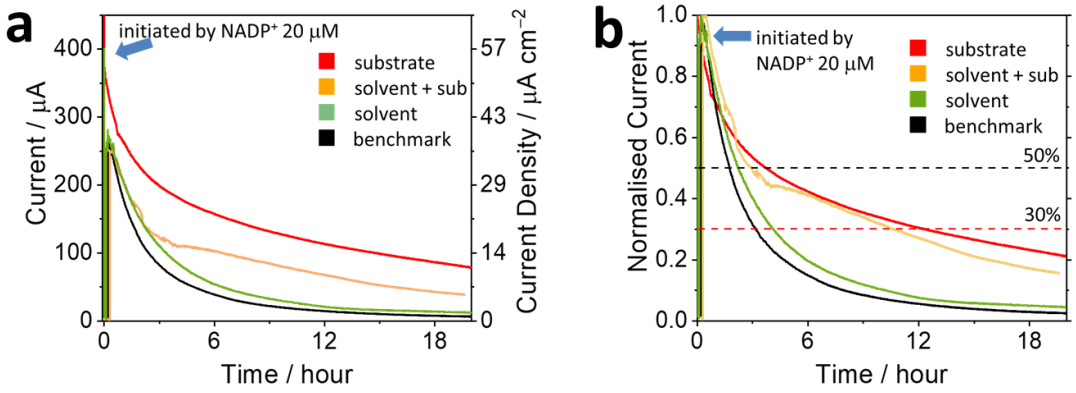


Figure 5.20. Overlaid chronoamperograms of biphasic reaction process with e-Leaf. **a)** original curves and **b)** normalised curves.

(3) Organic phase added in the middle of a reaction

As a comparison to the previous series of experiment, tests are conducted with organic phase added in the middle of a reaction instead of at beginning. The purpose is to further investigate how substrate and solvent affects the current pattern of the reaction process. It is also desired to see abrupt changes on the introducing of the second phase due to either substrate supplying or product-inhibition relief.

The two chronoamperograms are shown in figure 5.21. The starting solution contained 8 mM of racemic substrate 4-phenyl-2-butanol. The reaction was initiated by the addition of $NADP^+$ in real-time. The current quickly increased to the peak current after initiation. After approximately 1 hour, the organic phase (alcohol or solvent) is live injected. The 1-hour reaction time is chosen for building up the consumption of substrate and the accumulation of product-inhibition, with the expectation for a sharp change of current to be observed at the injection of an organic phase. However, the injection of solvent and substrate did not induce any immediate current change. The substrate in the solution was still sufficient and the product-inhibition was not built up so the addition of the organic phase did not cause direct change to the current. The current then decreased as the reaction proceeded and finally to a low level at the end of the reaction in 20 hours. The charge passed in the oxidation within 18 hours are 6.6 C and 3.5 C for pure substrate and pure solvent respectively, corresponding to 34.2 μmol and 18.1 μmol of product, which are corresponding to conversion rate of 85% and 45% in a typical monophasic batch reactor (8 mM in 5 mL).

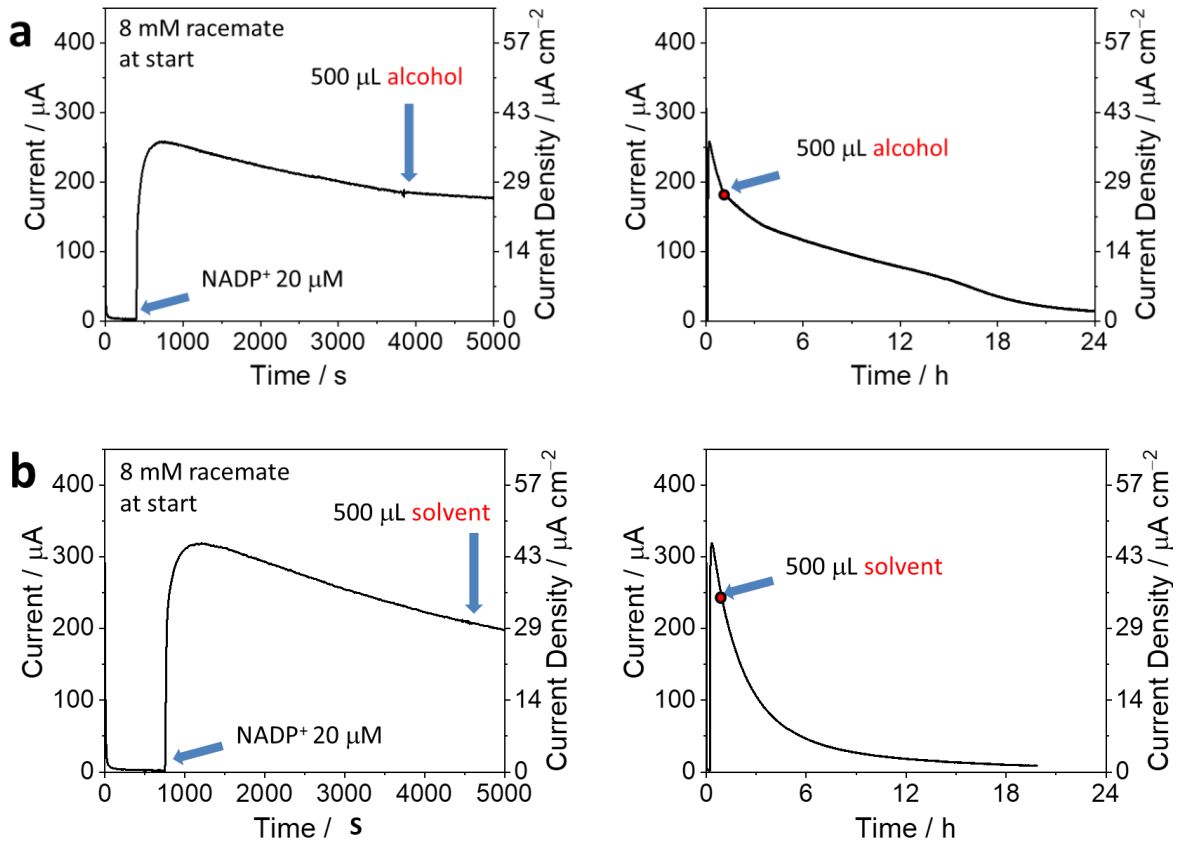


Figure 5.21. Chronoamperograms of ADH-catalysed oxidation of 4-phenyl-2-butanol with 10% v/v organic phase added at halfway of reaction. Organic phase: **a)** 500 µL pure substrate **b)** 500 µL pure solvent dodecane. Conditions: starting solution volume 5 mL; buffer: 100 mM TAPS pH 9.0; temperature: 25 ℃. Experiments performed in an anaerobic glovebox to avoid any contribution to the current form the reduction of O_2. substrate [4-phenyl-2-butanol] = 8 mM, [$NADP^+$] = 20 µM; Potential held at 0 V vs. Ag/AgCl (3 M KCl) to drive oxidation. Electrode SA = 7 cm^2. Enzymes loaded by stir-loading in 2.5 mL pH 9.0 TAPS buffer containing 11.5 nmol FNR + 5.7 nmol ADH.

The overlaid diagram is plotted in following figure 5.22. Panel (a) shows the normalised curves of the two experiments with organic phase injection in the middle of reaction. It can be observed that the reaction with pure substrate has a distinguishable effect of boosting the reaction rate and yield. The current pattern drifts away from the benchmark pattern immediately after the introducing of pure substrate. In contrast, the reaction with pure solvent has almost an identical current pattern as the monophasic reaction, indicating that the pure solvent dodecane in this case has hardly any influence on the reaction course. This agrees with the results from previous experiments that it is likely that the relief of product inhibition did not seem to occur.

Panel (b) shows the comparison of organic phase injection at different times, in which the normalised current changes with pure substrate added at beginning and at the middle of the reaction are plotted against the monophasic benchmark. Despite some difference at the ending stage of the processes, the two biphasic reactions share a much similar pattern of the timecourses, indicating that both operations have increased the overall conversion rate comparing to the monophasic reaction.

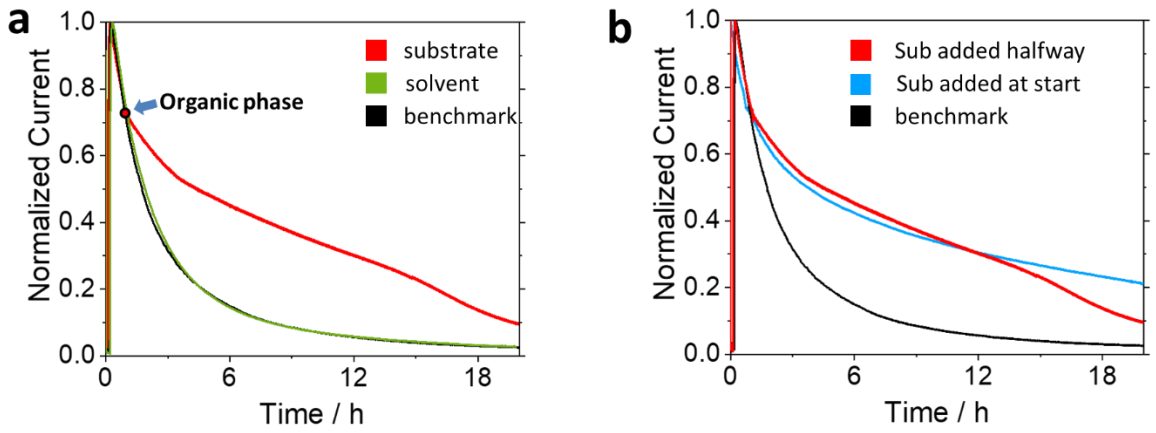


Figure 5.22. Overlaid chronoamperograms of biphasic reaction process with e-Leaf. **a)** comparison of halfway injection of different organic phases. **b)** comparison of organic phase injected halfway and at start.

In reviewing the biphasic oxidation experiments, several observations have been made. First, the additional supply of alcohol from the organic phase can boost the overall performance of the biocatalytic process by increasing the reaction current and therefore a higher conversion is achieved in a given reaction time. Second, dodecane as the organic solvent has no obvious effect on the reaction rate in these biocatalytic process, as it has a similar timecourse as the monophasic reaction. Third, introducing the organic phase to a monophasic system during the reaction will change the curve pattern similar to the biphasic system that has the same organic phase to start with. The later-stage experiments show the fact that in this specific reaction setting, only the pure substrate as the organic layer is improving the performance of the e-Leaf.

5.7. Conclusion and Potential Improvement

The introduction of an organic phase to the e-Leaf to make the ‘biphasic e-Leaf’ has been tested and its feasibility has been proved in principle. The organic layer of the e-Leaf consists of pure substrate and/or a common organic solvent. The aqueous solution is holding the working electrode as in a normal monophasic reactor. The mass transfer of the organic molecule of substrate and product is occurring between the two phases through the interface. The partitioning is determined by the affinity of substrate to both phases, also affected by the agitation condition.

The biphasic e-Leaf targets two issues from the monophasic reactor. First, a substrate with low solubility in water restricts the yield in a batch reaction. An organic layer containing high concentration of substrate can serve as a ‘reservoir’, providing continuous supply to the aqueous phase. The reaction is therefore free from restrictions of insufficient substrate and the activity and lifetime of the system is mainly depend on the stability of the biocatalysts. Second, some reactions are product-inhibited like the model reaction of ADH. The organic solvent which has stronger affinity to the organic molecule of product can extract product from the aqueous bulk solution and ease the inhibition effect. The inhibition will still exist as the organic solvent is not able to fully extract the product. This process is also limited by slow mass transfer.

Experiments in this chapter have covered the optimisation of the e-Leaf setup (enzyme loading, scale-up feasibility), organic solvent test and the performance of the biphasic reaction under different conditions. Successful tests have shown the ideas of substrate ‘reservoir’ and product inhibition relief work to some extent. The e-Leaf is proved to be available for deeper incorporation with biocatalytic organic synthesis.

Nevertheless, there are still questions remained to be answered and potential improvements available. First, organic solvent does not fully eliminate the product inhibition. There is always product in the aqueous phase due to partial extraction. In addition, the product is formed on the enzymes in the nanopores of ITO electrode, so its

diffusion to the bulk solution is slow. The production inhibition that can only happen in the bulk solution, is therefore less effective. Second, the life and stability of the enzyme ADH is not long-lasting enough for long-term investigation. The system normally has a stable and robust performance within 24 hours (the longest duration reported in this chapter is 72 hours). In addition, the activity of the system tends to decrease quickly in the reduction process in the presence of pure substrate. More stable enzymes or other reactions with different substrates that is less detrimental to the system are needed to fully explore systematic optimisation. Third, adding pure substrate or organic solvent containing pure substrate can cause a waste of chemicals, as the yield is less than the substrate applied, even though the conversion is many times higher than a monophasic batch reaction. This issue can possibly be solved by separating and recycling the organic layer after each reaction, which is possible in practice though not carried out in these research for lab experiments. Fourth, it would be better to focus on one question at a time rather than mixing several factors together. The model reaction has both low-soluble substrates and product inhibition. The experiments to investigate the function of substrate supply and product-inhibition relief are conducted under both restrictions. It is better to adopt a model reaction that have product-inhibition with soluble substrate, or a model reaction with low-soluble substrate but without product-inhibition. The result and comparison shall be more distinguishable.

CHAPTER VI

6. The Electrochemical Leaf Under Flow

6.1. Introduction

As a further step towards the application of the e-Leaf, the design of an e-Leaf under flow is explored and discussed in this chapter. Continuous-flow chemistry has become an attractive topic in academic and industrial research, popular in this field are microreactors due to their higher efficiency in mass and heat transfer, bringing increased process safety, and the potential to implement automation protocols and process analytical technology.[127] Bioelectrochemistry has also received increasing attention for its high efficiency, selectivity and the use of green and sustainable electricity as its driving force.[3–5] The e-Leaf has the feature of live monitoring and electrochemical to control which can be automated, which provides a good combination the two approaches.[48,51,60] This inspired the attempts to use the e-Leaf under flow to introduce the advantages of flow chemistry.

The flow reactor e-Leaf is inspired by previous chapters involving the design of the biphasic system and larger-sized reactors, and it is an extension of the e-Leaf scaling up project with a goal to solve the limited supply of substrate. Limitation by amount of substrate was also addressed in the larger-sized reactor to provide higher yields by increasing the batch amount and also the biphasic reactor by adding a layer of pure substrate. A flow reactor would continuously supply substrate by flowing from a storage tank, in addition, the flow reactor is convenient for carrying out the live interventions that are possible with the e-Leaf. The biphasic reactor is not ideal in regard to frequent live interventions for the limited space crowded with electrodes. For instance, the product extraction may be performed badly in a biphasic reactor due to lack of extraction solvent and mild mixing. In addition, there is the mixing of organic solvent with the aqueous layer (from stirring to maintain a good mass transport) with which can have a negative effect on the enzymes. A flow reactor can transport the reaction solution to a separate vessel, which allows various operations like product extraction, addition of substrates and live sampling, with less agitation to the electrode.

The blueprint of transforming the e-Leaf into a flow system for the use in industry will have three stages, as shown in figure 6.1, which are (i) a circulating flow reactor, (ii) a continuous reactor, and ultimately, (iii) a reactor series (with hypothetic reactions conditions for each reactor). Plenty of successful examples regarding to scaled-up electrochemical reactor, packed bed reactor and flow reactor have proved the feasibility of making a packed-flow e-Leaf.[16,127,128]

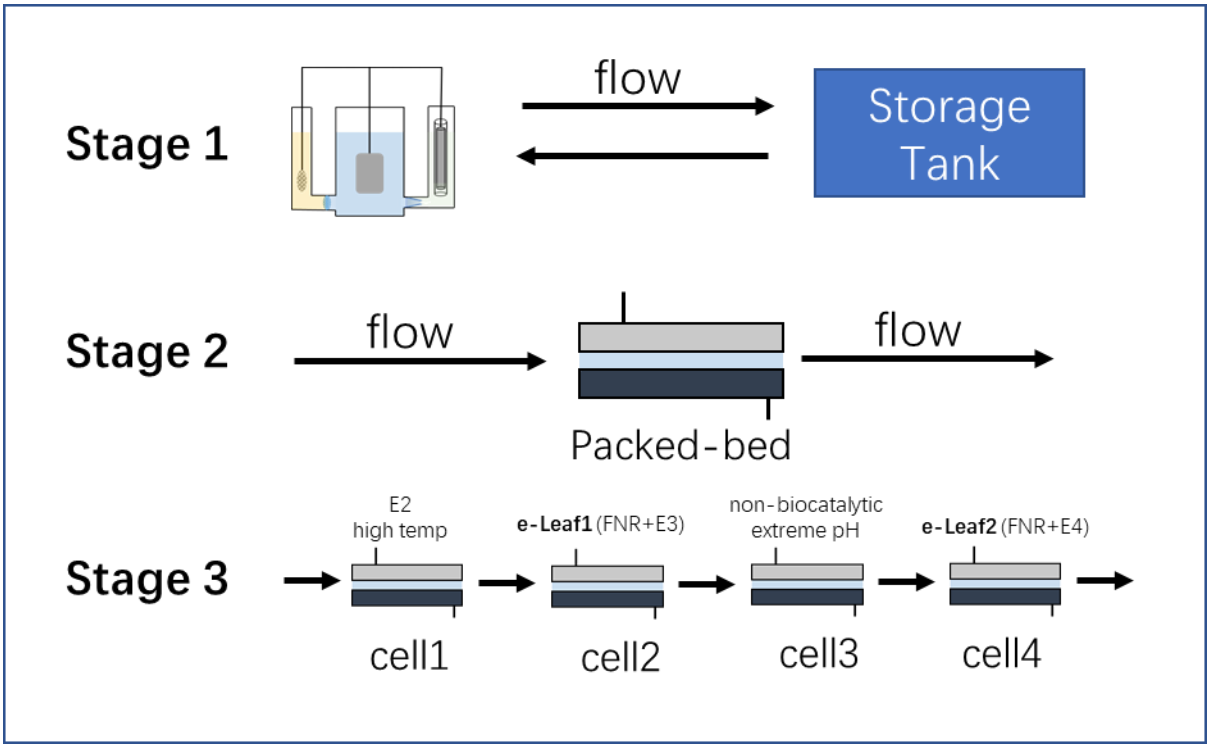


Figure 6.1. Stages of transforming the e-Leaf into a flow system for the use in industry

(1) Circulating flow reactor: To start with, e-Leaf will be directly connected to a storage tank with solution flowing and circulating in between. The obvious feature of this design is the improved supply of substrate and product collection by introducing the storage tank which is a separated environment from the reaction solution. The storage tank holding a large volume of solution can maintain a steady supply of both soluble and insoluble substrates. An organic layer can be introduced in the tank for insoluble organic substrate supply and product extraction and the independent space separated from the electrode allows for mixing and extraction without disturbing the electrode. The batch

can be recharged by real-time buffer exchange. The storage tank is relatively independent, only connected to the reactor by flow which can be switched on and off manually. The operation in the storage tank can be 'sensed' and reacted to by the electrode in the reactor, as the properties of the storage solution change. Therefore, a lot of operations can be conducted without physical disturbance of the biocatalyst, such as adding inhibitor, adjusting pH and buffer exchange. The potential usage at industry-level could be to replace batch without influencing the production unit. The purpose of such a circulating flow reactor in this work, is to test the feasibility of this combination and the stability of the e-Leaf under flow. The electrochemical cell design and improvement are the main questions to address in this stage.

(2) Packed-bed electrochemical reactor (PBER): The second stage is a continuous reactor with the e-Leaf. After the concept of the e-Leaf working under flow is confirmed, it is desired to make the reactor more efficient, robust, and of higher space efficiency. The feasibility of packed-bed electrochemical reactors (PBER) has been proved by plenty of research.[97,129,130] As the electrodes are packed, the density of the catalytic unit will become extremely high. This design prevents unnecessary dead space that is a common issue in the previous work in standard electrochemical cells. High space-time-yield (STY) will be achieved, and the e-Leaf will be more competent as a researching tool as well as a synthesis technology. At this stage, there will be a high requirement in regard to engineering design, such as the arrangement of electrode and the detailed flow control to achieve lower residual concentration.[131,132]. The e-Leaf shall be turned into a more application-oriented form, and research methods will include physical test and modelling, more than electrochemical reactions.[133,134] This is also the pre-requirement of making the reactor series, in which the high space time yield is needed to finish each step of a reaction to a high extent.

(3) Reactor series: The third stage is based on the previous two steps; the final industry-ready version of an e-Leaf flow reactor. This design will incorporate the well-

developed reactor series design from industry. The e-Leaf flow reactor will be a modular reactor which can be scaled up and be duplicated in series. The reactor cascade draws the inspiration from the enzyme cascades used in the e-Leaf. Nanoconfinement in the e-Leaf enables multi-step enzyme cascades in the same electrode with high efficiency. The reactor series, on a macro level of design, helps to further complete the application of the e-Leaf by allowing for a modular system where separate e-Leaf electrodes work in sequence but in separate reaction solutions. For example, some enzymes can be working in extreme conditions like high salinity, extreme pH, low or high temperature, at a higher speed whilst others in the next sequential module can work in milder conditions.[126,135] A reactor cascade can separate conditions that can be harmful to other enzymes thus allowing for different optimal conditions to run simultaneously.

The results presented in this chapter show three designs for stage (i) demonstrating the exploration to build the prototypes for the circulating e-Leaf flow reactor. There are three flow cells designed and tested for availability and stability using both the well-studied coupled reaction of GLDH in the e-Leaf and also the classic redox couple for electrochemical investigations, ferro-ferricyanide. The electrochemical reaction of this redox couple has often been used for demonstrating purpose in electrochemistry, since it is well-characterised and has reversible electrode reactions that can be catalysed directly on the e-Leaf without extra chemicals or process. The first cell is a premade small electrochemical cell. The second cell is a hand-made flow reactor using standard laboratory glassware used for distillation and gas flow. The third cell is a specially designed and blown cell for flow. This work is at the lab test level, it has deepened the understanding of e-Leaf performance under flow and provides guidance for future development. The flow reactor endeavour will grant the e-Leaf great potential for incorporation into the matured industrial process technologies such as continuous reactor, multistep series reactions and packed-bed reactors. The goal is to make the e-Leaf adaptive to common technologies such as automatic controls, kinetic screening in application purposes.[136,137]

6.2. Flow Cell I

6.2.1. Cell Design

The flow system I is the first step in the exploration of the e-Leaf under flow. The target is to start making a flow system by using a small-scale conventional electrochemical cell, combined with a peristaltic pump. It should be a small-sized prototype that runs a model reaction as a proof of concept.

Figure 6.2 shows the designed sketch and photo of the flow cell I. As the sketch shows (panel (a)), the flow cell I consists of two parts. The reactor part is an electrochemical cell where the reaction occurs under real-time control and monitoring. This reactor is similar to the 4 mL batch reactor commonly used in previous e-Leaf experiments (as described in chapter 1). The other part is a storage tank (not shown in the photo), which serves as the 'reservoir' for substrate supply, and it is the place for most of the live operations such as live injection, solution sampling, and buffer exchange (changes which previously were made directly in the reaction solution in which the working electrode was placed). These two parts are connected by silicone tubes. The flow is driven by a peristaltic pump.

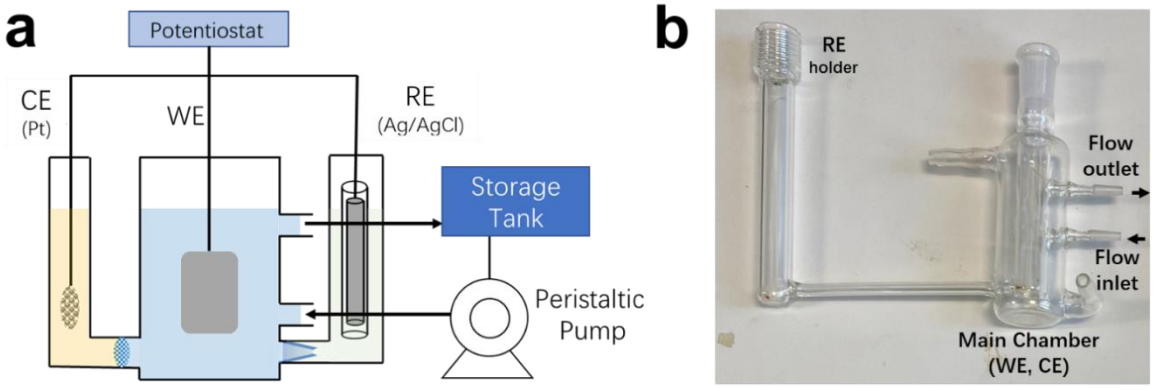


Figure 6.2. Design sketch (a) and the photo (b) of the flow reactor I

The glassware is adapted from a premade electrochemical cell with multiple side openings on the main compartments, shown in figure 6.2 panel (b). This cell was not

originally designed for a flow system and the side openings are made for gas inlet/outlet and a wired electrode; however it has been adapted for the purpose of flow. The two openings were used as the inflow (lower opening) and outflow (upper opening) for solution circulating between the reactor and the storage tanks by connecting to the tube and the pump in the flow system. This cell is slightly different from the design sketch in panel (a), as it does not have a side arm for the counter electrode. The counter electrode used in this cell is usually a Pt wire that is placed from the top to the main chamber with the working electrode.

When the pump is working, solution from the storage tank is transferred into the reactor through the inlet which is at a lower position. The solution will rise to reach the outlet and flow back to the storage tank naturally by gravity, thereby solution is circulating between the two parts. Both the reactor and the storage tank are made air-tight and are purged with argon to eliminate oxygen that may contribute to the reduction current. The tank is held in a water bath for temperature control. Both the storage solution and the main cell reaction solution are stirred using a magnetic flea.

6.2.2. Experiment Results and Discussion - Flow Cell I

The GLDH-catalysed reductive amination of alpha-ketoglutarate is adopted as a model reaction to test the performance of this flow reactor, with the electrode pre-loaded with FNR and GLDH before use. The flow is driven by a peristaltic pump with a relatively slow flow rate of 15 mL/min, circulating between the reactor and a storage tank containing 40 mL solution in total. Since the cell solution is stirred by a stirrer to prevent the limitation from mass transfer between the electrode and bulk solution, the flow rate was determined (in this cell and in following cell designs) for the purpose only to maintain a steady flow to circulate the solution between storage tank and cell with less possible agitation to the electrode. The flow rate is required to ensure uniform concentration across cell and storage tank solution. A chronoamperogram using this initial set-up is shown in figure 6.3, in which the graph on the right is a magnification of

the starting phase of the reaction (shown as the left graph). At the beginning stage of the reaction, $NADP^+$ was first injected in real-time to the storage tank that is under stirring (indicated by blue arrow), and a small increase in current was observed due to FNR reducing the cofactor. Then the substrate a-ketoglutarate was injected to the storage tank (indicated as blue arrow), the coupled reaction is initiated rapidly after the injection, as the substrate is dissolved and circulated to the reactor. The current reached its maximum at initiation which is approximately 95 $\mu A\ cm^{-2}$ which is similar to the current density achieved in a normal batch reactor (table 3.1 in chapter 3). The current was as stable as the 4 mL batch reactor in the first 6 hours. However, the long-term stability is not satisfactory in the flow reactor since the current decreased right after the peak current over the whole process. The possible cause could be that the flowing conditions requires a more robust and stable construction of the electrode. Another potential cause is the fluctuation of liquid level in the cell observed during the reaction, which is discussed in following paragraphs.

The whole process lasted for ~25 hours before the activity was fully lost. The charge passed was 38.6 C, corresponding to 0.2 mmol of substrate consumed, with a coulometric conversion of 62.5% (of 0.32 mmol substrate). Despite noise in the electrical signals and the shorter lifetime of catalytic activity, the system yields more than 6 times the product comparing to a batch in the 4 mL benchmark reactor (figure 3.7 in chapter 3). The high yield was achieved due to the continuous supply of the substrate from the storage tank and the removal (dilution) of the product which reduces potential product-inhibition. For the cell at 4 mL scale, the flow reactor I has a better performance than the batch reactor.

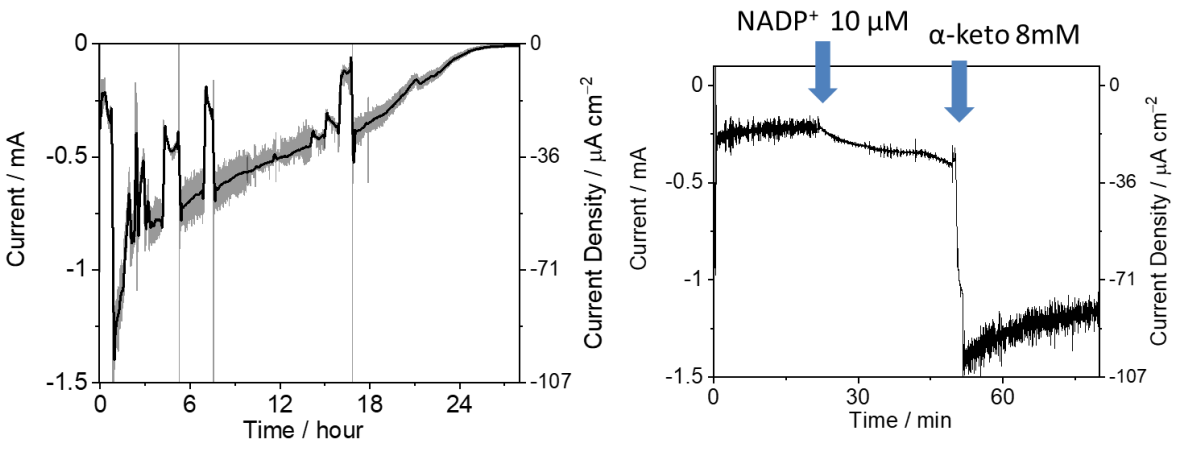


Figure 6.3. The e-Leaf under flow: Chronoamperogram showing GLDH-catalysed reductive amination in flow cell I. The right-hand side graph is a magnification of the beginning stage of the left diagram. Conditions: solution volume 40 mL, reactor volume 4 mL; buffer: 50 HEPES pH 7.5; temperature: 25 ℃, reactor cell and storage tank are purged with argon to remove O_2 and argon flow maintained in headspace thereafter; substrate [α-ketoglutarate] = 8 mM, [NH_4Cl] = 10 mM, [$NADP^+$] = 10 µM; Potential held at -0.72 V vs. Ag/AgCl (3 M KCl) to drive reduction. Solution agitation: stirred by a stirring flea in both the reactor and the storage tank; solution flow is driven by a peristaltic pump in a loop from the reservoir tank into the cell and to the reservoir tank again; flow rate: 15 mL/min. Enzyme loading: 29.2 nmol FNR + 11.9 nmol GLDH are mixed and loaded by drop-casting followed by rinsing to remove unadsorbed enzyme; electrode SA (Ti foil): 14 cm^2.

This experiment shows how feasible it is to use the e-Leaf in a flow system in a simple way with a cell that was not even designed for this. It proves several ideas and brings inspirations in making an e-Leaf under flow. First, it provides another angle on the scaling up of the e-Leaf. Rather than making a larger monolithic reactor which requires a complicated design, a flow system has a large storage tank, which serves as a reservoir of substrate. The flow system is an extension of the e-Leaf scaling-up, with a separated reaction compartment and the storage compartment which means the e-Leaf is free from the limitation of the reactor size now, which benefit future reactor design.

Second, the experiment shows the feasibility of doing live interventions to the storage tank because they are rapidly sensed in the reactor compartment even though they are separated. Real-time operations and interferences like live injection directly in the reactor can physically impact the electrode, causing electrical noise, inconsistency in catalytic rate and even deactivation. In contrast, the storage tank is a ‘safer’ place for the

physical impact and other changes (change in pH, addition of inhibitor, etc.) to occur in the first place, after which the solution is transported to the electrode in a milder way. It even allows for more types of operations that are impossible to conduct in a batch reactor. For example, live buffer exchange on the bench is difficult since oxygen would be introduced and contribute to a reduction current, and when exchanging the buffer in the separate compartment, a thorough purging can be conducted throughout without risk of electrical noise. The buffer exchange can be carried out in the storage tank with the pump switched off for a couple of minutes, while the reactor remains unaffected. Simultaneous product separation and extraction can be carried out in the side tank without disturbing the reactor, which could lead to ultimately a continuous reactor series. In addition, the separated also brings the potential to the e-Leaf for coupling its live monitoring feature to other time point analysis methods such as GC or NMR.

Third, when the e-Leaf under flow is free from the limitation of storage size and substrate amount, the enzymes are likely to work to their limit until deactivation. As shown in above experiment, the flow system can be coupled to the substrate supply, leading to several times more yield than a batch reactor of similar size. In regard to substrates with lower solubility, the separate storage tank connected to the reactor can provide more time and better mixing for such substrates to go into solution, while the biphasic reactor (in chapter 5) may be limited in stirring due to the caution to avoid disturbing the electrode.

The issue in this experiment is apparent: the signal has a high noise level originating from the experiment setup, and multiple current jumps (spikes) in the curve. Fluctuation of liquid level in the reactor is likely the cause observed during the reaction. The cell design is not intended for this purpose as the size of the outflowing openings are designed for placing a wire electrode and for gas flow so they are too narrow (can be seen in photos in figure 6.2) for liquid. The process of liquid level fluctuating is shown in figure 6.4. The system was installed before reaction, to the state shown as ①, in which

the working electrode was submerged under the liquid level. It had been expected that the solution would circulate without changing the level of the liquid. However, the whole system was sealed to be air-tight, and the storage tank is purged with argon which had an extra pressure preventing the solution flowing back to the tank. As shown in ①, the flow could not leave the cell when it reaches the exact same height as the outflow port. Therefore, the liquid kept rising high over the outflow port to build up pressure (shown as ②) before it was driven out by gravity (shown as ③). The liquid level dropped to the height of the outflow port which is lower than where the WE and CE were placed (shown as ④), which caused partially disconnection of electrode and the spikes in the chronoamperogram. The fluctuation of liquid level in the reactor can add to the instability of the system and was also a possible cause for the decreasing activity of the electrode.

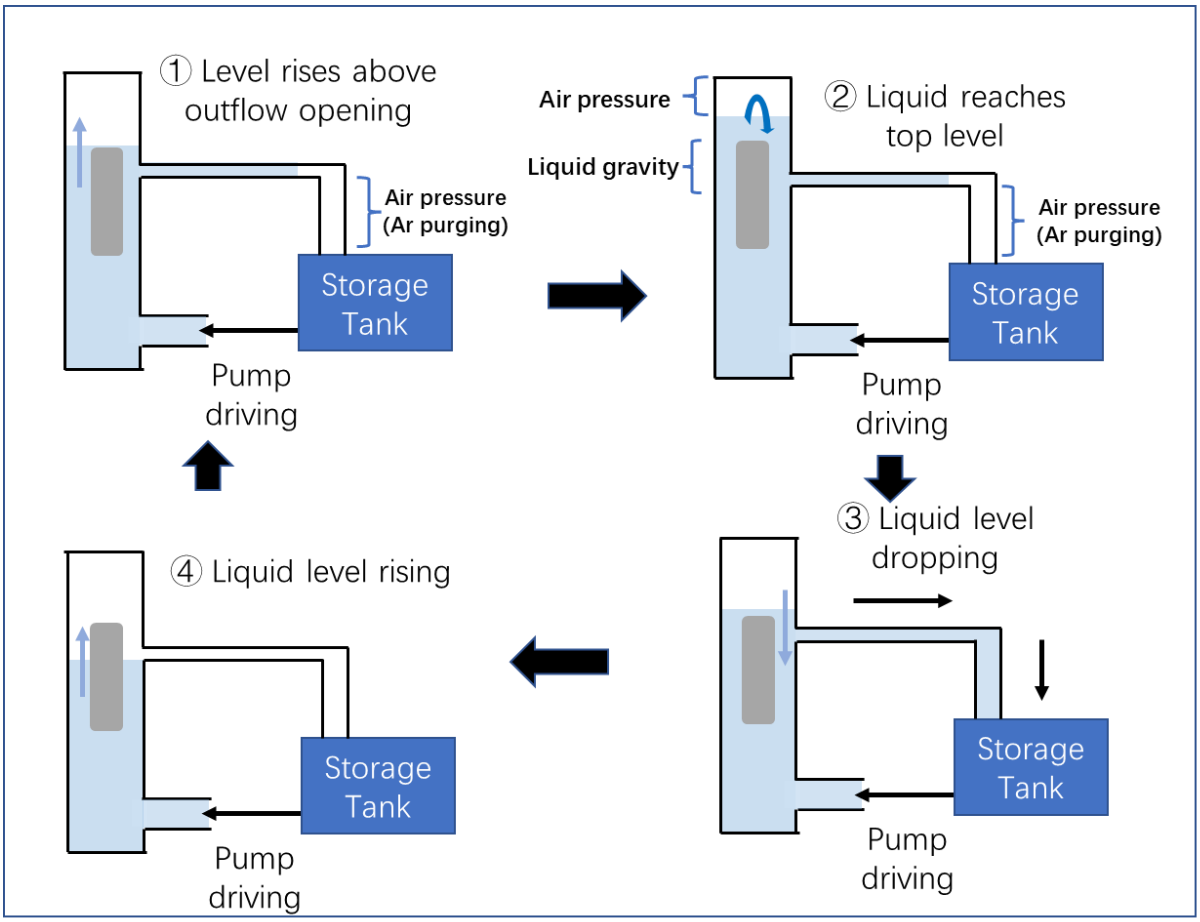


Figure 6.4. Fluctuation of solution level in flow cell I

In conclusion, even though the experiment is a good proof of concept, flow cell I is not a perfect design. There are a few issues to be addressed and improvements to be made: the narrow space in the cell is not suitable for flow conditions; electrical noises obvious due to the unstable positioning of the counter electrode; the sealed (air-tight) space within the cell is causing resistance against the designed flow path; the catalytic activity drops quite quickly due to possible weak construction for a flow condition and liquid level fluctuation. A new design of reactor that can yield a steady signal is desired.

6.3. Flow Cell II

6.3.1. Cell design

Flow cell II has been made based on the experience from flow cell I. As shown in figure 6.5, the new flow cell has been hand-made by assembling multiple standard chemistry lab glassware parts typically used for organic synthesis but adapted here for a new function. The sketch shows the detailed configuration of the cell which is divided into three parts: inlet, reaction compartment, and headspace. There are 5 openings including two at both ends and three at the side of each section that are marked as openings 1-3. The flow driven by peristaltic pump from the storage tank enters the cell through the bottom opening of the inlet section. The working electrode is placed above the glass frit separating the inlet section as shown. This glass frit is not for the typical purpose as discussed in previous chapters, it has a high porosity and cut-off so that it will allow chemicals to travel through. Its main use is as a platform, holding either the stir bar in the working compartment, or for holding Ti tube electrodes which are not able to be held in place by wire only (like Ti foil electrodes), whilst allowing flow. Opening 2 in is the flow outlet with a switch. The head space sector is where the reference electrode is placed; the modular holder of reference electrode is installed through the top of the cell and has a Luggin capillary. Opening 3 in this sector is one of the positions for counter electrode (the other is opening 1) and in the original design, the counter electrode is at opening 3 and opening 1 is used for releasing air trapped under the glass frit.

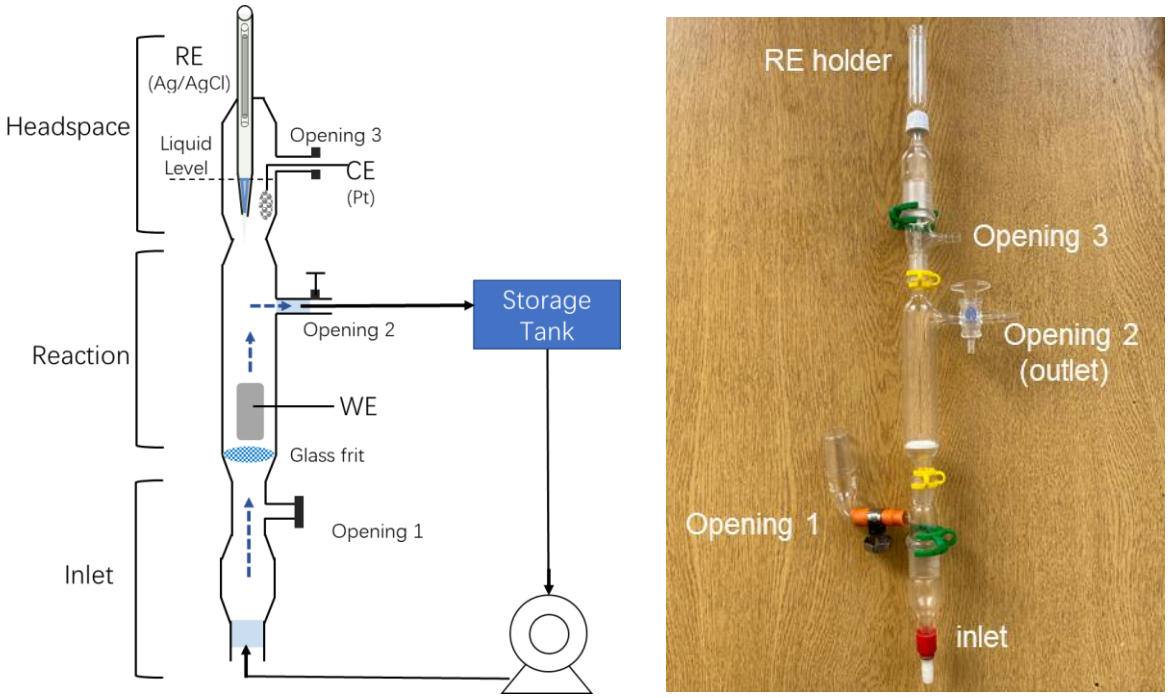


Figure 6.5. The design sketch (left) and photo (right) of flow reactor II

6.3.2. Flow cell II Test with Ferro-ferricyanide Oxidation

6.3.2.1. Cell Construction and Feasibility Test

Flow cell II was first tested using the simple model redox reaction of ferrocyanide-ferricyanide which has been commonly used in electrochemistry. The reaction is non-biocatalytic and can be driven by overpotential on a working electrode; Pt mesh was used as the working electrode to drive the oxidation of ferrocyanide.

Because the reactor is 'handmade' from common labware parts used for the different purpose of organic synthesis i.e. not made specifically for electrochemistry and a flow system, the first goal was to develop the right process for setting up the reactor before the e-Leaf reaction and to check its stability and reproducibility. After the reactor was set up, the performance of the system as an electrochemical cell was evaluated and the stability as a flow system was also checked and improved.

(1) Cell construction before reaction

Multiple trials of cell construction have finally concluded with the step-by-step setting up procedure of the detachable flow reactor. The cell is built up from the bottom to the top with the flow filling the cell, and the reactor was made air-tight and free of air bubbles on the flow path. The following are the steps required for setting up the flow cell II ready for reaction:

1) Fill pump tube with solution from the storage tank and make sure to get rid of any air bubbles in the pump tube.

2) Connect the inlet and reaction sectors of the cell; attach the pump tube to the inlet of the reactor.

3) Switch on the pump and let the solution flow in the reactor; hold the reactor horizontally with opening 1 facing upward; make sure liquid fills the inlet sector without any air trapped under the glass frit.

4) Put the working electrode in the reactor; switch off the opening 2 and continue flowing the liquid to fill the reaction sector.

5) Install the reference electrode holder onto the headspace sector but leave the screw open; install the counter electrode on the headspace sector and connect the headspace sector to the main body of the cell.

6) Flow the liquid to raise the level above the reference and counter electrode in the headspace and switch off the flow.

7) Connect the opening 2 to the tube leading to the storage tank; make sure the storage tank is at a lower level than opening 2 (but the height difference is within that which the pump can handle).

8) Tighten all the connectors on the reactor; switch on opening 2 and check how air-tight the system is. The liquid should not flow out by itself.

9) Switch on opening 2 and turn on the pump and let the flow circulate for a few minutes to make sure it is stable; the system is then ready for the reaction.

(2) Electrochemical performance

The performance of the flow reactor II as an electrochemical cell was then tested after the cell configuration process was optimised. Cyclic voltammetry and chronoamperometry were used to test the electrochemical activity with the Pt mesh working electrode. It is worth pointing out that the cell volume increased from 4 mL (flow cell I) to approximately 100 mL (flow cell II), and the flow rate was therefore increased from 15 mL/min to 50 mL/min to keep efficient circulation the solution in the system. The rate was determined by multiple trials of changing flow rate. The flow rate was not increased to the ratio as volume increased since higher flow rate can cause accelerated falling-off of ITO from the electrode thus deteriorate the activity of the e-Leaf.

Cyclic Voltammetry

Figure 6.6 shows the cyclic voltammograms (left) for the ferro-ferricyanide couple in flow cell II with the counter electrode placed at different positions (highlighted in the sketch on the right). A pair of redox peaks were observed and minimal electrical noise detected.

The three-electrode system turns out to be working well in the cell. There is an artificial current limit at approximately 4 mM though and it is resolved in later experiments. Despite all reaction conditions being the same apart from the position of the CE, the black trace shows a smaller peak separation (0.18V) compared to the red trace (0.43V), suggesting that the electron transfer is more efficient in the former. While it appears that the position of the counter electrode is causing the difference in peak separation, it is more likely to be caused by the distance between the WE and the RE which has likely been increased during the repositioning of the CE and subsequent reassembly of the cell components. The extra potential required could be due to the increase of the solution resistance caused by this increased distance between RE and WE.

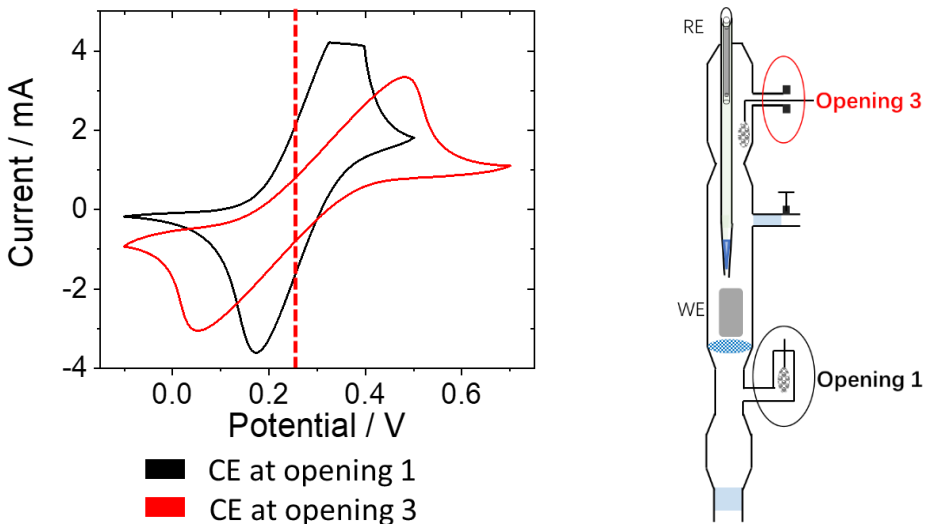


Figure 6.6. Cyclic voltammograms of ferrocyanide redox peaks with counter electrode at different positions. Scan rate = 4 mV/s. Conditions: WE: Pt mesh, solution volume 100 mL in reactor; temperature: 25 ℃; substrate: [ferrocyanide] = 10 mM, [KCl] = 500 mM; flow rate (when flow is on): 50 mL/min. Electrode (Pt mesh) geometric area: 1 cm^2.

Chronoamperometry

Figure 6.7 shows a chronoamperogram for the oxidation of ferricyanide in flow cell II (left) with the magnified beginning stage (right). The CE was held at opening 3. The reaction was initiated by applying a potential of +0.5 V (vs. Ag/AgCl 3 M KCl) at time=0 which caused the current to increase rapidly to a steady level of 1.5 mA. After 10 minutes the flow was switched on (as indicated) and the current increased again to 4.5 mA. This is because the flow increased the mass transfer, which was insufficient before the flow switch-on and limited the reaction rate. Stirring and flowing are the two main ways of maintaining sufficient mass transfer in the flow reactor.

The reaction rate was stable for over 12 hours until the connection was lost by the drop in liquid level due to the gas bubble accumulated on the headspace sector pushing down the liquid level. The liquid level at beginning of the reaction was held above the outlet openings with the system being sealed air-tight. However, as the process carried on, gas formed from water electrolysis on the CE accumulated on the headspace and

pushed down the liquid level. The liquid finally dropped below the counter electrode (held at opening 3) and the connection was lost.

The charge passed was 180 C, corresponding to 1.87 mmol of substrate converted, 37.4% of the starting amount. The chronoamperogram shows a steady current and good connection before disconnection happened indicating the potential of flow reactor II to function well as an electrochemical cell for the e-Leaf under flow.

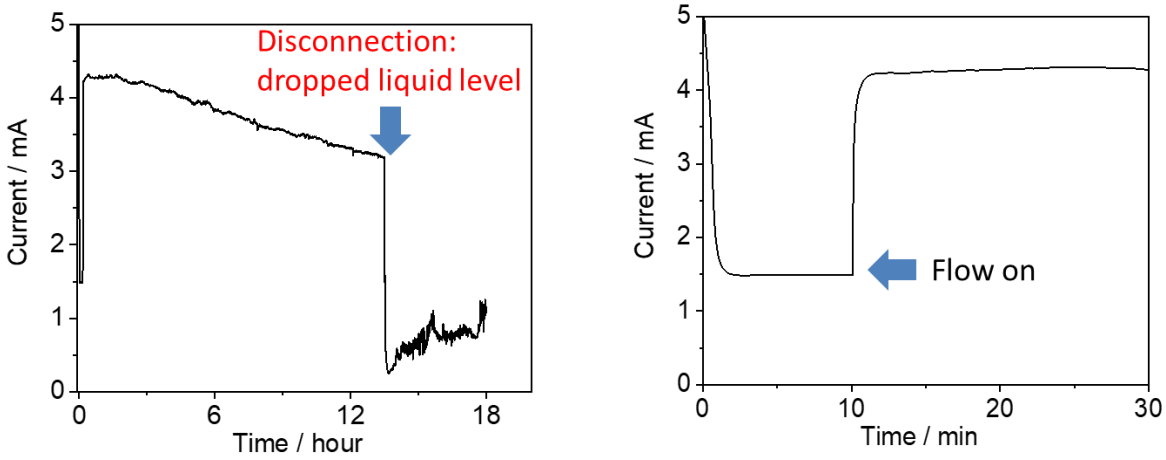


Figure 6.7. Flow Cell II used for the oxidation of ferrocyanide monitored by chronoamperometry. Conditions: WE: Pt mesh. solution volume: 500 mL, reactor volume: 50 mL; temperature: 25 ℃; substrate: [ferrocyanide] = 10 mM, [KCl] = 500 mM; Potential held at +0.5 V vs. Ag/AgCl (3 M KCl) to drive oxidation. Solution agitation: flow by peristaltic pump; flow rate: 50 mL/min. Electrode (Pt mesh) geometric area: 1 cm^2.

However, the disconnection has raised a serious question about the cell design. The disconnection during the reaction was caused by a drop in liquid level in the flow cell which resulted in a final solution level below the reference and counter electrodes. During the reaction, the counter electrode had hydrogen evolution since the WE was at an oxidative potential (as discussed in chapter 3.) The reactor is air-tight therefore the gas gets trapped in the headspace and pushes the solution level down until the reference and counter electrode are no longer in the solution. It has been commonly observed in a large-scale reactor that the liquid level in the CE modular holder is dropping fast over the reaction. In summary, although flow cell II can work as an

electrochemical cell, it needs further improvement to handle the gas formed at the counter electrode to become a feasible flow cell for the e-Leaf.

6.3.2.2. Improved Flow Cell II with Tube Electrodes

(1) Cell design improvement

To address the problem of disconnection caused by the build-up of gas at the counter electrode, a side arm was attached to opening 1 as an interchangeable holder for the counter electrode. It is a glass holder similar to the side arm in the conventional batch reactor, connected by the silicone tube to the main reactor, as shown in the photo of figure 6.8 and as shown in the sketch, the reference electrode is still placed in the headspace sector but has been moved down to be closer to the working electrode. The whole reactor remains air-tight. The counter electrode was originally placed in the side arm. To avoid potential liquid level dropping caused by the accumulation of gas formed on the CE, the electrode was finally placed in the middle of the flow path.

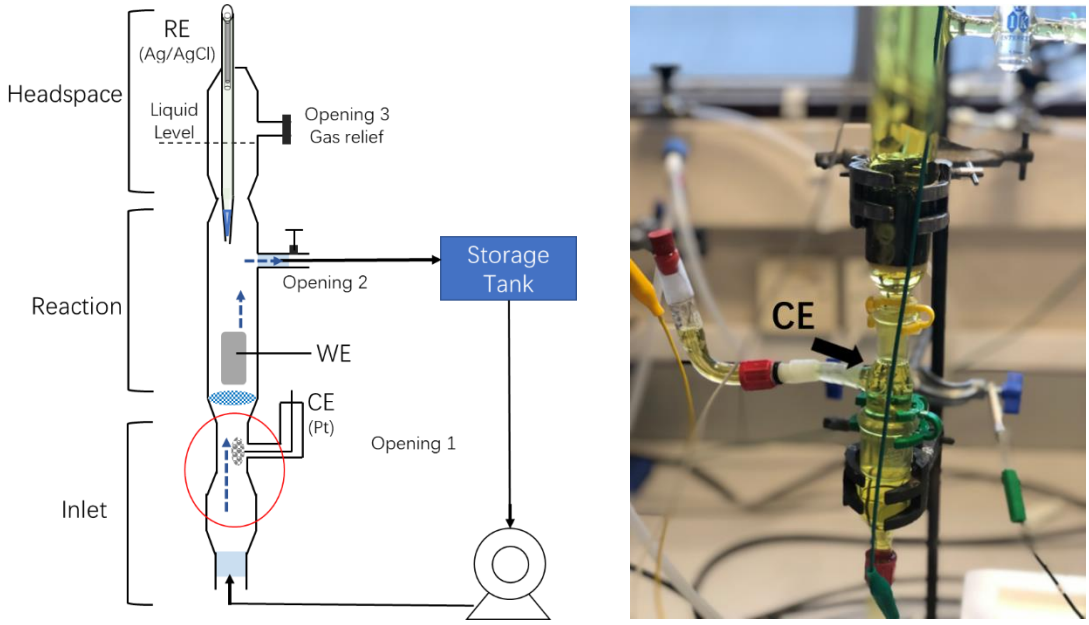


Figure 6.8. Improved design of the flow reactor II with counter electrode in the middle of the flow path from a side-arm.

In this adjusted design, gas formed on the counter electrode will still travel upward and accumulate in the headspace section leading to a solution level drop. However, opening

3 can now be used as a switch for gas relief. Since the whole system is air-tight (including the storage tank), opening 3 can be manually opened regularly to allow the liquid level to rise and compensate for the drop. This was impossible when the counter electrode is installed at opening 3. Considering the reaction current being not too high to generate gas quickly, a manual switch is enough for maintaining a steady solution level for reaction.

(2) Titanium tubes in flow reactor

In addition to the adjustment in the cell configuration, Ti tubes were tested for their feasibility in the flow reactor to explore the possibility of increasing the 'electrode to space' ratio, making the most use of space in the reactor. The Ti tubes' cylindrical structure allows them to be easily packed in the cylindrical reactor, filling most of the space in a regular way.

The Ti tube electrodes were coated with ITO by the doctor's blade method (see chapter 7 for experimental methods details) before use, and were placed on the glass frit (for support) in the reaction sector; Figure 6.9 shows the Ti tube electrodes packed in from above. Twenty-four Ti tubes (OD: 4.25 mm, ID: 3.75 mm, length: 33 mm) are packed to fill the available space in the reactor (ID: 25 mm). In practice, a piece of quartz fibre was jammed to the side of electrodes to keep the tubes held in position. The surface area to volume ratio in the 'tube cylinder' is 12.3 cm^2 / mL, which is extremely high for e-Leaf experiments (the 500 mL batch reactor being 1.05 cm^2 / mL, chapter 3). Electrode packing in a reactor is a key factor in designing a packed-bed reactor for an industrial level synthesis, thus Ti tube is a good material to start with.

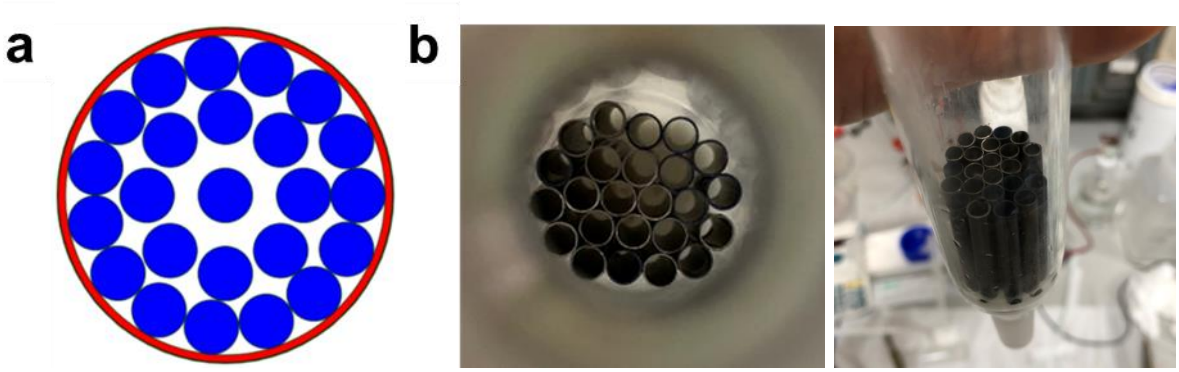


Figure 6.9. The sketch (c) and photos (b) of the Ti tubes packing in a cylindrical reactor.

Figure 6.10 shows cyclic voltammograms using ferri-ferrocyanide with the tube electrode design in the adjusted flow cell II. Panel (a) shows the CV for the ferri-ferrocyanide couple using a single tube working electrode and panel (b) shows the CV with 24 tubes (electrically connected), under flowing and stationary conditions.

Panel (a) show the CV obtained using one Ti tube electrode, in which the oxidation peak is much broader than the reduction peak. The Ti tube, unlike other commonly used electrodes with a flat surface, has a curved surface and the diffusion of substrate from the bulk solution may be enhanced due to this special geometric shape, supplying enough substrate to sustain a high current at oxidative potentials (leading to the observed plateaued shape). The reduction scan, in contrast, is more peak-like because it has limited substrate (ferricyanide) formed only during the oxidation scan and therefore it is easily depleted at the electrode surface to give the peak-like shape. The peak separation is similar to the previous CV, indicating a good reproducibility of the flow cell setup with repeatable electrochemical environment.

Panel (b) shows the CVs obtained using 24 Ti tubes in stationary conditions (black) and under flow (red). The CV obtained with 24 tubes does not present the same shape as the CV obtained with one Ti tube (panel (a)). This may be due to the fact that the 24 tubes may not be in perfect contact with each other which would cause the electrode to have a much higher resistance than the very low resistance expected from one piece of metal tube. In addition, the slightly different shapes are observed in panel (b) of 24 tubes

under flow (red) and at stationary conditions (black). This can be due to the similar reason that the increased agitation from flow may bring about loose contact among the tubes, causing increased resistance therefore the shape of the CV changed.

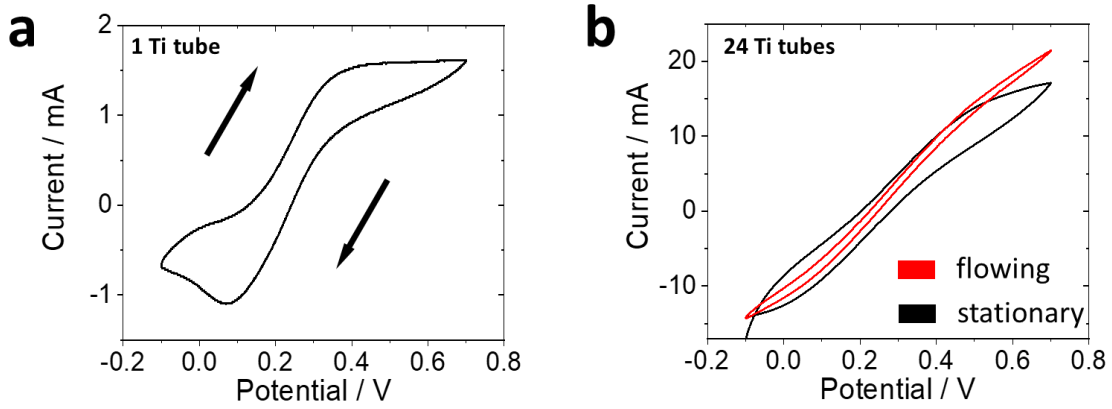


Figure 6.10. Titanium tube(s) used as the working electrode in the e-Leaf with redox couple ferri-ferrocyanide monitored using cyclic voltammetry. **a)** CV of one tube; **b)** CV of 24 tubes monitored in stationary condition (black) and under flow (red). Scan rate = 4 mV/s. Conditions: solution volume 100 mL in reactor; temperature: 25 ℃; substrate: [ferrocyanide] = 10 mM, [KCl] = 500 mM. Electrode SA: 8.3 cm^2 (1 tube) and 199.2 cm^2 (24 tubes).

The oxidation reaction was monitored by chronoamperometry with 24 tube electrodes as shown in figure 6.11. The reactor volume was approximately 100 mL and the volume of the 10 mM ferrocyanide solution, 500 mL. Without flow, the reaction was initiated by the potential applied and the current rapidly reached a stable level of 2.7 mA. The flow was switched on after 80 minutes and the current increased to 16.9 mA due to the increased substrate supply. The overall current slowly decreased over time, which could be due to the loss of ITO layer. This was confirmed by a test in which the Ti electrode without ITO coating shows a much lower rate in catalysing the conversion while ITO-coated Ti electrode has much higher rate. The process was manually stopped at 22 hours, by which time, the charge passed was 769 C, corresponding to 7.97 mmol substrate converted, a conversion of 159%. The over 100% conversion was due to extra substrate (ferricyanide) being produced on the counter electrode on the flow path where the reduction was proceeded. The adjustment made to the cell has proved effective in avoiding the liquid level dropping issue as the reaction went on steadily for over 20

hours and the experiment also shows that flowing overcame limitation by mass transport and the capability of flow cell II as an electrochemical cell for the e-Leaf under flow.

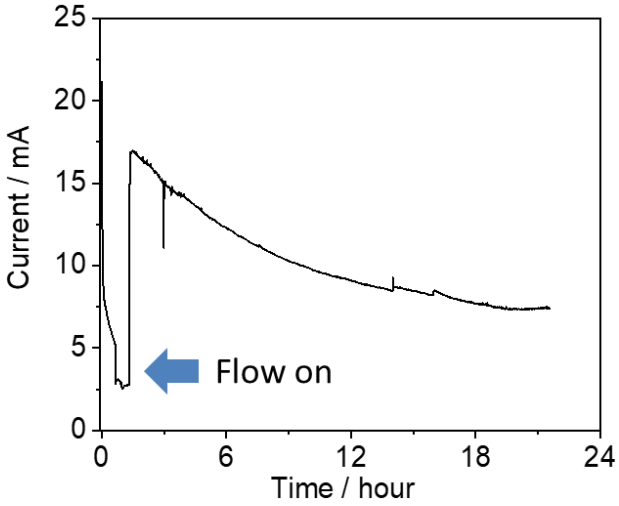


Figure 6.11. The e-Leaf under flow with improved cell (CE positioning) and a tube-shaped working electrode, tested using ferrocyanide oxidation. Conditions: solution volume: 500 mL, reactor volume: 100 mL; temperature: 25 ℃; substrate: [ferrocyanide] = 10 mM, [KCl] = 500 mM; Potential held at +0.6 V vs. Ag/AgCl (3 M KCl) to drive oxidation. Solution agitation: flow by peristaltic pump; flow rate: 50 mL/min; electrode SA: 199.2 cm^2.

6.3.3. Flow cell II: GLDH-catalysed Reduction with Ti Tube Electrodes

6.3.3.1. Cell Setup

Flow cell II was tested on biocatalytic reactions after the successful test with ferrocyanide. More adjustments were made to the cell design for better performance and stability: the reactor part was made open to the atmosphere (opening 3 was kept open) rather than being a closed air-tight system, with argon purging the headspace. This was to ensure a steady solution level at the height of the outlet (opening 2). These adjustments make the pressure in the system stable, avoiding unbalanced pressure and fluctuation of flow speed. The solution will flow out once it reaches opening 2 and will not accumulate in the headspace sector. Accordingly, the reference electrode reaches below the solution level to be close to the WE, which helps lowers the need for voltage

compensation, comparing to the setup shown in figure 6.12; the counter electrode is still held in the side arm below the glass frit.

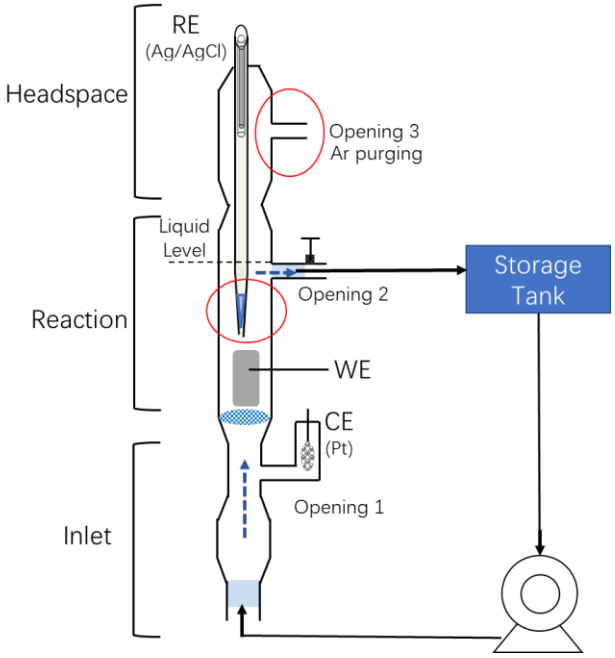


Figure 6.12. Adjusted design of flow reactor II for GLDH reaction with Ti tubes.

6.3.3.2. GLDH-catalysed reduction in flow cell II

(1) cyclic voltammetry

Figure 6.13 shows the cyclic voltammograms of the (FNR + GLDH)@ITO/Ti tube electrode tested in flow cell II. Panel (a) shows the CV for a single tube before (black trace) and after enzyme loading (red trace). The FNR non-turnover peaks indicates a loading amount of 54 pmol/cm^2, which is similar to the amount on Ti foil electrode. Panel (b) shows comparison of two CVs for 1 tube (red trace) and 24 tubes (blue trace). The capacitance change is a good indication that all tubes are electrically connected as a whole unit.

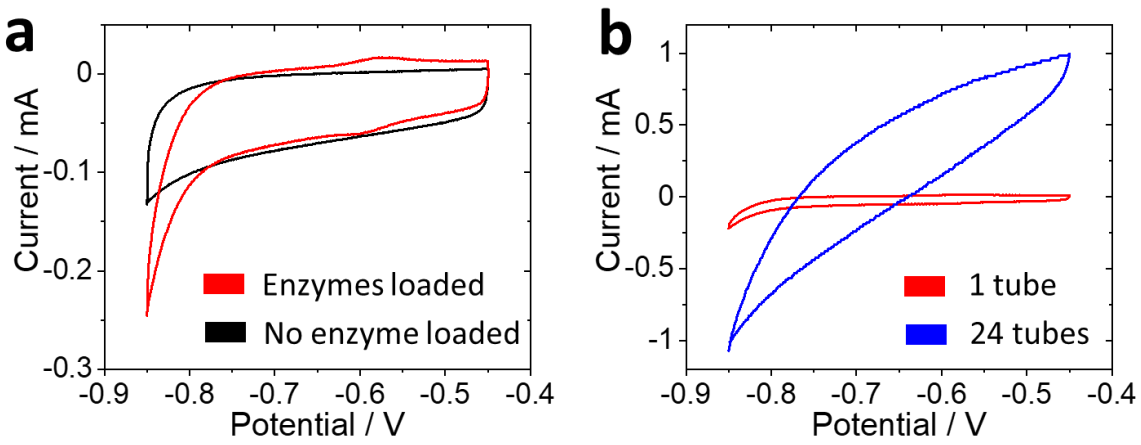


Figure 6.13. A comparison of FNR loading and the feasibility of a 24-tube electrode in the flow cell II, with (FNR + GLDH)@ITO/Ti tube electrode. **a)** CVs of one tube before and after enzyme loading **b)** CVs showing capacitance comparison between one and twenty-four tubes with enzyme loaded. Scan rate = 4 mV/s. Conditions: solution volume 100 mL in reactor; temperature: 25 ℃; buffer: 50 mM HEPES pH 7.5; temperature: 25 ℃, solution in storage tank is purged with argon to remove O_2 and argon flow maintained in headspace thereafter; Electrode SA: 8.3 cm^2 (1 tube) and 199.2 cm^2 (24 tubes). Enzyme loading: 414.3 nmol FNR + 42.2 nmol GLDH are mixed and loaded by stir-loading for 18 hours; electrode SA: 199.2 cm^2

(2) chronoamperometry

Figure 6.14 shows chronoamperograms of the two repeats for GLDH-catalysed reduction of α-ketoglutarate coupled to FNR in the e-Leaf. GLDH is a model reaction used in previous investigations. The two tests share identical preparation and reaction conditions. All substrates for GLDH were present from the start and the flow was on. The reaction was initiated by applying a potential of -0.8 V (vs. Ag/AgCl in 3 M KCl). As in indicated in the figure, reaction (a) had the flow on for the whole process and reaction (b) turned on flow at the initiation.

Both reactions had stable rates during the process, and the reaction (b) had a higher overall activity than reaction in panel (a). The current in (a) was almost unchanged in 20 hours and the current in (b) decreased by only by 25% (b) over 24 hours. The cells were agitated only by flow and the introduction of stirring would improve mass transfer. The coulometric yields were 0.62 (reaction a) and 2.2 mmol (reaction b) respectively, which,

although is less than 15% of the total amount of substrate, is still a good proof of concept.

Nevertheless, both reactions have the same problem that both were shut down by disconnection at the end, which was caused by a drop in cell solution from leaking. The leaking occurred from the connecting joints of the glass parts as well as the pump tube and the inlet opening. The volume losses were 200 – 300 mL, which is a significant amount. The cell was water-tight at its initial setting up but it may become loose in long operations. The glassware is not made for a flow system originally and 24 hours seems to be a limit for such a configuration.

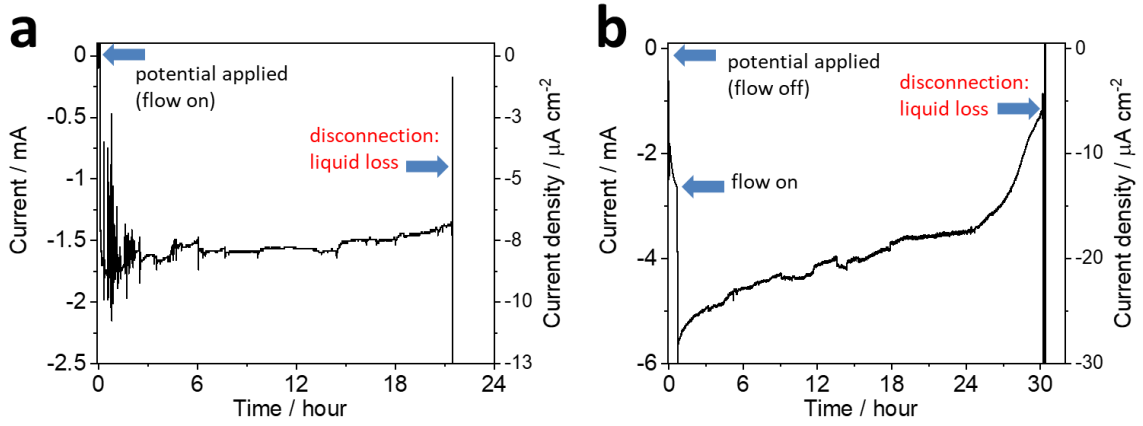


Figure 6.14. Biocatalytic process in e-Leaf under flow with tube-shaped working electrode, tested using the GLDH-catalysed reductive amination. (a) (b) were two repeats with same conditions. Conditions: solution volume 500 mL, reactor volume 100 mL (approx.); No buffer pH 7.5; temperature: 25 ℃, solution is purged with argon to remove O_2 and argon flow maintained in headspace thereafter; substrate [α-ketoglutarate] = 40 mM, [NH_4Cl] = 80 mM, [$NADP^+$] = 10 µM; Potential held at -0.8 V vs. Ag/AgCl (3 M KCl) to drive reduction. Solution agitation: stirred by stirring flea and flow by peristaltic pump, flow rate: 50 mL/min. Enzyme loading: 414.3 nmol FNR + 42.2 nmol GLDH are mixed and loaded by stir-loading for 18 hours; electrode SA: 199.2 cm^2.

The weaknesses in the current version of the flow cell are obvious: since it is assembled from non-specific lab glassware, it is clumsy in general. First, it has too much dead space; the reactor has a volume of nearly 100 mL which needs a large amount of solution to fill before use. Most of the volume is from the connector and joints that are redundant. The complex configuration is inconvenient to be set up. Second, the opening of the compartment holding the working electrode is extremely narrow (approx. 1.5 cm

diameter), which prevents the use of any larger-sized electrodes, limiting the versatility of the e-Leaf. Third, the distance between the working, counter and reference electrodes are still far, which can lead to limit on the current flow and solution resistance. Fourth, the porosity and the pore size of the supporting glass frit in the reaction chamber should be further increased as it causes much resistance to the solution flow. Fifth, leaking must be completely stopped for a continuous flow reaction. A further improved version of the flow reactor is required to address those problems.

6.4. Flow cell III

6.4.1. Cell Design

The new cell design presented in this section is targeting the problems listed for flow cell II. Several key features are expected in a new cell. First, the cell should be a customised reactor for the specific use of electrochemical analysis under flow by avoiding using the standardised interchangeable glassware parts, meaning that the reactor should be less clumsy and easy to set up. Second, the reference electrode should be close to the working electrode, allowing stable current flow and lowering the possible IR drop caused by the distant current path. Third, the cell should be both air-tight and water-tight. Based on these requirements, a new flow reactor has been made, flow cell III.

Flow cell III has a more compact monolithic structure (figure 6.15). It consists of two parts, the main body and a detachable cap. The main body has the flow inlet at the bottom end and the outlet at the higher position of the reaction chamber that holds the working electrode. A supporting glass frit is in the flow path, and it serves as a platform that can hold a stir bar or working electrode. The supporting glass frit has larger pore sizes and porosity comparing to that in the flow cell II, minimising resistance to the flow. An air relief valve was installed below the glass frit as air bubbles sometimes can accumulate below the supporting glass frit during the reaction process. The counter

electrode is held in the side arm connected to the main chamber, separated by a finer glass frit to prevent substrate crossover. The detachable cap has three openings, among which, the one in the middle is specifically made for the installation of the modular holder of the reference electrode. The other two openings can be used for multiple purposes such as real-time interventions.

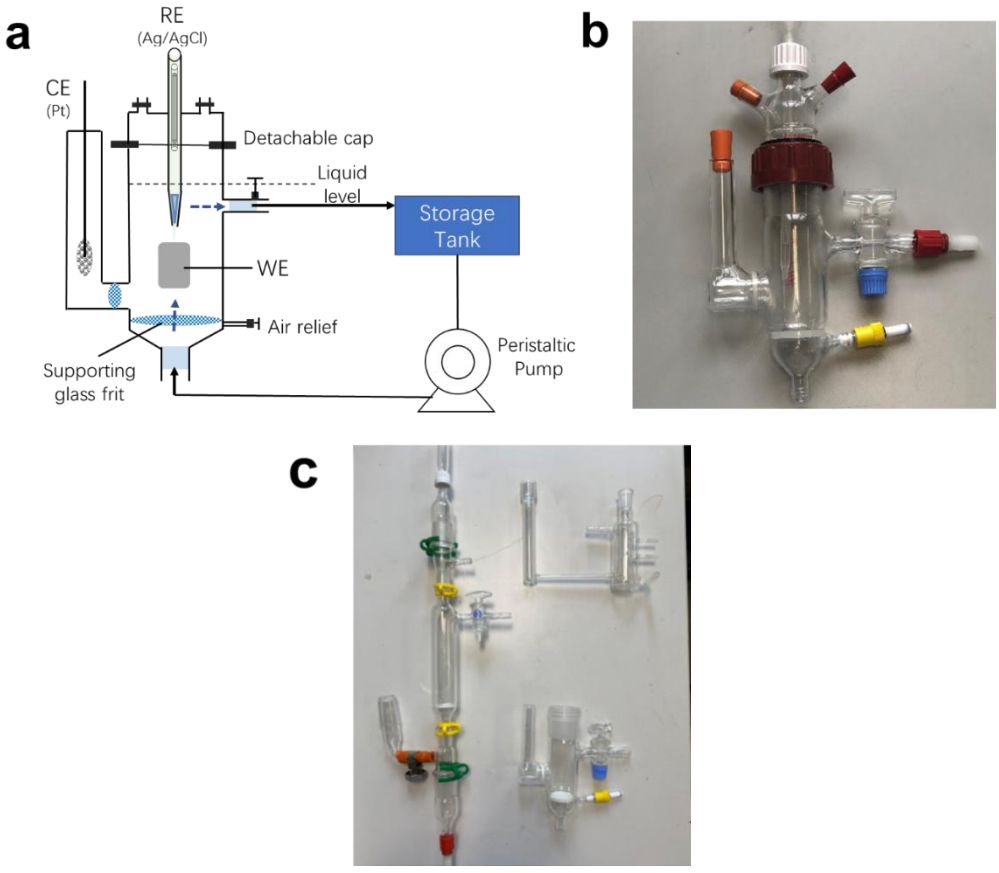


Figure 6.15. Design Sketch (a) and photo (b) of flow reactor III; Size comparison of flow systems (c)

In regard to sizes, the main chamber has a volume of ~60 mL, the diameter of the opening being 35 mm, allowing for the use of electrodes of multiple sizes and shapes. The side arm for the counter electrode was deliberately made larger to handle gas formation from water electrolysis and it has a volume of 15 mL. The cell can be working in an air-tight water-tight state, and it can work in open air as well. Panel (b) in figure 6.15 shows the direct comparison to the cell II. Flow cell III is more compact and has much less dead space. It is also smaller and more convenient to handle.

Flow cell III can provide a more stable working environment and it is convenient to set up. It is also a modular reactor and can work series. It is promising as a demonstrative example of an e-Leaf flow system.

6.4.2. Batch Mode Test with Ti mesh

The flow cell III was first tested for its basic function as an electrochemical cell in the 'batch mode' with its inlet and outlet openings closed. The following shows a comparison experiment carried out in a real batch reactor and in flow cell III with Ti mesh as the working electrode. As introduced in chapter 2, Ti mesh has a high surface area and is convenient to be made into an enzyme-loaded electrode. The mesh and honeycomb structure is widely used for catalysts under flow such as emission catalysts.[138] For the e-Leaf, a mesh electrode has potential use for making a packed-bed flow reactor, therefore it has been used in the tests for the flow reactor.

(1) Benchmark: reaction in a conventional batch reactor

The electrochemical test in a conventional batch reactor is shown in figure 6.16. The cyclic voltammograms in panel (a) show the comparison of a mesh electrode at each step of manufacturing (before and after ITO coating and also enzyme loading). The capacitance increased after ITO coating (black and blue traces), and the FNR non-turnover peak was detected after enzyme loading (red and blue traces), with a coverage of 285 pmol FNR cm^{-2}, which is 4 – 6 times that for a Ti foil electrode. The mesh is favoured for the idea of packed reactor with high density of reaction unit. The chronoamperogram (panel (b)) shows the reaction process catalysed using the (FNR +GLDH)-loaded mesh electrode. The reduction reaction was initiated by the real-time injection of $NADP^+$, the current took some time to become stable after the noisy stage of initiation. The noise was caused from air bubbles trapped on the porous structure of the mesh (as discussed in chapter 2). The charge passed was 81 C with a coulometric conversion of 95% in 18 hours.

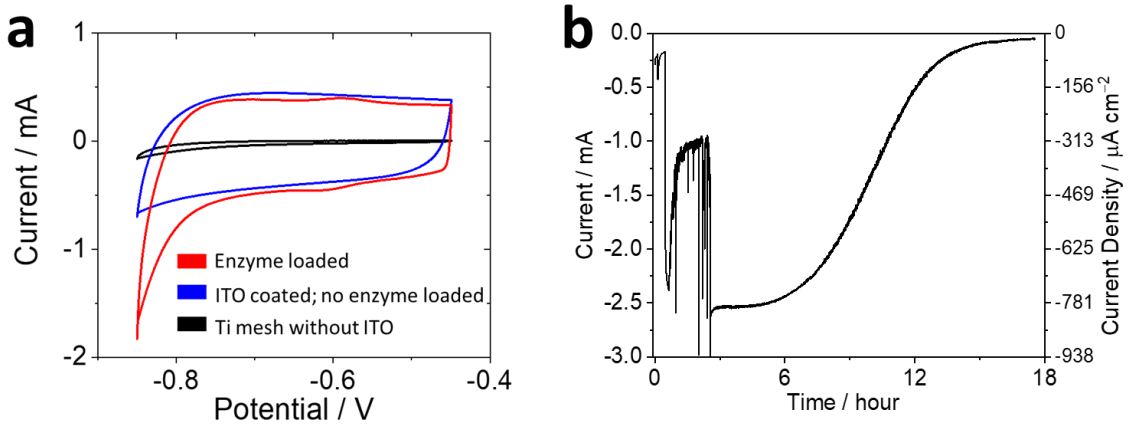


Figure 6.16. Flow cell III tested using an ITO/Ti mesh electrode with GLDH-catalysed reduction **a)** Cyclic voltammograms of ITO coating and enzyme loading comparison for Ti mesh electrode. **b)** chronoamperogram of GLDH-catalysed reduction. Conditions: solution volume 44 mL, buffer: 50 mM HEPES pH 7.5; temperature: 25 ℃, solution is purged with argon to remove O_2 and argon flow maintained in headspace thereafter; Enzyme loading: 75.8 nmol FNR + 7.6 nmol GLDH are mixed and loaded by drop-casting; electrode SA (mesh face area): 19.2 cm^2 .CV scan rate: 4 mV/s; Chrono conditions: substrate [α-ketoglutarate] = 10 mM, [NH_4Cl] = 20 mM, [$NADP^+$] = 10 µM; the solution was stirred using a stir flea on the supporting glass frit; potential held at -0.8 V vs. Ag/AgCl (3 M KCl) to drive reduction.

(2) Flow cell III: reaction at 'batch mode'

The test is then moving on to the flow cell III. A mesh electrode was used to test the batch mode of flow cell III, using the ADH-catalysed reduction of 4-phenyl-2-butanone as the model reaction. As shown in figure 6.17, the reaction was initiated by the potential applied (-0.85V vs Ag/AgCl in 3 M KCl), with substrate and cofactors already present in the 50 mL cell solution (stirred). The current was stable at approximately -0.4 mA for 24 hours and slowly decreased due to the depletion of the substrate, over another 36 hours. The final charge passed was 70 C, corresponding to a coulometric conversion of 91%. The 72-hour long-time stability of the biocatalysts and the completeness of the conversion has provided solid proof for the feasibility of flow cell III to work as an electrochemical cell.

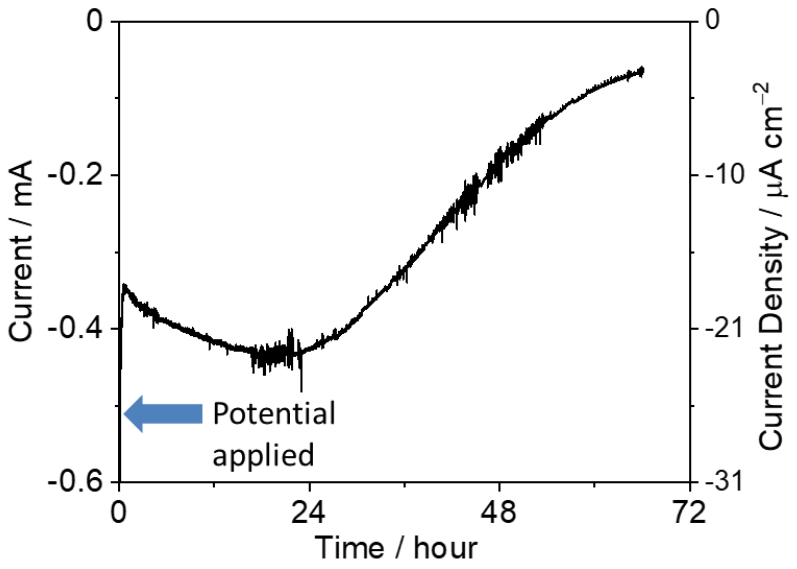


Figure 6.17. Batch mode of flow cell III tested using an ITO/Ti mesh electrode with ADH-catalysed reduction. Conditions: solution volume 50 mL; buffer: 50 mM HEPES pH 7.5; temperature: 25 ℃, solution is purged in storage tank with argon to remove O_2 and argon flow maintained in headspace thereafter; substrate [4-phenyl-2-butanone] = 8 mM, [$NADP^+$] = 20 µM; Potential held at -0.85 V vs. Ag/AgCl (3 M KCl) to drive reduction; solution stirred by stirring flea. Enzyme loading: 75.8 nmol FNR + 7.6 nmol ADH (W110G) are mixed and loaded by drop-casting; electrode SA (mesh face area): 19.2 cm^2.

6.4.3. First Trial in Flow Cell III Under Flow

The first experiment in flow cell III without prior optimisation for flow (cell design previously tested for feasibility as a batch reactor only) is shown in figure 6.18. In this experiment the classic GLDH enzyme was used. Panel (a) shows the whole timecourse which contains 3 stages. Panels (b-d) show the magnified time periods at the start of each stage. Panel (b) shows the starting stage (at 0 – 3 hours); panel (c) shows the electrode switch after 18 hours of reaction; panel (d) shows the change to batch mode after 35 hours of reaction.

In the stage 1, $NADP^+$ was first added, and then reduction was initiated by the addition of the substrate into the storage tank whilst the system is under flow (panel (b)). The e-Leaf quickly reacts to the change in this solution by a sudden increase of activity (current) which carries on with a decreasing activity for 18 hours after which it was manually paused.

The stage 2 was to investigate the cause of current deactivation. An electrode switch was conducted (panel (c)) and the current remained low, suggesting that deactivation of the enzyme-loaded electrode was not the decisive factor in the decreasing current. Surprisingly, an addition of a further 10 μM $NADP^+$ brought about an increase in current i.e. the recovery of catalytic activity (approximately 3.0 mA), suggesting that the $NADP^+$ could have degraded and thus caused the drop in current. This was due to the aggresive flowing in this system (explained in following paragraphs). The recovered current was higher than that at the start of stage 1, which was likely from the difference in the batches of electrode. The reaction was left running for 18 hours and the current again gradually decreased, which was also due to the flowing agitation.

In stage 3, the pump was turned off and the reactor was switched to batch mode; the reactor was agitated only by stirring. An injection of extra 10 μM $NADP^+$ restored the current again. The restored current was 1.2 mA, which was much less than the restored current at the beginning of stage 2 (3.0 mA), indicating that the deactivation of the e-Leaf electrode itself also contributes to the decreasing activity. The reaction was then left running for another 18 hours with a similar gradual decrease in rate.

Comparing to reactions in the batch reactor (chapter 3), NADP(H) deactivation is observed in a flow cell (figure 6.18). The assumption is that in a batch cell, the NADP(H) in the nanopores tends to be more retained due to the nanoconfinement and the cofactor channelling effect (introduced in chapter 1), therefore cofactor may be protected/stabilised. In addition, the stirring in a batch cell with a stirring flea may not be aggressive enough to displace the cofactor molecules from the nanopores. In the batch reactor, only the redundant cofactor in the bulk solution is exposed to stirring without massive movement as in a flow reactor. In contrast, the system is exposed to a more aggressive agitation under flow. The agitation in the reactor chamber consists of both stirring and flow, which could possibly displace cofactor molecules, thus lower the effective concentration (local concentration) in the nanopores.

In addition to the cofactor, the electrode is also exposed to more impact in a flow reactor, which can cause faster falling of the ITO layer, and therefore the accelerated decreasing of the overall activity. Improvement regarding electrode stability and protection must therefore be considered for the purpose of long-timescales application.

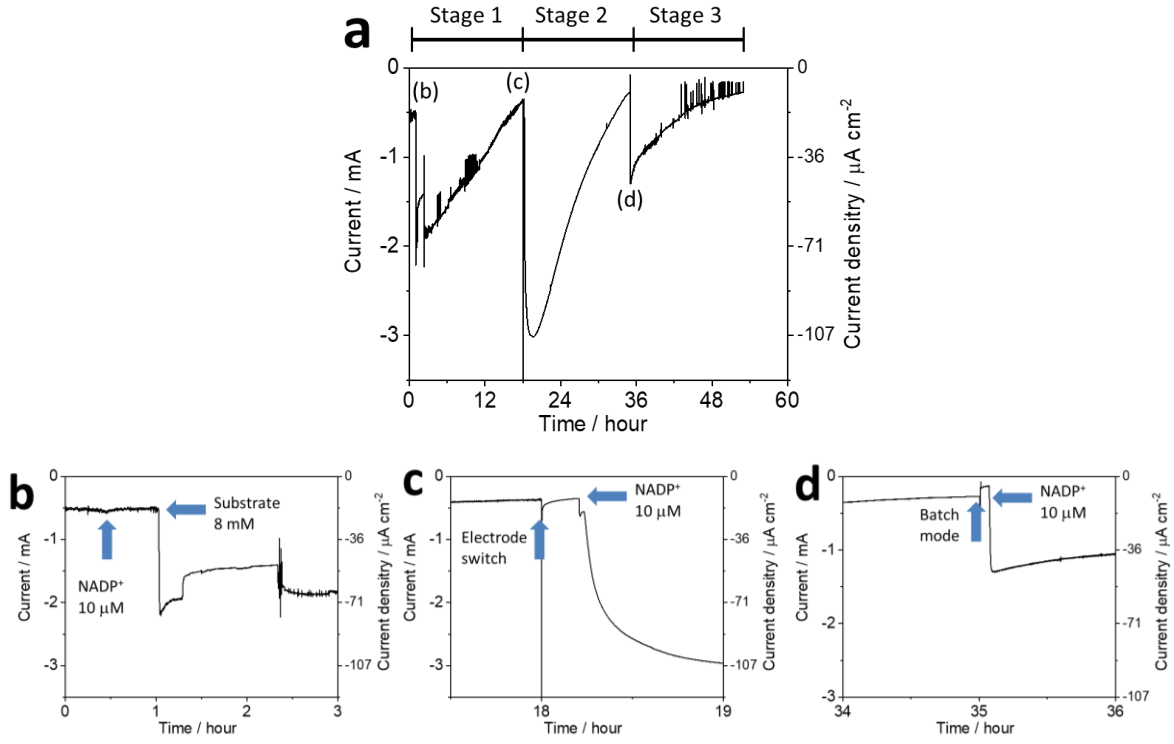


Figure 6.18. Flow cell III tested under flow with GLDH-catalysed reduction. Conditions: solution volume 500 mL, reactor volume 50 mL (approx.); buffer: 100 mM TAPS pH 8.0; temperature: 25 ℃, solution is purged in storage tank with argon to remove O_2 and argon flow maintained in headspace thereafter; substrate [α-ketoglutarate] = 8 mM, [NH_4Cl] = 16 mM, [$NADP^+$] = 10 µM; Potential held at -0.8 V vs. Ag/AgCl (3 M KCl) to drive reduction. Solution agitation: stirred by stirring flea and flow by peristaltic pump, flow rate: 50 mL/min. Enzyme loading: 29.2 nmol FNR + 11.3 nmol GLDH are mixed and loaded by drop-casting; electrode SA: 28 cm^2.

6.4.4. **Flow cell III in the Glovebox**

(1) Electrode switch experiment for long-time process

The flow reactor was moved to the glovebox for the remaining experiments to prevent the need for argon purging of both the storage tank and reactor headspace which would cause less disturbance to the electrode and reduce electrical noise.

An electrode switch experiment was conducted in the flow cell III and the chronoamperogram is shown in figure 6.19. The first reaction started with the Ti mesh as the working electrode (geometric area: 19.2 cm^2). With all substrates in the solution, the reaction was initiated by the addition of $NADP^+$ in real-time, and the current rapidly reached the peak 2.4 mA. The reaction proceeded for 18 hours and was paused for an electrode switch which involved pausing the potential and replacing the Ti mesh electrode by a Ti foil electrode (24 cm^2). The reaction with the new Ti foil electrode started with the peak current of approximately 0.5 mA, and was left running for another 18 hours before being manually stopped. In the first reaction with Ti mesh electrode, the charge passed was 129 C which equated to 0.67 mmol product yield, a conversion of 16.7% of total substrate in the bulk solution. The reaction with Ti foil has a charge passed of 30 C which equated to 0.16 mmol product yield, a conversion of 4% of total substrate.

The result is encouraging. The current was more stable than the reaction previously shown with a much slower decreasing trend. The stability and lifetime of the e-Leaf under flow has been improved by moving the cell into the glovebox due to milder agitation. In addition, the switching of the electrode has proved to be an achievable operation in the flow reactor. Electrode switching can be potential used to sustain the reaction/production process when the old batch of electrode has lost activity by a large scale. The e-Leaf has the potential to be exploited further as a modular, sustainable and reusable device.

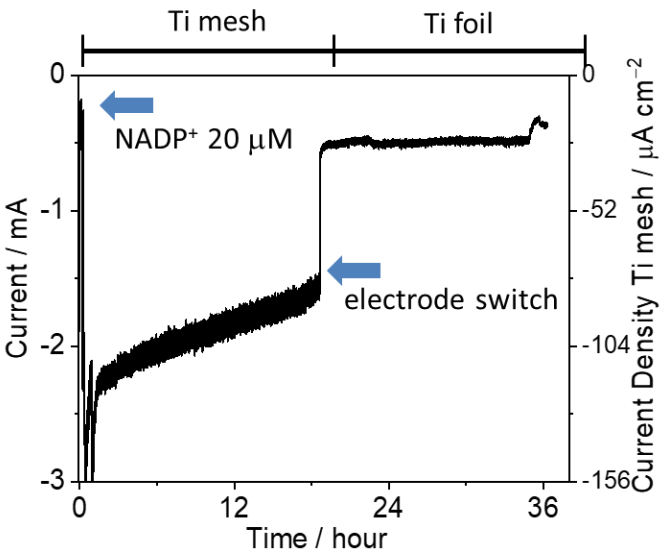


Figure 6.19. An investigation of the e-Leaf under flow in reactor III, in an anaerobic glovebox with an electrode switch step. Conditions: solution volume 500 mL; Experiments performed in an anaerobic glovebox to avoid any contribution to the current form the reduction of O_2. buffer: 100 mM TAPS pH 8.0, temperature: 25 ℃, substrate [α-ketoglutarate] = 8 mM, [NH_4Cl] = 16 mM, [$NADP^+$] = 20 μM; Potential held at -0.8 V vs. Ag/AgCl (3 M KCl) to drive reduction; solution agitation: stirred by stirring flea and flow by peristaltic pump, flow rate: 50 mL/min. Enzyme loading (mesh): 75.8 nmol FNR + 7.6 nmol GLDH are mixed and loaded by drop-casting; electrode SA (mesh face area): 19.2 cm^2. Enzyme loading (Ti foil): 50.0 nmol FNR + 5.0 nmol GLDH are mixed and loaded by drop-casting; electrode SA (Ti foil): 24 cm^2.

(2) Optimised experiment in flow cell III

The leaking issue with silicone tubes used for the peristaltic pump has been discovered (details in the appendix). The peristaltic pump was upgraded to one with increased stability and finer control. The photos of pumps are shown in figure 6.20. Panel (a) shows the previous pump used in flow reactor II and flow reactor III, which has analogous control only. Panel (b) shows the new pump (BT100-1F from Premier Control Technologies) which has finer control and monitoring, allows 0.17 – 500 mL / min output depending on the pump head and tubing choices. The pump tube comparison is shown in panel (c). The tube in the new pump is thicker and more robust with a wall thickness of 2.5 mm and inner diameter of 6.4 mm, while the old one has inner diameter of 4 mm and wall thickness of 1 mm. The flow rate is still 50 mL/min and the pump will run at a

lower rpm. The stability has been increased with less wearing of tube and lower chance of tube breakage.

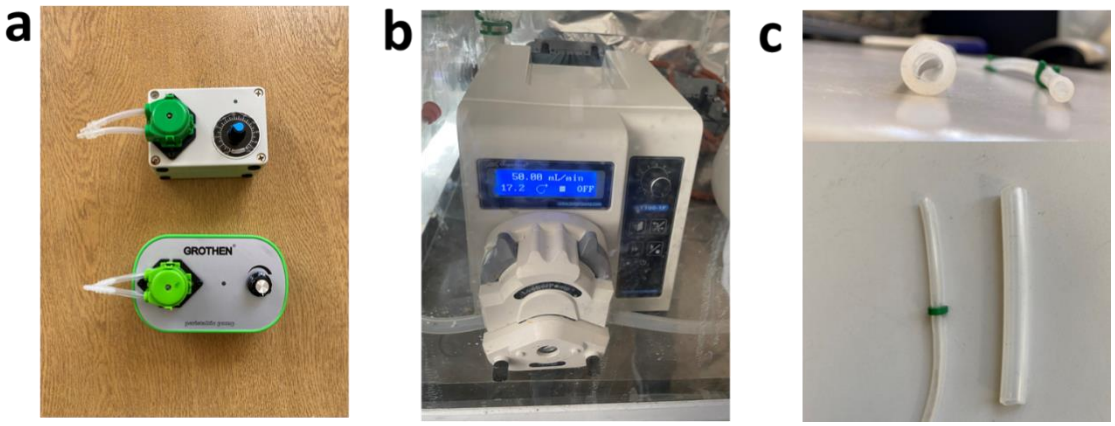


Figure 6.20. Photos of pumps used in flow reactor II and III (a) and the new pump for reactor III (b); tubes used in old pumps and the new pump (c).

Figure 6.21 shows the test of flow cell III under flow with the upgraded pump in the glovebox, with the optimised conditions so far. The GLDH-catalysed reduction was initiated by the addition of $NADP^+$ under flow and the current rapidly increased to the peak current 6.47 mA. The current gradually decreased over the 18-hour reaction process before a buffer exchange was conducted, which restored the current from 1.3 mA to 2.4 mA. The buffer exchange was to detect the cause of the decreasing current. As discussed previously, the deactivation of NADP(H) was one of the causes of decreased current, which was confirmed by the buffer exchange. The buffer exchange containing fresh substrate and cofactor has restored the current. In addition, the deactivation of the electrode also contributed to the decreased current since the restored current did not reach the same level as when reaction was initiated. The working electrode was observed to have a burned trace at the position facing the counter electrode side arm which can be due to that the working electrode being placed too close to the side arm openings that almost blocked the joints; the extremely large flux of charges converges at that part of the electrode and the unevenly distributed high current caused the sear.

The second stage of reaction took another 18 hours with a much lower current which finally decreased to almost zero. The reaction before buffer exchange has a charge passed of 230 C, corresponding to 1.2 mmol of substrate converted, a conversion rate of 74% which is 38 times that for a 4 mL batch reactor. This experiment revealed the problem of deactivation once again in the flow system. The rate decreased over 50% in 18 hours which is not ideal for application in industry.

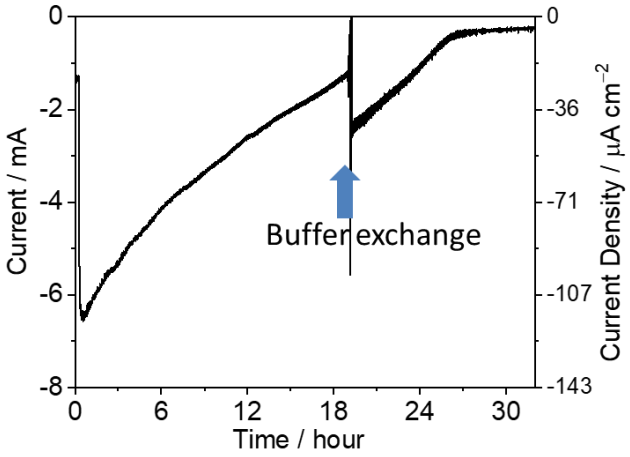


Figure 6.21. Investigation of the performance of flow reactor III with GLDH-catalysed reduction in under upgraded peristaltic pump, with buffer a exchange. Conditions: solution volume 200 mL; buffer: 50 mM TAPS pH 8.0, temperature: RT; experiments performed in an anaerobic glovebox to avoid any contribution to the current form the reduction of O_2. substrate [α-ketoglutarate] = 8 mM, [NH_4Cl] = 16 mM, [$NADP^+$] = 20 μM; Potential held at -0.85 V vs. Ag/AgCl (3 M KCl) to drive reduction; solution agitation: stirred by stirring flea and flow by peristaltic pump, flow rate: 50 mL/min. Enzyme loading: 102 nmol FNR + 10.2 nmol GLDH are mixed and loaded by drop-casting; electrode SA (Ti foil): 56 cm^2.

An ADH-catalysed ketone reduction was performed to further confirm the deactivation in flow reactor III. The test aimed to determine whether the deactivation is related to the physical configuration of the flow cell or is reaction-specific to the GLDH-catalysed reaction.

The chronoamperogram is shown in figure 6.22. Stage 1 had a steady current after initiation. After 18 hours of reaction, additional pieces of Ti foil electrode were connected to the working electrode already in the cell, aiming to increase the reaction rate. However, the current remained at a similar level, and continued to decrease. It is worth

pointing out that this operation disturbed the electrodes' positioning direction and the placement relative to the flow path, which may have caused a loss of stability after the operation. The reaction has a charge passed of 106 C, corresponding to 0.56 mmol substrate converted, a conversion rate of 34% which is 17 times that for a 4 mL batch reactor.

The deactivation was observed in this experiment (stage 2), therefore it is likely related to the physical cell setup. In addition, stage 1 has demonstrated the possibility that the e-Leaf could somehow work at a steady current, even though the reproducibility is not good based on tests conducted so far. Further improvement is needed boost the stability of the electrode, such as enhancing the nanoconfinement of on the electrode (different coating methods, coating materials) and designing a flow path that has less agitation directly to the electrode.

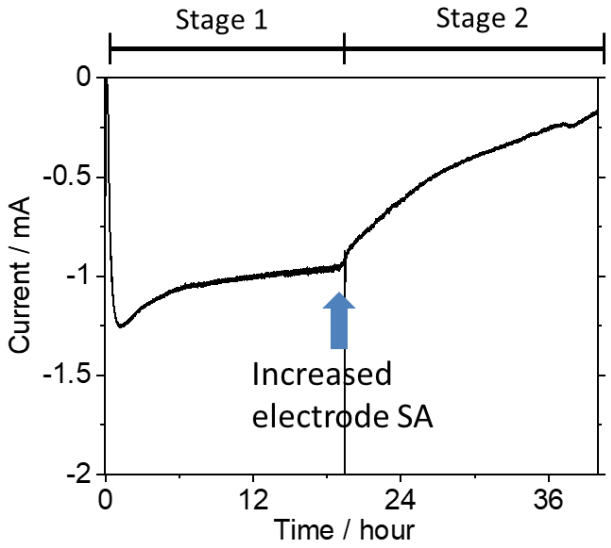


Figure 6.22. Chronoamperograms of ADH-catalysed reduction in flow reactor III under new peristaltic pump. Conditions: solution volume 200 mL; buffer: 50 mM TAPS pH 7.5, temperature: RT; experiments performed in an anaerobic glovebox to avoid any contribution to the current form the reduction of O_2; substrate [4-phenyl-2-butanol] = 8 mM, [$NADP^+$] = 20 µM; Potential held at -0.85 V vs. Ag/AgCl (3 M KCl) to drive reduction; solution agitation: stirred by stirring flea and flow by peristaltic pump, flow rate:50 mL/min. Enzyme loading: 68.4 nmol FNR + 34.2 nmol ADH (W110A) are mixed and loaded by stir-loading for 18 hours; electrode SA: 56 cm^2 to 112 cm^2.

6.5. Conclusion and Potential Improvement

Work in this chapter has explored the possibility of making e-Leaf into a flow reactor. Three flow reactors have been designed, constructed, and tested for their performance. Improvement has been made based on their performances in the electrochemical processes monitored. The feasibility of conducting biocatalytic processes in an electrochemical flow cell with the enzyme-loaded electrode of the e-Leaf is proved and is a step forward based on the scaling up project.

Flow reactor is a scaled-up reactor in a different sense, with the continuous supply from flow and the pool (storage tank) collecting substrate and products. In addition, the flow reactor features the decoupling of reactor and the chemical supply section, which allows live operation with more convenience and also the potential to couple to other technologies. Nevertheless, the flow cell for the e-Leaf is still not perfect; the increased agitation is preventing the cell from long-time and large-scale conversions. The aggressive agitation causes increased degradation of NADP(H), deactivation of the electrode by enzyme falling out from pores, and even accelerated ITO falling.

Future work should first include the improvement on both enzyme side and the reactor design side to boost the stability of biocatalyst under flow. In regard to the cell design, the flow path can be redesigned to avoid the direct impact to the electrode, since it is not a good alternative for stirring as a solution mixing method. The reaction chamber can be made as a side arm which is not in the main flow path as it is now. In regard to the stability of biocatalyst, electrode switch is a good method to compensate for the deactivation of the e-Leaf, but the e-Leaf itself also needs to be stable under harsh conditions. This could be achieved by engineering enzymes for certain tolerance (extreme temperature, pHs), improve the nanostructure on the electrode by using different coating technologies (such as doctor’s blade methods and electrochemically assisted deposition) or coating materials (antimony tin oxide (ATO)), change the

geometric shape of the electrode support material to accommodate the fluid mechanics under flow.

In addition, packed-bed flow reactor will be a good way to make the e-Leaf under flow more compact and modular, and it is the ultimate goal for this project. This would transform the lab level reactor to a synthesis technology with higher space-time yield. Such a modular reactor could then be coupled to other processes (such as automatic control, kinetic screening and product separation), and the e-Leaf can be evolved to a higher level as a versatile platform for biocatalysis.

CHAPTER VII

7. Experimental Methods and Materials

7.1. Introduction

This chapter is a complementary chapter to present in more detail, the experimental methods and materials involved in the experiments carried out in the thesis. Due to the nature of this thesis being an exploration and engineering of the e-Leaf for application, some of the experimental methods have been explained and discussed in the results chapters since this was the purpose of the work. For instance, the basics of the e-Leaf, the electrochemical analysis methods and the making of protein film electrode are introduced in chapter 1. This chapter is focused more on details with five sections introducing the experimental methods.

The first section is about the enzyme preparation, from its transformation to the expression, purification, and the concentration determination. The second section details the making of the protein film electrode, including the ITO coating methods and also enzyme loading. The third section describes electrochemical analysis methods which are mainly cyclic voltammetry (CV) and chronoamperometry (chrono). The fourth section introduces the methods used for product detection and enzyme activity such as NMR, UV-Vis and GC. The fifth section records the key equipment, devices and chemicals involved in all experiments.

7.2. Enzyme Production

7.2.1. Enzyme Preparation and Purification

Ferredoxin-NADP$^+$ reductase (FNR)

A vector (aLICator pLATE 51) containing the gene encoding N-terminal His-tagged FNR from *Chlamydomonas reinhardtii* and the genes which confer resistance to ampicillin was used to transform *Escherichia coli* cells (BL21 (DE3)). The cells were then plated on Lysongeny broth (LB) agar containing ampicillin at 0.1 mg/mL. Positive transformants were selected by resistance to ampicillin. A single colony was used to inoculate 100 mL

LB media containing same concentration of ampicillin (0.1 mg/mL) and grown shaking (200 rpm) overnight at 37 ℃. This culture was split and diluted into 500 mL of the same medium (15 mL in 500 mL containing same concentration of ampicillin) and was grown at 37 ℃, 200 rpm for approximately 3 hours (until mid-log phase, optical density (OD) ~0.5), at which point the cells were induced by the addition of isopropyl β-D-1-thiogalactopyranoside (IPTG) to a final concentration of 1 mM, and grown for a further 3 – 4 hours. The cells were then harvested by centrifugation and the pellets resuspended in cold cell resuspension buffer (50 mM HEPES; 150 mM NaCl; 10% V/V Glycerol pH 7.4) and stored at -80 °C. The cells were thawed and disrupted using a French press at 20 psi. The cell debris was removed by centrifugation at 45000 rpm for 1 hour (Beckman Ultracentrifuge). The supernatant was loaded onto a Ni^{2+} HisTrap affinity column (GE Healthcare Life Sciences) using an Äkta purification system with dual wavelength absorbance detector. The column was washed with 50 column volumes of buffer A (50 mM HEPES, 500 mM NaCl, 1 mM dithiothreitol (DTT) pH 7.4). Then buffer B (50 mM HEPES, 500 mM NaCl, 1 mM dithiothreitol (DTT) and 250 mM imidazole pH 7.4) was used with a linear increasing concentration gradient of imidazole reaching a maximum of 250 mM in 30 minutes at a rate of 1.5 mL/min, to elute FNR in 1 mL fractions. Those containing FNR were selected based on the absorbance at 280 nm (protein absorption) and 460 nm(FAD absorption), and based on the appearance of bright yellow (colour from FNR). The fractions were pooled and further concentrated by centrifugation (3,000 rpm at 4℃) protein using the Amicon Ultra 4 Merck 10 K centricons. The protein was desalted through a desalting column, aliquoted, flash frozen in liquid nitrogen and stored at -80 ℃ before use.

L-Glutamate dehydrogenase (GLDH)

Under sterile conditions, competent cells (BL21 (DE3)) were transformed with a vector (aLICator pLATE 51) containing an N-terminal HIS-tag *E. coli* GLDH gene and the

genes to confer ampicillin resistance (previously constructed by first, colony PCR to amplify the GDH gene using *E. coli* BL21 De3 cells as template, followed by ligation-independent cloning into an N-terminal Histag vector (Thermo Scientific aLICator system #K1251[1]). Colonies were grown on LB agar containing ampicillin at 0.1 mg/mL and positive transformants selected by their resistance to ampicillin. A single colony was used to inoculate 500 mL LB media containing ampicillin at 0.1 mg/mL and also IPTG to a final concentration of 1 mM, and left grown for 16 hours at 37 ℃, 200 rpm. Then the cells were centrifuged at 6000 rpm (4 ℃) for 30 minutes and resuspended in cold buffer (50 mM HEPES; 150 mM NaCl; 10% V/V Glycerol pH 7.4). The cells were then disrupted using a French press at 20 psi. The cell debris was removed by centrifugation at 45000 rpm for 1 hour (Beckman Ultracentrifuge). The supernatant was loaded onto a Ni^{2+} HisTrap affinity column (GE Healthcare Life Sciences) using an Äkta purification system with dual wavelength absorbance detector. The column was washed with 50 column volumes of buffer A (50 mM HEPES, 500 mM NaCl, 1 mM dithiothreitol (DTT) pH 7.4). Then buffer B (50 mM HEPES, 500 mM NaCl, 1 mM dithiothreitol (DTT) and 250 mM imidazole pH 7.4) was used with a linear increase in concentration of imidazole reaching a maximum of 250 mM in 30 minutes at a rate of 1.5 mL min^{-1}, to elute protein in 1 mL fractions. Fractions were selected based on the absorbance at 280 nm and also the enzyme activity tested by solution assay using a UV-Vis spectrophotometer (Perkin Elmer, Lambda 19) (see section 7.5.1 for details) .

The fractions were pooled and concentrated by centrifugation (3,000 rpm at 4℃) protein using the Amicon Ultra 4 Merck 10 K centricons. The protein was then dialysed overnight against 1 L of dialysis buffer (50 mM HEPES, 150 mM NaCl, 1 mM DTT and 10% glycerol). The protein was then aliquoted, flash frozen in liquid nitrogen and stored at -80 ℃ before use.

Alcohol Dehydrogenase (ADH): TeSADH W110A, W110V

A pET28 vector containing the gene for the alcohol dehydrogenase with mutation W110A or W110V (TesADH) and the genes to confer resistance to kanamycin, was transformed into *E. coli* BL21 (DE3) cells (New England Biolabs). Colonies were grown on LB agar containing 30 µg/ mL kanamycin overnight at 37°C (positive transformants selected based on kanamycin resistance). A single colony was used to inoculate 5 mL LB media containing same concentration of kanamycin (30 µg/mL) and grown overnight at 37°C, 250 rpm. This overnight culture was then used to inoculate 600 mL of TB autoinduction media (Formedium) (containing kanamycin 30 µg/mL) in a 2 L flask and incubated for 16 - 20 hours at 37 ℃, 250 rpm. The cells were then harvested by centrifugation and the pellets resuspended in cold cell resuspension buffer (100 mM potassium phosphate, pH 7.7, 300 mM NaCl, 20 mM imidazole, 1 mM dithiothreitol (DTT)). The cells were disrupted using a French press at 20 psi. The cell debris was removed by centrifugation (Beckman Ultracentrifuge) at 45000 rpm for 1 hour. The supernatant was loaded onto a Ni^{2+} HisTrap FF column (GE Healthcare Life Sciences) using an Äkta purification system with dual wavelength absorbance detector. The column was equilibrated with 10 column volumes of buffer A (100 mM potassium phosphate, pH 7.7, 300 mM NaCl, 20 mM imidazole, 1 mM dithiothreitol (DTT)). Then the column was washed with 10 column volumes of the buffer A. Then buffer B (100 mM potassium phosphate, pH 7.7, 300 mM NaCl, 300 mM imidazole, 1 mM DTT) was used with a linear increase in concentration of imidazole reaching a maximum of 300 mM to elute protein in 1 mL fractions. Fractions containing the ADH enzyme were selected based on absorbance at 280 nm and also the activity tested by solution assays using UV-Vis. Fractions containing the enzyme were then pooled and dialysed overnight against 1 litre of dialysis buffer (Tris (50 mM pH 8.0) supplemented with 1 mM DTT) at 4°C. The desalted enzyme was then concentrated using a 10K centrifugal filter (Amicon Ultra 4 Merck), aliquoted, flash frozen in liquid nitrogen and stored at -80 ℃ before use.

Alcohol Dehydrogenase (ADH) from *Lactobacillus Kefir* (LK)

The gene encoding ADH from *Lactobacillus kefir* was previously inserted into a vector using ligation independent cloning (LIC) (aLICator, Thermo Scientific, N-terminal His-tag/EK, #K1251) to confer ampicillin resistance.[56] The vector was also encoded an N-terminal hexa- HIS-tag and the sequence was confirmed by Source Bioscience. The plasmid was transformed into *E. coli* BL21 (DE3) cells (New England Biolabs) and was grown overnight at 37°C on LB agar plates supplemented with ampicillin to a final concentration of 0.1 mg/mL.

Positive transformants were selected by resistance to ampicillin. A single colony was used to inoculate 100 mL LB (25 g/L) media containing same concentration of ampicillin (0.1 mg/mL) and grown shaking overnight at 250 rpm at 37 ℃. This culture was diluted into six flasks of 500 mL of the same medium (15 mL in 500 mL containing the same concentration of ampicillin) and was grown at 37 ℃, 200 rpm for approximately 2 – 2.5 hours (until mid-log phase), at which point isopropyl β-D-1-thiogalactopyranoside (IPTG) was introduced to a final concentration of 1.3 mM, to induce the cells. The temperature was reduced to 30°C and overexpression of the protein was allowed to continue for approximately 20 hours (at 250 rpm). The cells were then harvested by centrifugation at 6000 rpm for 30 minutes and the pellets was resuspended in cold cell resuspension buffer (50 mM Tris, 500 mM NaCl, 1 mM MgCl2, 10 % glycerol, pH 8.0). The cells were disrupted using a French press at 20 psi. The cell debris was removed by centrifugation (Beckman Ultracentrifuge) at 45000 rpm for 1 hour at 4℃. The supernatant was loaded onto a His-Select Ni^{2+} column (GE Healthcare Life Sciences) using an Äkta purification system with dual wavelength absorbance detector. The column was equilibrated with 10 column volumes of buffer A 50 mM Tris, 500 mM NaCl, 1 mM DTT, 1 mM $MgCl_2$, pH 8.0). Then buffer B (50 mM Tris, 500 mM NaCl, 1 mM DTT, 1 mM $MgCl_2$, 250 mM imidazole, pH 8.0) was used with a linear increase in concentration of imidazole reaching a maximum of 250 mM to elute protein in 1 mL fractions. Fractions containing

the ADH enzyme were selected based on absorbance at 280 nm and also the activity tested by solution assays using UV-Vis. The fractions containing the enzyme were then pooled and dialysed overnight against 1 - 2 litres of dialysis buffer (Tris (50 mM pH 8.0) supplemented with 1 mM DTT) at 4°C. The desalted enzyme was then concentrated using a 10K centrifugal filter (Amicon Ultra 4 Merck), aliquoted, flash frozen in liquid nitrogen and stored at -80 ℃ before use.

7.2.2. Visualisation of Enzyme Purity by gel Electrophoresis and Determination of Enzyme Concentration

Sodium dodecyl sulfate–polyacrylamide gel (SDS gel)

The precast SDS gel (NuPage 4-12% Bis-Tris Midi Gel, ThermoFischer) was used to visualize the protein fractions. A potential of 200 V was applied to the gel in a running buffer (104.6 g MOPS, 60.6 g Tris Base, 10 g SDS, 3.0 g EDTA, pH 7.7; diluted 20 times for use) for approximately 30 minutes. InstantBlue (Sigma) was used to stain the gel at room temperature for 20 minutes. The gel was then rinsed with DI H_2O and viewed using a lightbox. Figure 7.1 shows a gel used for one LK preparation as an example.

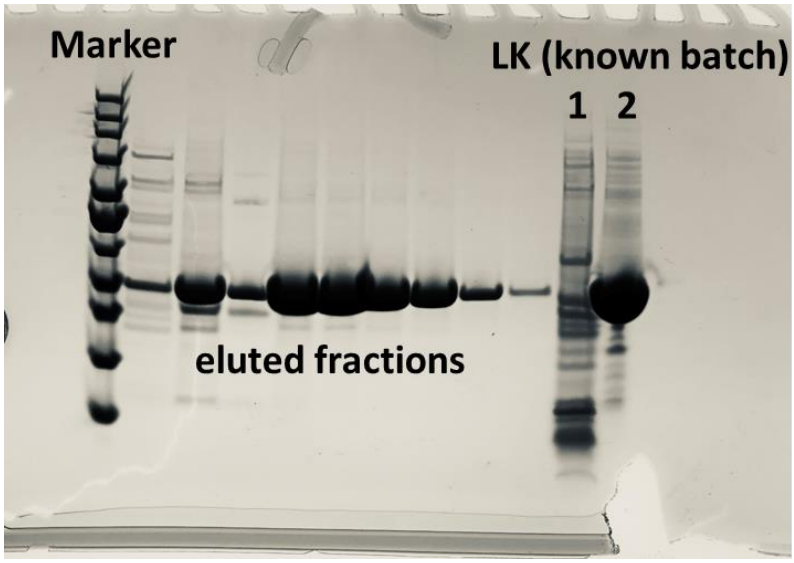


Figure 7.1. Photo of SDS gel used in detecting the target enzyme from fractions in the enzyme preparation.

Bradford Test

The Bradford method was used for determining the concentration of freshly purified enzymes. The method was first developed by M.M. Bradford and was commonly used for protein concentration test.[139] It is an assay based on the absorption shift of a dye called Coomassie Brilliant Blue G-250. For the test involved in this thesis, the standard reference sample was bovine serum albumin (BSA, 2 mg/mL) from Sigma-Aldrich which was used to construct a standard curve. And the Bradford dye reagent was purchased from Alfa Aesar.

7.3. Electrode Construction

Protein film electrode manufacturing is discussed with optimisation of each step outlined in chapter 1 and 2.

7.3.1. Electrode Materials

Materials

Titanium foil is the most commonly used electrode material for the e-Leaf. Ti foil was purchased from Sigma-Aldrich, 0.127 mm thickness and 99.7% trace metals basis. The typical size of Ti foil electrodes are 2.5 cm* 0.7 cm (SA: 3.5 cm2) for a small-scale cell, 3.5 cm* 3.5 cm (SA: 24.5 cm2) for a middle-scale cell (50 mL batch cell, 80 mL batch cell, flow cell III) and 7.5 cm* 3.5 cm (SA: 52.5 cm2) for a large-scale cell (500 mL batch cell). Other materials include Ti tubes (GoodFellow, inner diameter: 3.75 mm, outer diameter: 4.25 mm), Ti mesh (GoodFellow, open area 20%, nominal aperture:0.19 mm, wire diameter: 0.23 mm),carbon cloths were purchased from C-Tex. Before ITO coating, electrode materials were cleaned by

sonicating in water, ethanol and acetone for 15 min each, and then allowed to dry in an oven at 80 ℃.

ITO coating – Electrophoretic Deposition (EPD)

Indium tin oxide (ITO) nanopowder (Sigma-Aldrich, < 50 nm) was suspended in acetone solution. The solution is made of ITO (0.02 g), I_2 (0.01 g) and 20 mL of acetone, or larger volumes of acetone (depending on the size of the electrode to be covered) containing corresponding amount of ITO and iodine. The solution is suspended by sonicating for at least 30 minutes. The piece of Ti foil to be modified is held parallel to a counter electrode (which can be another piece of Ti foil or a piece of ITO glass) and placed in the ITO suspension at a close distance apart (ca. 1 - 2 cm). A 10 V potential is applied between the two electrodes for 5 – 10 min.

During this process, free protons are generated from acetone in the presence of iodine, which are then adsorbed on the surface of ITO nanoparticles. The positive-charged ITO nanoparticles migrate to the cathode which is the electrode support material to be coated. A dense and coherent deposition layer is being formed.[140] The electrode was left to dry in air and thoroughly rinsed in water and dried again before loading enzymes for use.

ITO coating - Doctor's blade

The doctor's blade method is based on the TiO_2 paste method.[141] ITO (0.5 g) was mixed with acetic acid (0.1 mL), MQ water (2 mL) and ethanol (4 mL). The mixture was then diluted in ethanol (70 mL), stirred for 15 minutes and sonicate for 30 minutes. Then α-terpineol (2 g) was added to the solution, followed by further stirring and sonicating for 30 minutes. Another 100 mL of ethanol with 0.3 g ethyl-cellulose dissolved (by sonicating) was then mixed with the nanoparticle solution (by 15 min stirring and 30 min sonicating). Then the suspension was concentrated by heating to evaporate ethanol at 70°C until the paste with high viscosity was acquired. The electrode support was painted

with a thin layer of this paste and then placed in a furnace at 450 ℃ for 30 minutes, with a heat ramp of 5 ℃/min.

7.3.2. Enzyme Loading

Drop-cast

In drop-casting, concentrated enzyme solution was first diluted to the required volume to ensure covering of the surface area of the electrode before loading (8 μL enzyme solution /cm^2 electrode). The enzyme solution dropped on the surface of electrode, and then was spread out by a pipette tip (making sure not to scrape the ITO surface) to cover the surface. The electrode was covered or held in an enclosed space/vessel to avoid dying and placed on ice. The incubation time for enzyme loading usually lasted for 20 – 30 minutes. Finally, the electrode was taken out, rinsed by buffer (same as the one to be used for reaction) to remove unbound enzyme, and kept in fresh buffer immediately before use.

Stirring

The electrode was placed in a vessel (for example a glass vial) containing a specific amount of buffer which was enough to submerge the electrode. The desired amount of each enzyme was injected into the solution. The solution was stirred by a magnetic flea. The loading process normally lasted overnight, after which the electrode was taken out and rinsed with buffer, then stored in fresh buffer immediately before use.

Live-injecting

When the electrochemical measurement was occurring, enzymes were injected using a syringe and needle directly into the reaction solution. The solution was usually stirred by a stirring flea to accelerate the loading process. The loading process could be monitored by the increase in current due to the coupled biocatalytic activity.

7.4. Electrochemistry

The two main electrochemical analytic methods used for the thesis are cyclic voltammetry and chronoamperometry, which has been introduced in chapter 1. The basic cell setup for the e-Leaf and the scaled-up versions are introduced in chapter 3 and flow version in chapter 6. Here shows a supplementary section on the electrochemical analysis process.

7.4.1. Three-electrode System

A three-electrode system was used for all electrochemical analysis experiments. A three-electrode system consists of a working electrode (WE), a counter electrode (CE) and a reference electrode (RE).

An electrochemical cell consists of two half-cells which hold two half-reactions. The reaction on the WE is the one of interest and is under monitoring. The other half-reaction is occurring on the CE, together with the WE, forms a full electrochemical reaction. The circuit is connected by electrolyte. The potential applied on the working electrode is:

$$E = E_{\mathrm{WE}} - E_{\mathrm{RE}} - iR \qquad (7.1)$$

Where E_{WE} is the potential on the surface of the WE, E_{RE} is the potential on the surface of the RE, R is the resistance of the electrolyte between the WE and RE, and i is the current between the two electrodes. The three-electrode system ensures the applied potential matches the actual potential on the WE against the RE since the current flows through the WE and RE is negligible due to the high resistance between them (connected by a Luggin capillary).[142] In the electrochemical system, the current passes between WE and CE, while the potential between WE and RE remains stable which is used for control and reference purpose.

The reference electrodes used in this thesis were SCE (saturated calomel electrode stored in saturated KCl) and Ag/AgCl (stored in 3 M KCl). The reference electrodes were calibrated against Pt in saturated quinhydrone solution at pH 4.0 and pH 7.0. The conversion of each potential to the standard hydrogen electrode (SHE) were carried out as follows:[142,143]

$$E_{SHE} = E_{Ag/AgCl} + 0.211\ \text{V at } 25\ ^{\circ}\text{C in 3M KCl} \qquad (7.2)$$

$$E_{SHE} = E_{SCE} + 0.241\ \text{V at } 25\ ^{\circ}\text{C in saturated KCl} \qquad (7.3)$$

7.4.2. Cell Operation in measurement

Live-injection

Live-injection is an operation occurring during the electrochemical measurement in real-time. A long needle was positioned into the cell solution prior to the experiment and either remained in the solution or was positioned through a rubber bung such that it could be inserted into it easily. When the injection was made, the plunger of the syringe was pulled in and out at least ten times to guarantee mixing and complete injection. Care should be taken that the needle does not touch the working electrode or create too much turbulence in the cell, which would increase electrical noise and also may deteriorate the stability of the working electrode. Real-time injections were used for additions of cofactor, substrate, inhibitor, enzyme, EDTA and also for pH-adjustment by acid/base injection.

Sampling

Sampling has a similar operation as live-injection. An empty syringe connected to a needle was used to remove cell solution directly from the reactor either in real-time or when paused.

Buffer exchange

Buffer exchange were performed during a paused electrochemical measurement (e.g. chronoamperometry). The working electrode was disconnected, taken out of the cell solution and kept in the same buffer to one side. The cell solution was removed from the cell and the cell was rinsed thoroughly by ultrapure water (Millipore, 18 MΩ cm) multiple times before the fresh buffer or reaction solution was refilled. The fresh buffer could contain cofactors and substrate or not, depending on the different test purposes. The working electrode was taken back into the cell and connected to the potentiostat and measurement resumed。

Electrode switch

An electrode switch was similar to buffer exchange. The switch was performed during the pause of a measurement. The working electrode was disconnected, taken out of the cell and stored in buffer to one side. The new electrode was then submerged in the cell solution and connected to the potentiostat and measurement resumed

7.5. Detection of Product and Monitoring Enzyme Activity

7.5.1. Ultraviolet–visible (UV-VIS) Spectroscopy

Absorbance spectra were recorded with a Perkin-Elmer Lambda 19 UV-vis spectrometer with software Lambda-SPX/P. This instrument was used for Bradford method (at 280 nm wavelength) and solution assays to detect enzyme activity based on the NADPH concentration change (at 340 nm). The path length of the quartz cuvette was 10 mm and the slit was set to be 1 nm. There were several functions for different test purposes: ‘Waveprog’ was to collect absorbance at the set wavelength at one time point. Bradford assays were tested with this mode. ‘Timedrive’ continuously monitored the change in absorbance. This was used for the live monitoring of NADPH concentration change to detect the enzyme activities for all E2 enzymes (since they were all NADPH-dependent). The initial rates were measured

as the initial gradient of the rate of change of A_{340} attributable to the change in NADPH concentration. The A_{340} was converted to a rate of change on concentration of NADPH using the Beer-Lambert law with the molar extinction coefficient of 6.22 l/mmol/cm.[144] The initial rates were plotted against the concentration of E2 substrate and fitted to the Michaelis-Menten equation using non-linear curve fitting (software Origin 2021b) or for the case of E2 enzyme (GLDH in chapter 3).

7.5.2. Proton Nuclear Magnetic Resonance (^{1}H NMR)

NMR was used to determine the concentrations of reaction products. The test result was used to confirm the coulometric conversions, and also used for concentration determination on its own.

The internal standard was used with 3-(Trimethylsilyl)propionic-2,2,3,3-d4 acid sodium salt (TMSP) as the standard. The standard was prepared by filling glass capillaries with TMSP solution. The concentration of effective TMSP standard was then calculated based on a solution with known concentration of compound (α-ketoglutarate, 10 mM) and the standard was ready. In the NMR test, the sample solution (aqueous) was mixed with D_2O at a volume ratio of 90:10. The instrument was a Bruker AVIIIHD 400, and the setting for water suppression selected. The spectra results were analysed in the software MestreNova. The position of the TMSP peak (9 H) is normally at 0 ppm in the water suppression method selected. The concentration of the chemical of interest was calculated based on the relative peak areas comparing to the internal standard of known concentration. It is worth pointing out that the calibration process of the internal standard with substrate (a-ketoglutarate, L-glutamate, 4-phenyl-2-butanone and 4-phenyl-2-butaol) of known concentration has confirmed that the ratio between substrate and internal standard peak areas is very close to the ratio of their corresponding numbers of H to give an accurate detection. Therefore, the internal standard method is viable and convenient in the NMR quantification of substrate and product.

7.5.3. Gas Chromatography - Flame Ionization Detection (GC-FID)

GC-FID was used to determine the relative amount of alcohol enantiomers for the deracemisation and inversion processes in chapter 4. Samples taken for GC analysis were first extracted into methyl tert-butyl ether (MTBE) and analysed by the previously established method.[145]

In brief, the gas chromatography (GC) was coupled with flame-ionization detection (FID), using a GC 6850 instrument fitted with an autosampler (Agilent) and a chiral BetaDex™ 325 column (30 m x 0.25 mm x 0.25 µm) (Supelco). The GC program setting for the analysis of ketone and alcohols: inlet temperature 200 °C, detector temperature 250 °C, oven 110 °C/hold 20 mins; 10 °C/min to 200 °C. Rt (4-phenyl-2-butanone) = 20.8 minutes. Retention time: Rt((*R*)-4-phenyl-2-butanol) = 23.7 minutes, Rt ((*S*)-4-phenyl-2-butanol) = 23.6 minutes, Rt(4-phenyl-2-butanone) = 21.1 minutes. The relative amount and concentration were calculated based on the peak areas as shown in figure 7.2.

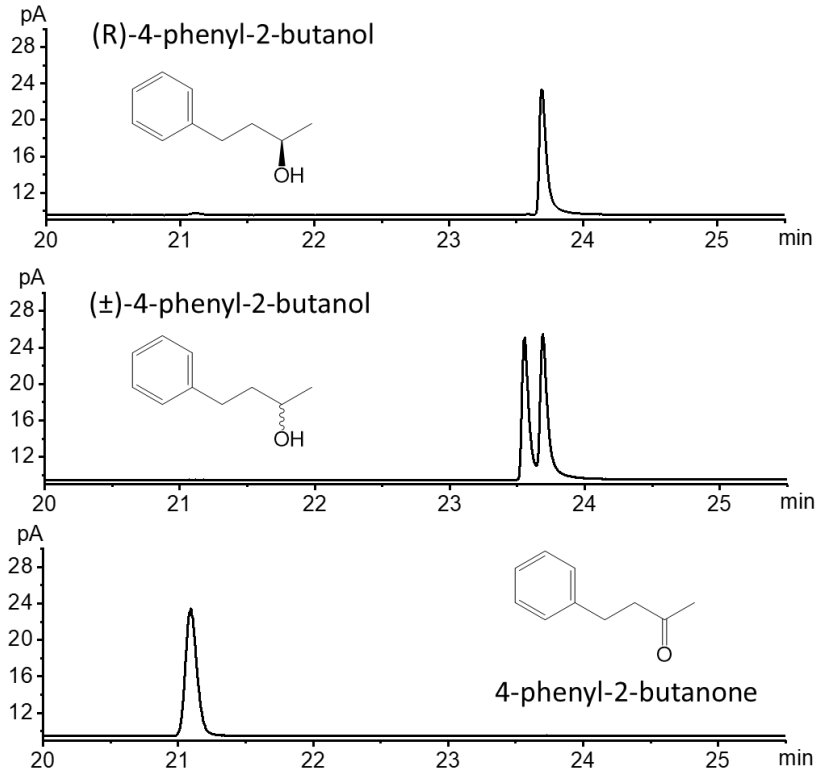


Figure 7.2. GC-FID spectrum of (*R*)-4-phenyl-2-butanol, (rac)-4-phenyl-2-butanol and 4- phenyl-2-butanone.

7.6. Equipment and Chemicals

7.6.1. Glovebox

Most of the reduction reaction driven by negative overpotential should avoid oxygen which can cause the rise of faradaic reduction current. Experiments conducted in chapter 4 are mostly in the glovebox (Belle Technologies, O_2 < 5 ppm). Early-stage experiments in chapter 2,3,5 and 6 were carried out on the bench. For the reaction carried out on the bench, electrochemical measurements were conducted with Ar purging the electrochemical cell.

7.6.2. Potentiostat

The potentiostat used for electrochemical measurements on the bench is a multichannel potentiostat from Alvatek (MultiEmStat) with the software Multitrace 3.4. The potentiostat with higher current range (Compactstat from Ivium technologies) was used for the measurement in large-scale reactions in chapter 3, with the software IviumSoft. For electrochemical measurement conducted in the glovebox, the potentiostat used was from Autolab (PGSTAT20) with the software Nova1.1.

7.6.3. Peristaltic Pump

Three peristaltic pumps were used in the exploration of flow reactor. The first pump (GE Healthcare, P-1 Cytiva) was to drive the slow flow in a small-scale. The second pumps (Yanmis G628-1) were used to drive flow in the larger handmade flow reactor II. The third pump (LongerPump, BT100-1F) had digital control and was more stable for long-time sessions. It was mostly used in the flow cell III.

7.6.4. Key Chemicals

Buffers

The buffer used in this thesis were TAPS and HEPES (Melford). TAPS buffer has a buffer range of 7.7-9.1, and it was used for reactions at pH 8.0, pH 8.5 and pH 9.0. HEPES buffer has a buffer range of pH 6.8- 8.2, and it was used for reactions at pH 7.5.

To make these buffers, the buffer salt of required amount was weighed and dissolved into distilled water or MQ water of a volume slightly less than the target volume. After being stirred uniformly, the solution was ready for pH adjustment. The pH was adjusted by titration of dilute NaOH or HCl solution under the monitoring of a pH meter (Mettler Toledo SevenEasy). Once the desired pH was reached. The solution was transferred to a volumetric flask and was replenished with water to reach the target volume. The buffer was then transferred and kept in a bottle in a proper environment.

α-ketoglutarate

α-ketoglutaric acid disodium salt dihydrate was purchased from Aldrich, dried material with >98% purity. It was used in the model reactions in the optimisation work of e-Leaf in chapter 2, scaling-up work in chapter 3 and the flow reactor work in chapter 6.

4-phenyl-2-butanoe, (*R*)-4-phenyl-2-butanol, (*S*)-4-phenyl-2-butanol

These were the substrates involved in the oxidation and reduction catalysed by ADH. They were used in the model reactions in the optimisation work of e-Leaf in chapter2, deracemiser and inverter work in chapter 4, biphasic reactor work in chapter 5 and the flow reactor work in chapter 6. 4-phenyl-2-butanoe was purchased from Aldrich with 98% purity. (±)-4-phenyl-2-butanol was purchased from Alfa Aesar with 98% purity. (*S*)-4-phenyl-2-butanol was purchased from ChemCruz. And (*R*)-4-phenyl-2-butanol was purchased from Aldrich with 98% purity.

$NADP^+$ and NADPH

NADP(H) is the vital cofactor in all the biocatalytic reactions involved in the e-Leaf. NADP(H) was purchased from Melford and kept at 4 ℃ fridge.

Appendix

Appendix of Chapter 2

A2.1 Carbon cloth electrode

Several carbon materials were tested as working electrode (photo shown in figure A2.1). Three carbon cloths (a, b and c) and two carbon felts (d and e) were first coated with ITO by EPD and then loaded with FNR by stirring in solution. Electrical activity was tested by cyclic voltammetry and chronoamperometry shown in figure A2.2.

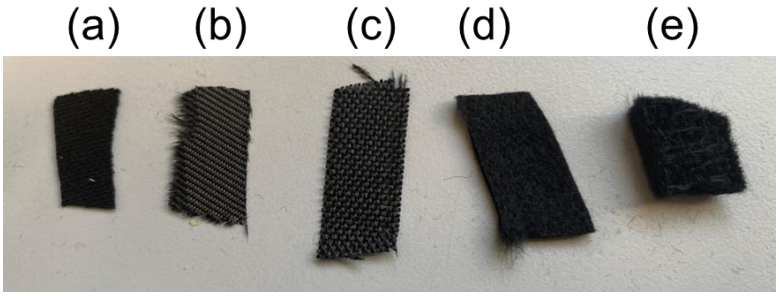


Figure A2.1. Carbon cloth material for potential use as electrode support

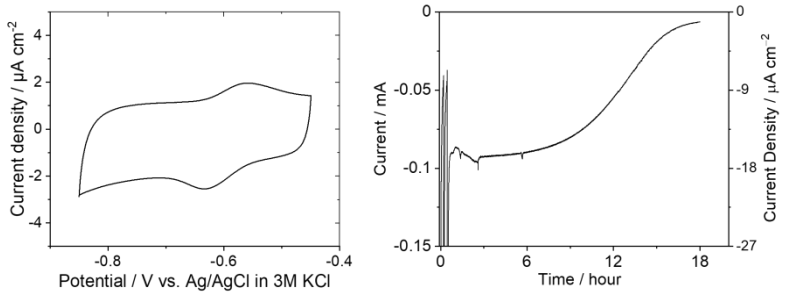


Figure A2.2. Cyclic Voltammetry of NADP(H) turnover peaks on carbon cloth electrode with FNR loaded (left) and Chronoamperogram of reduction of 4-phenyl-2-butanone catalysed by ADH on carbon cloth electrode (right). Conditions: solution volume 4 mL; substrate [4-phenyl-2-butanone] = 8 mM, [$NADP^+$] = 20 μM, buffer 100 mM TAPS pH 8.0, temperature: 25 ℃. Potential held at −0.9 V for reduction. Solution is purged with argon to remove O_2 and argon flow maintained in headspace thereafter. Enzyme loading: FNR loaded first by stir-loading, ADH is live injected to the final concentration of 0.16 μM in reaction solution. ITO coated by pasting method. Electrode SA: 14 cm^2.

Among all five carbon materials, the thick carbon felt (e) is not able to retain ITO after EPD because of its sponge-like texture. ITO particles peel off given mild pressure on carbon felt. In addition, ITO keeps falling off during the stirring process of enzyme loading. Carbon textiles (a) (c) and (d) have bad electrical signal. Only carbon cloth (b)

yields regular and clean electrical signal after FNR being load. In the experiment, carbon cloth is coated with ITO by EPD. FNR is stirring loaded before reaction and E2 (ADH) is applied by live-injection, which is also the initiation of reaction depicted in the chronoamperogram (figure A2.2). The current is rapidly increasing to its peak and then decrease sharply due to the depletion of substrate. 0.032 mmol of substrate is converted with a conversion rate of 70% within 18 hours. Carbon cloth and felt was not an ideal choice for the e-Leaf at current stage. Unlike the metal material, carbon cloth is too soft to hold a rigid structure and its positioning can be easily disturbed by external agitation. It has been observed that ITO coated on the electrode surface tends to fall on slight distortion of the cloth which is quite common in handling such electrode. The ITO falling in the cell can be observed, indicating loss of catalytic activity during the conversion.

A2.2 Electrical Assisted Deposition (EAD) method

Electrical assisted deposition method is another potential ITO coating method tested. Instead of coating ITO, EAD uses electrochemical process to produce and form a layer of ITO on the surface of support material. To start with, a reaction solution of 10 mM $In(NO_3)_3$ and 4.3 mM $SnCl_4$ is prepared and heated to 80 °C. Temperature is controlled by the water bath jacket of the cell. Ti foil, Ti tube and ITO glass have been tried as the working electrode. The counter electrode is Pt and an Ag/AgCl as reference electrode. A potential of -0.6 V is applied to the working electrode for 30 minutes to syntheses a layer of InSnOH on the working electrode. The electrode is taken out and rinsed by DI water after reaction and then put into the furnace and heated up to 320 for 45 minutes for calcination.

The trial with EAD is an unsuccessful one. The ITO did not form in the reaction step. Further optimisation and troubleshooting have not been carried out since this method is of lower efficiency when comparing to EPD method. The EAD method takes more steps, involves electrochemical reaction and high temperature calcination. Purchasing ITO

directly is more convenient and cheaper than using electrochemical reaction to synthesise ITO on electrode. It is of lower efficiency comparing to EPD method.

Appendix of Chapter 3

A3.1 Cost of e-Leaf manufacturing

In addition to the convenience in making an e-Leaf set-up, its cost is also relatively low based on the following estimated calculation. The cost of e-Leaf manufacturing has been calculated based on the 0.5 L reaction. The cost of manufacturing FNR@ITO/Ti electrode from raw materials including enzyme production and the electrode material making is 0.035 GBP per cm^2 (detailed below).

Due to optimised protocols, lab-level costs for the e-Leaf are extremely low. FNR is produced by overexpression (details in chapter 7) which yields higher amount of protein in one batch comparing to normal protein expression process; The supportive material for the electrode is titanium foil, which can be reused for very long periods of time without deterioration (> 5 years), accounting for no operation cost. The ITO nanoparticles are one of the main consumables which contribute to a large part of the cost. It is potentially recyclable provided further protocol optimisation is carried out. Another opportunity for potential optimisation lies in the difference between the amount of enzyme added to the loading solution (either that drop-casted or in a stirred dilute solution), and the exact enzyme amount loaded in the electrode. The amount of loaded enzyme is usually much lower than the amount applied (<10%) based on the FNR non-turnover peak and the amount dissolved in the loading solution. Lowering the waste on redundant enzyme can also cut down the cost for the e-Leaf. It is possible to reach or at least push towards the lowest possible cost of enzyme via the optimisation of the enzyme loading process, which holds more value in application-oriented practice.

Detailed calculation

(1) Calculation is based on the 500 mL reaction. Detailed item prices are shown in reference published work.

(2) The cost of the e-Leaf breaks down to two parts: electrode material and FNR prep cost. Downstream enzyme(s) are variable and the cost of these enzyme preparations

depend on different protocols. The cost would be paid for by the client or the client supplies the enzymes. Therefore, it is excluded from the calculation despite being an essential part of the e-Leaf.

(3) Ti foil as the key supportive material of electrode can be reused. Based on experience, the same piece of Ti foil can be reused more than 5 years. Cost of Ti foil could be counted as a fixed cost on initiation.

(4) Reactants (substrates, buffers, and cofactors) in reaction are not included in the cost since they are highly case-specific and depend on the exact catalytic process.

(5) The cost of setup and running of the lab conditions are not included, which contains cost like purchase and depreciation of instruments and devices, human labour cost and utility.

(6) The prices are based on suppliers' discounted prices for research institutes, which are usually much lower than the commercial prices when purchasing chemicals and materials.

Cost of electrode:

Cost of Initial electrode manufacturing (Ti foil cost included) = 0.15 GBP/cm^2

Cost of electrode manufacturing (Ti foil cost not included) = 0.02 GBP/cm^2

Cost of FNR:

Cost of FNR Preparation = 3.05 GBP/ mmol

In practice, concentrated enzyme solution is typically drop-casted onto the electrode. Based on the experiment shown in this chapter, typically 17 nmol of FNR is applied to 3.5 cm^2 electrode,

Cost of FNR = 0.015 GBP / cm^2

In an ideal situation where the amount of enzyme loaded is equal to the amount applied (i.e excess FNR rinsed off is recaptured for use), assuming FNR loading on the ITO/Ti electrode is 100 pmol/cm^2,

Cost of FNR (ideal) = 0.0003 GBP / cm^2

Total cost

Total cost in long run = cost of electrode (Ti not included) + cost of FNR

= 0.035 GBP/cm^2

Appendix of Chapter 4

A4.1 Possible causes for reaction errors in coulometry or substance loss

The reactor is a small-scale cell which has a side arm (5 mL) for the counter electrode, separated from the main compartment by a glass frit (as introduced in chapter 1 and 2). Substances in the main compartment can travel through the frit over time and react at the Pt, particularly relevant to these experiments which can take at least 18 hours and up to 2-3 days to finish. As shown in table 4.3 for the reaction shown in figure 4.4 (main text), the side arm contains approximately 17.7% of the total amount of product. The average amount in the side arm after the reaction is 15% - 20% of the total amount of substrate and product on average.

Second, most of the experiments are carried out in an anaerobic glovebox but some experiments during the early stage were conducted on the bench in open air. In this case, the solution is purged with argon to remove O_2 before the reaction and an argonflow is maintained in the headspace. The constant purging could take away the alcohol and ketone dissolved in the solution since they are volatile.

Third, there is some impurity in the starting solution. For example, in table 4.2 (main text) the starting racemic alcohol solution has small amount of ketone in it. The impurities could originate at the commercial production. This could also be due to the oxidation of alcohol during the storage time in air. This was more obvious in with experiments carried out on the bench in open air, since separate batches of storage solution were used for the experiments on the bench and in the oxygen-free glovebox.

A4.2 Calculation assumptions and errors caused

It is vital to elaborate the calculation and the assumptions.

(1) Coulometric conversion calculation

The charge passed can be converted into product amount. The starting solution is a premade storage buffer, which is only tested by GC analysis once before the whole series experiments. Therefore, in the calculation of conversion, it is assumed that starting concentration of substrate is known and no substrate or product loss occurs during experiment (see next section).

(2) Solution GC analysis data calculation

Amounts in the GC analysis tables are calculated based on the GC signal peak area and concentration and percentage in the table are calculated on the assumption of a known starting concentration and no loss of substrate and product during experiment. In this chapter, the starting concentrations of substrates are normally [(±)-4-phenyl-2-butanol] = 8 mM for deracemiser and [(*R*)-4-phenyl-2-butanol] = 4 mM for inverter. The loss of product or substrate in main compartment rises from the crossover to the side arm through the glass frit, and approximately 15%-20% substance will crossover based on the experiment. This has been noticed in the later stages of this research so in some of the experiments (including this one) the side arm solution has also been analysed by GC after reduction. The post-oxidation side arm solution is not suitable for GC analysis since it is midway in the ongoing experiment. Accordingly, the calculation of post-oxidation assumes that the substances remain in the main solution and add up to the starting concentration (8 mM in table 4.8 in the main text), since the side-arm data is not attainable. For the post-reduction solution, the calculation assumes the concentration of all substances in main part and side arm add up to the starting concentration (8 mM).

(3) Errors and Causes

The coulometric conversion and GC analysis data should match each other in the ideal situation. However, as just mentioned inevitable factors can cause errors and discrepancy between them.

The starting concentration assumed in both coulometry and GC solution analysis is not necessarily stable and constant, because the premade storage solution could be exposed to substrate loss over time. This could cause an underestimated coulometry conversion which are based on the assumed concentration, and an overestimation in GC analysis data which are absolute values detected.

Second, the all substrate-in-main compartment assumption for post-oxidation solution GC analysis is a compromise when the post-oxidation solution from side arm is not attainable. This could cause possible over- and underestimation in the calculation depending on the crossover between the side arm and the main compartment. This effect is more obvious in the process of a longer time.

In addition, the baseline determination in calculating coulometry also adds to the errors. The artificial baseline current differs in each run there can be a lot of errors in determining it.

With above said, the experiment in figure 4.21 (section 4.5.2.2) is used here as an example. The absolute amount of substrate consumed by charge passed is 3.46 mM (17.3 μmol in 5 mL) which is close to the actual value of the reaction. The coulometric conversion in oxidation is 86.5%, assuming a 4 mM starting concentration of substrate. In the solution GC analysis, the post-oxidation solution has 3.43 mM ketone produced from 3.93 mM (*R*)-alcohol, with a conversion of 87.3%. The oxidation conversion and substrate consumed from coulometry and solution analysis are closely matched in this experiment. In reduction, the coulometric conversion is 81.3% * 3.46 mM = 2.81 mM in 4 mL. The solution analysis shows ketone concentration decreases by 3.14 mM. There is a difference of 10.5% within acceptable range. The experiment takes 40 hours to

complete, and the time length is typical. For some longer experiments the discrepancy between coulometry and solution analysis could increase.

A4.3 Optimisation of the enzyme loading process

Enzyme loading method for this specific system is explored in this section. The investigation here takes previous work shown in early chapters as a good reference point and is built from it. The aim was to find a loading process that has each enzyme with optimal rates for the conversion process.

This section has tried to investigate and cover a more in-depth investigation in terms of competition for the pores between the enzymes and the subsequent optimisation of loading for taking the work forward. Other conditions are also examined such as pH, enzyme amount (in the loading solution) and enzyme batch stability.

A4.3.1 Loading methods choice – based on two enzymes

The loading method test starts with a simplified scenario in which only two enzymes FNR and one E2 are to be loaded. The common loading methods for a Ti foil electrode as mentioned in chapter 1 and 2, include drop-cast loading and stir-loading. Different enzymes can also be loaded together (co-loading) or stepwise.

Figure A4.1 panel (a) shows the chronoamperogram of a co-stirred FNR+W110A electrode. This is an early-stage loading method for loading FNR + W110A on an ITO/Ti foil that enzymes were co-stirred in buffer solution overnight, a simple one-step operation chosen as the first test method in the current section. The performance was evaluated by the reaction current in the oxidation. This reaction achieved a 48.1% conversion of 8 mM racemic alcohol in a 4 mL reaction in 18 hours. This is a replicated results and is therefore consistent. It is necessary to point out that the standard of a good loading performance here is judged by whether the electrode (7 cm^2) can achieve

a >90% conversion (>45% in racemic substrate) of 4 mL 8 mM racemic alcohol in approximately 18 hours.

Panel (b) shows two loading methods tested to load FNR + LK which takes the reaction in the panel (a) as a reference. The co-stirring (red trace) method involves the injection of 11.5 nmol FNR and 2.88 nmol of LK together into a 2.5 mL solution (50 mM TAPS buffer pH 9.0) and stirring for 18 hours. In the FNR preload + LK stirred loading methods (black trace), FNR is loaded first by drop-casting, and LK is loaded afterwards by stirring in a 2.5 mL solution containing 4.96 nmols of LK for 18 hours. The current achieved for the LK + FNR loading shows that the stepwise loading is better since it shows a peak current at 360 μA (black trace) comparing to the 50 μA from the co-stirring of two enzymes (red trace). The competition that exists between enzymes for adsorption into the nanopores may in part explain this result.[48] According to this result, it was decided that FNR being pre-loaded by drop-casting and E2s simultaneously loaded by stirring from solution was optimal for enzyme loading with LK involved.

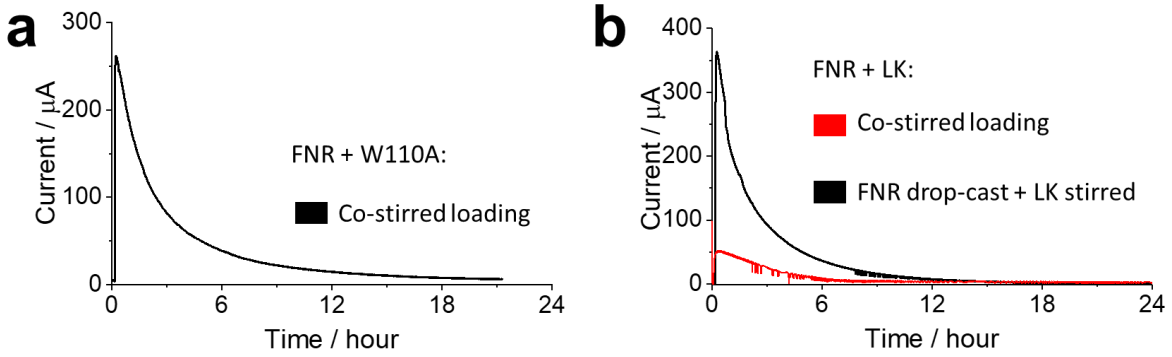


Figure A4.1. Chronoamperograms monitoring the oxidation of (±)-4-phenyl-2-butanol **a)** catalysed by LK comparing two loading method; FNR + LK co-inject loading (red) vs. FNR-preload + LK stir-loading (black). **b)** catalysed by FNR + W110A, enzyme loaded by co-stirring Conditions: cell volume 4 mL; solution stirred throughout using a magnetic flea; substrate [(±)-4-phenyl-2-butanol] = 8 mM, [$NADP^+$] = 20 μM, [Mg^{2+}] = 5 mM buffer: 50 mM TAPS pH 9.0; temperature: 25 ℃, Potential held at -0.175 V vs. SCE to drive oxidation. Experiments performed in an anaerobic glovebox to avoid any contribution to the current form the reduction of O_2.

A4.3.2 Loading Ratio LK to W110A

A balance is needed in the ratio of the two E2 enzyme. Since there is product inhibition in oxidation for the ADHs, a higher amount of LK is desired to convert as much of the R-type alcohol as possible during the oxidation phase, before the oxidation rate becomes extremely slow (since the system goes from racemic to (*S*), or (*R*) to (*S*) in the oxidation). Yet a sufficient amount of (*S*)-selective enzyme (W110A, W110V) is also necessary for the reduction phase to fully convert all the ketone produced in oxidation. Hereby three different ratios of LK to W110A have been tested, with chronoamperograms shown in figure A4.2.

For the enzyme loading process, an ITO-coated Ti foil was preloaded with FNR by the drop-cast method. The electrode was then rinsed to remove redundant FNR and held in a 2.5 mL solution (pH 9.0, 50 mM TAPS buffer with 5 mM Mg^{2+}) containing different amount of LK and 110A. The solution was stirred overnight (18 – 20 hours) at 4 ℃. The electrode was rinsed before placing in the electrochemical cell.

The chronoamperograms in figure A4.2 shows the performance of an electrode prepared with different enzyme loading ratios. The electrodes are first used for (*S*)-alcohol and the oxidative current gives an indication of the activity of (*S*)-selectivity which is mainly due to W110A. A buffer exchange to racemic alcohol was carried out afterwards, and the electrodes were rinsed before being put in the new solution. The current in the racemic alcohol solution indicates the activity combined by LK's selectivity towards (*R*) alcohol and W110A's selectivity towards (*S*) alcohol. The relative amount of active W110A loaded was reflected in the currents in panel (a). The blue trace has the least W110A, the red trace has more W110A hence a higher current and the black has the most therefore the highest current.

The 10:1 LK to W110A (blue trace) is chosen to be a preferred ratio, which has the lowest current attributed to (*S*)-alcohol being oxidised while the system still has a high enough overall current in the racemic mixture, indicating a high rate from LK. The low current from W110A in oxidation is preferred as the R-type alcohol needs to be

converted as much as possible during the oxidation phase, as stated above, in order to achieve a high purity of target enantiomer in the end.

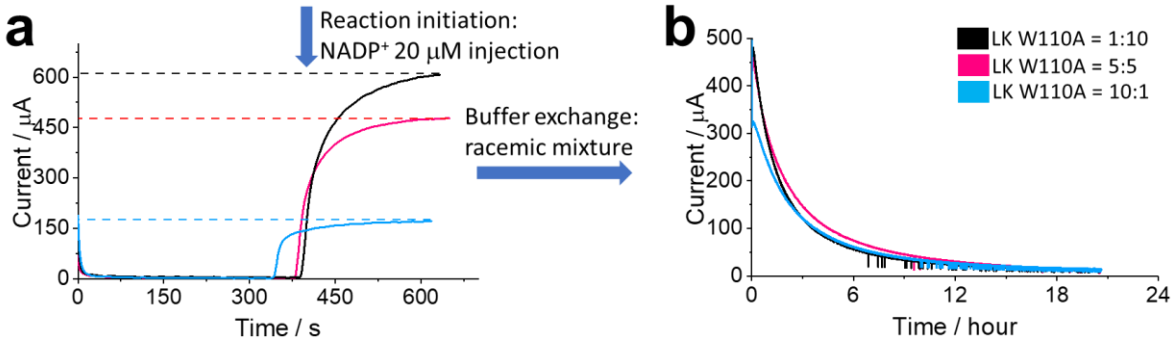


Figure A4.2. An investigation of the effect of varying the ratio of LK: W110A, on the bulk oxidation of racemic alcohol. **a)** Chronoamperometry experiment in 4 mM (*S*)-alcohol before buffer exchange to racemic alcohol; **b)** Chronoamperometry experiment in racemic alcohol 8 mM. Conditions: cell volume 4 mL; solution stirred throughout using a magnetic flea; substrate **(a)** [(*S*)-4-phenyl-2-butanol] = 4 mM, **(b)** [(±)-4-phenyl-2-butanol] = 8 mM; [$NADP^+$] = 20 µM, [Mg^{2+}] = 5 mM buffer: 50 mM TAPS pH 9.0; temperature: 25 ℃, Potential held at 0 V vs. Ag/AgCl (3 M KCl) to drive oxidation. Solution purged with argon to remove O_2; argon flow maintained in headspace thereafter. electrode (Ti foil) SA: 7 cm^2. Enzyme loading: FNR loaded first by drop-casting, LK and W110A loaded after FNR, by stirring in a 2.5 mL solution containing different ratios of two enzymes in 50 mM TAPS buffer pH 9.0. For 1LK:10W110A, 5.3 nmol LK + 0.58 nmol W110A; for 5LK:5W110A, 2.7 nmol LK + 2.7 nmol W110A; for 1LKW110A, 0.53 nmol LK + 5.8 nmol W110A.

A4.3.3 Enzyme-ITO Interactions: displacement and rate-limiting factors (FNR, LK and W110A)

It was mentioned previously that when E2 is stir-loaded into the porous electrode, there is possibly a competition between the enzymes as FNR, W110A and LK may have different affinity for the porous ITO. The question also arises from the observation that W110A and FNR can be loaded by stirring together overnight (18 hours at 4℃.) to achieve high activity, yet LK + FNR loaded in the same way, do not achieve high activity (figure A4.1). The following experiments investigate about interactions among these three enzymes.

A4.3.3.1 E2 displacement

FNR displacing LK:

The test of whether the redundant FNR in solution would displace E2 (in the pores) is shown in figure A4.3 panel (a) (LK) and b (W110A). In both chronoamperograms, FNR was preloaded in the electrode pores before the reaction and E2 was injected into the bulk solution in real-time at the start of reaction and was allowed to adsorb into the pores for 30 - 40 minutes before FNR was then injected in the bulk solution. The loading process is indicated by the increasing of the current[51]. For the electrode loaded with LK (panel (a)), the current started to decrease upon the real-time addition of FNR. The current decreased approximately 60% in 2 hours, even with the LK still present in the solution (since a buffer exchange was not carried out here). In panel (b), buffer exchange removed the W110A in solution before FNR was added. The current decreased by approximately 13% upon the FNR injection and decreased at a very slow rate afterwards (decreased 6% in 15 minutes). The FNR injection into solution seemed to have a greater effect on the LK. The current continued to drop even though a reservoir of LK was still in the solution since there was no buffer exchange; the result for W110A, implies that W110A is more secure in the pores than LK. It can be observed that in this condition, LK is 'weaker' in the competition of adsorbing into the pores against FNR, and W110A and FNR are similar.

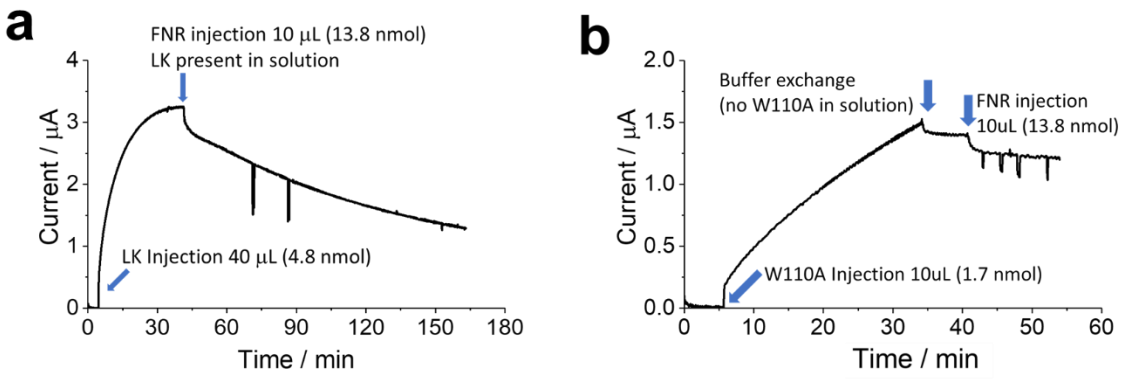


Figure A4.3. Competition between FNR and E2 with E2 loaded for the adsorption into the porous ITO layer **a)** LK loaded with extra FNR addition and **b)** W110A loaded with extra FNR addition. Conditions:

cell volume 4 mL; substrate [(±)-4-phenyl-2-butanol] = 8 mM, [$NADP^+$] = 10 µM, [Mg^{2+}] = 5 mM buffer: 50 mM TAPS pH 9.0; temperature: 25 ℃, Potential held at −0.175 V vs. SCE to drive oxidation. Solution purged with argon to remove O_2; argon flow maintained in headspace thereafter. Rotating disk electrode (RDE) SA: 0.07 cm^2, 1000 rpm. Enzyme loading: FNR loaded by drop-casting and rinsing before the experiment; LK 4.8 nmol or W110A 1.7 nmol was injected in real-time during the experiment as indicated.

A4.3.3.2 FNR displacement

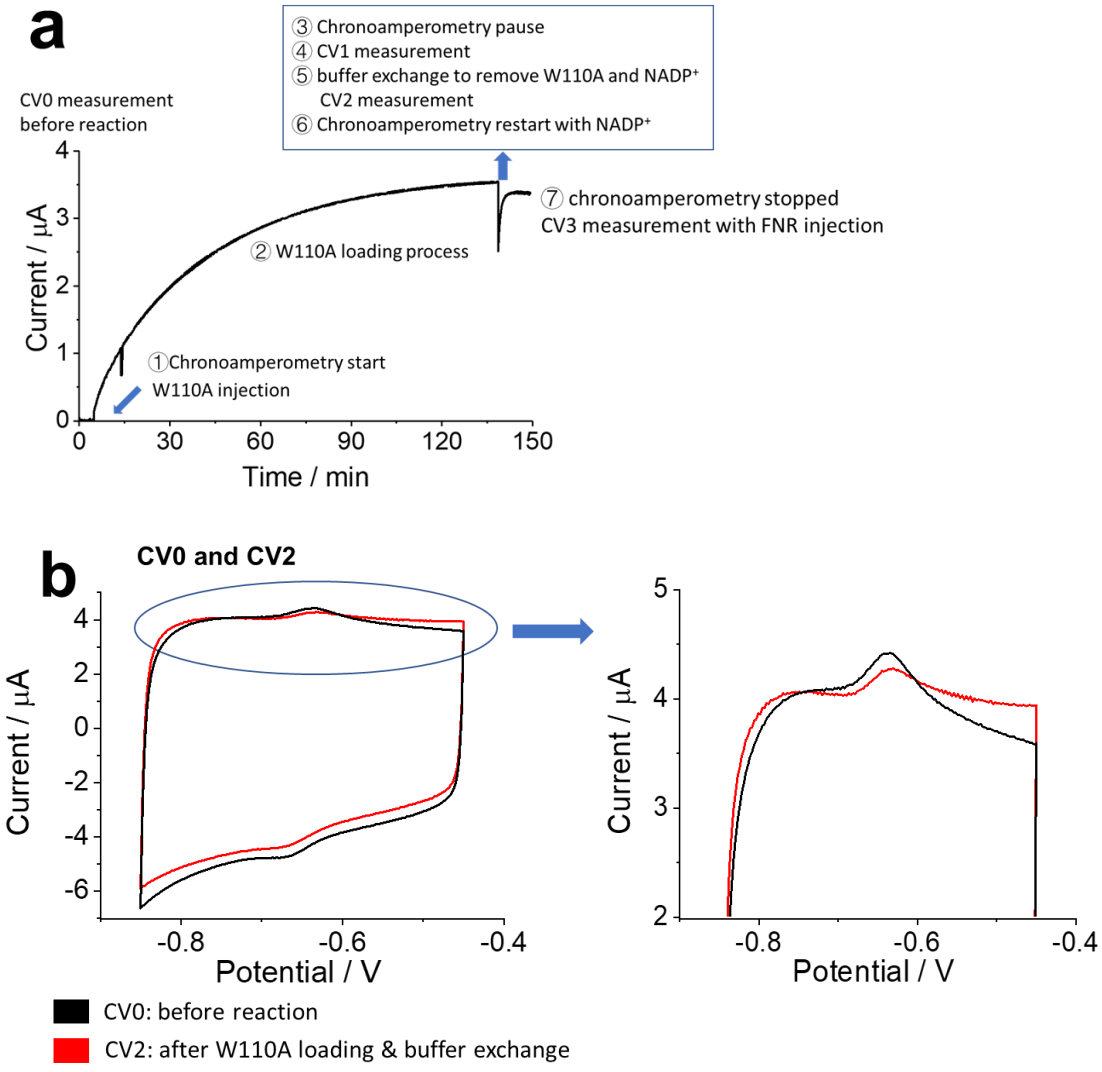
The purpose of the following experiments is not only to detect which enzyme is more competitive in the loading process as discussed in th last section. This section also focuses on the change of rate-limiting enzyme during the loading process. The loading method for enzymes mostly used in this chapter pre-loading FNR by drop-casting followed by loading two E2s (LK and W110A) together by stirring in solution. Thus, the process of E2s displacing FNR during their loading is relevant to the work later when the electrode is used for bulk deracemisation or inversion.

(1) W110A displacing FNR

Figure A4.4 is a chronoamperogram showing the W110A loading process together with CVs measured during and afterwards to depict the rate-limiting factor switching throughout the process. The experimenet steps were as followings, corresponding to the number marked in figure A4.4 panel (a):

0) A CV measurement of FNR non-turnover peak(CV0) was conducted before the reaction for later comparison of FNR loading amount (shown in panel (b) with CV2). 1) The chronoamperometry started with reaction initiated by the live injection of W110A. At this point, E2 loading is the rate-limiting factor. The current growth is due to the W110A binding in the sites in nanopores. 2) During the loading process, the growth in current slows down as the pores become more and more saturated with enzyme. At this point, W110A now could also compete with and may displace FNR to get in their pore sites. 3) The chronoamperometry was paused for CV measurement. 4) As shown in panel (c), the successive CVs (CV1) show a decrease of oxidation current over time, caused by the loading of W110A displacing FNR, which suggests the rate limiting factor is FNR.

This is also confirmed by the non-plateu shape on the end of oxidation side of the curve. 5) Buffer exchange was carried out to remove W110A from the solution and also $NADP^+$, CV2 was then measured to compare the FNR non-turnover peak with CV0 (in panel (b)). The displacement of FNR is confirmed by the CV measured before and after the E2 loading process as CV0 and CV2 in panel (b), which shows a decrease in the area of FNR non-turnover peak. The FNR coverage was 655 pmol/cm^2 in CV0 and 355 pmol/cm^2 in CV2) The chronoamperometry was restarted with $NADP^+$ added, to check the activity of the electrode via the recovery of and current.(panel (a)) 7) The chronoampometry measurement was stopped and continuous CV (CV3) was measured to monitor further changes in oxidation current on extra FNR addtions (panel (d)).



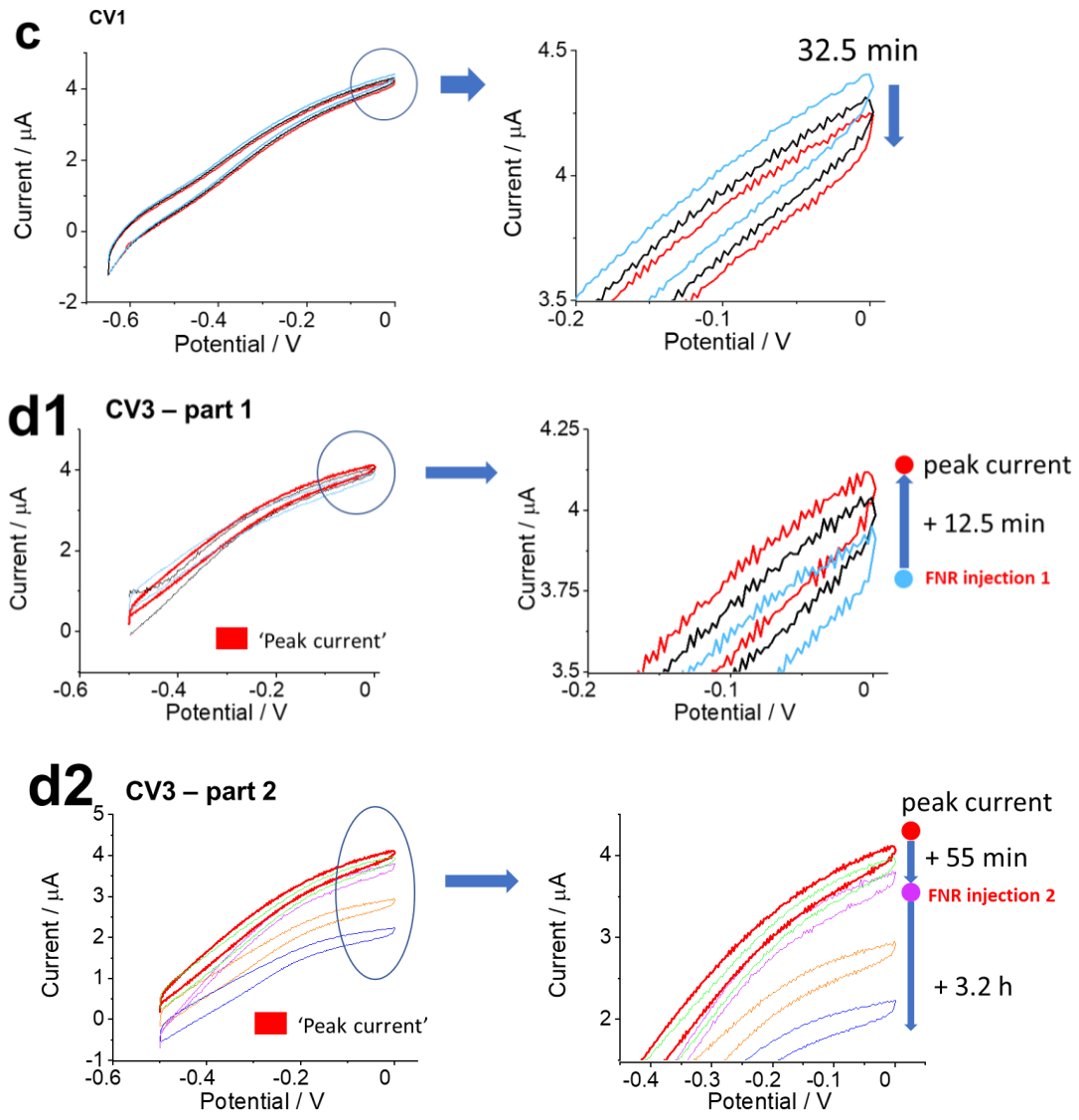


Figure A4.4. The competition between W110A and FNR for adsorption into the porous ITO electrode. **a)** Chronoamperograms monitoring the W110A-catalysed oxidation of alcohol. Conditions: cell volume 4 mL; substrate [(±)-4-phenyl-2-butanol] = 8 mM, [$NADP^+$] = 10 µM, [Mg^{2+}] = 5 mM buffer: 50 mM TAPS pH 9.0; temperature: 25 ℃, Potential held at –0.175 V vs. SCE to drive oxidation. Solution purged with argon to remove O_2; argon flow maintained in headspace thereafter. Rotating disk electrode (RDE) SA: 0.07 cm^2, 1000 rpm. Enzyme loading: FNR loaded by drop-casting before the experiment; W110A 3.5 nmol is live injected during the experiment as shown in (a). **b)** continuous cyclic voltammetry (CV1) after chronoamperometry stopped, scan rate = 4 mV/s **c)** cyclic voltammetry 2 (**CV2**, red curve) taken after chronoamperometry stopped and buffer exchange removing $NADP^+$, comparing to cyclic voltammetry before reaction and LK loading (**CV0**, black curve); scan rate = 20 mV/s **d)** Repetitive cyclic voltammetry with FNR injected; scan rate = 4 mV/s; oxidation current increased first (d1) then decreased (d2).

Panel (d) depicts the change in oxidation current with the injection of FNR (the electrode had already been loaded with FNR and LK as shown in (a) and the system was now FNR-limited as discussed previously). When FNR was injected (FNR injection 1 in d1) the oxidation current increased. During the first 12.5 minutes, the current increases from the blue trace to the red trace which is the ‘peak current’. The current then decreased due to more FNR displacing W110A in the electrode, indicating that the electrode is W110A-limiting now. Another 13.8 nmol of FNR was injected (FNR injection 2 in panel (d2)) and the current continued to decrease.

There is an optimal point of enzyme loading in the electrode that yields the peak current. At this specific loading ratio, all effective nanopores of the eletrode are occupied by enzyme and the level of current can no longer be improved by adjusting the loading ratio of enzymes - this should be the goal of enzyme loading. Even though it is impractible to keep monitoring the reaction current during theenzyme loading, the theoretical optimal loading point can give a reference to the amount of enzyme and time of loading. It is difficult to get a precise calculation of the speed at which one enzyme is displacing another. The electrochemistry here at least provides solid proof with a three-enzyme system that each of these enzymes competes with/displace others.

(2) LK displacing FNR

Based on the W110A experiment in last section, a simplified repeat experiment was carried out for LK loading. This experiment simply tests the displacement of LK by FNR. Similar steps are in this experiment and the results are shown in figure A4.5. 0) A CV measurement of FNR non-turnover peak (CV0) was conducted before the reaction for later comparison of FNR loading amount (shown in panel (b) with CV2). 1) At the beginning of the chronoamperometry measurement, when LK is injected, LK is the rate-limiting factor until a maximum current is reached. The current growth is due to the LK binding in the nanopores. 2) During the loading process, the current growth levels off with loading time, indicating that the pores became more and more saturated with

enzymes and LK now needed to also compete with and may displace FNR to get in their pore sites. 3) The chronoamperometry was paused for CV measurement. 4) The continuous CV measurement was conducted (CV1 in panel (c)) with excess LK remianing in the solution. As shown in the figure, the repeatitive CVs showed no change over the measurement (45 minutes), suggesting that the enzyme loading sitution was unchanged with the excess LK present. LK, unlike W110A, was less aggressive in displacing FNR loaded in the electrode. In addition, the current on the oxidisation side that does not fully plateau. The oxidation side current increases with increasing driving force (potential) giving rise to the non-plateaued shape. This indicates that the system could be limited by FNR. 5) Buffer exchange removes W110A in the solution and $NADP^+$, CV2 was then measured to compare the FNR non-turnover peak with CV0 (in panel (b)). The displacement of FNR is confirmed by the CV measured before and after the E2 loading process as CV0 and CV2 in panel (b), which shows a decrease in the area of FNR non-turnover peak. The FNR coverage was 870 pmol/cm^2 in CV0 and 455 pmol/cm^2 in CV2. The observation seems to contradict the inference that LK did not displace FNR. The FNR displacement could be due to the manual operation in buffer exchanges (rinsing, moving in and out the buffer, etc.) or may be a natural loss during the reaction using the RDE. 6) Chronoamperometry restarts and continues overnight to finish the reaction.

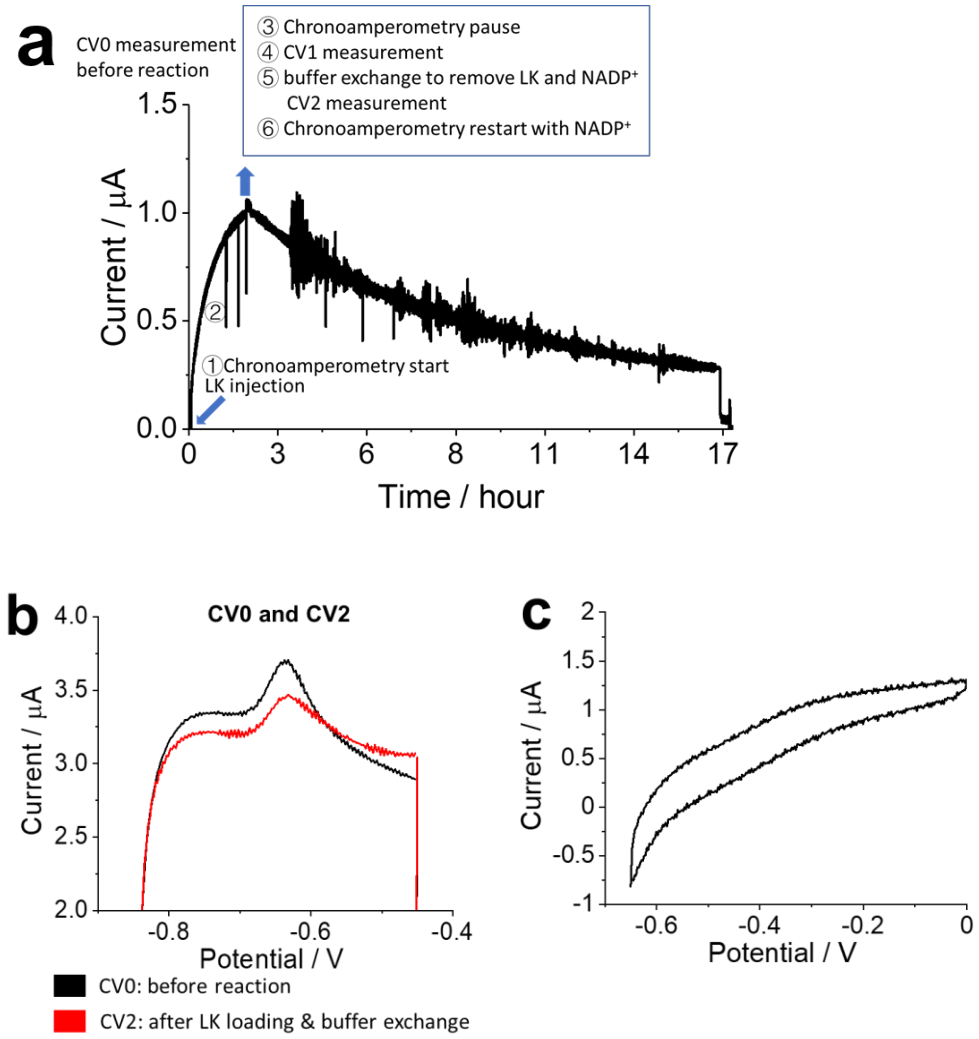


Figure A4.5. The competition between LK and FNR for adsorption into the porous ITO electrode. **a)** Chronoamperograms of LK-catalysed alcohol oxidation with LK live injection. **b)** cyclic voltammetry 1 **(CV1)** when chronoamperometry stopped, measure time: 45 minutes (2 repeats), scan rate = 1 mV/s **c)** cyclic voltammetry 2 (**CV2**, red curve) taken after chronoamperometry stopped and buffer exchange removing $NADP^+$, comparing to cyclic voltammetry before reaction and LK loading (**CV0**, black curve); scan rate = 20 mV/s. Cell conditions: cell volume 4 mL; substrate [(±)-4-phenyl-2-butanol] = 8 mM, [$NADP^+$] = 10 µM, [Mg^{2+}] = 5 mM buffer: 50 mM TAPS pH 9.0; temperature: 25 ℃, Potential held at −0.175 V vs. SCE to drive oxidation. Solution purged with argon to remove O_2; argon flow maintained in headspace thereafter. Rotating disk electrode (RDE) SA: 0.07 cm^2, 1000 rpm. Enzyme loading: FNR loaded by drop-casting before the experiment; LK 2.3 nmol is live injected during the experiment as shown in (a).

In summary, results of this section are trying to answer two questions. The first question is what the optimal loading point is. There is a theoretical 'optimal' ratio of the three enzymes in the pore when all the pore sites are occupied, and the current is maximum.

That means, an increase of any enzyme (FNR or E2s) will cause the decrease of reaction current; the optimal point is close to the maximum oxidation current.

The second question is, why W110A loaded by co-stirring with FNR is optimal but when LK is loaded in this way it is not. Perhaps LK is less aggressive in adsorbing into the pores compared to W110A, thus co-stirring FNR with LK will result in less LK loaded as it competes with excess FNR in the solution. FNR needs to be pre-loaded for avoiding it competing for nanopores against ADHs (especially LK). In the co-stirring process for LK and W110A, the amount of LK added to the loading solution also needs to be more than W110A to have a better loading result, which corresponds to the results in figure A4.2 about the loading ratio.

A4.3.4 pH of the LK-catalysed reaction

Alcohol dehydrogenases shows different activity in the e-Leaf at different pH values (discussed in the section 4.5.2.2 of the main text). Since LK is relatively new the electrochemical leaf, and (*R*)-alcohol conversion catalysed by LK in oxidation is more important for the proposed deracemiser and inverter, tests on the LK-loaded electrode are necessary. Figure A4.6 shows reaction performance at different pHs with (a) electrodes loaded with both LK and W110A (and FNR), and (b) a single-E2 electrode loaded with LK (and FNR). Reactions were initiated by injecting $NADP^+$. Each experiment involves the use of the same electrode with buffer exchanges in between to change the pH. The current immediately after buffer exchange did not start at zero. This is because some $NADP^+$ from the previous experiment was still trapped in the pores.

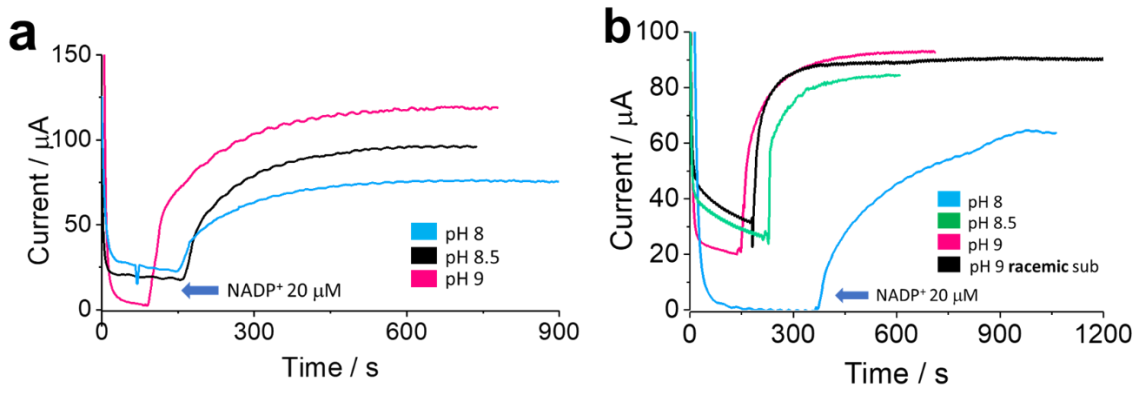
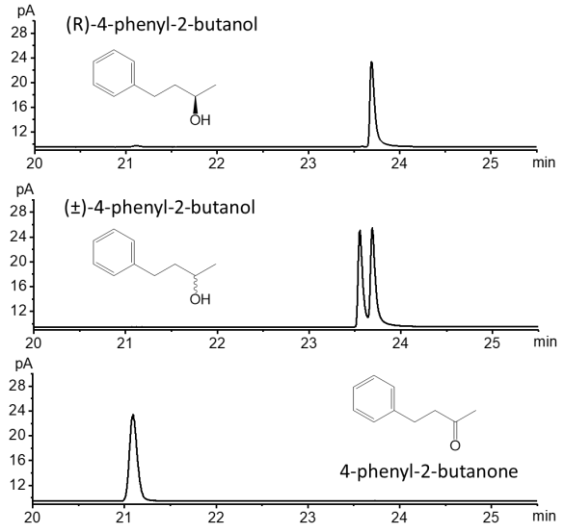


Figure A4.6. The effect of pH on the oxidation activity of LK. (*R*)-4-phenyl-2-butanol oxidation in solution of different pH **(a)** LK and W110A coloaded in the electrode **(b)** LK only, loaded electrode. Conditions: cell volume 4 mL and 1 mL sample is taken at potential switch; solution stirred throughout using a magnetic flea; substrate [(*R*)-4-phenyl-2-butanol] = 4 mM, [(±)-4-phenyl-2-butanol] = 8 mM, [$NADP^+$] = 20 µM, [Mg^{2+}] = 5 mM buffer: 50 mM TAPS pH 9.0, pH 8.5 and pH 8.0; temperature: 25 ℃, Potential held at 0 V vs. Ag/AgCl (3 M KCl) to drive oxidation. Solution purged with argon to remove O_2; argon flow maintained in headspace thereafter. Enzyme loading: FNR loaded first by drop-casting and rinsing, LK and W110A loaded after FNR by stirring in a 2.5 mL solution containing (a) 5.12 nmols LK and 0.53 nmols W110A (b) 5.12 nmol LK only, in 50 mM TAPS buffer pH 9.0; electrode (Ti foil) SA: 7 cm^2.

In the experiment with two-ADHs coloaded, the electrode was first tested in pH 9.0 and then in pH 8.5 and pH 8.0, and for the single-ADH electrode, the pH was 8, 8.5 and 9 sequentially. The electrode was taken out and rinsed between buffer exchanges and the substrate is (*R*)-alcohol so that the current is contributed to by LK. The trend is clear that at higher pH values, the reaction is favoured. The black trace in (b) corresponds to an extra measurement with racemic alcohol and it has similar current as that with (*R*)-alcohol, as expected from the selectivity of LK. As a result, pH 9.0 was chosen as the pH to perform the deracemisation and inversion.

A4.4 GC analysis results for the optimised inverter and deracemiser

Benchmarks



Original inverter

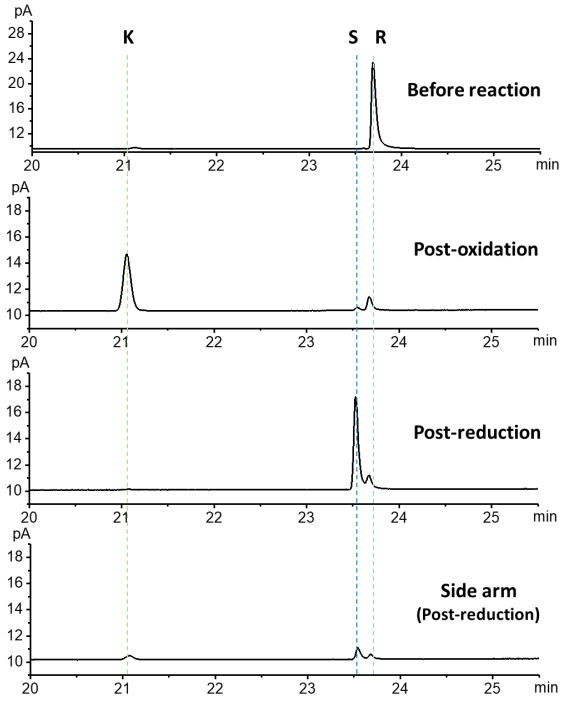


Figure A4.7. GC signals of the initial version of inverter in figure 4.19. Reprinted from Cheng et al with permission from the Royal Society of Chemistry.[57]

Optimised inverter

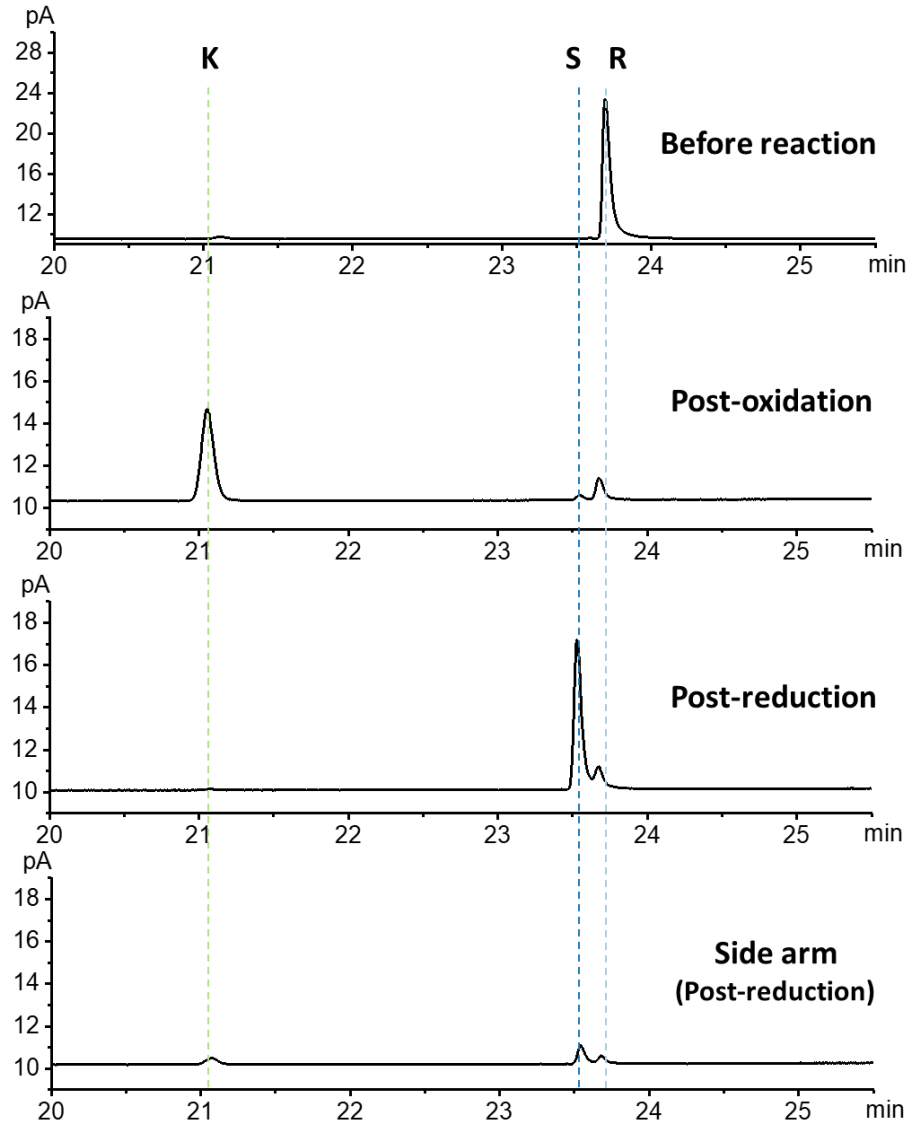


Figure A4.8. GC signals of the improved version of inverter in figure 4.24 panel (a). Reprinted from Cheng et al with permission from the Royal Society of Chemistry.[57]

Optimised deracemiser

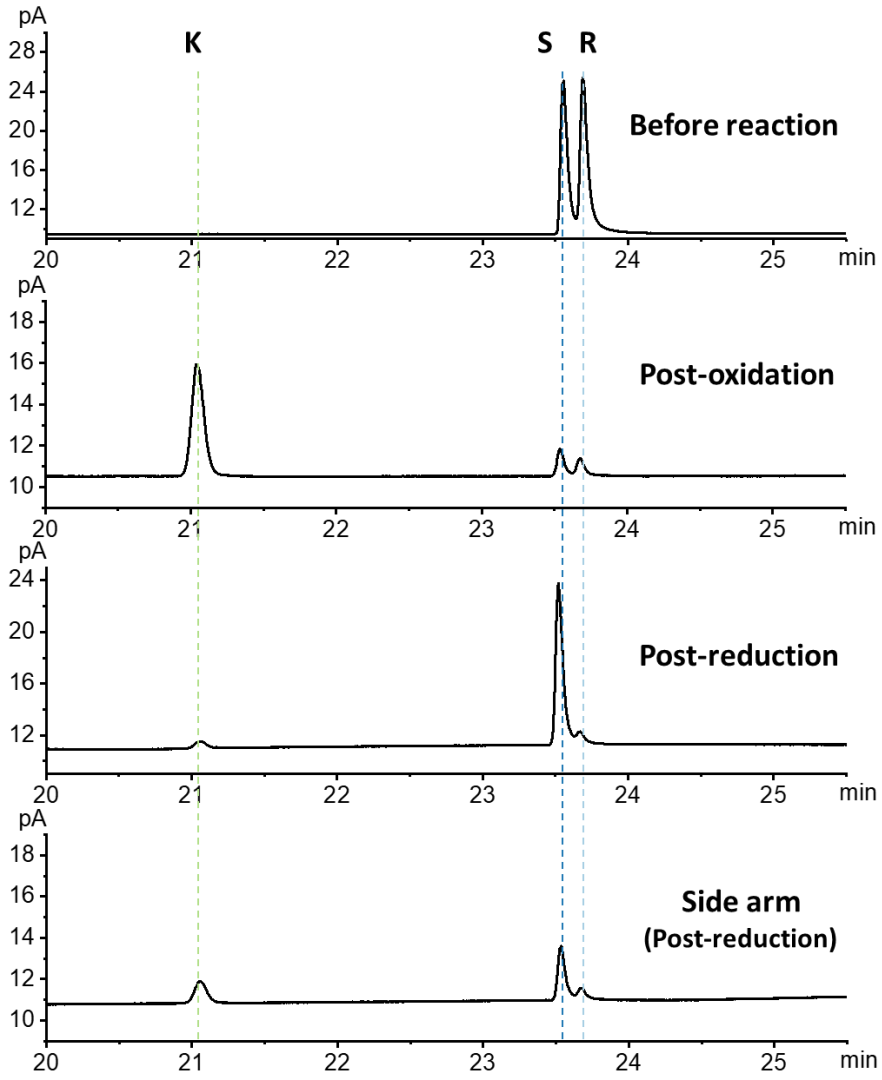


Figure A4.9. GC signals of the improved version of deracemiser in figure 4.24 (panel (b)). Reprinted from Cheng et al with permission from the Royal Society of Chemistry.[57]

A4.5. Enzyme loading: W110V

A4.5.1. W110V loading experiments

With FNR preloaded in the electrode, W110V and LK were loaded simultaneously from a stirred solution overnight and several repeats of experiments have the same outcome that the selectivity towards (*S*) – alcohol is still extremely low (despite using W110V). One typical experiment is shown in figure A4.10. The first CV shows FNR non-turnover peak indicating a successful loading of FNR and rules out the possibility of poor FNR loading. In the chronoamperograms with (*S*)-alcohol, (*R*)-alcohol and ketone, no current increase after $NADP^+$ injection, showing no E2 activity.

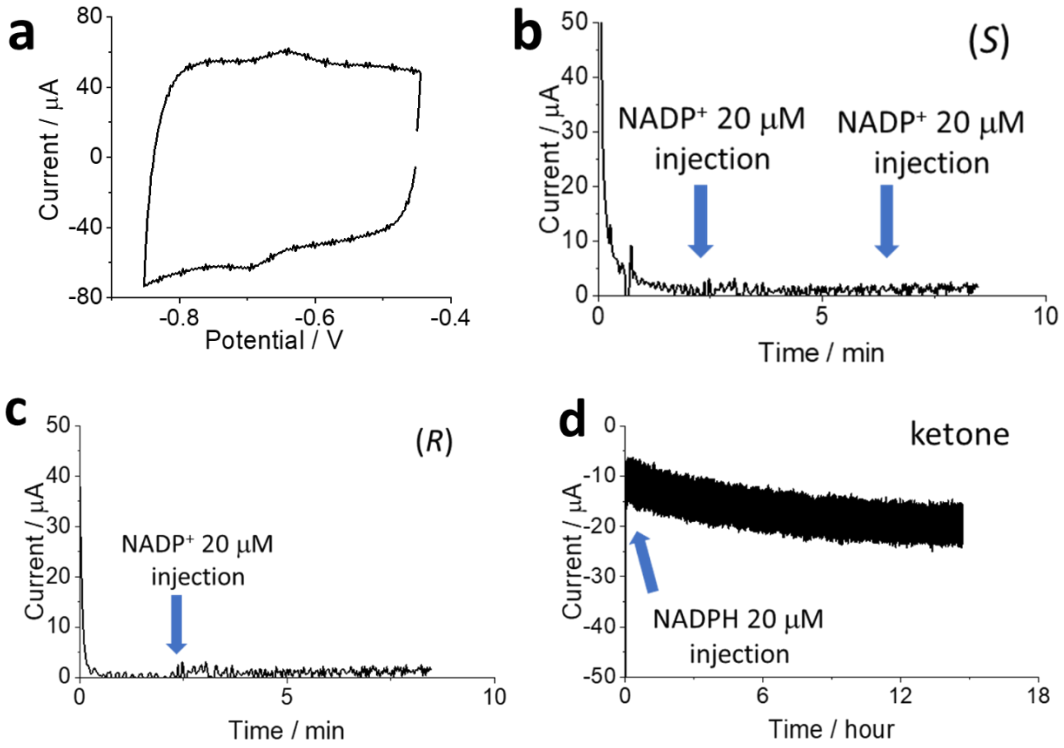


Figure A4.10. W110V loading activity test **a)** Non-turnover peak of FNR **b)** Chronoamperogram in (*S*)-alcohol **c)** Chronoamperogram in (*R*)-alcohol **d)** Chronoamperogram in ketone. Conditions: starting cell volume 5 mL; solution stirred throughout using a magnetic flea; substrate [(*S*)-4-phenyl-2-butanol] = 4 mM or [(*R*)-4-phenyl-2-butanol] = 4 mM for oxidation and [4-phenyl-2-butanone] = 8 mM for reduction, $[Mg^{2+}]$ = 5 mM buffer: 50 mM TAPS pH 9.0 for oxidation and pH 8.0 for reduction; temperature: 25 ℃, Potential held at 0 V vs. Ag/AgCl (3 M KCl) to drive oxidation and −0.74 V for reduction. Experiments performed in an anaerobic glovebox to avoid any contribution to the current form the reduction of O_2. Enzyme loading: FNR loaded first by drop-casting, W110V loaded after

FNR, by stirring in a 2.5 mL solution containing 3.28 nmols of W110V in 50 mM TAPS buffer pH 9.0 at 4 ℃ for 18 hours; electrode (Ti foil) SA: 7 cm^2.

A real-time W110V injection experiment was carried out first to check whether the unexpected result in Figure A4.11 was due to low W110V loading. Surprisingly, as figure 3.31 shows, the injection of W110V shows high activity, suggesting a good loading of W110V in these experimental conditions.

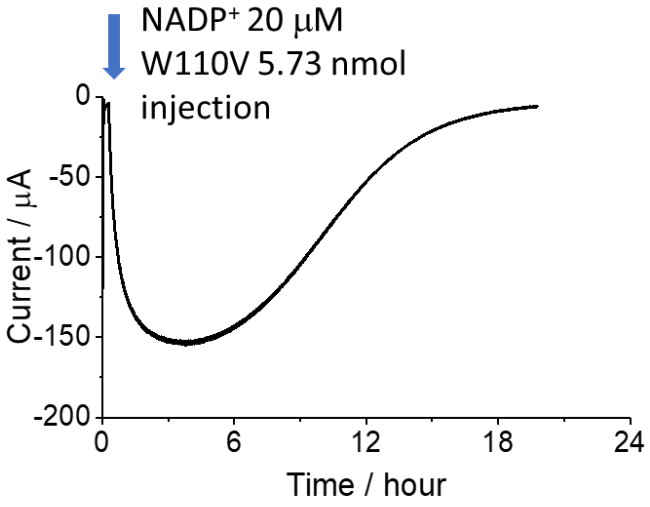


Figure A4.11. Chronoamperogram showing ketone reduction catalysed by W110V injected in real-time to the bulk solution. Conditions: starting cell volume 5 mL; solution stirred throughout using a magnetic flea; substrate [(±)-4-phenyl-2-butanol] = 8 mM, [$NADP^+$] = 20 µM, [Mg^{2+}] = 5 mM buffer: 50 mM TAPS pH 9.0; temperature: 25 ℃, Potential held at −0.74 V vs. Ag/AgCl (3 M KCl) to drive reduction. Experiments performed in an anaerobic glovebox to avoid any contribution to the current form the reduction of O_2. Enzyme loading: FNR loaded first by drop-casting, W110V live-injected during reaction as shown in curve; electrode (Ti foil) SA: 7 cm^2.

By comparing multiple aspects of these two experiments(i.e. W110V stirred on overnight to an FNR preloaded electrode and live injection of W110V to an FNR preloaded electrode), factor(s) that would probably hinder the W110V loading process are listed in the table A4.1. The conditions in this table are explored.

Table A4.1. Possible causes of poor W110V loading

	Factors	W110V Load from dilute solution overnight: LOW ACTIVITY	Live injection experiment HIGH ACTIVITY
1	pH	9	8
2	Loading Temperature	4 ℃	25 ℃
3	Loading Time	18 hours	Reaches peak in 5 hours
4	Redundant Enzyme	No, in reaction cell	Yes, in reaction cell
5	Reaction (potential applied)	No	Yes. – 0.74V
6	Substances (NADP(H), ketone)	No	Yes. 20 μM NADPH, 8 mM ketone
7	Oxygen	Yes	No

A4.5.2. Exploration of W110V loading conditions

A4.5.2.1. W110V activity, pH and loading temperature

(1) W110V activity

As mentioned in last section, W110V activity is the first factor that has been checked and excluded. The live injection experiment proves that W110V is inherently active.

(2) pH

Enzyme loading in pH 8.0 solution has been tested as a comparison to the original pH 9.0 solution loading. The chronoamperogram is shown in figure A4.12. There is a small increase in current when $NADP^+$ is injected. Loading enzyme in pH 8.0 instead of pH 9.0 can be a good improvement for W110V but the current shown in the figure is still not high enough for the reaction.

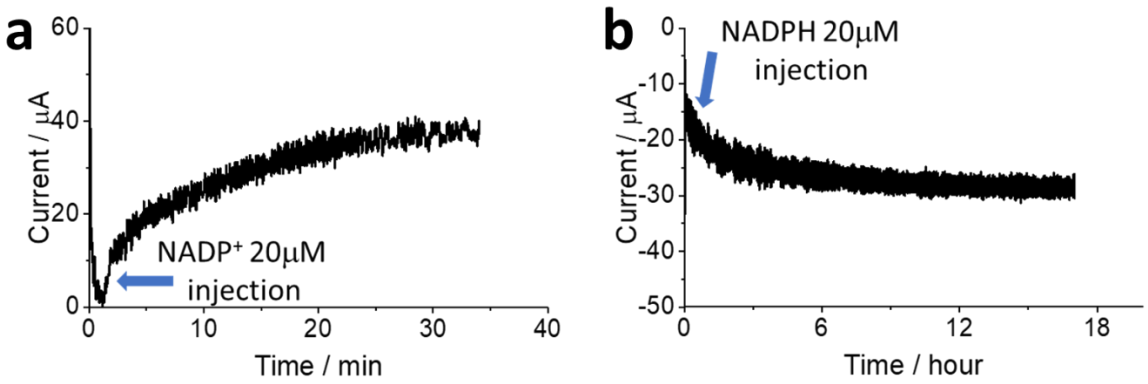


Figure A4.12. Chronoamperograms of **a)** oxidation and **b)** reduction with W110V loaded in pH 8.0 solution. Conditions: starting cell volume 5 mL; solution stirred throughout using a magnetic flea; substrate [(±)-4-phenyl-2-butanol] = 8 mM for oxidation and [4-phenyl-2-butanone] = 8 mM for reduction, [$NADP^+$] in oxidation [NADPH] in reduction = 20 µM, [Mg^{2+}] = 5 mM buffer: 50 mM TAPS pH 9.0 for oxidation and pH 8.0 for reduction; temperature: 25 ℃, Potential held at 0 V vs. Ag/AgCl (3 M KCl) to drive oxidation and −0.74 V for reduction. Experiments performed in an anaerobic glovebox to avoid any contribution to the current form the reduction of O_2. Enzyme loading: FNR loaded first by drop-casting, W110V loaded after FNR, by stirring in a 2.5 mL solution containing 3.28 nmols of W110V in 50 mM TAPS buffer pH 8.0; electrode (Ti foil) SA: 7 cm^2.

(3) Loading temperature and loading time

With FNR preloaded, W110V is then loaded on the bench at room temperature instead of at 4 ℃. The loading solution was stirred for 4 hours instead of overnight (18 hours). Chronoamperograms in figure A4.13 show the oxidation of racemic alcohol solution and the reduction in ketone solution. No E2 turnover current is observed for either experiment, indicating poor W110V loading, ruling out loading temperature and time as possible causes.

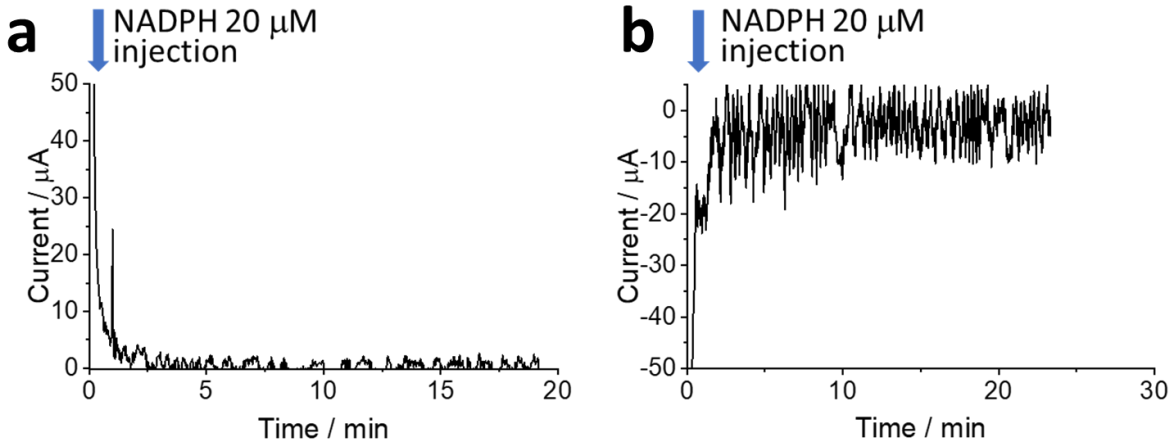


Figure A4.13. Chronoamperograms of a) oxidation and b) reduction with W110V loaded in room temperature for 4 hours. Conditions: starting cell volume 5 mL; solution stirred throughout using a magnetic flea; substrate [(±)-4-phenyl-2-butanol] = 8 mM for oxidation and [4-phenyl-2-butanone] = 8 mM for reduction, [NADPH] = 20 µM, [Mg^{2+}] = 5 mM buffer: **50** mM TAPS pH 9.0 for oxidation and pH 8.0 for reduction; temperature: 25 ℃, Potential held at 0 V vs. Ag/AgCl (3 M KCl) to drive oxidation and −0.74 V for reduction. Experiments performed in an anaerobic glovebox to avoid any contribution to the current form the reduction of O_2. Enzyme loading: FNR loaded first by drop-casting, W110V loaded after FNR, by stirring in a 2.5 mL solution containing 3.28 nmols of W110V in 50 mM TAPS buffer pH 9.0 at room temperature for 4 hours; electrode (Ti foil) SA: 7 cm^2.

A4.5.2.2. Electrode potential, presence of substrates, Oxygen

(1) Potential applied

The real-time injection experiment was repeated except no potential was applied. Buffer exchange was conducted after 5 hours, after which the chronoamperometry measurement began. The figure A4.14 has shown good activity which means that W110V has been loaded (left). The loading process is a physical process rather than a chemical or electrical process, and potential applied to the electrode while loading has not affected the W110V loading.

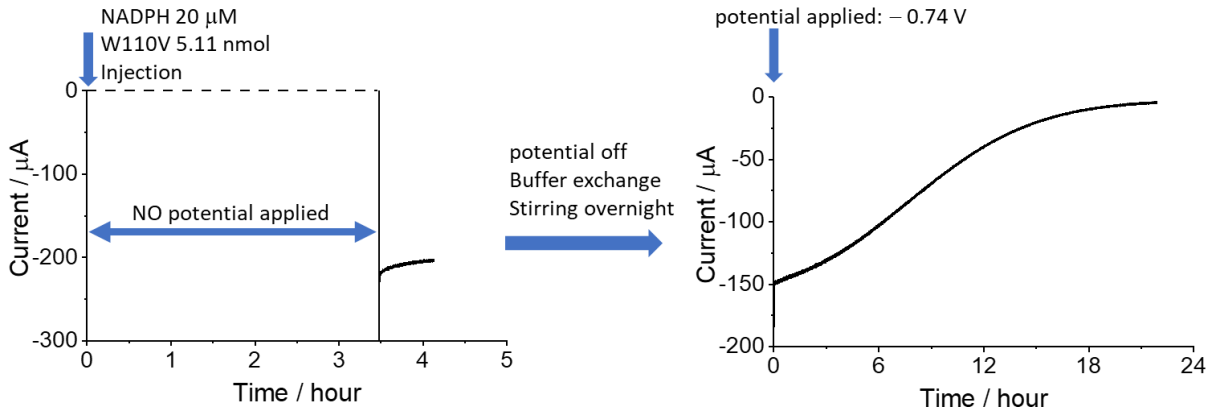


Figure A4.14. Chronoamperogram of ketone reduction with W110V injection loading and buffer exchange. Conditions: starting cell volume 5 mL; solution stirred throughout using a magnetic flea; substrate [(4-phenyl-2-butanone] = 8 mM, [NADPH] = 20 µM, [Mg^{2+}] = 5 mM buffer: 50 mM TAPS pH 8.0; temperature: 25 ℃, Potential held at 0 V vs. Ag/AgCl (3 M KCl) to drive oxidation and –0.74 V for reduction. Experiments performed in an anaerobic glovebox to avoid any contribution to the current form the reduction of O_2. Enzyme loading: FNR loaded first by drop-casting, W110V loaded by injection 5.73 nmol into the cell, stirring at room temperature for 5 hours; electrode (Ti foil) SA: 7 cm^2.

(2) Redundant enzyme

The experiment in figure A4.14 was carried on and followed by a buffer exchange (right). The buffer exchange is at 1 hour after the potential was applied initially to check the activity of W110V to confirm whether it had loaded. The potential was switched off at this buffer exchange and the solution was then stirred overnight before the potential was applied again one day later (figure A4.14 right). The current level was still high after 18 hours in the solution without redundant enzymes. The reaction continued for 20 hours to finish the conversion.

Another buffer exchange test experiment for redundant enzyme was repeated and shown in figure A4.15. W110V was injected together with $NADP^+$ at the beginning of the reaction. The current grew afterwards and after ~3.5 hours when the current growth slowed down, a buffer exchange was carried out to remove the excess enzymes in solution. The system still holds an active conversion rate, and the conversion finished over time, which proves that W110V injected is loaded well in the electrode in the first several hours and can do the ketone reduction in the reaction conditions.

Therefore, enzyme loaded holds stable activity even without redundant enzyme in the solution. This is not a cause for the poor loading of W110V.

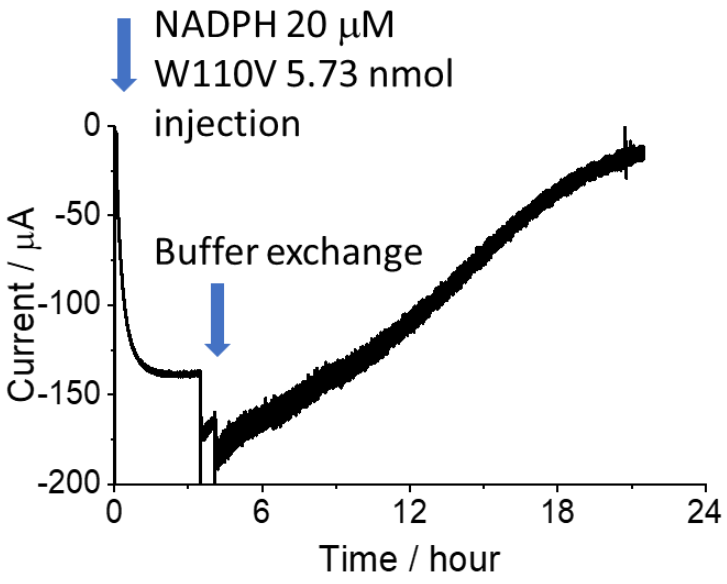


Figure A4.15 Chronoamperogram of ketone reduction with W110V live injection and buffer exchange. Conditions: starting cell volume 5 mL; solution stirred throughout using a magnetic flea; substrate [(4-phenyl-2-butanone] = 8 mM, [NADPH] = 20 μM, [Mg^{2+}] = 5 mM buffer: 50 mM TAPS pH 8.0; temperature: 25 ℃, Potential held at 0 V vs. Ag/AgCl (3 M KCl) to drive oxidation and −0.74 V for reduction. Experiments performed in an anaerobic glovebox to avoid any contribution to the current form the reduction of O_2. Enzyme loading: FNR loaded first by drop-casting, W110V loaded by injection 5.11 nmol into the cell, stirring at room temperature for 5 hours; electrode (Ti foil) SA: 7 cm^2.

(3) Presence of NADP(H) and ketone

With FNR preloaded, 2.87 nmol W110V was then stirred in 2.5 mL 50 mM TAPS buffer pH 9.0 containing either 8 mM ketone or 20 μM of NADPH. The rest of the loading process was identical. The activity was tested by chronoamperometry, as shown in figure A4.16. The electrode with enzyme loaded from the ketone-containing solution shows no current increase after NADPH is injected to initiate the reaction, suggesting poor loading of W110V. For the electrode with enzyme loaded in NADPH-containing solution, a clear current increase is observed after NADPH injection, suggesting the

activity from W110V loaded. NADPH is likely related to the successful loading of W110V. This is discussed at the end of this set of exploration experiments.

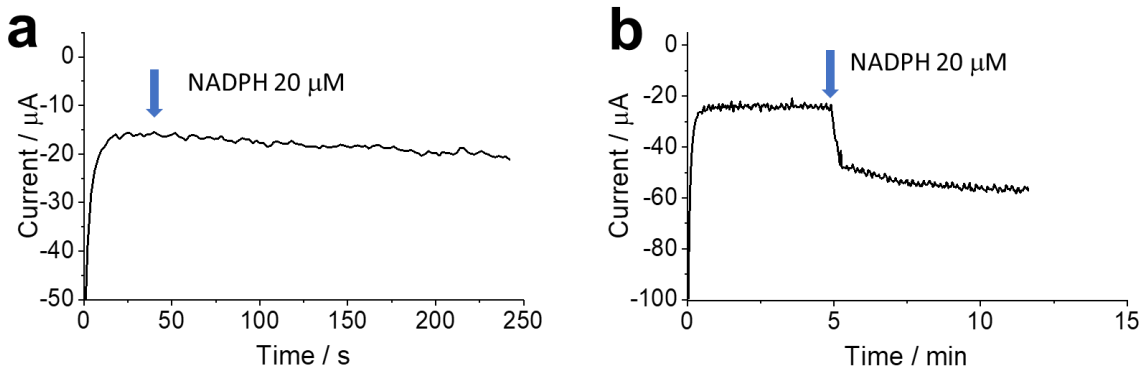


Figure A4.16. Chronoamperogram of ketone reduction **a)** W110V loaded with ketone in solution **b)** W110V loaded with $NADP^+$ in solution. Conditions: starting cell volume 5 mL; solution stirred throughout using a magnetic flea; substrate [(±)-4-phenyl-2-butanol] = 8 mM for oxidation and [4-phenyl-2-butanone] = 8 mM for reduction, [NADPH] = 20 μM, [Mg^{2+}] = 5 mM buffer: 50 mM TAPS pH 9.0 for oxidation and pH 8.0 for reduction; temperature: 25 ℃, Potential held at 0 V vs. Ag/AgCl (3 M KCl) to drive oxidation and −0.74 V for reduction. Experiments performed in an anaerobic glovebox to avoid any contribution to the current form the reduction of O_2. Enzyme loading: FNR loaded first by drop-casting, W110V loaded after FNR, by stirring in a 2.5 mL solution containing 2.87 nmols of W110V in 50 mM TAPS buffer pH 9.0 at 4℃ for 5 hours; loading solution also contains 20 μM $NADP^+$ for (a), and 8 mM ketone for (b). electrode (Ti foil) SA: 7 cm^2.

(4) Presence of oxygen

The reaction process in all the experiments were conducted in an anaerobic glovebox however, the enzyme loading process is conducted in open air before the electrode is taken into the oxygen-free environment. The loading process takes from 5 hours to 18 hours, during which the enzymes are exposed to oxygen.

In the following test, the W110V enzyme is loaded in glovebox at room temperature, by stirring in 2.5 mL solution for 5 hours. The chronoamperogram in figure A4.17 has shown distinguishable activity once NADPH is injected to initiate the reaction.

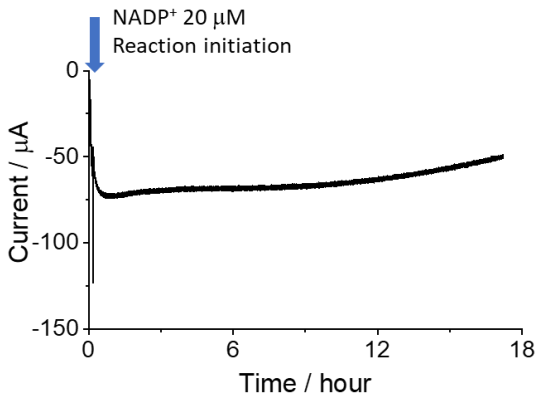


Figure A4.17. Chronoamperogram of ketone reduction with W110V loaded in oxygen-free environment. Conditions: starting cell volume 5 mL; solution stirred throughout using a magnetic flea; substrate [(±)-4-phenyl-2-butanol] = 8 mM for oxidation and [4-phenyl-2-butanone] = 8 mM for reduction, [$NADP^+$] = 20 µM, [Mg^{2+}] = 5 mM buffer: 50 mM TAPS pH 9.0 for oxidation and pH 8.0 for reduction; temperature: 25 ℃, Potential held at 0 V vs. Ag/AgCl (3 M KCl) to drive oxidation and −0.74 V for reduction. Experiments performed in an anaerobic glovebox to avoid any contribution to the current form the reduction of O_2. Enzyme loading: FNR loaded first by drop-casting, W110V loaded after FNR, by stirring in a 2.5 mL solution containing 2.87 nmols of W110V in 50 mM TAPS buffer pH 8.0; electrode (Ti foil) SA: 7 cm^2.

The enzyme loading in oxygen-free environment and with NADPH (oxygen present) have a good activity of W110V. It is hypothesised that the W110V loading process can be easily affected by oxidative conditions. NAPDH in the loading solution is a reductive that can fill into nanopores and create a reductive environment that help protect the enzyme loading from being slowed by oxygen's presence. It is worth pointing out that the hypothesis suggests that the oxidative environment is affecting only the loading process of W110V and does not harm the viability and activity of the enzyme itself. It can be observed from the experiments that the W110V is still active in catalysing the reduction process after one-day oxidative potential applied to the electrode, Further experiments are needed to further explore this effect.

A4.6 LK +W110A Inverter and deracemiser with more substrate

The reaction with more substrates has been conducted with the LK+W110A system. Figure A4.18 shows the chronoamperograms for the inverter (a) and deracemiser (b). The same problems arise: the conversion rate of (*R*)-alcohol in oxidation is lower due to product inhibition. The final ee% is less than previous experiments. The reduction current for the inverter is low, a likely result of poor loading process and the low amount of W110A relative to LK used when loading.

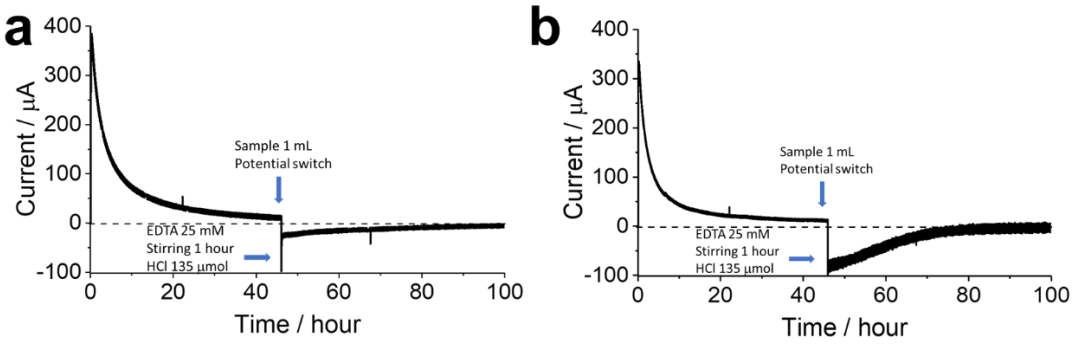


Figure A4.18. Chronoamperogram of **a)** Inversion of (*R*)-alcohol and **b)** deracemisation of (±)-alcohol catalysed by ADHs (W110A + LK) bidirectional control with 10 mM substrate at start. Conditions: starting cell volume 5 mL and 1 mL sample is taken at potential switch; solution stirred throughout using a magnetic flea; substrate [(*R*)-4-phenyl-2-butanol] = 10 mM for inverter or [(±)-4-phenyl-2-butanol] = 10 mM for deracemiser, [$NADP^+$] = 20 µM, [Mg^{2+}] = 5 mM buffer: 50 mM TAPS pH 9.0, pH is adjusted by HCl injection to approximately pH 8.0 at potential switch; temperature: 25 ℃, Potential held at 0 V vs. Ag/AgCl (3 M KCl) to drive oxidation and −0.74 V for reduction. Experiments performed in an anaerobic glovebox to avoid any contribution to the current form the reduction of O_2. Enzyme loading: FNR loaded first by drop-casting, LK and W110A loaded after FNR, by stirring in a 2.5 mL solution containing 2.56 nmols of LK and 0.95 nmols of W110A in 50 mM TAPS buffer pH 9.0; electrode (Ti foil) SA: 14 cm^2.

Table A4.2. GC Enantiomer analysis for the inverter (LK+W110A) with more substrate

	[S]/mM	[R]/mM	[ketone]/mM	ketone%	S%	R%	ee%(*S*)
Starting	0.03	9.84	0.13	1.3	0.3	98.4	-99.3
Post-oxidation	0.00	2.78	7.22	72.2	0.0	27.8	-100.0
Post-reduction	2.23	1.81	2.05	33.7	36.6	29.7	10.5
Side-arm	0.75	1.26	1.90	48.7	19.1	32.2	-25.4

*Coulometric Conversion (oxidation): 97.1 % Conversion (reduction): 31.4% (produced in oxidation)

Table A4.3. GC Enantiomer analysis for the deracemiser (LK+W110A) with more substrate

	[S]/mM	[R]/mM	[ketone]/mM	ketone%	S%	R%	ee%(*S*)
Starting	4.87	5.13	0.00	0.0	48.7	51.3	-2.5
Post-oxidation	3.16	1.35	5.49	54.9	31.6	13.5	40.1
Post-reduction	5.30	0.72	0.24	3.8	84.6	11.6	76.0
Side-arm	2.44	0.41	0.89	23.7	65.3	11.0	71.2

*Coulometric Conversion (oxidation): 67.9% Conversion (reduction): 91.1% (produced in oxidation)

Appendix of Chapter 5

A5.1. Enzyme loading methods – from live injection to drop-casting and co-stiring

As introduced in previous chapters, several methods are available for FNR and E2 enzyme loading. Enzymes can be loaded by drop-casting and stirring in dilute solution and can either be preloaded or loading by live injection under electrochemical monitoring. FNR and E2 can be loaded together and stepwise. This section presents the optimisation attempts for enzyme loading, from the early-stage loading process in which FNR is preloaded and ADH is live injected, to the later-stage loading process in which FNR and ADH are preloaded by drop-casting and co-stirring. The test reaction for enzyme loading optimisation is only reduction of ketone since the oxidation direction catalysed by ADH has product inhibition effect on it and the racemic alcohol used cannot reach a completion.

A5.1.1 FNR preloaded and E2 Live injection

As one of the frequently used loading methods at early stage, live injection of E2 is worth investigating in order to determine an optimal E2 loading situation. A typical chronoamperogram of ADH-catalysed 4-phenyl-2-buanone reduction is shown in the figure A5.1, a whole process of the chronoamperogram (left) with a zoom-in part of its starting stage (right). In this experiment, the ITO/Ti electrode was preloaded with FNR by either drop-casting or stirring with dilute solution. A negative potential was applied to drive reduction, followed by the injection of $NADP^+$, which yielded a small reduction current from its reduction. Then E2 (ADH) was then injected giving rise to a current due to the entrapment of E2 into the ITO nanopores over time and reacting with substrate and cofactors. The growth last for 3 hours until the peak current was reached. Then the current decreased swiftly due to the depletion of the substrate. The current reached zero in the end. The baseline current was resulted from the minor oxygen introduced from the environment.

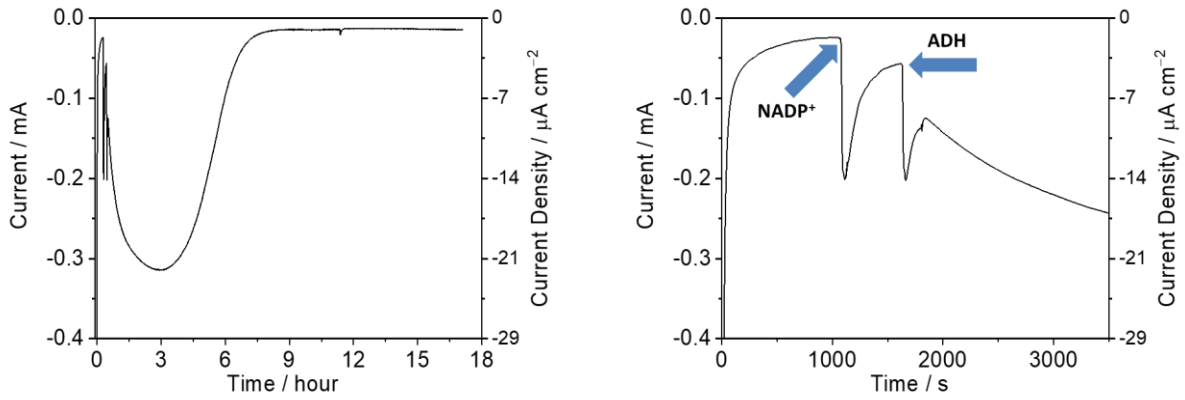


Figure A5.1. Chronoamperogram of the reduction reaction catalysed by ADH with E2(ADH) live injected as initiation of reaction. Conditions: solution volume 4 mL; buffer: 100 mM TAPS pH 9.0; temperature: 25 ℃, solution is purged with argon to remove O_2 and argon flow maintained in headspace thereafter. substrate [4-phenyl-2-butanone] = 8 mM, [$NADP^+$] = 20 µM; Potential held at -0.9 V vs. Ag/AgCl (3 M KCl). Electrode SA = 14 cm^2. Enzyme loading: FNR pre-loaded by drop-cast, ADH loaded by live injection 2.18 nmol.

E2 loading can be optimised conveniently based on the electronic signals, as the loading process of ADH, its adsorption into the nanoconfined system and incorporation to the catalytic cascade is directly reflected as the current change which is monitored live. However, the obvious issue with ADH loading is that there is not a stage when the current plateaus to show the steady peak current. The change of current close to peak current shown is mixed with the increase from E2 loading and the decrease from substrate depletion. Therefore, the peak current (also the turning point of the curve) is not the indicator of E2 maximum loading. It is only the point where the current decrease from substrate limit outweighs the current increase from the loading of E2.

The limitation in the typical run is that it is impossible to determine the time required for E2 to be fully loaded. The solubility of substrate is low and can hardly be increased to allow for longer reaction time before the substrate limitation dominates the current change. In addition, the loading takes quite a long time (>3 hours) and the slowly increasing reaction rate is not ideal for conversion purpose. These limitations inspired further investigation of monitoring E2 loading, loading with different methods, and introduction of organic phase of pure substrate.

(1) Monitoring E2 loading: extra substrate supply and non-catalytic process

To get a current change mainly caused by E2 loading, there should not be other limits like the insufficient substrate. This inspired adding an organic layer to the e-Leaf. Two tests are conducted regarding to this purpose, process shown in figure A5.2.

Panel (a) shows the process in which a steady supply of substrate is provided by adding a layer of pure substrate on the top of aqueous solution at beginning, with ADH live injected to initiate the enzyme loading and the reaction. The current increasing stage was approximately 1.5 hours and a steady peak current is reached. The reaction continued until 8 hours and was then paused. A buffer exchange was conducted to replace the biphasic solution containing redundant ADH to a fresh batch of aqueous solution containing only substrate and $NADP^+$. The current level after buffer exchange was similar to the biphasic loading process. The substrate was then depleted over time. The charge passed in the loading phase is 6.5 C, indicating a coulometric yield of 33 μmol of product (103.1% of 8 mM starting concentration in aqueous phase). After buffer exchange, the charge passed is 5.7 C, indicating a coulometric yield of 29 μmol of product, a conversion of 90.6% of the 8 mM starting concentration. This experiment solved the concentration limit from poorly soluble substrates by adding a layer of pure substrate. This is the first inspiration of introducing organic phase to the e-Leaf. Organic substrate serves as a reservoir that keeps refill the aqueous phase with substrate at a saturated concentration and keeps the e-Leaf working with sufficient substrate of low solubility in one batch.

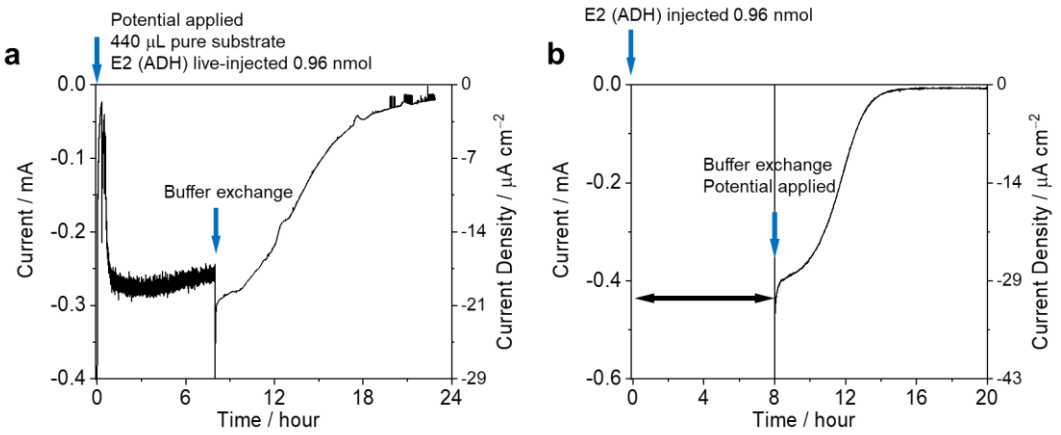


Figure A5.2. Monitoring of ADH loading process with the ketone reduction. **a)** loading stage live-monitored by chronoamperometry; **b)** no reaction and monitoring in the loading stage. Conditions: volume 4 mL; solution stirred throughout using a magnetic flea; substrate [4-phenyl-2-butanone] = 8 mM, [NADPH] = 20 μM, buffer: 100 mM TAPS pH 8.0; temperature: 25 ℃, Potential held at −0.9 V vs. Ag/AgCl (3 M KCl) to drive reduction. Solution purged with argon to remove O_2; argon flow maintained in headspace thereafter. Enzyme loading: FNR loaded first by drop-casting, ADH loaded by live injection 0.96 nmol into the cell, electrode (Ti foil) SA: 14 cm^2.

A potential problem is that since the ADH is injected into the aqueous phase, it may have intense direct contact with the organic layer. Possible deactivation of the enzyme can be occurring during its interaction with pure organic chemicals. Panel (b) shows a control experiment, where the loading of ADH was in aqueous solution without adding pure substrate. The loading process was 'blind' to us without monitoring and last for the same loading time (8 hours). After the loading process, buffer exchange was conducted, and potential was applied to initiate the reaction. The current (-0.4 mA) showed up on the applying of potential, indicating the outcome of the enzyme loading. The substrate was then depleted and reaction came to an end. The charge passed in the loading phase is 5.4 C, indicating a coulometric yield of 28 μmol of product, a conversion of 87.5% of the 8 mM starting concentration.

By comparing two experiments, some observations can be made. The peak current of 'blind' loading (-0.4 mA) is higher than the peak current from live monitoring with organic layer (-0.28 mA). This suggests that the extra organic layer may be holding back the E2 loading process, probably by the direct contact to the redundant ADH in the aqueous

bulk solution during the loading stage. Other factors may also come to play. For example, the pure organic substrate can have direct contact with the electrode due to agitation of the solution, or in the operation of buffer exchange, which may harm the activity of the system for the subsequent experiment. It could also be due to the operation errors between different reactions. In brief, each experiment shown here provides a different angle of depicting the process and performance of E2 live injection with certain restrictions. Reaction with pure substrate has no limit of substrate supply but has potential effect from pure substrate to the system. The control experiment has no monitoring of the loading process, with only the resulting activity shown as reaction current in a new batch.

(2) Monitoring E2 loading: cyclic voltammetry

Another way to monitor the ADH loading process is by cyclic voltammetry (CV). With substrate and $NADP^+$ presented, the injection of E2 would result in a shape change with an increasing reduction current, and thus the loading process can be monitored by checking the current at reductive potential. As shown in figure A5.3 (panel (a), b, c in chronic sequence), the starting CV of the electrode preloaded with FNR in the solution containing ketone and $NADP^+$ was shown as the black trace in panel (a). ADH was injected live as the continuous CV scanning started. The current at reductive potential (-0.9 V) was increasing over time and finally reached the peak at 4 hours and this peak current remained at the level until 10.5 hours (approximately 0.4 mA at -0.9V, blue trace). The current then decreased as time passes due to the depletion of substrate. The monitoring was stopped at 17.5 hour (red trace) and a buffer exchange was conducted. Reduction current returns to high level after buffer exchange (approximately 0.6 mA at -0.9 V, green trace), which was slightly higher than the peak current (blue trace) in loading process.

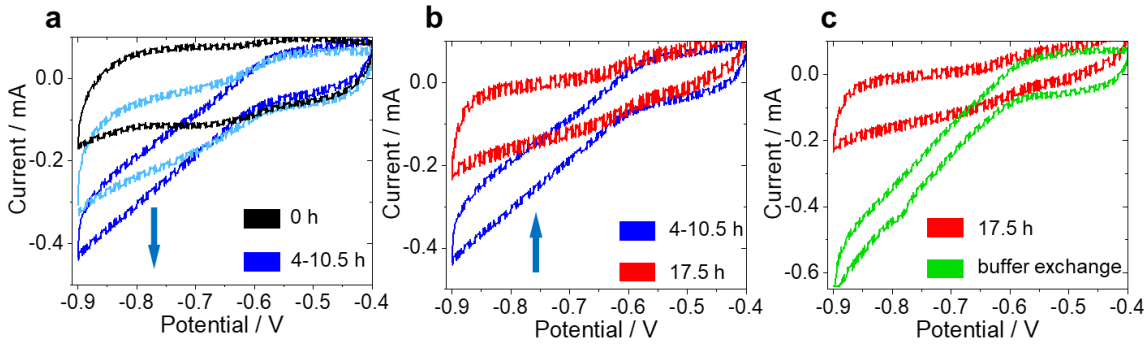


Figure A5.3. Cyclic voltammograms for ADH-catalysed ketone reduction current over time monitoring the loading of E2 injected. **a)** 0 – 10.5 hours, **b)** 10.5 – 17.5 hours, **c)** buffer exchange vs. peak current at 10.5 hours. Conditions: volume 4 mL; solution stirred throughout using a magnetic flea; substrate [4-phenyl-2-butanone] = 8 mM, [$NADP^+$] = 20 µM, buffer:100 mM TAPS pH 8.0; temperature: 25 ℃. Solution purged with argon to remove O_2; argon flow maintained in headspace thereafter. Scan rate: 2 mV/s. Enzyme loading: FNR loaded first by drop-cast (29.4 nmol in 2.5 mL TAPS buffer pH 9.0), ADH loaded by live injection 0.96 nmol, electrode (Ti foil) SA: 14 cm^2.

Continuous cyclic voltammetry as a monitoring method for enzyme loading, comparing to chronoamperometry, has the same feature of live monitoring with less substrate consuming rate. The potential is sweeping over a range, in which only negative enough potential can drive the conversion. The peak current remains at 10.5 hour, longer than the 8-hour loading time used in chronoamperometry. The experiment suggests that the loading process of ADH could take a long time approximately 4-10 hours.

There are some disadvantages with this method as well. First, most of the data points acquired are less valuable for the aim of this experiment. Only the reduction current at the potential held to drive reaction is of our interest. This is a trade-off for less consumption of substrate over a long time. Second, it is difficult to calculate the amount of substrate converted over time. Therefore, it is hard to determine whether the E2 loading is finished when the current starts to decrease from the peak current due to substrate depletion, even though it is likely. Third, the current after buffer exchange is higher than the peak current in loading process. The higher current is from the minor amount of oxygen left in the new batch of solution being reduced that adds to the current.

(3) Monitoring E2 loading: intermittent chronoamperometry for semi-monitoring

The previous experiments have pointed out the features a proper way of monitoring the ADH loading with limited substrate should have. 1. The system should be kept oxygen free for reduction reaction. 2. Substrate should be above the threshold of becoming rate-limiting during a time length of 4-10 hours. 3. Conditions should be kept constant, and the test should be in shorter period time when the overall stability is good (ideally within 18 hours). 4. Live monitoring with the electrochemical signal is preferred.

Such requirement inspires a new way of E2 monitoring, which is intermittent monitoring by chronoamperometry. The new method is called ‘intermittent’ chronoamperometry, in that the potential is applied for 1000 seconds to drive reaction and then paused for 2 hours. This ‘reaction and pause’ was repeated 10 times in an 18-hour process. The accumulated reaction time was 2.8 hours. It is a semi-monitoring process. The chronoamperogram with currents aligned is shown in figure A5.4. The current increases as stages from different time of loading. ADH was live injected at beginning (0 hour). The current increases for approximately 6 to 8 hours loading time and the peak current remained unchanged until the 10 hours loading time. The current after 10-hour loading time started to decrease due to substrate limit and turns to nearly 0 in the end. It can be observed from the results that the loading time for ADH in this process is approximately 6 to 8 hours.

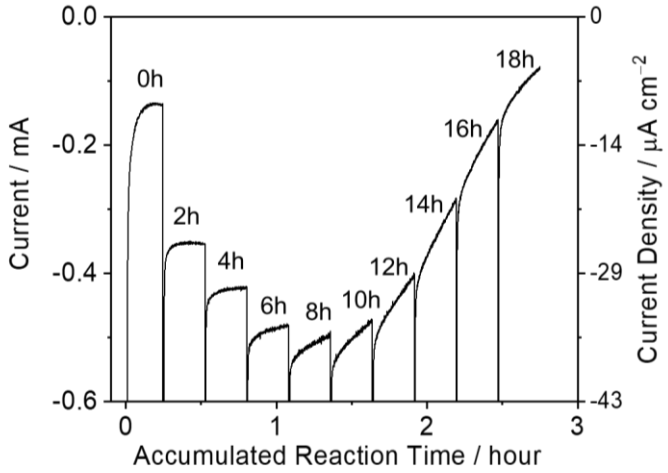


Figure A5.4. Chronoamperograms of 'semi-monitored' enzyme loading. Conditions: volume 4 mL; solution stirred throughout using a magnetic flea; substrate [4-phenyl-2-butanone] = 8 mM, [NADPH] = 20 μM, buffer: 100 mM TAPS pH 8.0; temperature: 25 ℃, Potential held at −0.9 V vs. Ag/AgCl (3 M KCl) to drive reduction. Solution purged with argon to remove O_2; argon flow maintained in headspace thereafter. Enzyme loading: FNR loaded first by drop-casting, ADH loaded by live injection 0.96 nmol into the cell, electrode (Ti foil) SA: 14 cm^2.

The advantages of the intermittent chronoamperometry in monitoring ADH loading can be easily observed comparing to other methods. The system has no organic phase, meaning no potential negative effect on the overall activity. The substrate consumption is low comparing to normal continuous chronoamperometry. The insufficient substrate limitation occurs far after the fully loading of ADH. There is only 2.8 hours of reactions time in 18 hours of loading time indicating the slowing of substrate consumption speed in multiple times. The loading process as the reaction current can still be monitored despite of less data points collected. The intermittent monitoring look more time take snapshot samples as commonly conducted in analysis, yet the 'sampling' of reaction rate (current) is exclusive to electrochemical analysis. This experiment solved the conflict of concentration limit from poorly soluble substrates and live monitoring.

(4) Substrate limit point of 4-phenyl-2-butanone

A supplementary experiment has been carried out to show the limiting effect of insufficient substrate to the reaction current. The chronoamperogram is shown in figure A5.5, in which ADH was live injected at the beginning to initiate the reaction as well as

the enzyme loading process. A buffer exchange was conducted to remove the excess ADH in the solution, at the point where current increasing almost ceases. The e-Leaf loaded with FNR and ADH then started to work converts all the substrates of the new batch and current reaches zero at the end of the process.

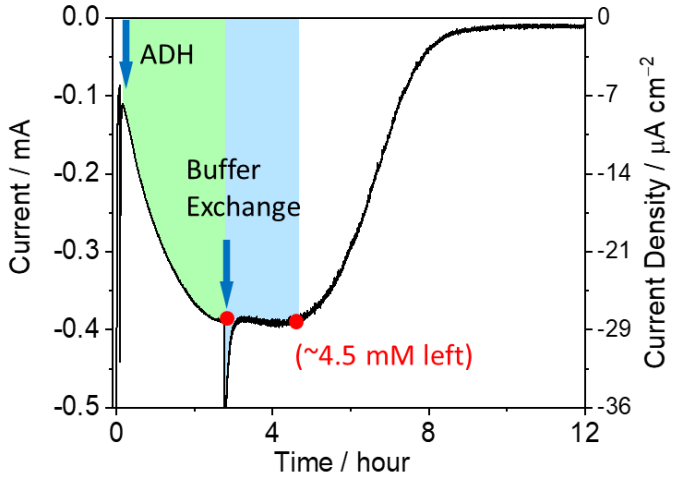


Figure A5.5. Chronoamperograms of ketone reduction with ADH live injected at beginning and buffer exchange after 2.8 hour. Conditions: volume 4 mL; solution stirred throughout using a magnetic flea; substrate [4-phenyl-2-butanone] = 8 mM, [NADPH] = 20 μM, buffer: 100 mM TAPS pH 8.0; temperature: 25 ℃, Potential held at –0.9 V vs. Ag/AgCl (3 M KCl) to drive reduction. Solution purged with argon to remove O_2; argon flow maintained in headspace thereafter. Enzyme loading: FNR loaded first by drop-casting, ADH loaded by live injection 0.96 nmol into the cell, electrode (Ti foil) SA: 14 cm^2.

The charge passed before buffer exchange (shaded in green) is 2.8 C corresponding to 14.5 μmol of substrate, 3.6 mM in the solution. The charge passed after buffer exchange and before the current decreases from substrate limits (shaded in blue) is 2.6 C corresponding to 13.5 μmol of substrate, 3.4 mM in the solution. Therefore, it can be determined that for this specific system, the concentration of substrate at which substrate limitation starts to occur, is approximately 4.5 mM. This justifies the semi-monitored loading process shown in figure A5.4. The coulometric consumption of substrate from the intermittent chronoamperometry before the 8-hour loading time (1.4 hours of accumulated reaction time) is 12 μmol, indicating approximately 5 mM substrate is left in the solution at that point. So the loading phase recorded by the intermittent chronoamperometry is free from the substrate limitation effect.

In summary, live injection for enzyme loading has the advantage of real-time data for loading progress monitoring. This method takes advantage of the informative electrochemical analysis, which is an excellent way of picturing the progress. The disadvantages of such method are equally obvious. For conversion, its efficiency is low since the conversion rate cannot reach its potential after several-hour's enzyme loading. For monitoring loading process, the concentration limit from substrate of low solubility remains. The intermittent chronoamperometry is not suitable in regard to conversion. Nevertheless, it would be a universal way of progress monitoring given no substrate limitation. Another shortcoming is that the cell solution is not 'clean' as there are redundant enzymes presented. Since enzymes can be nanoconfined in the pores of ITO layer, the enzymes in solution seems unnecessary after enzyme loading. In addition, the amount of enzymes live injected will increase accordingly to the volume change of reactor in scaling up, causing a large increase and waste of enzyme usage. The features of live injection inspired the idea of exploring other options for enzyme loading. Drop-cast loading is tested and optimised for the FNR + ADH e-Leaf biphasic system next.

A5.1.2 Stepwise Drop-cast Loading

Drop-cast method is as well introduced in previous chapters. The investigation of drop-cast loading method in this chapter is about two enzymes being drop-cast in sequence rather than together. The idea comes from that drop-cast is a 'faster' version of stir-loading or live injection loading. In previous experiments, FNR has been drop-cast while ADH is live injected, and the ADH loading process takes several hours and FNR loading takes only less than half hour. Despite the differences in the natures of two enzymes, it is interesting to check if ADH loading would be more efficient when it is drop-cast to the electrode after FNR being loaded first.

Four experiments have been carried out with different FNR and ADH drop-casting times. The purpose is to explore whether the stepwise drop-cast is capable for enzyme loading

and whether the loading is complete enough. Chronoamperograms are shown in figure A5.6. In stepwise drop-casting, the second enzyme was drop-cast after the first enzyme was rinsed off with buffer. The loading times are a) FNR 3 minutes and ADH 4 minutes, b) FNR 12 minutes and ADH 3minutes, c) FNR 3 minutes and ADH 12 minutes and d) FNR 3 minutes and ADH 1 minute.

All the experiments started with 8 mM ketone as substrate and were initiated by the addition of NADPH in real-time. Panel (a) shows the first test and serves as a benchmark experiment. A buffer exchange was conducted after the first batch reaction was finished and a high ratio of the peak current was recovered. The reaction was left running and finished in another 18 hours. The reactions in panel (b) and (c) have opposite times of loading of FNR and ADH. Reaction in panel (c) with longer ADH loading time has a 20% higher peak current than the reaction in panel (b). In panel (c), after the buffer exchange, separate addition of FNR and ADH were conducted. There was no change in current after the extra enzymes being introduce, indicating that the pre-reaction loading was complete. The hypothesis is that the pore sites were fully loaded with both enzymes, therefore no more enzymes could get in and increase the activity further. The reaction in panel (d) has the electrode with shortest loading time of ADH, and the starting current was also the lowest among the experiments. The reaction was paused and extra ADH is injected in the solution for an extra loading session for 8 hours. The reaction resumed with an increased current (highest amount the experiments) and finished the substrate in approximately 6 hours.

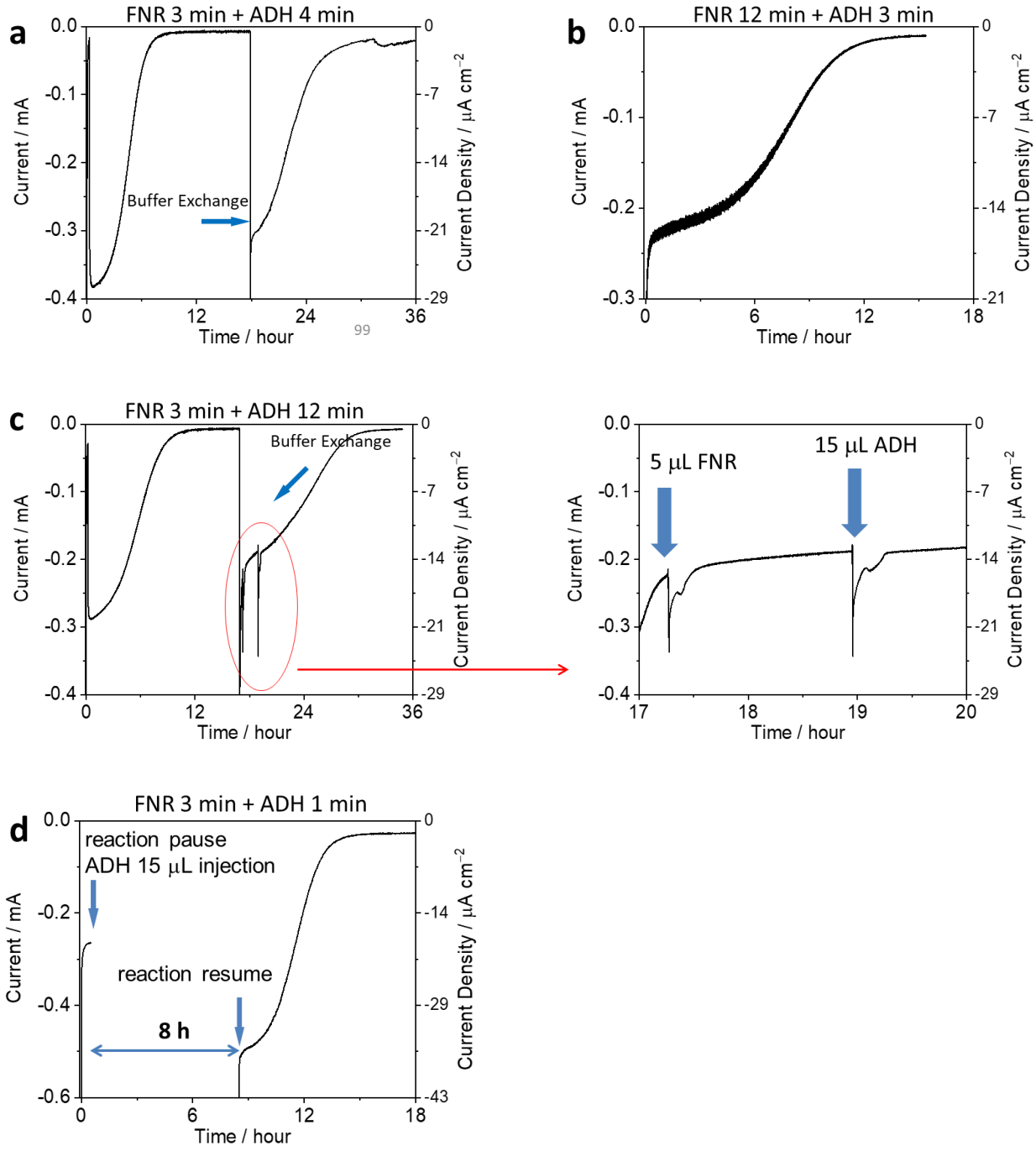


Figure A5.6. Chronoamperograms of ADH-catalysed reduction with two enzymes loaded stepwise by drop-casting. **a)** FNR 3 minutes and ADH 4 minutes, **b)** FNR 12 minutes and ADH 3 minutes, **c)** FNR 3 minutes and ADH 12 minutes, **d)** FNR 3 minutes and ADH 1 minutes. Conditions: volume 4 mL; solution stirred throughout using a magnetic flea; substrate [4-phenyl-2-butanone] = 8 mM, [NADPH] = 20 μM, buffer: 100 mM TAPS pH 8.0; temperature: 25 ℃, Potential held at −0.9 V vs. Ag/AgCl (3 M KCl) to drive reduction. Solution purged with argon to remove O_2; argon flow maintained in headspace thereafter. Enzyme loading amount: FNR 9.8 nmol, ADH 0.24 nmol. electrode (Ti foil) SA: 14 cm^2.

Several observations can be made from this group of experiments. First, drop-cast can work with both enzymes and drop-cast in sequence can work as an enzyme loading method. Second, by comparing the reactions in panel (b), (c) and (d), it can be concluded that FNR loading is relatively faster, while ADH is less competitive than FNR in loading and needs much longer time. This could be also due to the concentration of enzyme drops. The FNR solution from enzyme prep is 1.98 mM while ADH is only 0.068 mM. The concentrations differ a lot even though the drop concentration is already much higher than solution injection. Third, long time stir-loading can help the loading for enzymes that are somehow ‘reluctant’ in loading such as ADH and can get better loading activity than drop-cast. As shown in reaction (d), the current after ADH being stirring loaded for 8 hours is higher than that in reaction (c) where ADH is loaded by drop-casting for 12 minutes.

In brief, stepwise drop-cast is an available method for enzyme loading. It is more complex and has more factors to be considered for an excellent optimisation comparing to drop-cast all enzymes together. Therefore, this method has good potential for precise control on loading specific enzymes. On the other hand, the complexity sets a higher level of entrance. The normal drop-cast is easier and faster, with better repeatability, though stepwise drop-cast should always be in the toolkit for the e-Leaf manufacturing.

A5.1.3. Co-dropcast and co-injection loading

(1) Co drop-cast：

A step forward from stepwise drop-cast is co-dropcast, in which both enzymes are mixed and dropped on electrode together. This is one of the most convenient and efficient enzyme loading methods and it is has been tested for the FNR + ADH system. Figure A5.7 shows the cyclic voltammogram (left) of the electrode in pH 8.0 buffer after enzyme loading, and the chronoamperogram (right) of ketone reduction catalysed by the e-Leaf. Before the test, 0.97 nmol ADH and 9.8 nmol FNR were mixed and dropped on the electrode with a surface area of 14 cm^2. The drop was held for 3 minutes for

incubation before being rinsed off with buffer. The chronoamperogram shows a peak current at start approximately 0.3 mA at start, close to the level of some peak currents from stepwise drop-cast loading tests. Co-dropcast loading turns out to be an efficient way of loading enzymes, which has a short time of preparation, and is convenient in the operation with excellent reaction performance.

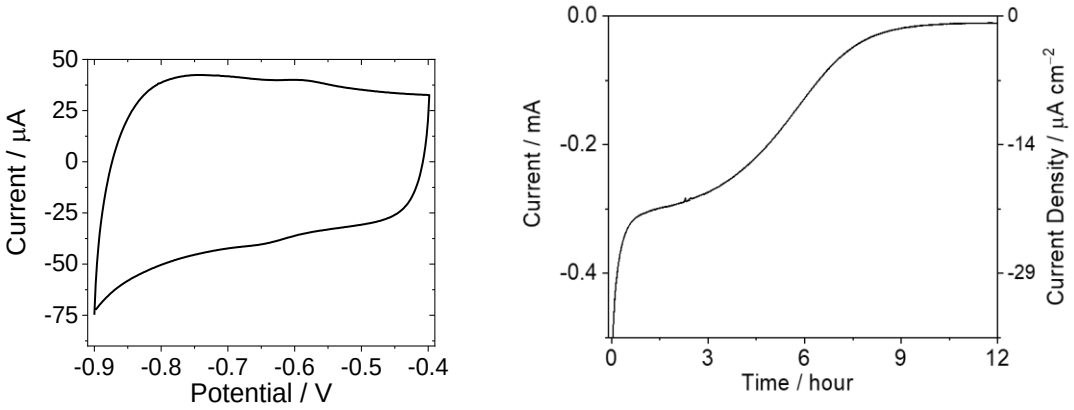


Figure A5.7. Cyclic Voltammogram and chronoamperogram of electrode loaded with FNR and ADH by co-dropcast. Conditions: volume 4 mL; solution stirred throughout using a magnetic flea; substrate [4-phenyl-2-butanone] = 8 mM, [NADPH] = 20 µM, buffer: 100 mM TAPS pH 8.0; temperature: 25 ℃, Potential held at −0.9 V vs. Ag/AgCl (3 M KCl) to drive reduction. Solution purged with argon to remove O_2; argon flow maintained in headspace thereafter. Enzyme loading amount: FNR 9.8 nmol, ADH 0.97 nmol. electrode (Ti foil) SA: 14cm^2.

(2) Co-injection and co-stirring

Stir-loading with longer time than drop-casting can help the loading for some enzymes that are slow to get into the pores of ITO layers and achieve better performance as discussed in previous section. Co-injection is the live-monitored version of co-stirriing. The chronoamperogram of a typical co-injection reaction is shown in figure A5.8. FNR and ADH are injected at the beginning of the reaction. The current grows as the enzyme loading is occurring. The substrate is fully converted in approximately 6 hours. A buffer exchange is conducted after 17 hours. The current in fresh batch reaches higher than the peak current in loading process as the peak current in loading process is masked by substrate limitation. The current is approximately 0.55 mA which is higher than the drop-

cast loading with same amount of enzyme applied. Co-stir loading is also an excellent method for enzyme loading. Drop-cast and stir-loading are complementary.

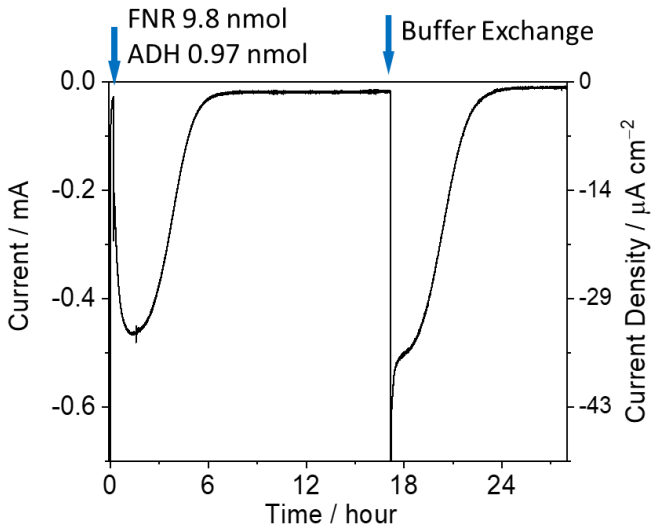


Figure A5.8. Chronoamperogram of electrode loaded with FNR and ADH by live co-injection. Conditions: volume 4 mL; solution stirred throughout using a magnetic flea; substrate [4-phenyl-2-butanone] = 8 mM, [NADPH] = 20 μM, buffer: 100 mM TAPS pH 8.0; temperature: 25 ℃, Potential held at −0.9 V vs. Ag/AgCl (3 M KCl) to drive reduction. Solution purged with argon to remove O_2; argon flow maintained in headspace thereafter. Enzyme loading amount: FNR 9.8 nmol, ADH 0.97 nmol live injected. Electrode (Ti foil) SA: 14cm^2.

A test of FNR redox peak with different loading methods provides further comparison of drop-cast and stir-loading. FNR redox peak area is directly related to the amount of FNR that is electroactive in the electrode. In this test, the ITO electrode is loaded with only the FNR. As shown in figure A5.9, the cyclic voltammograms of three electrodes have different area of FNR non-turnover peak. In stir-loading 1 (green trace), 9.8 nmol of FNR is diluted in 4 mL of pH 9.0 TAPS buffer, in which the electrode is held and solution is stirred for 2 hours. Stir-loading 2 (red trace) has the same condition as stir-loading 1 with a longer loading time of 6 hours. The drop-cast loading takes only 3 minutes, 28 μL buffer containing 9.8 nmol of FNR is dropped on the electrode before being rinsed off by buffer. The FNR coverage calculated based on the areas of FNR non-turnover peak are 48, 32 and 88 pmol cm^{-2} for drop-cast, stir-loading 1 hour and stir-loading 6 hours. This

result confirms again that drop-cast is fast and takes shorter time for a decent loading, while stir-loading is slow but can achieved better loading given enough time.

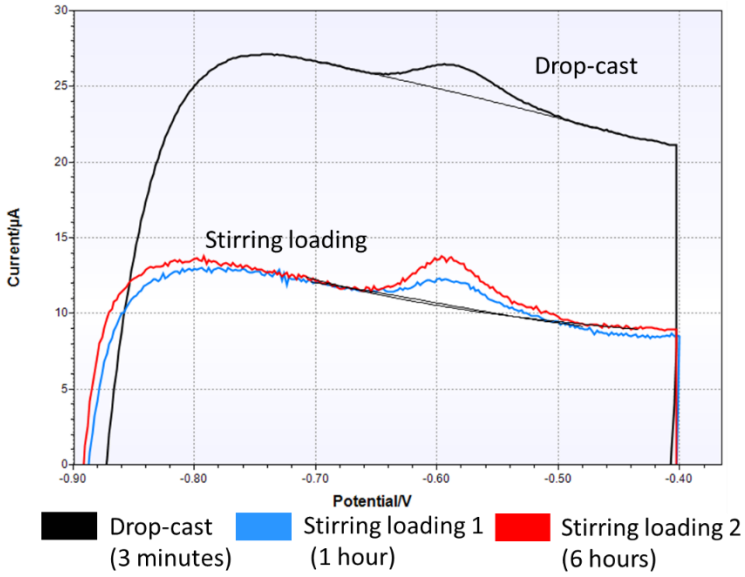


Figure A5.9. Cyclic Voltammograms of electrode with different FNR loading methods. Conditions: solution volume 4 mL, buffer: 100 mM TAPS pH 9.0; temperature: 25 ℃, solution is purged with argon to remove O_2 and argon flow maintained in headspace thereafter. Electrode SA = 3.5 cm^2; FNR amounts: 9.8 nmol. Scan rate: 4 mV/s.

The comparison of stir-loading and drop-casting has also been conducted by chronoamperometry. As shown in figure A5.10, drop-casting loading (green trace) given long enough time of 20 hours as the stir-loading, still achieves lower current than the stir-loading method (black trace). Stir-loading is slower but with larger potential than the drop-cast loading that is a static loading process with higher concentration. The static loading with similar condition as the stir-loading (diluted enzyme in solution) is shown as the blue trace, having an extremely low current.

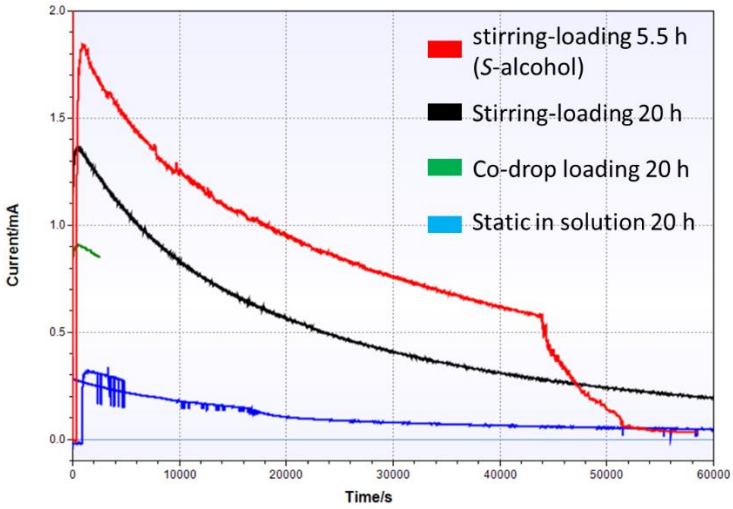


Figure 5.10. Chronoamperograms of ADH-catalysed oxidation with enzymes loaded by stirring, drop-cast and holding staticall. Conditions: volume 40 mL; solution stirred throughout using a magnetic flea; substrate [4-phenyl-2-butanol] = 8 mM, [NADPH] = 20 µM, buffer: 100 mM TAPS pH 9.0; temperature: 25 ℃, Potential held at −0.34 V vs. Ag/AgCl (3 M KCl) to drive reduction. Solution purged with argon to remove O_2; argon flow maintained in headspace thereafter. Enzyme loading amount: FNR 34.2 nmol, ADH 17.1 nmol. Electrode (Ti foil) SA: 28 cm^2.

On reviewing the difference of drop-cast and dilute solution stirring method, the key inference is that each method relies on different main mass transfer process. Diffusion driven by high concentration is the dominant force. It is more of a 'kinetic'-driving process. In stir-loading, the agitation of solution contributes to the thinner diffusion layer of enzyme getting into the nanopores. The adsorption of enzymes into the nanopores is thermodynamically favoured, therefore an optimal loading point can be reached given enough time in stirring.

A5.2. Enzyme loading amount and ratio

A5.2.1. Enzyme loading amount

The test was carried out to compare the loading process with different amount of ADH by continuous cyclic voltammetry, in order to investigate the effect of E2 injection amount on the enzyme loading process. Figure A5.11 shows the current changes in the loading process with different amount of ADH injected. The starting cyclic voltammetry is

marked as the black trace, and the peak current is red. The time taken to reach the peak current and the current increase is listed in table A5.1. Intuitively, the faster current increases, indicating the faster loading process, were observed with higher amount of ADH injected despite some inconsistent results. The flaw with this series test was that the amount of ADH used did not yet reach the upper cap, in which enzyme amount was no longer the rate determining factor for enzyme loading. In addition, the continuous CV was also exposed to possible substrate limitation, even though the current is low with less surface area of electrode.

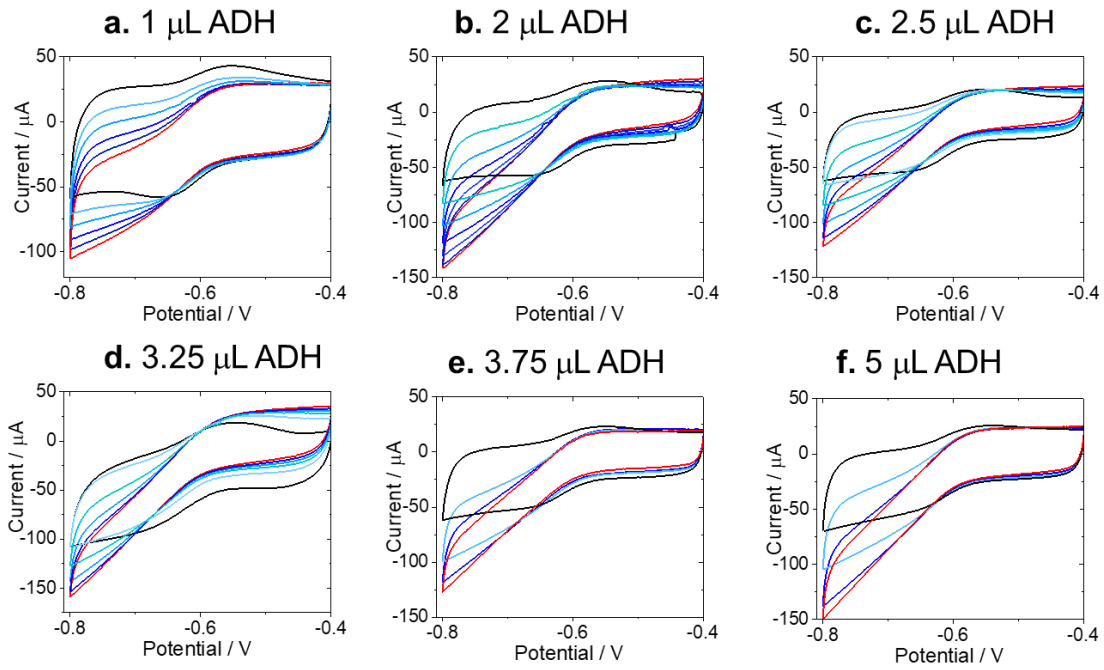


Figure A5.11. Cyclic Voltammograms over time monitoring the loading process with different amount of E2 (ADH). Conditions: solution volume 4 mL; solution stirred throughout using a magnetic flea; buffer: 100 mM TAPS pH 8.0; temperature: 25 ℃, substrate [4-phenyl-2-butanol] = 8 mM, [NADPH] = 20 µM; solution is purged with argon to remove O_2 and argon flow maintained in headspace thereafter. Electrode SA = 3.5 cm^2; Scan rate: 2 mV/s (a – d and f) and 4 mV/s (e).

Table A5.1. ADH injection amount and current change performance in figure A5.11

	ADH injection volume / μL	ADH injection amount* / nmol	Current increased / mA	Time to reach maximum current /hour
a	1	0.11	51	29
b	2	0.22	79	33
c	2.5	0.28	58.6	26
d	3.25	0.36	51	26
e	3.75	0.41	65	7.6
f	5	0.55	81.6	15

* Concentration of injected ADH is 0.109 mM. Scan rate: entry a - d and f: 2 mV/s, entry e: 4 mV/s.

A5.2.2. Enzyme loading ratio (FNR to ADH)

Figure A5.12 shows the reaction current change with three electrodes loaded with FNR and ADH (W110A) of three different ratios (10:1, 10:10, and 1:10). All the curves have similar timecourses. The reaction rate remained at a steady level over the reaction, despite the oxygen peak introduced at the initiation of the reaction by addition of NADPH in real-time. The substrate did not deplete due to low reaction rate. Despite low current level and some noises of the curves, it is distinguishable that the 10:1 ratio of FNR:ADH has the best catalytic activity. The ratios in FNR + ADH loading can be tailored for different batches of enzyme, reaction purposes and loading methods. For example, the amount of ADH can be increased when FNR is preloaded and ADH is being loaded alone by stirring in dilute solution. This reaction is not an excellent one due to the low activity of the electrode and the large oxygen spike on the initiation of the reaction. This experiment only provides a rough idea that different FNR to E2 ratios will have different catalytic performance and it is a key factor to consider for optimisation.

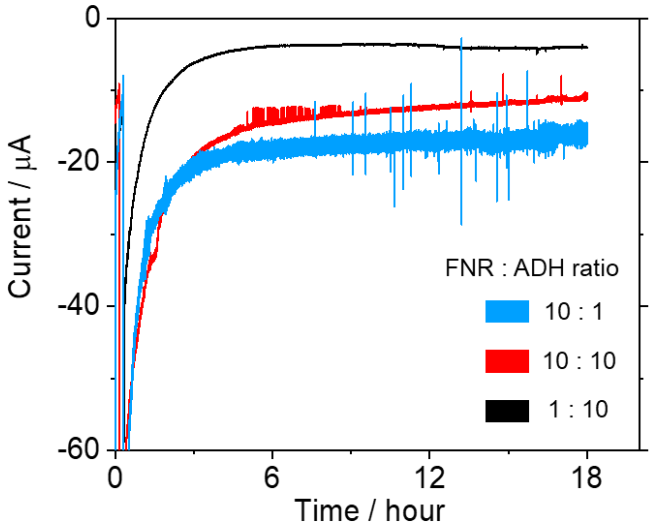


Figure A5.12. Chronoamperograms of ADH-catalysed reduction with enzyme loading of different FNR to GLDH ratios. Conditions: solution volume 4 mL, buffer: 100 mM TAPS pH 7.5; temperature: 25 ℃, solution is purged with argon to remove O_2 and argon flow maintained in headspace thereafter. substrate [4-phenyl-2-butanone] = 8 mM, [$NADP^+$] = 20 µM; Potential held at -0.69 V vs. Ag/AgCl (3 M KCl) to drive reduction. Electrode SA = 3.5 cm^2; enzyme loaded by co-dropcast, enzyme amounts: 3.25 nmol FNR + 0.325 nmol ADH (10:1); 3.25 nmol FNR + 3.25 nmol ADH (10:10); 0.325 nmol FNR + 3.25 nmol ADH (1:10).

Appendix of Chapter 6

Leaking issue from pump tube breaking

The silicone tube used in the peristaltic pump is worn fast under a heavy work load and the abrasion caused leaking. Figure A6.1 shows two typical chronoamperograms with leaking occurring. The pump is a simple model with the silicone tube of a thin wall thickness (1 mm) and is not suitable for prolonged experiments thus a new pump of a higher standard was used for later experiments.

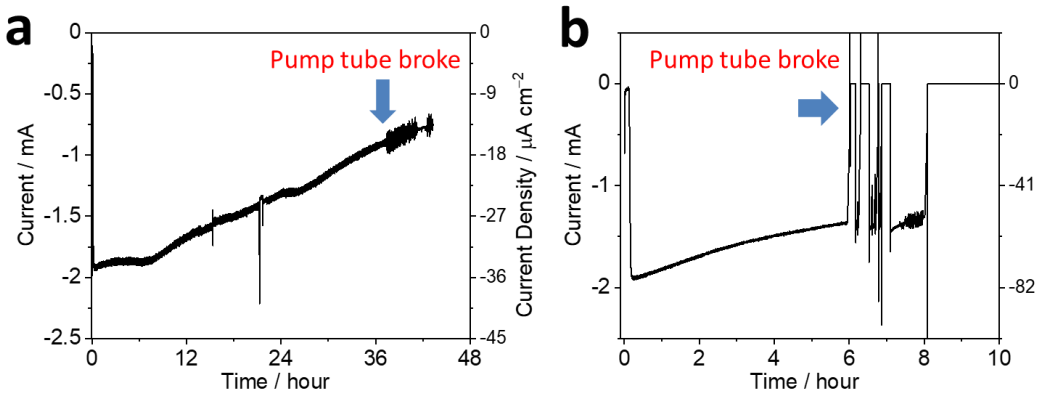


Figure A6.1 Leaking problems in reaction processes in flow reactor III. Conditions: solution volume 200 mL; buffer: 50 mM TAPS pH 8.0, temperature: RT; experiments performed in an anaerobic glovebox to avoid any contribution to the current form the reduction of O_2. substrate [-ketoglutarate] = 8 mM, [NH_4Cl] = 16 mM, [$NADP^+$] = 20 µM; Potential held at -0.8 V vs. Ag/AgCl (3 M KCl) to drive reduction; solution agitation: stirred by stirring flea and flow by peristaltic pump, flow rate: 50 mL/min. Enzyme loading (a): 102 nmol FNR + 10.2 nmol GLDH are mixed and loaded by drop-casting; electrode SA: 56 cm^2. Enzyme loading (b): 51.1 nmol FNR + 5.1 nmol GLDH are mixed and loaded by drop-casting; electrode SA: 24 cm^2.

Reference

1. Siritanaratkul, B. *et al.* Transfer of photosynthetic NADP + /NADPH recycling activity to a porous metal oxide for highly specific, electrochemically-driven organic synthesis. *Chem. Sci.* **8**, 4579–4586 (2017).

2. Berg, J., Tymoczko, J. & Stryer, L. *Biochemistry, 5th edition*. *Biochemistry* (W H Freeman, 2002).

3. Turner, N. J. Directed evolution drives the next generation of biocatalysts. *Nat. Chem. Biol.* **5**, 567–573 (2009).

4. Zhao, H. & Van Der Donk, W. A. A. Regeneration of cofactors for use in biocatalysis. *Curr. Opin. Biotechnol.* **14**, 583–589 (2003).

5. Bugg, T. D. H. *Introduction to Enzyme and Coenzyme Chemistry*. *Introduction to Enzyme and Coenzyme Chemistry: Third Edition* (Wiley, 2012). doi:10.1002/9781118348970

6. Sheldon, R. A. & Brady, D. Broadening the Scope of Biocatalysis in Sustainable Organic Synthesis. *ChemSusChem* **12**, 2859–2881 (2019).

7. Tatta, E. R., Imchen, M., Moopantakath, J. & Kumavath, R. Bioprospecting of microbial enzymes: current trends in industry and healthcare. *Appl. Microbiol. Biotechnol.* **106**, 1813–1835 (2022).

8. Morra, S. *et al.* Electrochemical control of [FeFe]-hydrogenase single crystals reveals complex redox populations at the catalytic site. *Dalt. Trans.* **50**, 12655–12663 (2021).

9. Yuan, M., Kummer, M. J., Milton, R. D., Quah, T. & Minteer, S. D. Efficient NADH Regeneration by a Redox Polymer-Immobilized Enzymatic System. *ACS Catal.* **9**, 5486–5495 (2019).

10. Adamson, H., Bond, A. M. & Parkin, A. Probing biological redox chemistry with large amplitude Fourier transformed ac voltammetry. *Chem. Commun.* **53**, 9519–9533 (2017).

11. WHITE, H. B. Evolution of Coenzymes and the Origin of Pyridine Nucleotides. in *The Pyridine Nucleotide Coenzymes* 1–17 (Elsevier, 1982). doi:10.1016/B978-0-12-244750-1.50010-5

12. Gorton, L. & Domínguez, E. Electrochemistry of NAD(P)+/NAD(P)H. in *Encyclopedia of Electrochemistry* (Wiley, 2002). doi:10.1002/9783527610426.bard090004

13. Sauer, U., Canonaco, F., Heri, S., Perrenoud, A. & Fischer, E. The Soluble and Membrane-bound Transhydrogenases UdhA and PntAB Have Divergent Functions in NADPH Metabolism of Escherichia coli. *J. Biol. Chem.* **279**, 6613–6619 (2004).

14. Drauz, K., Waldmann, H., Lalonde, J. & Margolin, A. *Enzyme Catalysis in Organic Synthesis*. *Enzyme Catalysis in Organic Synthesis* (Wiley, 2002). doi:10.1002/9783527618262

15. Hollmann, F. & Schmid, A. Electrochemical regeneration of oxidoreductases for cell-free biocatalytic redox reactions. *Biocatal. Biotransformation* **22**, 63–88 (2004).

16. Kochius, S. *et al.* Electrochemical regeneration of oxidised nicotinamide cofactors in a

scalable reactor. *J. Mol. Catal. B Enzym.* **103**, 94–99 (2014).

17. Wu, H. *et al.* Methods for the regeneration of nicotinamide coenzymes. *Green Chem.* **15**, 1773–1789 (2013).

18. Wichmann, R. & Vasic-Racki, D. Cofactor regeneration at the lab scale. *Advances in Biochemical Engineering/Biotechnology* **92**, 225–260 (2005).

19. Lee, Y. S., Gerulskis, R. & Minteer, S. D. Advances in electrochemical cofactor regeneration: enzymatic and non-enzymatic approaches. *Curr. Opin. Biotechnol.* **73**, 14–21 (2022).

20. Shaked, Z. & Whitesides, G. M. Enzyme-catalyzed organic synthesis: NADH regeneration by using formate dehydrogenase. *J. Am. Chem. Soc.* **102**, 7104–7105 (1980).

21. Yun, H., Yang, Y. H., Cho, B. K., Hwang, B. Y. & Kim, B. G. Simultaneous synthesis of enantiomerically pure (R)-1-phenylethanol and (R)-α-methylbenzylamine from racemic α-methylbenzylamine using ω-transaminase/alcohol dehydrogenase/glucose dehydrogenase coupling reaction. *Biotechnol. Lett.* **25**, 809–814 (2003).

22. Wada, M. *et al.* Production of a Doubly Chiral Compound , by Two-Step Enzymatic Asymmetric Reduction Production of a Doubly Chiral Compound , Enzymatic Asymmetric Reduction. *Appl. Environ. Microbiol.* **69**, 933–937 (2003).

23. Chenault, H. K., Simon, E. S. & Whitesides, G. M. Cofactor regeneration for enzyme-catalysed synthesis. *Biotechnol. Genet. Eng. Rev.* **6**, 221–270 (1988).

24. Jones, J. B., Sneddon, D. W., Higgins, W. & Lewis, A. J. Preparative-scale reductions of cyclic ketones and aldehyde substrates of horse liver alcohol dehydrogenase with in situ sodium dithionite recycling of catalytic amounts of NAD. *J. Chem. Soc. Chem. Commun.* 856 (1972). doi:10.1039/c39720000856

25. Maenaka, Y., Suenobu, T. & Fukuzumi, S. Hydrogen Evolution from Aliphatic Alcohols and 1,4-Selective Hydrogenation of NAD + Catalyzed by a [C,N] and a [C,C] Cyclometalated Organoiridium Complex at Room Temperature in Water. *J. Am. Chem. Soc.* **134**, 9417–9427 (2012).

26. Rueping, M., Dufour, J. & Schoepke, F. R. Advances in catalytic metal-free reductions: from bio-inspired concepts to applications in the organocatalytic synthesis of pharmaceuticals and natural products. *Green Chem.* **13**, 1084 (2011).

27. Wagenknecht, P. S., Penney, J. M. & Hembre, R. T. Transition-Metal-Catalyzed Regeneration of Nicotinamide Coenzymes with Hydrogen 1. *Organometallics* **22**, 1180–1182 (2003).

28. Ali, I., Khan, T. & Omanovic, S. Direct electrochemical regeneration of the cofactor NADH on bare Ti, Ni, Co and Cd electrodes: The influence of electrode potential and electrode material. *J. Mol. Catal. A Chem.* **387**, 86–91 (2014).

29. Kadowaki, J. T., Jones, T. H., Sengupta, A., Gopalan, V. & Subramaniam, V. V. Copper oxide-based cathode for direct NADPH regeneration. *Sci. Rep.* **11**, 180 (2021).

30. Cai, C. X. & Xue, K. H. Electrocatalysis of NADH oxidation with electropolymerized films of azure I. *J. Electroanal. Chem.* **427**, 147–153 (1997).

31. Burnett, J. W. H., Sun, Z., Li, J., Wang, X. & Wang, X. Comparative life cycle assessment of NAD(P)H regeneration technologies. *Green Chem.* **23**, 7162–7169 (2021).

32. Jiang, Z., Lü, C. & Wu, H. Photoregeneration of NADH using carbon-containing TiO2. *Ind. Eng. Chem. Res.* **44**, 4165–4170 (2005).

33. Miura, R. Versatility and specificity in flavoenzymes: control mechanisms of flavin reactivity. *Chem. Rec.* **1**, 183–194 (2001).

34. Shin, M., Tagawa, K. & Arnon, D. I. Crystallization of Ferredoxin-Tpn Reductase and its Role in the Photosynthetic Apparatus of Chloroplasts. *Biochem. Z.* **338**, 84–96 (1963).

35. Deng, Z. *et al.* A productive NADP+ binding mode of ferredoxin-NADP+ reductase revealed by protein engineering and crystallographic studies. *Nat. Struct. Biol.* **6**, 847–853 (1999).

36. Piubelli, L. *et al.* Competition between C-terminal tyrosine and nicotinamide modulates pyridine nucleotide affinity and specificity in plant ferredoxin-NADP+ reductase. *J. Biol. Chem.* **275**, 10472–10476 (2000).

37. Nascimento, A. S. *et al.* Crystal structures of Leptospira interrogans FAD-containing ferredoxin-NADP+ reductase and its complex with NADP+. *BMC Struct. Biol.* **7**, 1–12 (2007).

38. Mulo, P. Chloroplast-targeted ferredoxin-NADP+ oxidoreductase (FNR): Structure, function and location. *Biochim. Biophys. Acta - Bioenerg.* **1807**, 927–934 (2011).

39. Karplus, P. A., Daniels, M. J. & Herriott, J. R. Atomic Structure of Ferredoxin-NADP + Reductase: Prototype for a Structurally Novel Flavoenzyme Family. *Science (80-.).* **251**, 60–66 (1991).

40. Medina, M. Structural and mechanistic aspects of flavoproteins: Photosynthetic electron transfer from photosystem i to NADP+. *FEBS J.* **276**, 3942–3958 (2009).

41. Batie, C. J. & Kamin, H. The relation of pH and oxidation-reduction potential to the association state of the ferredoxin . ferredoxin:NADP+ reductase complex. *J. Biol. Chem.* **256**, 7756–7763 (1981).

42. Kurisu, G. *et al.* Structure of the electron transfer complex between ferredoxin and ferredoxin-NADP(+) reductase. *Nat. Struct. Biol.* **8**, 117–21 (2001).

43. Hurley, J. K. *et al.* Structure-function relationships in Anabaena ferredoxin/ferredoxin:NADP+ reductase electron transfer: Insights from site-directed mutagenesis, transient absorption spectroscopy and X-ray crystallography. *Biochim. Biophys. Acta - Bioenerg.* **1554**, 5–21 (2002).

44. Megarity, C. F., Siritanaratkul, B., Herold, R. A., Morello, G. & Armstrong, F. A. Electron flow between the worlds of Marcus and Warburg. *J. Chem. Phys.* **153**, (2020).

45. Armstrong, F. A., Evans, R. M. & Megarity, C. F. *Protein Film Electrochemistry of Iron–Sulfur Enzymes*. *Methods in Enzymology* **599**, (Elsevier Inc., 2018).

46. Armstrong, F. A. & Hirst, J. Reversibility and efficiency in electrocatalytic energy

conversion and lessons from enzymes. *Proc. Natl. Acad. Sci. U. S. A.* **108**, 14049–14051 (2011).

47. Armstrong, F. A. *et al.* Guiding Principles of Hydrogenase Catalysis Instigated and Clarified by Protein Film Electrochemistry. *Acc. Chem. Res.* **49**, 884–892 (2016).

48. Megarity, C. F. *et al.* Electrified Nanoconfined Biocatalysis with Rapid Cofactor Recycling. *ChemCatChem* **11**, 5662–5670 (2019).

49. Morello, G., Megarity, C. F. & Armstrong, F. A. The power of electrified nanoconfinement for energising, controlling and observing long enzyme cascades. *Nat. Commun.* **12**, 340 (2021).

50. Megarity, C. F., Weald, T. R. I., Heath, R. S., Turner, N. J. & Armstrong, F. A. A Nanoconfined Four-Enzyme Cascade Simultaneously Driven by Electrical and Chemical Energy, with Built-in Rapid, Confocal Recycling of NADP(H) and ATP. *ACS Catal.* **12**, 8811–8821 (2022).

51. Megarity, C. F. *et al.* Electrocatalytic Volleyball: Rapid Nanoconfined Nicotinamide Cycling for Organic Synthesis in Electrode Pores. *Angew. Chemie Int. Ed.* **58**, 4948–4952 (2019).

52. Wan, L., Megarity, C. F., Siritanaratkul, B. & Armstrong, F. A. A hydrogen fuel cell for rapid, enzyme-catalysed organic synthesis with continuous monitoring. *Chem. Commun.* **54**, 972–975 (2018).

53. Morello, G., Siritanaratkul, B., Megarity, C. F. & Armstrong, F. A. Efficient Electrocatalytic CO2 Fixation by Nanoconfined Enzymes via a C3-to-C4 Reaction That Is Favored over H2 Production. *ACS Catal.* **9**, 11255–11262 (2019).

54. Cheng, B., Wan, L. & Armstrong, F. A. Progress in Scaling up and Streamlining a Nanoconfined, Enzyme-Catalyzed Electrochemical Nicotinamide Recycling System for Biocatalytic Synthesis. *ChemElectroChem* **7**, 4672–4678 (2020).

55. Herold, R. A. *et al.* Exploiting Electrode Nanoconfinement to Investigate the Catalytic Properties of Isocitrate Dehydrogenase (IDH1) and a Cancer-Associated Variant. *J. Phys. Chem. Lett.* **12**, 6095–6101 (2021).

56. Wan, L. *et al.* Exploiting Bidirectional Electrocatalysis by a Nanoconfined Enzyme Cascade to Drive and Control Enantioselective Reactions. *ACS Catal.* **11**, 6526–6533 (2021).

57. Cheng, B., Heath, R. S., Turner, N. J., Armstrong, F. A. & Megarity, C. F. Deracemisation and stereoinversion by a nanoconfined bidirectional enzyme cascade: dual control by electrochemistry and selective metal ion activation. *Chem. Commun.* **58**, 11713–11716 (2022).

58. Ralston, G. B. Effects of ‘crowding’ in protein solutions. *J. Chem. Educ.* **67**, 857–860 (1990).

59. Tabaka, M., Sun, L., Kalwarczyk, T. & Hołyst, R. Implications of macromolecular crowding for protein-protein association kinetics in the cytoplasm of living cells. *Soft Matter* **9**, 4386–4389 (2013).

60. Armstrong, F. A., Cheng, B., Herold, R. A., Megarity, C. F. & Siritanaratkul, B. From Protein Film Electrochemistry to Nanoconfined Enzyme Cascades and the

Electrochemical Leaf. *Chem. Rev.* (2022). doi:10.1021/acs.chemrev.2c00397

61. Daido, T. & Akaike, T. Electrochemistry of cytochrome c: influence of coulombic attraction with indium tin oxide electrode. *J. Electroanal. Chem.* **344**, 91–106 (1993).

62. Lai, Y. H., King, T. C., Wright, D. S. & Reisner, E. Scalable one-step assembly of an inexpensive photoelectrode for water oxidation by deposition of a Ti- and Ni-containing molecular precursor on nanostructured WO3. *Chem. - A Eur. J.* **19**, 12943–12947 (2013).

63. Riesgo-Gonzalez, V. *et al.* Single-Source Deposition of Mixed-Metal Oxide Films Containing Zirconium and 3d Transition Metals for (Photo)electrocatalytic Water Oxidation. *Inorg. Chem.* **61**, 6223–6233 (2022).

64. Wang, C. & Liao, K. Recent Advances in Emerging Metal- And Covalent-Organic Frameworks for Enzyme Encapsulation. *ACS Appl. Mater. Interfaces* **13**, 56752–56776 (2021).

65. Minten, I. J. *et al.* Catalytic capsids: The art of confinement. *Chem. Sci.* **2**, 358–362 (2011).

66. Miller, T. E. *et al.* Supplementary Materials for with natural and synthetic parts. *Science (80-.).* **654**, 1–48 (2020).

67. Reeve, H. A., Lauterbach, L., Ash, P. A., Lenz, O. & Vincent, K. A. A modular system for regeneration of NAD cofactors using graphite particles modified with hydrogenase and diaphorase moieties. *Chem. Commun.* **48**, 1589–1591 (2012).

68. Pareek, V., Sha, Z., He, J., Wingreen, N. S. & Benkovic, S. J. Metabolic channeling: predictions, deductions, and evidence. *Mol. Cell* **81**, 3775–3785 (2021).

69. Rife, J. E. & Cleland, W. W. Kinetic Mechanism of Glutamate Dehydrogenase. *Biochemistry* **19**, 2321–2328 (1980).

70. Musa, M. M., Ziegelmann-Fjeld, K. I., Vieille, C., Zeikus, J. G. & Phillips, R. S. Xerogel-encapsulated W110A secondary alcohol dehydrogenase from Thermoanaerobacter ethanolicus performs asymmetric reduction of hydrophobic ketones in organic solvents. *Angew. Chemie - Int. Ed.* **46**, 3091–3094 (2007).

71. Kohls, H., Steffen-Munsberg, F. & Höhne, M. Recent achievements in developing the biocatalytic toolbox for chiral amine synthesis. *Curr. Opin. Chem. Biol.* **19**, 180–192 (2014).

72. Coccia, F. *et al.* Stereoselective double reduction of 3-methyl-2-cyclohexenone by use of palladium and platinum nanoparticles in tandem with alcohol dehydrogenase. *Nanomaterials* **8**, (2018).

73. Mutti, F. G., Knaus, T., Scrutton, N. S., Breuer, M. & Turner, N. J. Conversion of alcohols to enantiopure amines through dual-enzyme hydrogen-borrowing cascades. *Science (80-.).* **349**, 1525–1529 (2015).

74. Gröger, H. *et al.* Practical asymmetric enzymatic reduction through discovery of a dehydrogenase-compatible biphasic reaction media. *Org. Lett.* **5**, 173–176 (2003).

75. Musa, M. M., Ziegelmann-Fjeld, K. I., Vieille, C. & Phillips, R. S. Activity and selectivity of W110A secondary alcohol dehydrogenase from Thermoanaerobacter

ethanolicus in organic solvents and ionic liquids: mono- and biphasic media. *Org. Biomol. Chem.* **6**, 887 (2008).

76. Hamaker, H. C. Formation of a deposit by electrophoresis. *Trans. Faraday Soc.* **35**, 279 (1940).

77. Besra, L. & Liu, M. A review on fundamentals and applications of electrophoretic deposition (EPD). *Prog. Mater. Sci.* **52**, 1–61 (2007).

78. Compton, R. G. & Banks, C. E. *Understanding Voltammetry*. *Understanding Voltammetry* (WORLD SCIENTIFIC, 2007). doi:10.1142/6430

79. Compton, R. G. & Sanders, G. H. W. *Electrode Potentials*. (OUP Oxford, 1996).

80. Huynh, T.-P., Hoang, T.-T., Nguyen, P.-H., Tran, T.-N. & Nguyen, T.-V. Preparation of TiO2 thin film using modified doctor-blade method for improvement of dye-sensitized solar cell. in *2009 34th IEEE Photovoltaic Specialists Conference (PVSC)* 002168–002171 (IEEE, 2009). doi:10.1109/PVSC.2009.5411405

81. Nguyen, T. V., Lee, H. C. & Yang, O. B. The effect of pre-thermal treatment of TiO2 nano-particles on the performances of dye-sensitized solar cells. *Sol. Energy Mater. Sol. Cells* **90**, 967–981 (2006).

82. Weissman, S. A. & Anderson, N. G. Design of Experiments (DoE) and Process Optimization. A Review of Recent Publications. *Org. Process Res. Dev.* **19**, 1605–1633 (2015).

83. Veronese, F. M., Boccu, E. & Conventi, L. Glutamate dehydrogenase from Escherichia coli: Induction, purification and properties of the enzyme. *BBA - Enzymol.* **377**, 217–228 (1975).

84. Sharkey, M. A. & Engel, P. C. Apparent negative co-operativity and substrate inhibition in overexpressed glutamate dehydrogenase from Escherichia coli. *FEMS Microbiol. Lett.* **281**, 132–139 (2008).

85. Megarity, C. F. *et al.* Electrocatalytic Volleyball: Rapid Nanoconfined Nicotinamide Cycling for Organic Synthesis in Electrode Pores. *Angew. Chemie - Int. Ed.* **58**, 4948–4952 (2019).

86. Kusoglu, A. & Weber, A. Z. New Insights into Perfluorinated Sulfonic-Acid Ionomers. *Chem. Rev.* **117**, 987–1104 (2017).

87. Musa, M. M. *et al.* Thermoanaerobacter ethanolicus secondary alcohol dehydrogenase mutants with improved racemization activity. *J. Mol. Catal. B Enzym.* **115**, 155–159 (2015).

88. Hildebrand, F. & Lütz, S. Electroenzymatic synthesis of chiral alcohols in an aqueous-organic two-phase system. *Tetrahedron Asymmetry* **18**, 1187–1193 (2007).

89. Schöll, J., Vicum, L., Müller, M. & Mazzotti, M. Precipitation of L-glutamic acid: Determination of nucleation kinetics. *Chem. Eng. Technol.* **29**, 257–264 (2006).

90. Manzurola, E. & Apelblat, A. Solubilities of L-glutamic acid, 3-nitrobenzoic acid, p-toluic acid, calcium-L-lactate, calcium gluconate, magnesium-DL-aspartate, and magnesium-L-lactate in water. *J. Chem. Thermodyn.* **34**, 1127–1136 (2002).

91. Yalkowsky, S. H., He, Y. & Jain, P. *Handbook of Aqueous Solubility Data - Second*

edition. *CRC Press* (2010).

92. Herold, R. A., Reinbold, R., Schofield, C. J. & Armstrong, F. A. NADP(H)-dependent biocatalysis without adding NADP(H). *Proc. Natl. Acad. Sci.* **120**, (2023).

93. dos Santos, E. V. *et al.* Scale-up of electrochemical oxidation system for treatment of produced water generated by Brazilian petrochemical industry. *Environ. Sci. Pollut. Res.* **21**, 8466–8475 (2014).

94. Jiang, D. *et al.* A pilot-scale study on utilizing multi-anode/cathode microbial fuel cells (MAC MFCs) to enhance the power production in wastewater treatment. *Int. J. Hydrogen Energy* **36**, 876–884 (2011).

95. Zhuang, L., Yuan, Y., Wang, Y. & Zhou, S. Long-term evaluation of a 10-liter serpentine-type microbial fuel cell stack treating brewery wastewater. *Bioresour. Technol.* **123**, 406–412 (2012).

96. Sajana, T. K., Ghangrekar, M. M. & Mitra, A. Effect of operating parameters on the performance of sediment microbial fuel cell treating aquaculture water. *Aquac. Eng.* **61**, 17–26 (2014).

97. Siritanaratkul, B. *et al.* Zero-Gap Bipolar Membrane Electrolyzer for Carbon Dioxide Reduction Using Acid-Tolerant Molecular Electrocatalysts. *J. Am. Chem. Soc.* **144**, 7551–7556 (2022).

98. Nguyen, L. A., He, H. & Pham-Huy, C. Chiral drugs: an overview. *Int. J. Biomed. Sci.* **2**, 85–100 (2006).

99. Karume, I., Takahashi, M., Hamdan, S. M. & Musa, M. M. Deracemization of Secondary Alcohols by using a Single Alcohol Dehydrogenase. *ChemCatChem* **8**, 1459–1463 (2016).

100. Gihani, M. T. & Williams, J. M. J. Dynamic kinetic resolution. *Curr. Opin. Chem. Biol.* **3**, 11–5 (1999).

101. Intaraboonrod, K., Lerdwiriyanupap, T., Hoquante, M., Coquerel, G. & Flood, A. E. Temperature cycle induced deracemization. *Mendeleev Commun.* **30**, 395–405 (2020).

102. Shi, Q. & Ye, J. Deracemization Enabled by Visible-Light Photocatalysis. *Angew. Chemie Int. Ed.* **59**, 4998–5001 (2020).

103. Vedovello, P., Marcio Paranhos, C., Fernandes, C. & Elizabeth Tiritan, M. Chiral polymeric membranes: Recent applications and trends. *Sep. Purif. Technol.* **280**, 119800 (2022).

104. Foulkes, J. M., Malone, K. J., Coker, V. S., Turner, N. J. & Lloyd, J. R. Engineering a Biometallic Whole Cell Catalyst for Enantioselective Deracemization Reactions. *ACS Catal.* **1**, 1589–1594 (2011).

105. de Gonzalo, G. & Paul, C. E. Recent trends in synthetic enzymatic cascades promoted by alcohol dehydrogenases. *Curr. Opin. Green Sustain. Chem.* **32**, 100548 (2021).

106. Hermann, J. *et al.* Neutron and X-ray crystal structures of Lactobacillus brevis alcohol dehydrogenase reveal new insights into hydrogen-bonding pathways. *Acta*

Crystallogr. Sect. F Struct. Biol. Commun. **74**, 754–764 (2018).

107. Niefind, K., Müller, J., Riebel, B., Hummel, W. & Schomburg, D. The crystal structure of R-specific alcohol dehydrogenase from Lactobacillus brevis suggests the structural basis of its metal dependency. *J. Mol. Biol.* **327**, 317–328 (2003).

108. Hummel, W. Reduction of acetophenone to R(+)-phenylethanol by a new alcohol dehydrogenase from Lactobacillus kefir. *Appl. Microbiol. Biotechnol.* **34**, 15–19 (1990).

109. KAGI, J. H. & VALLEE, B. L. The role of zinc in alcohol dehydrogenase. V. The effect of metal-binding agents on thestructure of the yeast alcohol dehydrogenase molecule. *J. Biol. Chem.* **235**, 3188–92 (1960).

110. Ziegelmann-Fjeld, K. I., Musa, M. M., Phillips, R. S., Zeikus, J. G. & Vieille, C. A Thermoanaerobacter ethanolicus secondary alcohol dehydrogenase mutant derivative highly active and stereoselective on phenylacetone and benzylacetone. *Protein Eng. Des. Sel.* **20**, 47–55 (2007).

111. Weckbecker, A. & Hummel, W. Cloning, expression, and characterization of an (R)-specific alcohol dehydrogenase from Lactobacillus kefir. *Biocatal. Biotransformation* **24**, 380–389 (2006).

112. Wan, L. *et al.* Enzyme-catalysed enantioselective oxidation of alcohols by air exploiting fast electrochemical nicotinamide cycling in electrode nanopores. *Green Chem.* **21**, 4958–4963 (2019).

113. Musa, M. M. & Phillips, R. S. Recent advances in alcohol dehydrogenase-catalyzed asymmetric production of hydrophobic alcohols. *Catal. Sci. Technol.* **1**, 1311 (2011).

114. Chen, Q., Hu, Y., Zhao, W., Zhu, C. & Zhu, B. Cloning, expression, and characterization of a novel (s)-specific alcohol dehydrogenase from lactobacillus kefir. *Appl. Biochem. Biotechnol.* **160**, 19–29 (2010).

115. Vedha-Peters, K., Gunawardana, M., Rozzell, J. D. & Novick, S. J. Creation of a broad-range and highly stereoselective D-amino acid dehydrogenase for the one-step synthesis of D-amino acids. *J. Am. Chem. Soc.* **128**, 10923–10929 (2006).

116. Richter, N. *et al.* Characterization of a whole-cell catalyst co-expressing glycerol dehydrogenase and glucose dehydrogenase and its application in the synthesis of L-glyceraldehyde. *Biotechnol. Bioeng.* **106**, 541–552 (2010).

117. Wei, P. *et al.* Significantly enhancing the biocatalytic synthesis of chiral alcohols by semi-rationally engineering an anti-Prelog carbonyl reductase from Acetobacter sp. CCTCC M209061. *Mol. Catal.* **479**, 110613 (2019).

118. Höllrigl, V., Otto, K. & Schmid, A. Electroenzymatic asymmetric reduction of rac-3-methylcyclo-hexanone to (1S,3S)-3-methyleyclohexanol in organic/aqueous media catalyzed by a thermophilic alcohol dehydrogenase. *Adv. Synth. Catal.* **349**, 1337–1340 (2007).

119. Hollmann, F., Kleeb, A., Otto, K. & Schmid, A. Coupled chemoenzymatic transfer hydrogenation catalysis for enantioselective reduction and oxidation reactions. *Tetrahedron Asymmetry* **16**, 3512–3519 (2005).

120. Dong, F. *et al.* Biphasic Bioelectrocatalytic Synthesis of Chiral β-Hydroxy Nitriles. *J.*

Am. Chem. Soc. **142**, 8374–8382 (2020).

121. Kragl, U., Kruse, W., Hummel, W. & Wandrey, C. Enzyme engineering aspects of biocatalysis: Cofactor regeneration as example. *Biotechnol. Bioeng.* **52**, 309–319 (1996).

122. Lukito, B. R., Wu, S., Saw, H. J. J. & Li, Z. One-Pot Production of Natural 2-Phenylethanol from L-Phenylalanine via Cascade Biotransformations. *ChemCatChem* **11**, 831–840 (2019).

123. Chaudhari, R. V., Torres, A., Jin, X. & Subramaniam, B. Multiphase catalytic hydrogenolysis/hydrodeoxygenation processes for chemicals from renewable feedstocks: Kinetics, mechanism, and reaction engineering. *Ind. Eng. Chem. Res.* **52**, 15226–15243 (2013).

124. Moehlenbrock, M. J., Toby, T. K., Pelster, L. N. & Minteer, S. D. Metabolon catalysts: An efficient model for multi-enzyme cascades at electrode surfaces. *ChemCatChem* **3**, 561–570 (2011).

125. Wheeldon, I. *et al.* Substrate channelling as an approach to cascade reactions. *Nat. Chem.* **8**, 299–309 (2016).

126. Stepankova, V. *et al.* Strategies for stabilization of enzymes in organic solvents. *ACS Catal.* **3**, 2823–2836 (2013).

127. Noël, T., Cao, Y. & Laudadio, G. The Fundamentals behind the Use of Flow Reactors in Electrochemistry. *Acc. Chem. Res.* **52**, 2858–2869 (2019).

128. Krieg, T., Sydow, A., Schröder, U., Schrader, J. & Holtmann, D. Reactor concepts for bioelectrochemical syntheses and energy conversion. *Trends Biotechnol.* **32**, 645–655 (2014).

129. Tennakoon, C. L. K., Bhardwaji, R. C. & Bockris, J. O. M. Electrochemical treatment of human wastes in a packed bed reactor. *J. Appl. Electrochem.* **26**, 18–29 (1996).

130. Li, J., Hu, X., Su, Y. & Li, Q. Modeling of a packed-bed electrochemical reactor for producing glyoxylic acid from oxalic acid. *Chem. Eng. Sci.* **62**, 6784–6793 (2007).

131. Mascia, M., Vacca, A. & Palmas, S. Fixed bed reactors with three dimensional electrodes for electrochemical treatment of waters for disinfection. *Chem. Eng. J.* **211**–**212**, 479–487 (2012).

132. Perry, S. C., Ponce de León, C. & Walsh, F. C. Review—The Design, Performance and Continuing Development of Electrochemical Reactors for Clean Electrosynthesis. *J. Electrochem. Soc.* **167**, 155525 (2020).

133. Saravanan, A., Kumar, P. S. & Yaswanthraj, M. Modeling and analysis of a packed-bed column for the effective removal of zinc from aqueous solution using dual surface-modified biomass. *Part. Sci. Technol.* **36**, 934–944 (2018).

134. Menon, S. H., Madhu, G. & Mathew, J. Modeling Residence Time Distribution (RTD) Behavior in a Packed-Bed Electrochemical Reactor (PBER). *Int. J. Chem. Eng.* **2019**, 1–9 (2019).

135. Karan, R., Capes, M. D. & DasSarma, S. Function and biotechnology of extremophilic enzymes in low water activity. *Aquat. Biosyst.* **8**, 4 (2012).

136. Van Herck, J. & Junkers, T. Rapid Kinetic Screening via Transient Timesweep Experiments in Continuous Flow Reactors. *Chemistry–Methods* **2**, 1–6 (2022).

137. Cortés-Borda, D. *et al.* An Autonomous Self-Optimizing Flow Reactor for the Synthesis of Natural Product Carpanone. *J. Org. Chem.* **83**, 14286–14289 (2018).

138. Hightower, J. W. Catalysts for automobile emission control. *Stud. Surf. Sci. Catal.* **1**, 615–636 (1976).

139. Bradford, M. A Rapid and Sensitive Method for the Quantitation of Microgram Quantities of Protein Utilizing the Principle of Protein-Dye Binding. *Anal. Biochem.* **72**, 248–254 (1976).

140. Ciou, S.-J., Fung, K.-Z. & Chiang, K.-W. The mathematical expression for kinetics of electrophoretic deposition and the effects of applied voltage. *J. Power Sources* **172**, 358–362 (2007).

141. Wei, M. *et al.* Highly efficient dye-sensitized solar cells composed of mesoporous titanium dioxide. *J. Mater. Chem.* **16**, 1287 (2006).

142. Bard, A. J. & Faulkner, L. R. *Electrochemical Methods: Fundamentals and Applications*. *Annual Review of Materials Science* **30**, (2000).

143. Bates, R. G. & Macaskill, J. B. Standard Potential of the Silver-Silver Chloride Electrode. *Pure Appl. Chem.* **50**, 1701–1706 (1978).

144. Bergmeyer, H. U. New values of molar extinction coefficients of NADH and NADPH for routine laboratory use. *Med. Lab. (Stuttg).* **30**, 57–9 (1977).

145. Heath, R. S., Sangster, J. J. & Turner, N. J. An Engineered Cholesterol Oxidase Catalyses Enantioselective Oxidation of Non‐steroidal Secondary Alcohols. *ChemBioChem* **23**, (2022).